Science Report 2019 - 2021

Max Planck Institute for Extraterrestrial Physics

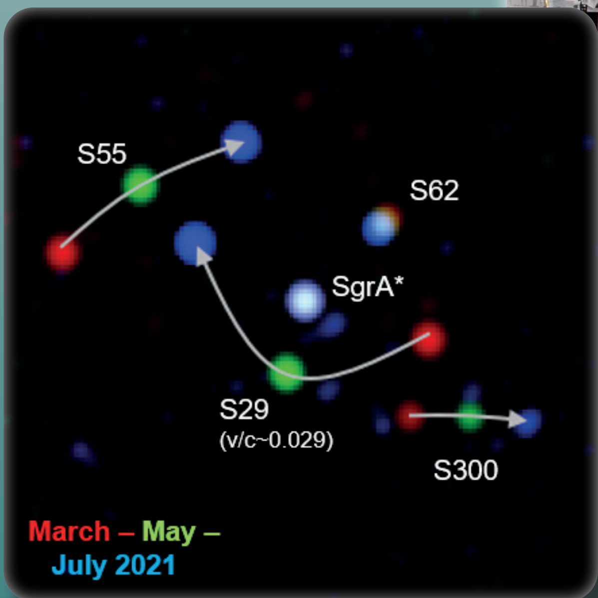

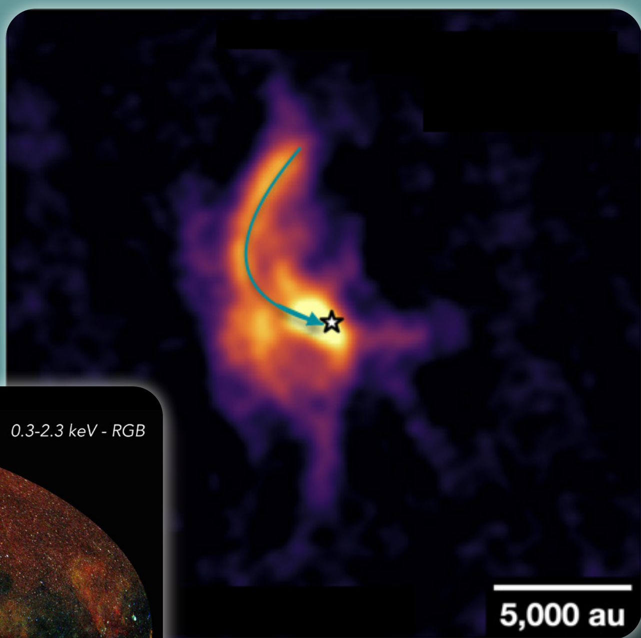

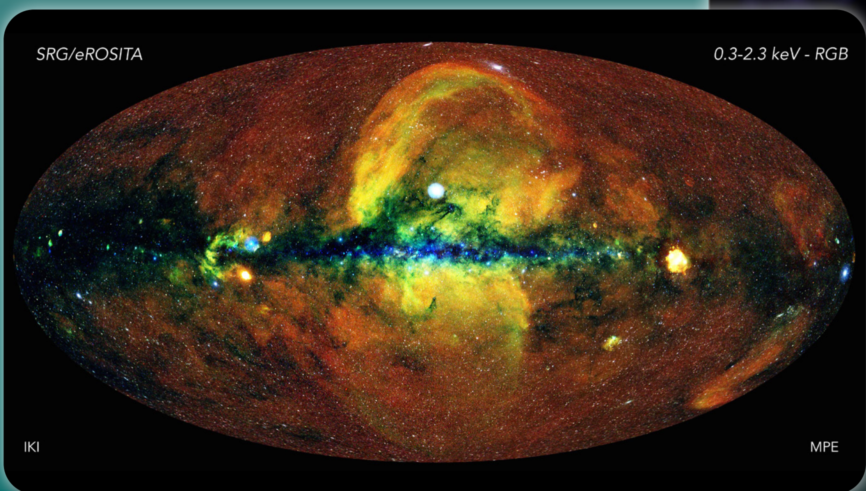

Top left: Stars orbiting the massive black hole in the center of our Galaxy.

Top right: The Euclid Pay-Load Module (consisting of the telescope with the NISP and VIS instruments) and the Service Module mated to form the Euclid space craft in Torino, Italy.

Bottom left: The energetic universe: The first eROSITA all-sky survey was conducted over a period of six months.

Bottom right: Discovery of the "streamer" of material that connects the "mother" cloud to the protoplanetary disk orbiting around the young star marked by a star, done with IRAM-NOEMA.

Report 2019 - 2021

MPE Science Report

Max Planck Institute for Extraterrestrial Physics

Imprint

Responsible for contents:	P. Caselli
Editors and Layout:	T. Herrmann, B. Niebisch
Text and Figure Contributions:	MPE Science and Research Groups

1. Edition June 2022

Table of Contents

PREFACE

The past three years have been literally glorious for MPE and I feel extremely honored and proud to be part of this outstanding Institute. I cannot think of a better place to be and carry out my research.

This Science Report is a summary of the impressive achievements in the past three years for the four scientific departments: Infrared/Submillimeter (IR; Section 2), Optical and Interpretative Astronomy (OPINAS; Section 3), High-Energy Astrophysics (HE; Section 4), Center for Astrochemical Studies (CAS; Section 5). This is followed by Section 6, which includes an overall glimpse to the rest of the Institute, starting with our Technical Services, the heart of MPE, continuing with the other vital department, our Administration, and ending with our educational efforts to train the next generation of scientists, such as the Vocational Training and the International Max Planck Research School (IMPRS); last but not least, we describe here our engagement with the public and outreach activities. Below, I very briefly summarize a few of the highlights that you will find in the next five sections.

IR - In 2020, Reinhard Genzel received the Nobel Prize for Physics, shared with Andrea Ghez, for the discovery of a supermassive compact object at the center of our Galaxy, and with Roger Penrose. Early results from GRAVITY in the Galactic Center have contributed to this fantastic achievement. In fact, the leader of GRAVITY, Frank Eisenhauer, has also been awarded with prestigious prizes, including the 2021 Tycho Brahe Medal of the European Astronomical Society and the 2022 Gruber Prize for Cosmology. Besides the precision tests of Einstein's General Theory of Relativity, GRAVITY has also obtained stunning results on Active Galactic Nuclei, Galactic star forming regions, hot Jupiter exoplanet atmospheres and orbital measurements of young exoplanets. The first upgrade (GRAVITY+) is now taking over and I am looking forward to see the new data. Great results have also been obtained in the area of Galaxy Evolution, with ground breaking surveys such as KMOS^{3D}@VLT and PHIBSS2@NOEMA which allowed the discovery of very low dark matter fractions in the most massive star forming galaxies at high redshift. Looking at the future, we are all thrilled about the 39m ELT and its first instrument, MICADO, which will allow 10 milliarcsecond near-IR images and high sensitivity spectroscopy. MPE is honored to be the MICADO PI-Institute, with Ric Davies (IR group) being the PI.

OPINAS – The main focus of the OPINAS group is on massive galaxies and their relation to Black Holes, Dark Matter and Dark Energy. Among the highlights, I mention here the development of a novel deprojection method, which allowed OPINAS scientists to derive for the first time the shapes of Brightest Cluster Galaxies (BCG) on an object-by-object basis and to make detailed comparison with comprehensive simulations of galaxy formation. A new fully 3-dimensional Schwarzschild orbit-superposition code (SMART) has also been developed to accurately measure the mass of supermassive Black Holes and Dark Matter halo properties. A major role has been played by the OPINAS group in the final analysis of the extended Baryon Oscillation Spectroscopic Survey (eBOSS) and as partners in the Dark Energy Survey (DES). Another great achievement has been the successful completion of the optics for the Near-Infrared Photometer and Spectrograph (NISP) of the ESA Dark Energy Mission Euclid (to be launched in 2024). In fact, OPINAS operates the German Euclid Science Data Center and they are in charge of making ground-based data available to Euclid. The OPINAS group is also one of the major partners of the MICADO consortium, in close collaboration with the IR group (see above). I would finally like to mention here the important results obtained by Ortwin Gerhard's group on the stellar halos of early-type galaxies, thanks to their detailed comparison between observations and Illustris TNG100 simulations, and on the Galactic bulge and bar.

HE – The HE-group (and the whole MPE) has celebrated the successful eROSITA launch on July 13th 2019. This was an emotional moment for all of us, considering the two decades of hard work by the group to arrive at this event. Since then, eROSITA has provided important new insights in our Milky Way and in the Universe, including the discovery of eROSITA bubbles extending more than 10 kpc above and below the Galactic plane; the X-ray detection of high redshift ($z > 5.5$) AGNs, providing clues on black hole growth; the discovery of Quasi-Periodic Eruptions of the central black hole in formerly quiescent galaxies, and many more highlights which can be found in the special issue of A&A on eROSITA, with 16 MPE first author papers (out of 30). For the development of eROSITA, Peter Predehl accepted on behalf of MPE the Institutional Marcel Grossmann award. I sincerely hope that eROSITA, now in safe-mode following the sanctions against Russia soon after the invasion of Ukraine, will soon come back to life and continue to bring sharper and sharper views of our hot Universe. The main focus of the HE-group now is on the WFI instrument for Athena, the next-generation X-ray telescope, scheduled to be launched in 2034.

CAS – It is for me a real privilege to be the director of CAS. Being surrounded by young and bright scientists with different backgrounds (both scientific and cultural) is refreshing and brings excitement every day. Even during the pandemic, we maintained our motivation and completed important work, including part of the fourth and last laboratory experiment, the Trap Laboratory, which has now started to provide accurate measurements of light ion-neutral reactions of astrophysical interest. We have measured frequencies of new molecules with our (CASAC and CASJET) laboratories and detected them in space; we have also continued to study the spectroscopy of molecules embedded in ices (in CASICE), providing important input for upcoming JWST observations. CAS scientists have found the first clear evidence of a large-scale streamer of material connecting a protostellar disk to the surrounding cloud, which has challenged standard theories of star formation. Fundamental work on cosmic ray propagation in the interstellar medium has been carried out, allowing a better understanding of the penetration in dense and quiescent media of these energetic particles, which provide the only ionization and heating source. The next steps will be to start exploring interstellar dust particle analogues, exploit all the CAS laboratories, continue our successful observational campaigns using mainly IRAM telescopes and ALMA, and unveil the physical and chemical structure of star- and planet-forming regions.

I would like to finish here by congratulating female colleagues who received distinguished honors, awards and prizes in the past few years, in particular Esra Bulbul, Natascha Förster Schreiber, Elena Redaelli, Silvia Spezzano, Linda Tacconi and our external scientific member Ewine van Dishoeck. Thank You all for being an inspiration to all women in science!

Paola Caselli

Paola Caselli
Managing Director of the
Max Planck Institute for Extraterrestrial Physics

1 Research Areas and Institute Structure

1 Research Areas and Institute Structure

The Max Planck Institute for Extraterrestrial Physics (MPE, Figure 1.1) is located on the University and Research Campus in Garching, near Munich, a vibrant environment with major research institutes in physics and astrophysics. Our Institute performs basic research in astrophysics, with particular emphasis on the following science areas:

- Astrochemistry, gas and dust processes in the Interstellar Medium
- Star and planet formation
- Compact Objects
- The Galactic Centre
- Active galactic nuclei
- Galaxy formation & evolution
- Galaxy-black hole co-evolution
- Galaxy clusters & large scale structure
- Cosmology and Dark Energy

To further our research aims, we combine hardware development with observations, data analysis, laboratory and theoretical work. Our experimental work in astrophysics is driven by our scientific interests and focuses on a relatively small number of key projects, spanning a broad range of the electromagnetic spectrum from the millimeter/submm, through infrared (IR) and optical-in- frared wavelengths, to the X- and γ-ray bands (Figure 1.2).

In many cases the observations must be made from space, and MPE has a proud history and reputation as Germany's premier space astrophysics Institute. Current satellites such as XMM-Newton, Chandra, Integral, Fermi and Swift feature MPE hardware contributions, as did the Herschel mission. In 2019 our eROSITA telescope was launched, and we are developing hardware for future space facilities, in particular Euclid and Athena. Most of these projects are implemented in collaboration with the European Space Agency (ESA), the German Space Agency (DLR), or NASA.

Our more than 30 year effort to build and use instruments at large ground-based telescopes has been crowned by the 2020 Nobel prize award to Reinhard Genzel. In the near infrared and optical bands MPE has developed and exploited such instruments at the Very Large Telescopes (VLTs) of the European South ern Observatory (ESO) and their combination in the VLTI interferometer, the Large Binocular Telescope (LBT) and others. MPE leads the development of MICADO, one of the first-light instruments for ESO's Extremely Large Telescope (ELT). In the mm range we are very active users of the telescopes of the Institute for Radio Astronomy in the Millimetre Range (IRAM), located in the Alps and in Spain, and the Atacama Large Millimetre Array (ALMA), located at high altitudes in the Atacama desert in Chile. Our experimental and observational work is complemented by analytical, numerical and observation-related interpretational work and theory. Several laboratory astrophysics experiments study molecules and dust as part of the CAS group activities.

Our scientific activities are organised into four major research fields, each of which is led by one of the Directors: (1) Infrared- and Submillimeter Astronomy (IR, Prof. Reinhard Genzel), (2) Optical and Interpretative Astronomy (OpInAs, Prof. Ralf Bender), (3) High-Energy Astrophysics (HE, Prof. Kirpal Nandra), (4) The Centre for Astrochemical Studies (CAS, Prof. Paola Caselli). The main departments often host quasi-autonomous

Fig. 1.1 *MPE (front) and MPA (background) buildings in Garching. The MPE building houses the vast majority of our 350+ staff of scientists, engineers, and technical, administrative and support personnel.*

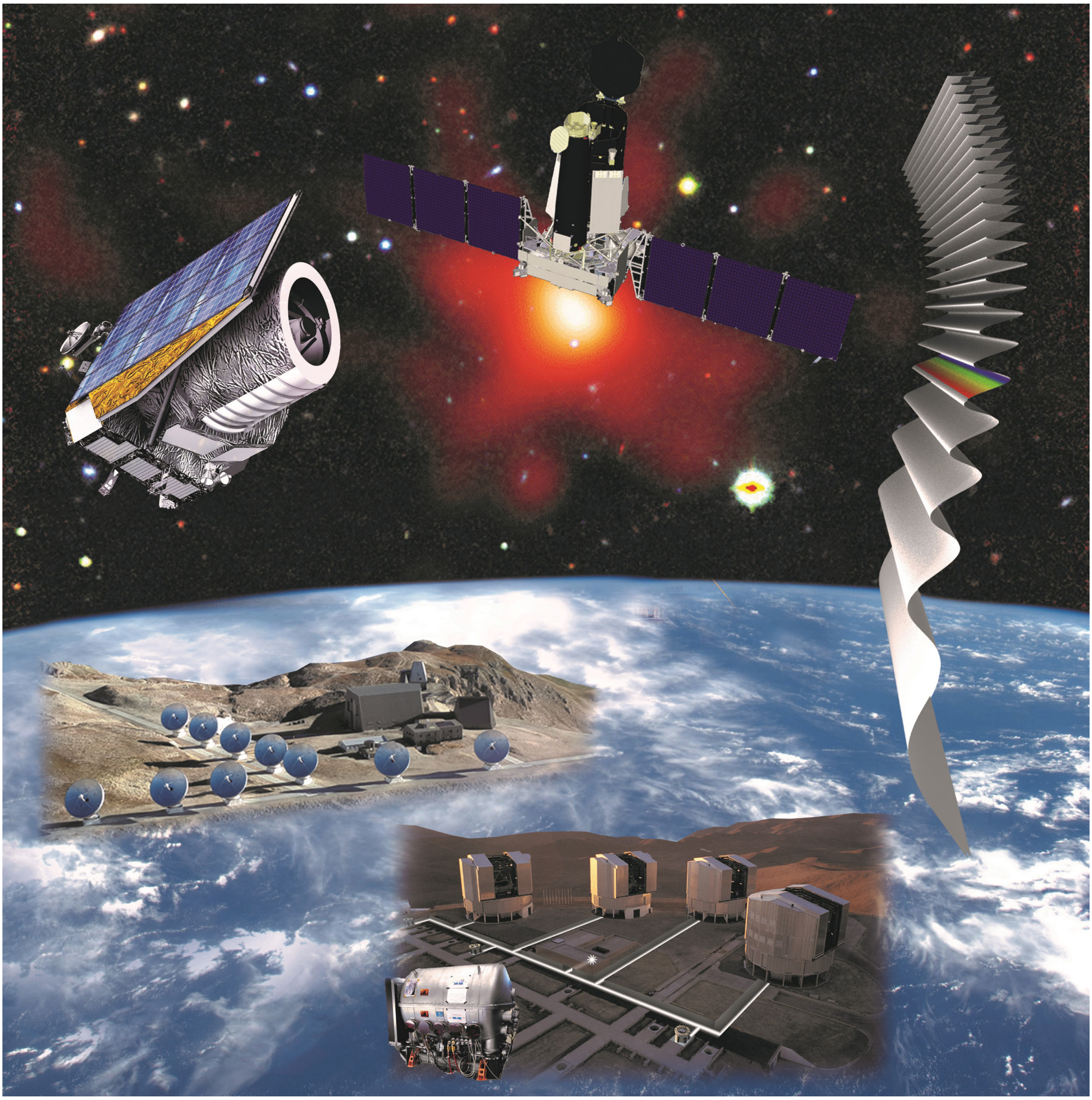

***Fig. 1.2** Scientists at MPE build and exploit state-of-the-art astronomical instruments and telescopes, both ground and space-based and across the whole span of the electromagnetic spectrum.*

research groups concentrating on particular sub-fields, supported either by internal (MPG) or external, third party funds. Close collaboration continues with the former Max Planck Fellowship holder Prof. Andreas Burkert.

While many of the major projects are driven at grouplevel, there are significant scientific synergies and collaborations in place between the different groups. The IR and OpInAs groups completed the KMOS^{3D} galaxy evolution survey. Their joint instrument development continues with MICADO for the ELT and GRAVITY+ for the VLTI interferometer. Star and planet formation processes and scaling laws from the smallest scales up to high redshift galaxies are being studied in the CAS group, the IR group, and the group of Ewine van Dishoeck. Andreas Burkert's group has a strong collaboration with the IR group, focussed on the dynamics of high redshift galaxies and gas clouds in the Galactic Center. The High Energy group and IR group have worked jointly on AGN hosts and their star forma- tion properties, in particular during the Herschel mission, and study the multi-wavelength properties and physics of Galactic Center flares. Complementary routes to explore the nature of Dark Energy are pursued by HE (eROSITA clusters) and OpInAs (Euclid weak lensing and baryonic acoustic oscillations), a synergy that extends to the collection of ancillary data and follow-up preparation for these missions. HE and OpInAs are also jointly studying AGN variability. Research programs at MPE are often organized into integrated project groups, which include scientists, postdocs, students from the main groups, and staff from the Institute's central support divisions. These central divisions play a key role in the development of our ambitious instruments and experiments and primarily consist of mechanical and electronic engineering staff and their associated workshops. We are also engaged in the development of software packages for the analysis of large amounts of data yielded by our instruments, and for instrument control. A central IT division assists in these efforts, while also supporting our computer hardware and networking infrastructure. A highly efficient administration and a technical and building services team, which also serve the neighbouring Max Planck Institute for Astrophysics and the Max Planck Computing and Data Facility, complete the team on campus in Garching. Off- campus, a key facility of the High-Energy Astrophysics Group, is the PANTER X-ray test facility located in Neuried.

The implementation of most of our experimental projects requires close cooperation with industry, both locally in the Munich area as well as all over Europe and worldwide. Our 50-year record of success in astrophysics and space research demonstrates the efficiency of such cooperations, primarily with space industry, speciality work- shops and electronics companies.

In addition to the institutional support by the Max Planck Gesellschaft, which is the most important element of our funding for personnel and projects, our research is supported by government institutions such as the German Federal Ministries for Education and Research (BMBF) and for Economy (BMWi), DLR and international organi- sation such ESO, ESA, the European Research Council and the EU. Additional financial contributions for specific projects and fellowships come from the German Science Foundation (DFG) and the Alexander von Humboldt Foundation (AvH).

Our institute is strongly engaged in vocational and aca- demic training. We cooperate closely with the major local Universities: Ludwig-Maximilians Universität (LMU) and the Technische Universität München (TUM). Staff at MPE supervise research students (Bachelor, Master and PhD), at both Munich Universities, as well as other German Universities and sometimes even further afield. Internships are offered to University, as well as high school students. The MPE Directors and many other senior staff have Professorial or Lecturer appointments at LMU, TUM and/or other Universities. The Institute hosts seminars, workshops and conferences in our own and adjacent research fields, often in cooperation with the Universities. Our very successful "International Max-Planck Research School on Astrophysics" at the LMU continues to attract many young motivated people to astrophysical research. We offer apprenticeships in our mechanical workshop.

MPE is also active in public outreach. Our aim is to communicate our work specifically and interest in astrophysics in general to the local and national press, and the public. We achieve this in part via our web pages, press releases, and personal contacts. Our scientists regularly give public talks in schools, planetaria, and other forums, and write articles in popular astronomy publications.

We are looking forward to reinvigorate after a pandemic low our in-person outreach efforts of School class and other group visits to the institute, annual participation in the national "Girls' Day" initiative, and Open House day every other year.

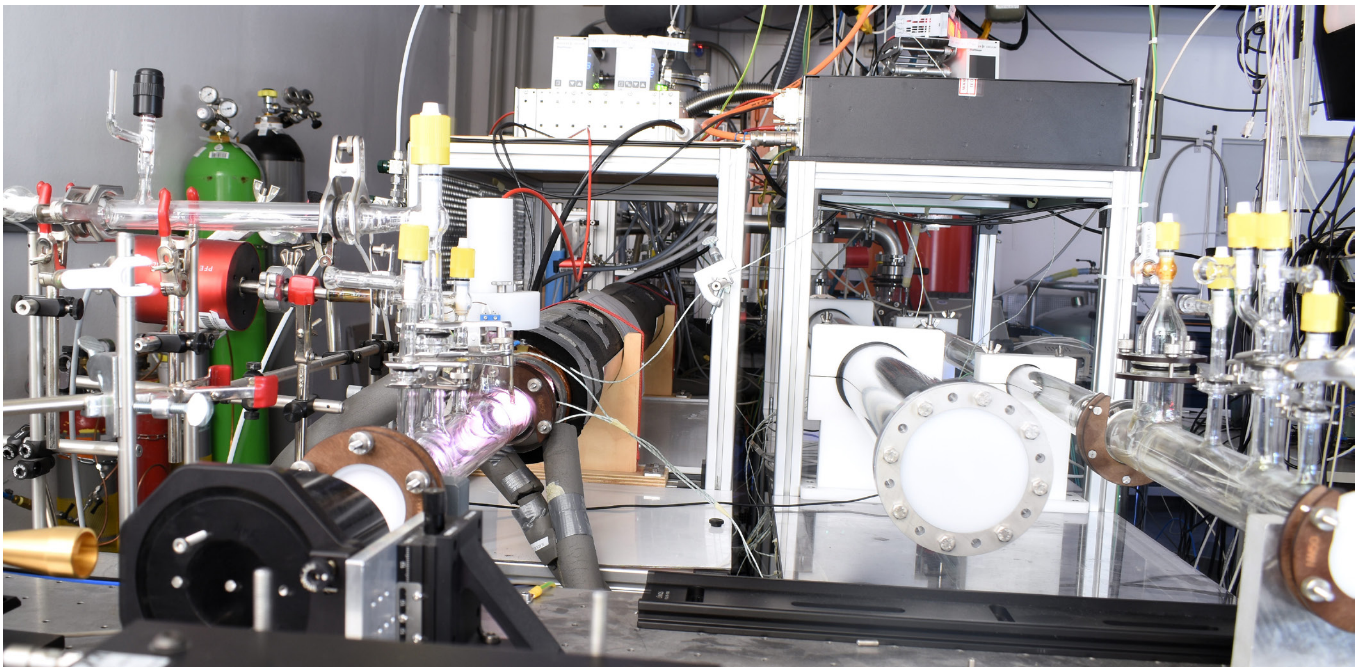

***Fig. 1.3** High resolution spectrometer CASAC for investigating the rotational spectrum of reactive species and molecular ions.*

2 Infrared and Submillimeter Astronomy

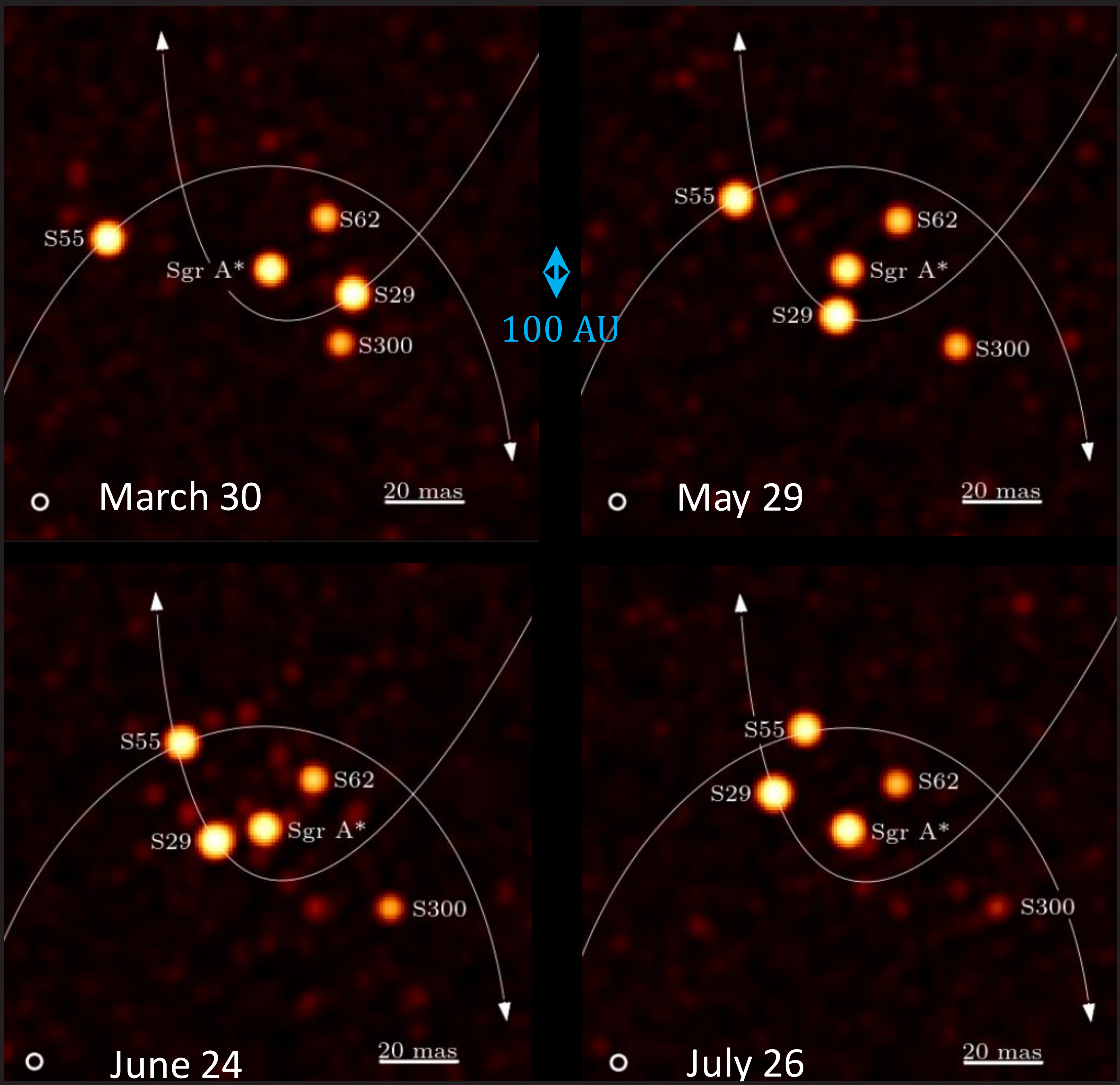

Stars in the immediate environment of the supermassive black hole in the center of our Galaxy (marked SgrA*). The images were taken with the GRAVITY instrument at the VLT interferometer during different nights in summer 2021. The rapid movement of these stars on their orbits around the supermassive black hole is obvious. GRAVITY resolves the stars that would appear blended in images taken with a single 8m-class telescope.

2. The MPE-Infrared/Submillimeter Group

2.1 Executive Summary

2.1.1 GRAVITY, Galactic Center, AGN and Exoplanets

Without doubt, the rich harvest of science from the **GRAVITY** interferometric beam combiner instrument at the VLT is at the top of the group's achievements of the last three years (Fig. 2.1.1). **GRAVITY** has provided ground-breaking results covering a broad range of astrophysical science:

- **GRAVITY** has delivered precision tests of Einstein's General Theory of Relativity (Gravitational redshift, Schwarzschild precession, relativistic gas motions and magnetic field structures near the Innermost Stable Orbit, thus providing the so far strongest experimental evidence that the compact mass in the Galactic Center (Sgr A*) is indeed a Schwarzschild-Kerr hole of 4 million times the mass of the Sun). These early results from **GRAVITY** in the Galactic Center have contributed to the 2020 Nobel Prize for Andrea Ghez and Reinhard Genzel (together with Roger Penrose, [https://www.nobelprize.org/uploads/2020/10/advanced-physicsprize2020.pdf], Nobel Committee of Physics). In his 'First Course of General Relativity (third edition, 2022)', Bernard Schutz writes "In one of the highest-precision measurements ever made in Astronomy, the **GRAVITY** team (Abuter et al. 2020) measured the peri-bothron shift of one of them, called S2". On the 2021 Tycho Brahe Medal of the European Astronomical Society (EAS) to Frank Eisenhauer, the EAS Laudatio says, "It is probably fair to say that **GRAVITY** is the most innovative optical/near-IR instrument of the last decade. After a mere 3 years of science operation, **GRAVITY** has already provided stunning results, ...";
- **GRAVITY** has revealed that the ionized gas in the broad line region in several AGN (including the famous quasar 3C 273) is comprised of an ~0.1 pc turbulent rotating disk. The **GRAVITY+** -"wide" upgrade of **GRAVITY** has demonstrated that similar measurements can now also be made in quasars at z~2;
- **GRAVITY** has mapped the hottest dust in the nearby Seyfert galaxy NGC 1068 and other type 2 AGN. **GRAVITY** finds that the hot dust emission in NGC1068 does not emanate from a thick torus, as postulated by the standard 'unified scheme' for AGN, but rather appears to be correlated with a ring/disk of about 1 parsec diameter associated with the H_2O masers;
- **GRAVITY** has provided clear evidence that the majority of the massive stars in the Orion Trapezium region are multiple;
- **GRAVITY** has yielded milliarcsecond imaging spectroscopy of the gas in ηCar and SS433 with remarkable detail and complexity;
- Finally, and perhaps least expected, **GRAVITY** has provided outstanding, high quality atmospheric spectra of young hot Jupiter exoplanets, better than previous coronographic spectroscopy, as well as the direct imagery and measurements of orbits of young exoplanets;

The key advance in **GRAVITY** is the superb sensitivity, which comes from the combination of novel low noise infrared detectors, external fringe tracking (phase-referencing), suppression of incoherent signals in single mode fibers, compact optics and high quality metrology. Together these features allow broadband imaging at K~19-20 in the Galactic Center, almost 10 magnitudes fainter than previously), as well has high precision (20-50 microarcseconds) astrometry, polarimetry and spectroscopy. The first upgrades of **GRAVITY+** are also being realized, such as off-axis fringe tracking on a bright star (**GRAVITY-wide**), dramatically improving the sky coverage for faint and distant AGN, and bringing the high-z Universe into the reach of interferometry.

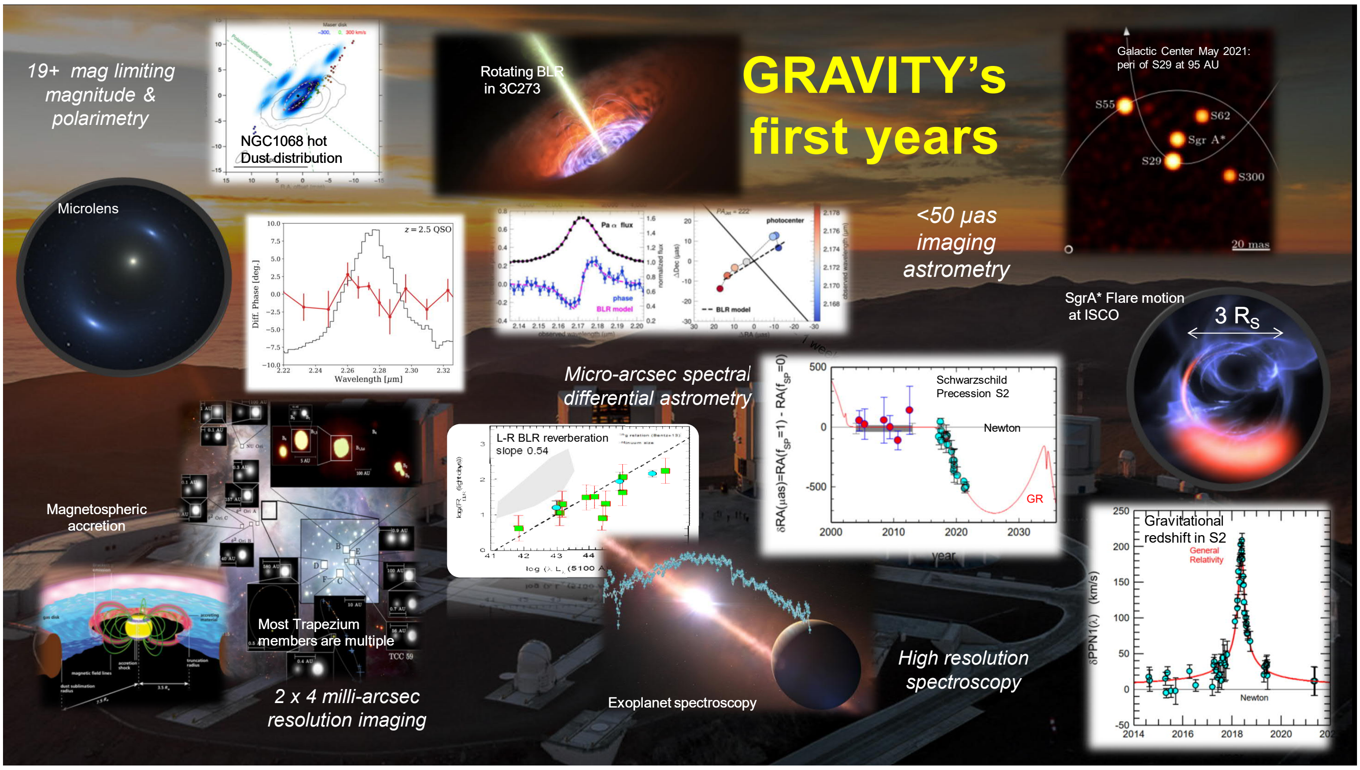

Fig. 2.1.1 Summary of the scientific results from the first four years of GRAVITY (2017-2021). This slide summarizes the remarkable depth and range of astronomy demonstrated with this new instrument, from circum-stellar gas and dust, to X-ray binaries and stellar black holes, to the detailed kinematics of dust and gas near the super-massive black hole in the Galactic Center, and then out to the circum-nuclear and broad-line regions around active galactic nuclei, including the first z>2 QSOs.

2.1.2 Galaxy Evolution

In our second main research area, the **cosmic evolution of star forming galaxies, and their-co-evolution with embedded active galactic nuclei**, we successfully completed two ground-breaking surveys: the 75 night **KMOS^{3D}@VLT** spectroscopic survey of Hα/[NII]/[SII] emission lines, and the 1500 hour **PHIBSS2@NOEMA** survey of CO in z~0.8-2.6 galaxies. These major surveys have provided quantitative ISM and kinematic properties of 750 (**KMOS^{3D}**) and 200 (**PHIBSS**) massive star forming galaxies at and after the peak of cosmic galaxy formation ten billion years ago, many with sub-galactic (a few to six kpc) resolution. **PHIBSS** has delivered statistically robust scaling relations of the relationship of (molecular) gas and star formation with redshift, stellar and baryonic mass and vertical location in the stellar mass – star formation rate plane. **KMOS^{3D}** gives a detailed census of galactic outflows driven by stars and central black holes, and provides robust gas kinematics and velocity dispersions for over half of the full sample. Our surveys confirm that massive star forming galaxies at z~0.5-2.6 were rotation dominated, but with a significant component of dispersion and radial motions. They grew mostly by 'equilibrium' gas accretion from the cosmic web. The quenching of star formation at high mass is at least in part driven by ubiquitous, nuclear black hole driven outflows. Combining **SINFONI, KMOS** and **NOEMA** data sets we have measured high quality outer disk rotation curves for ~100 z~0.6-2.6 galaxies, providing the first empirical determinations of dark matter fractions to ~2-4 R_e, during the assembly phase of massive halos. Perhaps the greatest surprise is that at the highest redshifts, where galaxies of masses $M_* \geq M_{Schechter}$ were becoming abundant, dark matter fractions at R_e of the most massive star forming galaxies are very low. This is unlike similar mass systems that formed later in the Universe, but is similar to the dark matter fractions of high mass, passive galaxies between z~0 and 1.7, which are probably descendants of the early massive star forming disks. Very substantial inflows in the ionized and molecular gas components of some of these galaxies suggest the presence of rapid inward gas transport and bulge formation, plausibly triggered by global disk instabilities, bars and gas streams. The upgraded capabilities of **NOEMA-12** (incorporated this winter) and **ERIS@VLT** (starting in summer 2022) will give us the appropriate tools for tackling the next big step, namely studying star forming galaxies at the peak of galaxy formation for the first time at the sub-Toomre scale of cloud formation and star cluster formation.

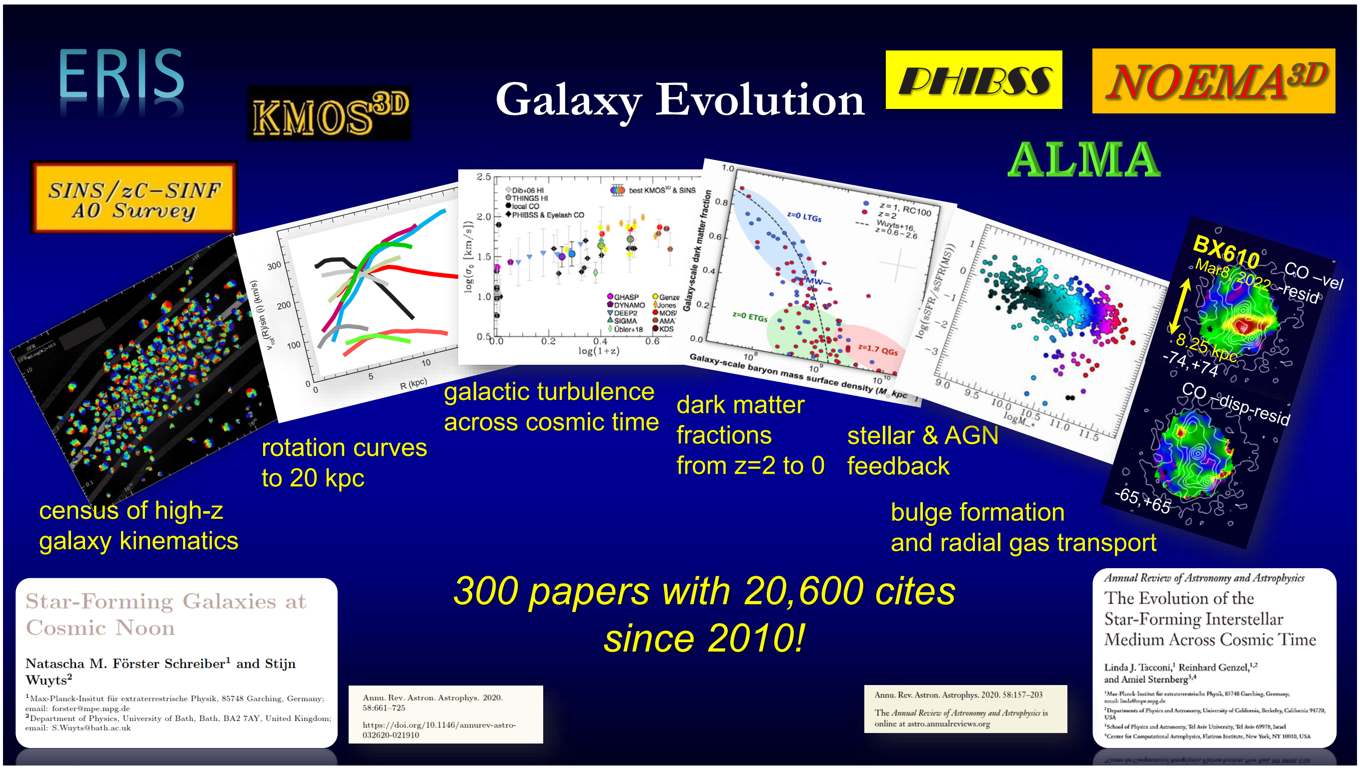

Fig. 2.1.2 Summary of the IR-group's scientific results in galaxy evolution. Using KMOS, SINFONI, NOEMA and ALMA (and with ERIS starting in summer 2022), our research focused on the sub-galactic scale physics of the baryon cycling across cosmic epochs, dark matter fractions and internal galaxy kinematics of star forming galaxies.

2.1.3 Group Philosophy and Instrumentation

Since the inception of the MPE-IR/Submm Group in 1985/86, our strategy has been to carry out group-wide research focused on selected major science themes. We have worked in Galactic and extragalactic star formation, studies of massive black holes and their environment and evolution, in the Galactic Center and in external galaxies, and in the physical properties driving galaxy evolution, from redshift ~6 to the present time.

We often work with external collaborators, national and international to enhance our main observational efforts with interpretational and theoretical work. My longstanding connection to the University of California, Berkeley, and our strong collaborations with several groups in Israel, France and the Max Planck Institutes for Astronomy (Heidelberg) and Radio Astronomy (Bonn) have played important roles.

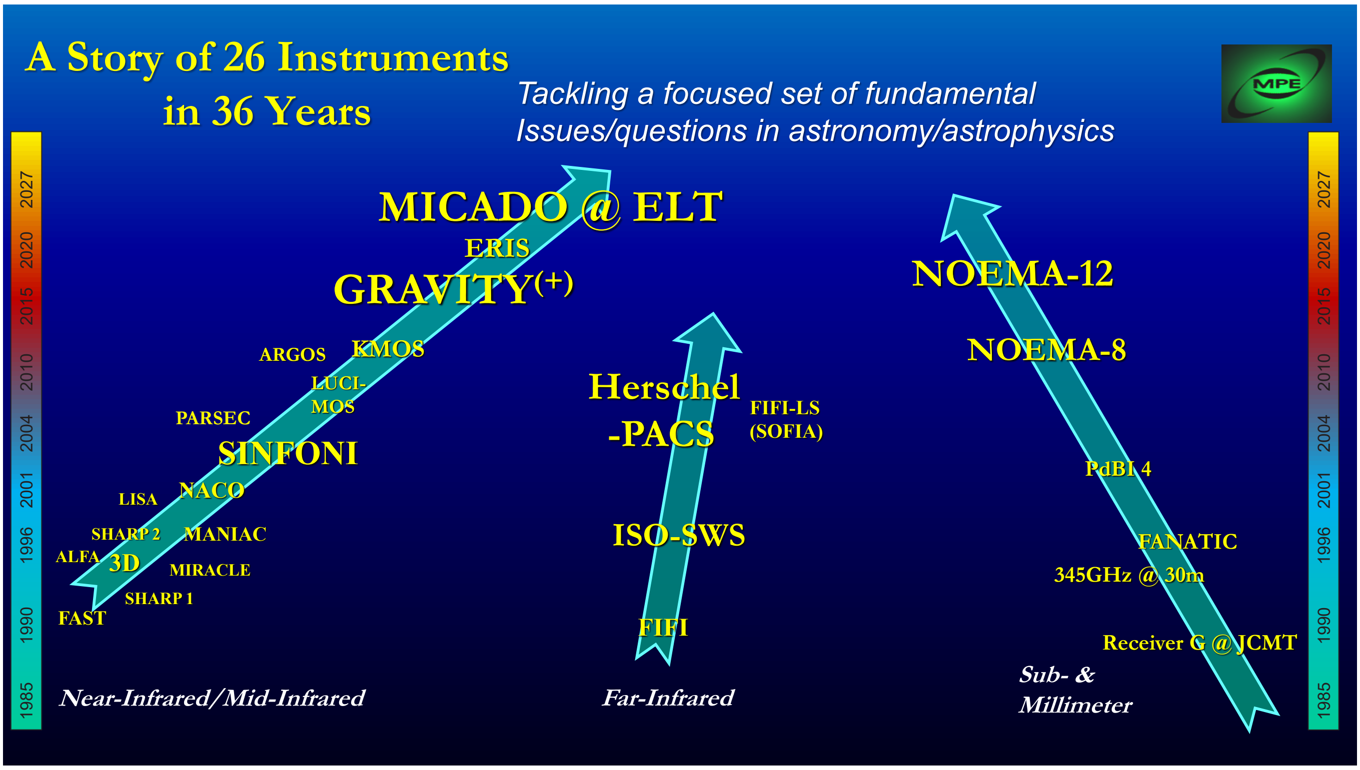

Fig. 2.1.3 *A Story of 26 Instruments in 36 Years*

To achieve our goals we develop innovative, state of the art, ground- or space-based instruments that address one or several of these themes. These instruments are built in house or in a consortium with MPE leadership (**3D, SINFONI, PACS, GRAVITY**), or with major MPE participation (**ISO-SWS, NACO, KMOS**). The left inset of Fig. 2.1.4 shows that ground-based **observations in the near-infrared are a "sweet spot" compared to other electromagnetic bands, in terms of atmospheric transparency, sensitivity and resolution**. Infrared Interferometry with **GRAVITY@VLT** is an obvious example, and perhaps the ultimate culmination of this philosophy. It took 13 years from initial design by Frank Eisenhauer and his team to **GRAVITY's** shipment to Paranal in late 2016, with the first results emerging already in 2017 and 2018 (Fig. 2.1.1). The upgraded successor of both **NACO** and **SINFONI**, called **ERIS**, is another example, which was commissioned earlier this year and is now ready for science exploitation.

2.1.3.1 The ESO ELT and MICADO

The next big step is the 39m **ELT** of ESO, currently under construction on Cerro Armazones in Chile, with an estimated time of completion of 2026/2027. MPE has the honor and privilege to be the PI-Institute (PI Ric Davies) of **MICADO**, the first instrument on the **ELT**, and likely two years before the second instrument (either **HARMONI** or **METIS**) will join. If everything goes well, **MICADO** will thus take 10 milliarcsecond near-IR images and spectroscopy at the same of better sensitivity as/than **JWST**, but 6 times higher angular resolution. This is a unique opportunity for MPE, and for ESO. **MICADO** is now in FDR and hopefully will have first light in 2027. This places the science exploitation at the end and beyond the active time of the two MPE Directors engaged in **MICADO**, Ralf Bender and myself. **We hope for the support of the younger directors, the SAB and the MPG that the Institute fulfills its commitments to ESO and MICADO even after Ralf's and my retirements, so that the IR and OPINAS teams at MPE/LMU can reap the unique science harvests we have worked for in the last 20 years.**

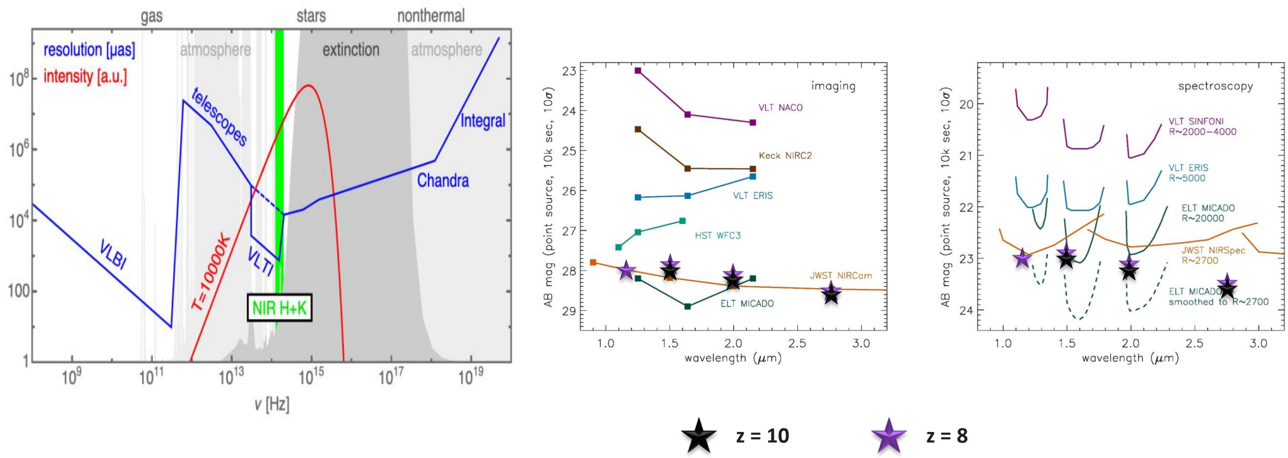

Fig. 2.1.4 Left: *Angular Resolution as a function of wavelength from radio to γ-ray bands (blue). The red curve shows a black-body thermal emitter of 10,000 K, typical for stars or ionized plasma. Light gray shading denotes those parts of the atmosphere where no ground-based observations are feasible. Dark grey shading denotes the additional effects of extinction in a dusty source. It is apparent that the near-infrared bands (J, H, K) are unique in that they naturally permit sensitive, very high angular resolution observations at 10 milliarcsecond resolution(ELT), and even 2 milliarcsecond resolution (with GRAVITY@VLT), with only modest sensitivity to dust obscuration, and ideally suited for studying dust, gas and stars in a wide range of environments and redshifts.* ***Right:*** *Imaging (left) and spectroscopic (right) sensitivities of various existing and future facilities. MICADO@ELT is en par with JWST in imaging and even superior by ~1mag for modest resolution spectroscopy. As an example, for a 10 ks exposure, MICADO can detect key lines at 10σ in z~8-10 galaxies of >$10^{9.5}$ $M_\odot$, as well as the continuum of a $10^{7.3}$ $M_\odot$ galaxy.*

Finally, since 1986 we have been deeply engaged at the Institute for Radio Astronomy in the mm-Range (**IRAM**, Grenoble). We have led the MPG-effort (since 2010) of expanding the Plateau de Bure Interferometer, now called **NOEMA**, by factors of two to five each in sensitivity, resolution and spectral bandwidth. As of this report, Antenna 12 has been incorporated into the array, and we have been able to carry out very sensitive observations in the longest configuration of the array. With its 12x15m antennas and their state-of-the-art receivers (factor 2 broader bandwidth and lower noise temperature than ALMA), two software correlators for dual-band operation and an expanded 1.6 km baseline, **NOEMA** will soon have comparable sensitivity to ALMA in the 3- and 2-mm continuum observations, and 40-60% of ALMA line sensitivity at 3, 2 and 1mm. NOEMA's future now is assured to 2034. The next generation of astrophysicists and the leadership of MPG need to decide within the next decade how to proceed beyond that time period.

We are grateful for the support and positive recommendations the Visiting Committee has given to the experimental program of the MPE-IR group over the years, which has been extremely helpful in getting additional resources from the MPG, such as recently for NOEMA, GRAVITY+ and MICADO.

2.1.4 The MPE-IR/Submm Group

Integrated over the last 3+ years the MPE-IR/Submm Group has had 63 members. This includes members who have left recently and moved onto other positions, as well recent additions, so that the group size at any given time is currently 45-50, down from 60+ a decade ago during the heydays of the **PACS@HERSCHEL** mission. It also includes a few long-term external collaborators, especially Ewine van Dishoeck (Leiden), who has led a small Galactic star formation studies group hosted by the IR-group for 15 years, as well as Andi Burkert (LMU Munich), Alvio Renzini (Padova) and Tim de Zeeuw (Leiden). Our group also has three MPG External Foreign Members, Ewine van Dishoeck (Leiden), Karl Schuster (IRAM, Grenoble) and Amiel Sternberg (Tel Aviv).

The MPE-IR/Submm Group: Composition & Diversity
Total: 63 (2019-2022: ~ 50 in a given year)

38 (60%) PhD scientists
25 (40%) female, 38 (60%) male
9 Tenured Senior Scientists/Group Leaders:
3 female, 6 male
44 European (D&E), 10 Asian (C&E), 9 American (N&S)

Fig. 2.1.5 *Images of the ~63 members of the wider MPE-IR/Submm group who were at MPE during the reporting period, and some statistics on its composition.*

Of the 63, 38 are PhD scientists, the remaining members are PhD students, master students, engineers and technicians, and general support staff. In addition to this group, we are closely interacting and often working together for a number of years with members of the central engineering groups of MPE who thus have made significant and sometimes critical contributions to our projects. Our project and science work is led by nine group/project leaders; of these, three are at the highest (W2) rank, two females and one male.

I am proud of the diversity in gender and origin of our group members. Overall 40% of the group are female. The number of European, Asian and American members is 44, 10 and 9.

2.1.5 Publications

The relevant statistical information about the refereed publications of members of the MPE-IR group is summarized in Fig. 2.1.6 below. We list the number of such publications as a function of time in the left panel, and their citation and h-value distribution in the two middle panels, as well as the names of all 12 Clarivate "Top Cited Researchers" in Space Science (of 104 worldwide) on the right panel. We only included those publications in which MPE-IR led (e.g. first or corresponding author) or co-led the work.

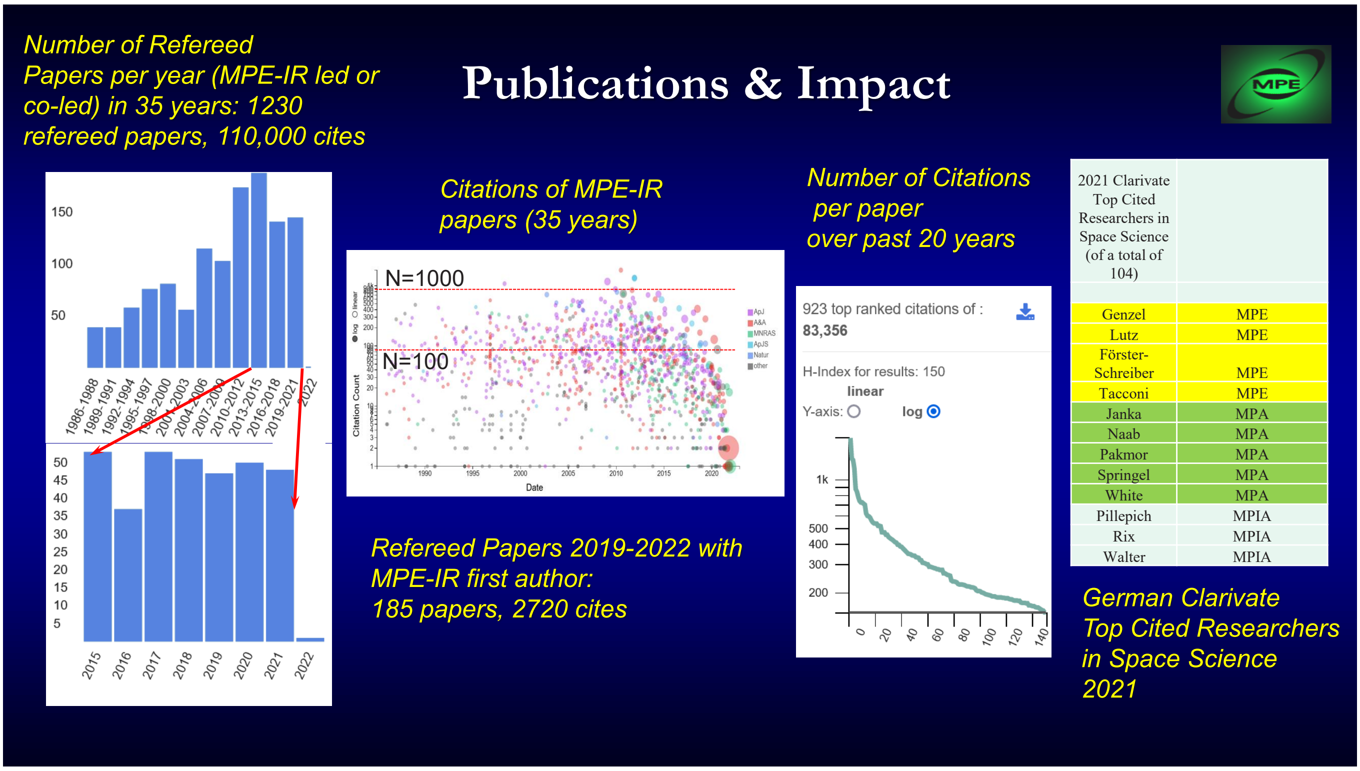

Fig. 2.1.6 Record of Publications, citations and standing of refereed papers with MPE-IR group members as leading or co-leading authors. ***Left:*** *Publication per 3 years during 1986-2022 (top), and for each year since 2015, along with citations over this period. Middle left: Citation distribution of individual papers during that period, with N=100 and 1000 citations (since publication) marked as red dotted lines. Middle right: h-index distribution of these papers (number of papers 1986-2022 with number of citations >h).* ***Right:*** *German scientists listed in 2021 as Clarivate "top cited researchers" in Space Science. There are 104 such highly cited scientists in the world, of those 12 are working in a German Institution, and of those 4 are in the MPE-IR group.*

2.1.6 Honors and Prizes

The last three years were very special to several individuals in our group, but also to our group as a team, to MPE and even the MPG. One of us received a Nobel Prize. In fact four MPG scientists garnered four Nobel Prizes in each Physics and Chemistry, two each in 2020 and 2021, a culmination that has never occurred during the last 120 years in the Max-Planck Society, or it predecessor, the Kaiser Wilhelm Society. Two MPE-IR scientists received not only one, but several high-level German or International Science Prizes. Four MPE-IR scientists were appointed as members of prestigious European Science Academies, one received a doctor honoris causa. One of us won a prestigious ERC Advanced Grant. Four of our younger scientists were recognized as an MPG Partner Group Leader, a Nobel Fellow, or in the Fundamental Breakthrough Prize in Physics for the EHT Group Award. Finally, three of us have been trusted with very senior committee Chair positions worldwide.

Fig. 2.1.7 *Summary of the Prizes, high level recognitions and honors given to MPE-IR group members during the reporting period 2019-2022.*

Reinhard Genzel

2.2 Detailed Reports

2.2.1 In Situ Surveys of Galaxy Evolution

Spatially and spectrally resolved observations of the rest-frame optical and mm line and continuum emission are very powerful for exploring galaxy evolution around the peak epoch of cosmic star formation, 5–10 billion years ago. Our major spectroscopic mapping programs at z~1–3 with the near-IR KMOS and SINFONI IFUs at ESO's Very Large Telescope (VLT) and with the IRAM NOEMA mm interferometer have established (1) the central role of molecular gas reservoirs and of internal galaxy dynamics in growing early disks and bulges, (2) the strong dominance of baryons on galactic scales at higher mass and redshift, and (3) the demographics of feedback via galactic-scale outflows. Capitalizing on the game-changing capabilities of the new VLT/ERIS IFU and the fully upgraded NOEMA, we will next be studying massive z~1–3 galaxies at the Toomre scale to pinpoint the physical drivers at play. With guaranteed time allocations of ~900h with ERIS and ~1700h with NOEMA, complemented by high-resolution ALMA and HST/JWST observations, we will build unrivalled data sets for galaxy evolution studies. These will pave the way for our major GTO program with MICADO at the Extremely Large Telescope (ELT) later this decade.

Our programs in context — cornerstones of the equilibrium growth scenario.
Lookback studies have assembled a fairly complete census of galaxies over 85% of cosmic time and established that the bulk of stars that today reside in massive ellipticals and spirals formed rapidly at redshift z~1–3 (e.g., Madau & Dickinson 1994). Most of this star formation took place in massive gas-rich, turbulent disks, which already followed tight scaling relations in their global properties, and in which dense bulges, fast growing central black holes, and galactic winds were ubiquitous (Förster Schreiber & Wuyts 2020; Tacconi et al. 2020). The existence of these scaling relations, the prevalence of disks among massive star-forming galaxies (SFGs), and the shape of the mass function indicate that since at least z~3, the growth of galaxies has been tightly regulated and largely driven by internal processes. Star formation is then quenched upon reaching $M_{*}\sim10^{11}\ M_{\odot}$ (e.g., Peng et al. 2010; Lilly et al. 2013). As highlighted in section 2.1.2, our pioneering multi-year near-IR IFU and mm interferometric surveys at z~0.5–3 provided linchpins of the *equilibrium growth* scenario of galaxy evolution. **SINS/zC-SINF** and **KMOS^{3D}** with **SINFONI** and **KMOS** at the VLT mapped the ionized gas kinematics and distribution in ~800 galaxies (Förster Schreiber et al. 2018; Wisnioski et al. 2019), and **PHIBSS1 and 2** surveyed the cold molecular gas for >200 galaxies (Tacconi et al. 2018; Freundlich et al. 2019). Key to their influential roles were (i) the coverage in parameter space, encompassing typical massive star-forming galaxies for an unbiased view of time- and population-averaged properties, and (ii) the high quality data for individual galaxies, also enabling the characterization of trends in physical properties.

The next frontier requires cloud/cluster-scale observations for studying the structure, radial inflows and outflows, and gravitational instabilities in these rapidly growing, gas-rich galaxies in the young Universe.
At z~2, the characteristic Toomre scale is ~1 kpc, which can be resolved with adaptive optics (AO) assisted observations with the new ERIS IFU at the VLT and the now fully upgraded NOEMA-12 facility. Exploiting the dramatic increase in sensitivity and resolution afforded by these instruments, our substantial GTO allocations, and our previous lower resolution IFU and mm surveys, we are undertaking the first major systematic studies of the internal physics of galaxy evolution at its peak (Fig. 2.2.1.1), with the main goals sketched out below.

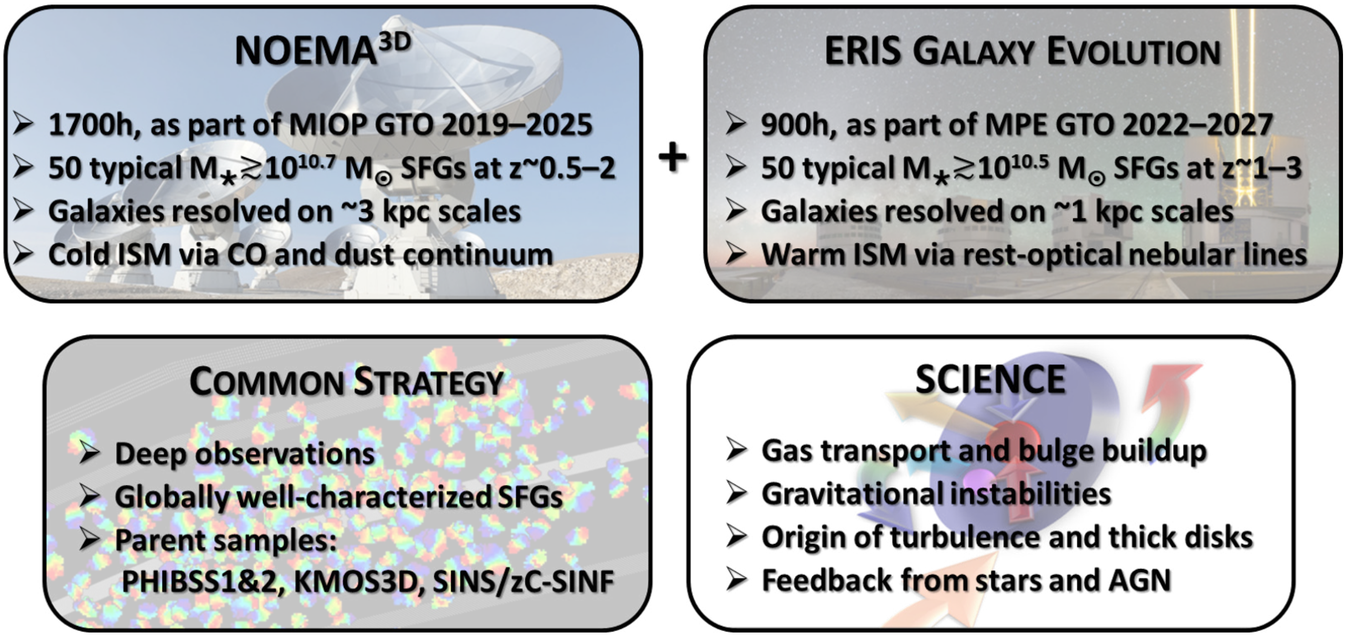

***Fig. 2.2.1.1** Our synergetic surveys with NOEMA and ERIS will each assemble very deep, high-resolution observations of ~50 massive typical SFGs around the peak epoch of star formation and galaxy growth. NOEMA^{3D} observations started in 2019, and will ramp up this year until 2025, leveraging the full capabilities afforded by the upgrade completion in 2022, including 12 antennas, full baseline extension, and dual-band receivers. The NOEMA^{3D} sample will be the first and largest of its kind – no such systematic study has been completed or approved with ALMA. The capabilities of ERIS, currently in commissioning, and the VLT Adaptive Optics Facility (AOF) bring unprecedented sensitivity to compact structure on 0.5–1 kpc scales at z≥1 with velocity resolution as fine as σ ~ 10-25 km/s, unmatched by any other near-IR IFU until the ELT and not even NIRSpec on JWST, which is limited to R≤2700. Our substantial GTO allocations with NOEMA and ERIS will uniquely allow us to address fundamental physical processes of galaxy and structure buildup.*

2.2.1.1 Gas Transport and the Buildup of Bulges

Most gas accreted by galaxies has substantial angular momentum and is deposited in their outer regions. Torques arising from global gravitational instabilities, non-axisymmetric structure, and galaxy interactions drive much of this gas inward. Efficient gas transport and angular momentum loss is expected in the turbulent gas-rich z~1–3 disks, and could lead to the rapid build-up of massive bulges. Greatly expanding on our previous rotation curve (RC) studies at z~1–3, our detailed modeling of 100 of the deepest KMOS, SINFONI, and NOEMA data sets reveals a strong anti-correlation between galaxy-scale dark matter (DM) mass fraction and baryonic mass and mass surface density. DM fractions reach $f_{DM}(<Re) \leq 0.2$ in the densest, most massive disks and preferentially at higher redshifts (Fig.2.2.1.2; Genzel et al. 2020; Price et al. 2021; Nestor et al. 2022). The analysis provides evidence for cored DM halo profiles in the denser galaxies, which may result from dynamical heating associated with rapidly inflowing material and/or feedback via outflows. The RC results strongly support bulge growth by efficient inward transport of accreted gas, a scenario we will directly test with ERIS, NOEMA, and complementary ALMA observations.

- ***Bulge mass.*** Current RC data best measure the galactic mid- and outer-disk regions. With higher spatial and spectral resolution, we will constrain the inner RC signature of a compact bulge component, in regions where the DM contribution is minimal. Estimates of bulge stellar masses from high-resolution HST imaging (e.g., Lang et al. 2014) miss the gas component, which may be large and/or whose distribution may not follow the stars (e.g., Tadaki et al. 2020; Liu et al. 2022). Dynamical measurements will weigh the total mass in the bulge, and allow us to assess the stage of bulge buildup.

- ***Gas transport.*** The kinematics of several SINS/zC-SINF/KMOS^{3D} and NOEMA^{3D} galaxies show signatures of radial motions (Price et al. 2021). We have firmly detected strong radial inflows in two galaxies with highest S/N and resolution data (Figs. 2.2.1.3 and 2.2.1.4). Theory predicts radial transport rates related to the amount of gas turbulence σ_0 and rotation velocity v_{rot}, $v_{rad} = C\,Q^{-1\ldots-3}\sigma_0^2/v_{rot}$ (with C~1–3; and Toomre Q~0.5; e.g., Dekel & Burkert 2014). This implies v_{rad}~20–40 km/s based on Hα and CO kinematic properties of massive z~1–3 disks. By studying the corresponding non-circular motions, we will determine the importance of radial transport among massive z~1–3 SFGs, and its role in early bulge growth.

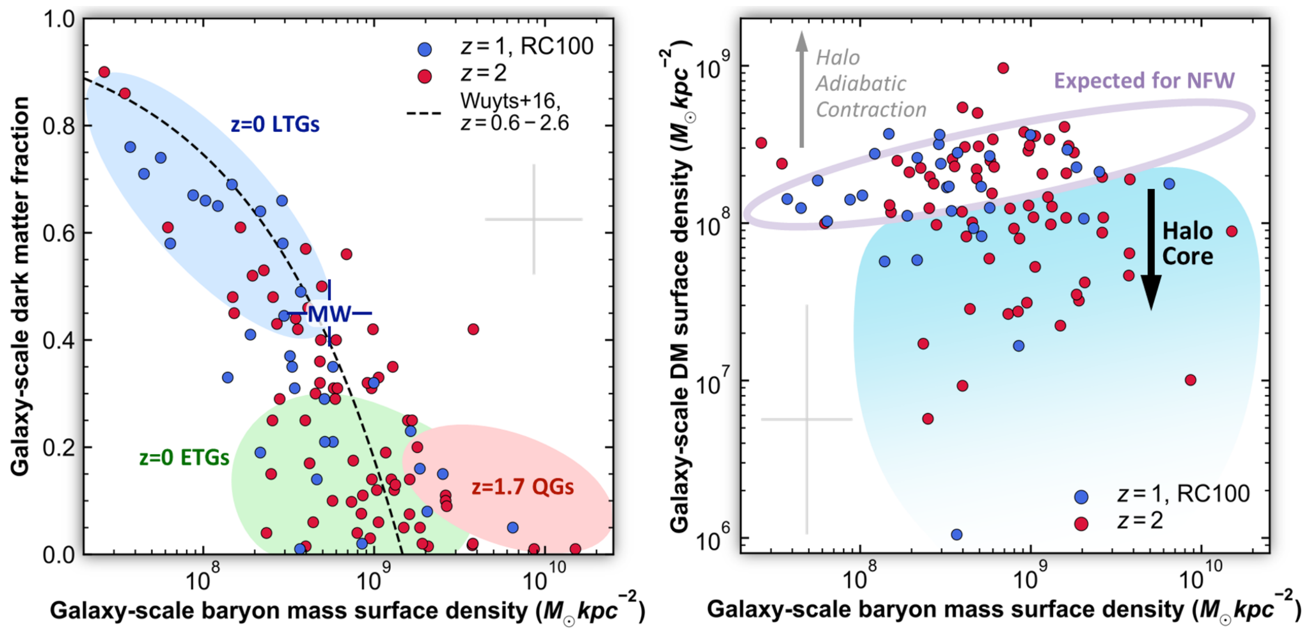

Fig. 2.2.1.2 ***Left:*** *Galaxy-scale DM mass fractions of massive z~1–3 star-forming disks anti-correlate with their baryonic mass surface densities. The denser, preferentially higher z galaxies reach very low fractions comparable to those of quiescent, early-type galaxies in the local and distant universe.* ***Right:*** *For an important fraction of star-forming disks, the low central DM fractions imply shallower inner DM halos than the commonly adopted "NFW" profiles. Such cored halos at high z may result from dynamical friction through efficient radial gas transport expected in turbulent gas-rich disks, and/or from galactic outflows largely driven by AGN in dense massive SFGs. The results were obtained from detailed, multi-component mass modeling of 100 rotation curves ("RC100") extracted to radii >10–15 kpc in the highest S/N data from our SINS/zC-SINF, KMOS^{3D}, and NOEMA^{3D} surveys.*

2.2.1.2 The Origin of Gas Turbulence and Thick Disks

Gas turbulence drives the dynamical friction/viscous timescales as well as the Toomre scale of gravitationally unstable gas-rich disks, and thus plays a crucial role in the buildup of galactic structure (e.g., Genzel et al. 2008, 2011). Star formation feedback and gas transport are both important for turbulence injection (e.g., Krumholz et al. 2018). Empirically, the driver of the elevated turbulence at z~1–3 remains elusive because global galactic scale measurements do not provide the necessary spatial detail (e.g., Übler et al. 2019). We are obtaining the missing constraints with our new programs(Fig. 2.2.1.5).

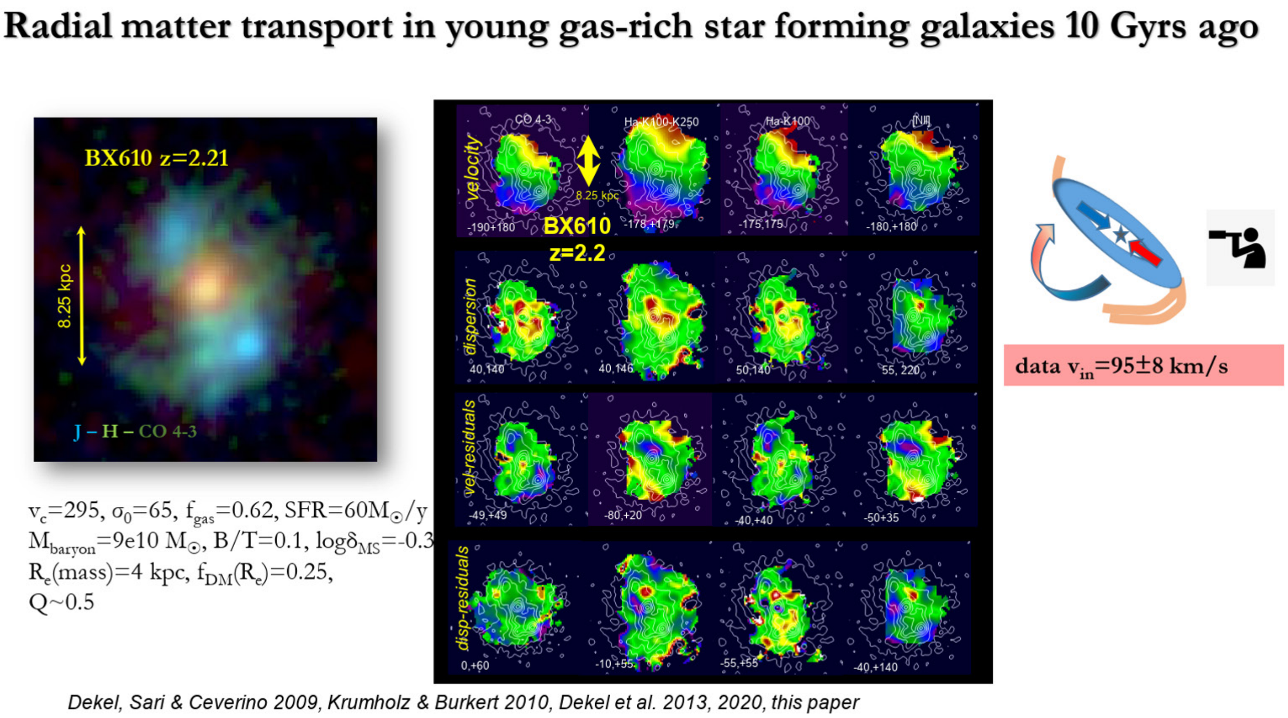

Figure 2.2.1.3 *In BX610, a typical massive star-forming galaxy at z=2.2, we detect signatures of radial inflow in both molecular and ionized gas kinematics. Deep high-resolution observations with ALMA, SINFONI+AO, and HST reveal (i) a clumpy star-forming disk in Hα emission, (ii) a small stellar bulge, clumps along a bar-like structure, and faint spiral-like features in rest-optical continuum light, and (iii) a large central concentration of molecular gas in CO(4-3) emission. Kinematic residuals from the best-fit axisymmetric bulge+disk+DM halo model are consistent with gas transport through the disk reaching de-projected velocities ~90 km/s; geometric arguments indicate the northern (top) side is tipped away from us, such that the blue-/redshifted residuals trace inward motions. BX610's bulge could rapidly grow further due to this inflow. Our 900h ERIS GTO program will resolve the inner rotation curve and quantify gas transport on the Toomre scale of ~1 kpc in a sample of at least 50 typical massive SFGs at z~1–3.*

- ***Spatial variations in turbulence.*** Theory predicts a strong scaling between σ_0 and v_{rad} (see above) and a local decoupling between σ_0 and the SFR, unlike pure feedback-driving theories. With sensitive, high-resolution maps of the gas kinematics and intrinsic SFR, we will test these dependences on the ~1 kpc scales of giant star-forming complexes. We will also determine radial variations in σ_0, important in setting the disk thickness across the galaxies, and for the role of pressure support in kinematic modeling.

- ***Molecular gas turbulence.*** The growing number of dispersion measurements from CO at z~1–3 are consistent with increasing turbulence at higher z but possibly lower than seen in H*α* (Übler et al. 2019). This suggests the molecular gas is in a dynamically colder disk than the ionized gas, as observed in local star-forming disks (e.g., Levy et al. 2018). CO kinematics from *NOEMA[3D]* are establishing the level of cold ISM turbulence of massive high-z SFGs, giving an additional handle on the driving mechanism.

2.2.1.3 Star Formation Complexes on kpc Scales and Gravitational Instabilities

Giant star-forming “clumps” are a ubiquitous feature in the rest-UV and Hα morphologies of massive z~1–3 disks (e.g., Genzel et al. 2008; Förster Schreiber et al. 2011; Wuyts et al. 2012, 2013). Their sizes match well the ~1 kpc Toomre scale for rotationally supported, turbulent gas-rich disks at z~1–3 and could thus be the imprint of recent gas fragmentation leading to star formation. Clump migration due to dynamical friction and torques may contribute to bulge formation, unless stellar feedback rapidly disperses their gas and/or strong tidal torques tear apart their stars before they reach the galaxy center (e.g., Genel et al. 2012).

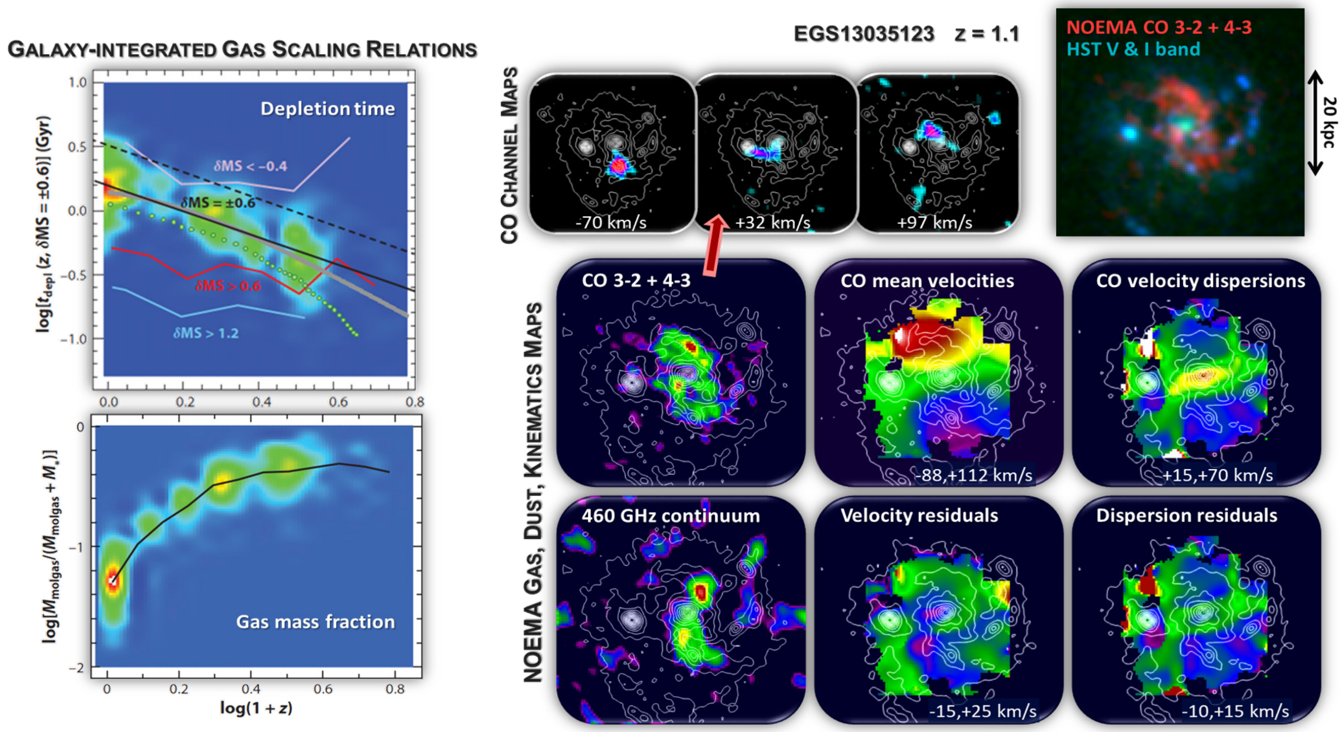

Fig. 2.2.1.4 ***Left:*** *Molecular gas scaling relations, derived from CO emission lines and dust continuum measurements of >2000 SFGs from z~0 to z~5 (Tacconi et al. 2020). The gas depletion time t_{dep} depends on redshift and offset in SFR from the “main sequence” (MS) of galaxies in stellar mass vs. SFR. The evolution of the galactic-scale t_{dep}, hence of the star formation efficiency, is modest, with a factor of ~3 change out to z~2. This contrasts with the ~20x increase in SFRs, such that typical massive MS SFGs are ~10x more gas-rich at z~2 than at z~0.* ***Right:*** *With greatly improved capabilities over its predecessor PdBI, NOEMA resolves molecular gas and dust continuum at mm wavelengths on scales down to ~3 kpc and ~10 km/s in z~1–3 SFGs. In EGS13035123, a typical massive MS SFG at z=1.1, CO is detected across the entire opticl disk; channel maps of 10 km/s illustrate the clumpy structure of the molecular gas. The CO velocity field is dominated by rotational motion, with non-circular motions of ~15-20 km/s evident in the velocity residuals. The CO velocity dispersion of ~25 km/s in the outer disk regions is typical of those measured from Hα at z~1. Our 1700h NOEMA^{3D} GTO program will resolve the molecular gas, dust, and CO kinematics on sub-galactic scales for an unprecedented sample of ~50 typical massive SFGs at z~0.5–2.*

- ***The nature of clumps.*** We will robustly identify clumps of cold gas and star formation in 3D (weeding out chance projections of unrelated structures, and brightness enhancements caused by patchy extinction). We will measure the global structure, kinematics, and dynamical mass of clumps, and push observations of the brightest clumps to the highest resolution and sensitivity to search for substructure, wherein globular clusters may be forming (Shapiro et al. 2010). Another aspect is angular momentum transport on the instability cascade below the Toomre scale. Neither in the local Universe, nor at high redshift, is there significant evidence that the gravitationally unstable, collapsing sub-Toomre scales are spun up with respect to the larger scales, suggesting that magnetic fields or other torques transport angular momentum back to large scales.
- ***The fate of clumps.*** Studies of clump lifetimes are inconclusive but rely largely on indirect inferences from colors in HST imaging (e.g., Wuyts et al. 2012), or on outflow properties in a few bright clumps or from stacking (Genzel et al. 2011; Newman et al. 2012). We will combine measurements of clump dynamical, gas, and stellar masses, intrinsic SFRs, and mass ejection, momentum, and energy rates from outflows to investigate their evolutionary stage and lifetime.

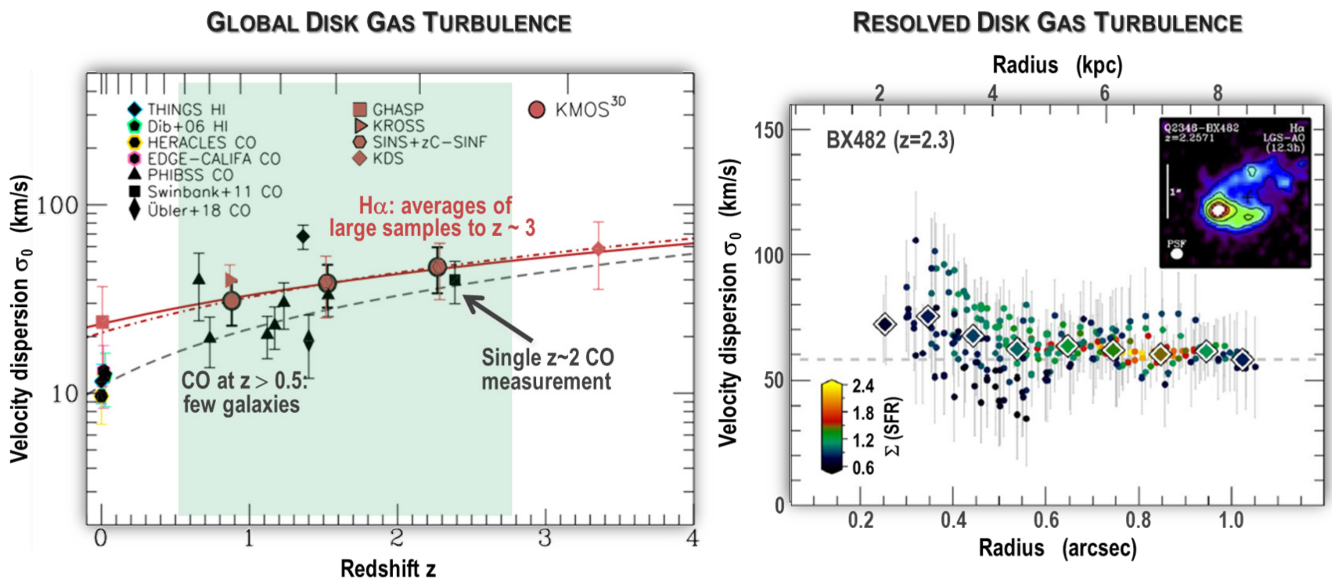

Fig. 2.2.1.5 *Elevated gas turbulence is a distinctive property of high redshift star-forming galaxies, and is tied to their elevated gas fraction in the framework of marginally stable gas-rich disks. Theoretical models and cosmological simulations indicate that gravity-driving gas transport should dominate the powering of turbulence at z > 1, whereas feedback from star formation may only dominate at lower redshift. With NOEMA^{3D} we will obtain the first census of global molecular gas disk velocity dispersions at z~0.5–2, to establish whether there is or not a significant difference between the cold and warm gas phases. With ERIS in particular, we will investigate spatial variations in gas turbulence on ~ 1 kpc scales, searching for trends with local physical properties such as radial motions and star formation surface density that will help disentangle gravity vs. feedback driving. The proof-of-concept example of BX482, one of the best resolved galaxies observed with SINFONI+AO at high S/N, supports dominant gravity driving, where the Hα velocity dispersion is fairly constant across the gas-rich disk even at the location of the bright star-forming clumps.*

2.2.1.4 Gas-Scaling Relations on Sub-Galactic Scales

Well-defined galaxy-integrated scaling relations of the molecular gas depletion time t_{dep} and gas mass fraction with redshift, star formation, and stellar mass indicate that the processes that regulate star formation on galactic scales have not changed significantly over the past ~11 Gyrs (Tacconi et al. 2020). This is also captured by the near constancy of the Schmidt-Kennicutt (SK) relation between galaxy-averaged SFR and molecular gas mass surface density. In local star-forming disks, the SK law holds down to a few 100 pc, where evolutionary effects on scales of molecular cloud complexes become important. With resolved molecular gas observations and intrinsic SFR maps from extinction-corrected Hα, cold dust continuum, and/or multi-band HST/JWST imaging, we will test whether the scaling relations and star formation efficiencies hold down to the ~kpc scales of giant gas and star-forming complexes at z~1–3.

2.2.1.5 The Role of Stellar and AGN Feedback

Galactic winds are ubiquitous at high redshift and a key element in mediating feedback from massive stars and AGN in baryon cycling models and numerical simulations (e.g., Naab & Ostriker 2017). The properties of outflows in the high-mass regime are crucial to elucidate their role in quenching star formation. Our near-IR IFU surveys established the demographics of ionized gas winds and revealed the importance of fast AGN-driven winds in massive galaxies (Förster Schreiber et al. 2019; Davies et al. 2019, 2020). We will now pin down the detailed physical properties of outflows at z~1–3.

• ***Drivers of outflows.*** The multi-line ERIS data will map the warm gas conditions and excitation (star formation, AGN, shocks), with outflows identified from broad emission tracing high velocity gas. With kpc-scale resolution, we will associate outflows with star-forming sites across galaxies and with nuclear regions, constrain their global geometry, and derive their mass and energetics. Comparing the luminosities, momenta, and energies of the power sources and outflows, we will assess the ISM coupling (energy-/momentum-conserving), and thus the impact of outflows.

• ***Role of molecular gas.*** Our studies of ionized gas outflows showed that gas is typically expelled at ~10-20% the star formation rate , even for AGN-driven winds. Ionized gas may only contribute a modest fraction of the wind mass budget, however. Our ALMA data from one massive z~2 SINS/zC-SINF galaxy showed its outflow to be ~4–5 times more massive in molecular than in ionized gas (Herrera-Camus et al. 2019). We will investigate population trends in molecular outflows with *NOEMA^{3D}*, and will link the ionized and molecular phases through ALMA follow-up of ERIS targets.

2.2.1.6 Witnessing the Early Phases of Galaxy Evolution

Theoretical and observational work indicates that chaotic accretion may drive the evolution of galaxies in the first two billion years after the Big Bang, with shorter timescales for gas transport within galaxies compared to gas depletion by star formation. Another key goal of our galaxy evolution programs is to investigate the assembly of z~1–3 massive galaxy progenitors at these early cosmic times. We are co-leading an ALMA Cycle 8 Large Program, CRISTAL, to resolve the kinematics, gas, and star formation distribution on ~1 kpc scales in 20 typical SFGs at z~4–6 using the bright [CII] 158μm line and far-IR dust continuum emission. This effort is part of the Max-Planck Partner Group between the MPE IR Group and University of Concepcíon in Chile, led by R. Herrera-Camus. We will expand our study of cold gas properties of nascent galaxies over the next few years, drawing sources from the considerably larger pool of spectroscopically confirmed targets from approved Cycle 1 JWST surveys.

2.2.1.7 Paving the Way for the Next Revolution with MICADO at the ELT

With the cutting-edge ERIS and NOEMA capabilities, our guaranteed time surveys will deliver world-unique data sets of lasting legacy for galaxy evolution studies. They will elucidate the inner workings of galaxies at the heyday of massive galaxy formation, and will set the stage for science with the next game-changer: the **first-light MICADO imager and spectrograph on the 39m ELT.** MICADO, built by a consortium led by MPE and optimized for diffraction-limited operations, will provide a 10-fold gain in angular resolution over AO at 8-10m telescopes and HST, and even a 6-fold increase compared to JWST. Together with its exquisite sensitivity and R~20000 spectroscopic capabilities, MICADO will enable studies of the structure, stellar populations, and kinematics down to ~100 pc at z≥1. Exciting prospects include characterizing globular cluster progenitors at z~2–8 and primordial galaxies out to z~10, resolving the stellar structure and kinematics of the puzzling population of compact massive quiescent galaxies at z~3–4, and weighing the first supermassive black holes at z>6 from stellar dynamics. We are already setting up the MPE/IR GTO program in anticipation of the transformative insights that MICADO will bring to our understanding of the physics of galaxy evolution.

Selected References:
Davies, R.L., et al. 2020, ApJ, 894, 28
Förster Schreiber, N.M. & Wuyts, S. 2020, ARAA, 58, 661
Genzel, R., et al. 2020, ApJ, 902, 98
Liu, D., et al. 2022, ApJ, submitted
Nestor, A., et al. 2022, ApJ, submitted
Price, S.H., et al. 2021, ApJ, 922, 14
Tacconi, L.J., Genzel, R., & Sternberg, A. 2020, ARAA, 58, 157
Tadaki, K., et al. 2020, ApJ, 901, 74
Übler, H., et al. 2019, ApJ, 880, 48
Wisnioski, E.S., et al. 2019, ApJ, 886, 124

Natascha M. Förster Schreiber

Linda J. Tacconi

(MPE collaborators: R. Genzel, S.H. Price, A. Burkert, R.I. Davies, R.L. Davies, R. Herrera-Camus, L. Lee, M.M. Lee, D. Liu, D. Lutz, T.T. Shimizu, A. Sternberg, E. Sturm, H. Übler)

2.2.2 High Resolution Studies of Accreting Massive Black Holes (AGN)

Many open questions concerning AGN and their environment are best addressed by our tools of high spatial and spectral resolution NIR and mm spectrometry and interferometry. Key aspects of our research in this area are the physics of the broad-line region (BLR), structure of the inner hot dust, SMBH mass measurements, and the feeding of and energetic feedback from AGNs. Our ESO/VLTI Large Program with GRAVITY in particular has led us to major recent breakthroughs. We have spatially resolved the BLR for three different nearby AGN, further reinforcing the rotating disk model, providing direct measurements of their SMBH masses, and testing the BLR radius-luminosity (R-L) scaling relation. We have measured the hot dust sizes for eight AGN and fully imaged the hot dust structure for two AGN. Our sample of dust sizes also tests the hot dust R-L scaling relation where we are beginning to see evidence for luminosity dependent deviations from the expected relation. With GRAVITY+, we will be able to vastly expand to both larger samples and higher redshifts with the ultimate goal of tracing black hole growth and galaxy coevolution through cosmic time.

2.2.2.1 The GRAVITY AGN Large Programme

At the time of the last Visiting Committee, we had been granted by ESO an open time Large Programme (17 nights over 4 semesters) to observe 11 nearby AGN with VLTI/GRAVITY that span four orders of magnitude in luminosity. GRAVITY, the near-infrared beam combiner built by an international consortium led by the IR Group, provides images with 3 mas angular resolution as well as 10 µas astrometric accuracy. This exquisite performance **opened the door to resolving the innermost regions of the brightest AGN: the BLR and surrounding hot dust.** Through our Large Programme we aimed to constrain questions like: How reliable are reverberation mapping (RM) based BLR sizes and black hole masses? Are BLR kinematics always dominated by ordered rotation? What is the size and shape of the obscuring structure? We further aimed to establish a new, GRAVITY-based R-L relation to form the basis for more robust black hole mass measurements in large samples in both the local and distant Universe.

The First Spatially Resolved BLR
Broad lines in AGN spectra can be used to measure the mass of the SMBH (assuming that the motions are due to gravity), and to constrain accretion and outflow models. However, because of its small radius it has been impossible to resolve the structure of the BLR directly, which introduces uncertainties in derived SMBH mass measurements. Studies of the BLR structure have relied mostly on reverberation mapping (RM) which use the time variability observed in the AGN continuum emission and the subsequent response of the gas in the BLR. These RM programs established a size-luminosity relation ($R_{BLR} \sim L^{\alpha}$) which allows black hole mass estimates from a single AGN spectrum. This is the only available method for measuring black hole masses in large surveys and out to high redshift and plays a key role in our understanding of black hole growth over cosmic time. However, recent velocity-resolved RM studies are starting to indicate a variety of BLR geometries and a previously unknown dependence on the Eddington ratio.

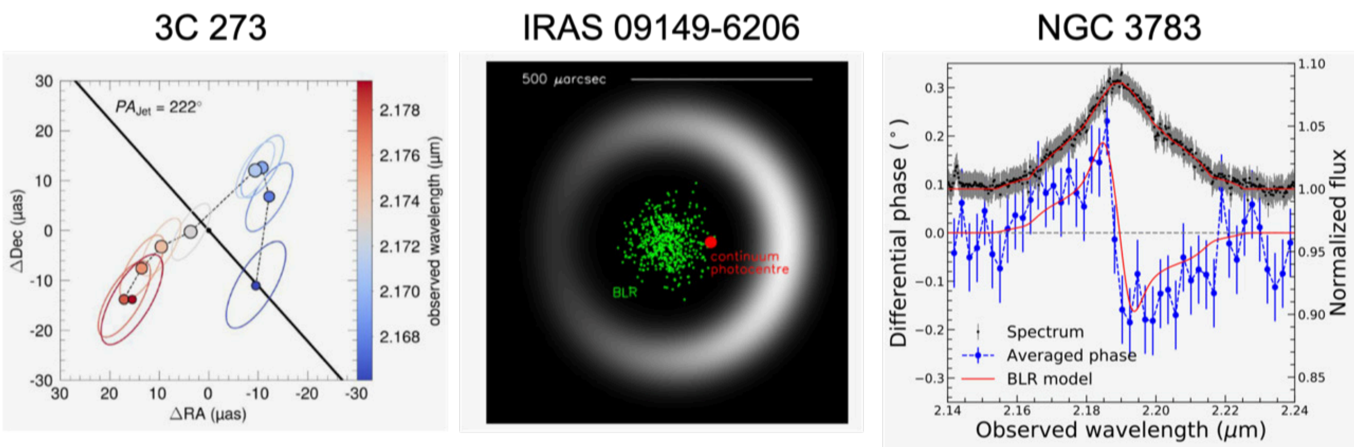

Fig.2.2.2.1 Left: *Observed velocity resolved photocenters for 3C 273 indicating a kinematic axis nearly perpendicular to the radio jet axis (black line).* ***Middle:*** *Cartoon illustrating a possible cause for the observed offset between the near-infrared continuum photocentre and the BLR for IRAS 09149-6206.* ***Right:*** *Observed BLR differential phase signal for NGC 3783 (blue points) together with the best-fit model (red lines) and emission line flux profile (black points)*

Spectro-astrometry with GRAVITY provides a new, direct probe of the BLR spatial and velocity structure, which can independently test and break degeneracies in these studies. This technique measures the flux weighted spatial offset from the continuum of each velocity channel across an emission line. Combining the six independent VLTI baselines, we can then map the velocity structure of the BLR and kinematically model it to measure both the BLR radius and ultimately the SMBH mass. In the previous Visiting Committee, we highlighted the power of spectro-astrometry by spatially resolving a velocity gradient across the BLR of the quasar 3C 273 (Gravity Collaboration et al. 2018). The gradient revealed rotation perpendicular to the jet (see left panel of Fig. 2.2.2.1), and was consistent with line emission from a thick disc of gravitationally bound material around a black hole of 3 x 10^8 solar masses. We measured a disc radius of 46 µas (0.12 pc, or 150 light-days) which was consistent with the RM measured size of 100-400 light-days.

The Large Programme has now yielded two further published spectro-astrometric BLR measurements for IRAS 09149−6206 and NGC 3783. Armed with an improved data reduction that came from this study, we significantly detected the BLR differential phase signal across the Brγ line. **Surprisingly, the signal primarily represented a systematic offset of ~120 µas (0.14 pc) between the BLR and the centroid of the hot dust distribution** traced by the 2.3 µm continuum (see middle panel of Fig. 2.2.2.1). This offset is well within the dust sublimation region, which matches the measured ~300 µas (0.35 pc) radius of the continuum and can be explained by an asymmetric hot dust continuum such that the photocenter of the continuum is shifted towards the brightest side of the dust structure. Including this "continuum phase" in our BLR model, we could then measure a BLR size of 65 µas (0.075 pc) and SMBH mass of 1 x 10^8 solar masses (Gravity Collaboration et al. 2020a).

In NGC 3783, a galaxy only ~40 Mpc away that hosts a bright type 1 AGN, we again were able to significantly detect the BLR differential phase signal (see right panel of Fig. 2.2.2.1). For this AGN, we measure a BLR size of 71 µas (0.013 pc) and SMBH mass of 5 x 10^7 solar masses. **Interestingly for this AGN, we measure a physical BLR size almost a factor of 2 larger than the one measured by RM** and found this is due to a radial distribution of clouds that peaks in the inner regions but is significantly extended to large radii. This creates a discrepancy between RM measurements, which are variability-weighted and thus biased towards the inner regions, and interferometric measurements, which are flux-weighted and more sensitive to outer radii (Gravity Collaboration et al. 2021a).

With these three published BLR size measurements, we have begun constructing our own GRAVITY-based R-L relation. The left panel of Fig. 2.2.2.2 shows as red stars the location of our measurements compared to the RM based measurements and relation (black and gray points with black dashed line). Our measurements so far are largely in agreement with RM and further we begin to see the recently observed Eddington ratio dependency that leads to smaller sizes for AGN accreting near the Eddington limit (e.g. 3C 273). From the Large Programme we have BLR data for another 4 more AGN that are under analysis and will be used to complete our GRAVITY-based R-L relation.

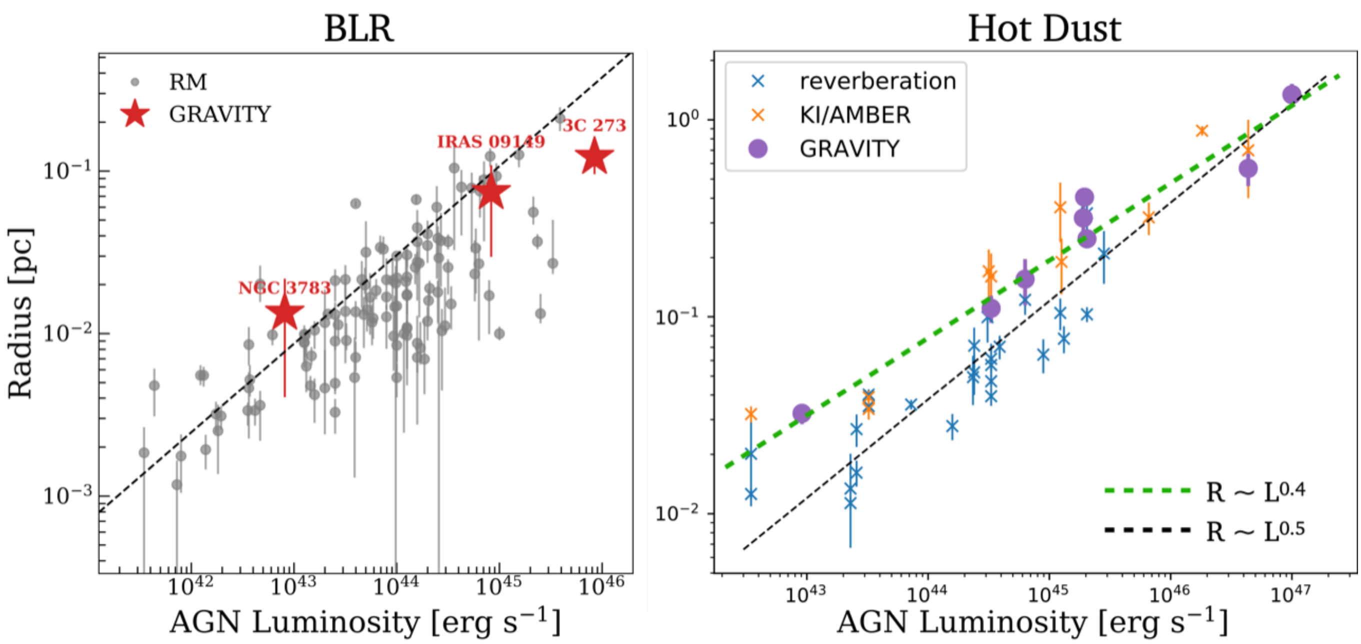

Fig. 2.2.2.2 Left: *BLR R-L relation with our new GRAVITY measurements plotted with RM data points (black points) and RM relation (black dashed line).* ***Right:*** *Hot dust R-L relation with our new GRAVITY measurements. Our interferometric hot dust sizes match previous Keck interferometer sizes. They seem to follow a flatter relationship than $R \propto L^{0.5}$ (which would be the expected relationship if hot dust radiation peaks near the dust sublimation radius).*

Imaging and Sizing up the Innermost Hot Dust

Another long-standing issue of AGN models is the size and structure of the obscuring, dust-emitting region: is it a torus or disk, inflowing or outflowing? The near and mid infrared luminosity associated with AGN originates in dust surrounding the AGN and heated by it. However, like the BLR, circum-nuclear dust in AGNs is unresolved in single telescope images. In the past decade, infrared interferometry has begun to shed light on the physical structure of this component. Detailed results from Circinus and NGC 1068 show evidence for an inner disk, but have also revealed dust in the polar regions indicative of outflow (López-Gonzaga et al. 2016). The presence of multiple components could have a severe impact on dust-RM methods that assume a torus origin. The NIR is thought to trace hot dust just beyond the sublimation limit at the inner edge of the torus. Measuring the emission size can therefore test the assumptions on which dust-RM methods are based. **GRAVITY observations provide the first resolved view of the shape and structure of the hot dust emission region whose size and orientation can be compared directly with that of the BLR.** With its enhanced sensitivity compared to previous NIR interferometers, it also allowed for more accurate size measurements for a larger sample of AGN. Therefore, through our Large Programme we have been able to both image the hot dust structure of individual AGN and measure sizes for the whole sample.

The data set of NGC 1068, the prototypical type 2 AGN, permitted us for the first time to image the nuclear hot dust in the sublimation region of an AGN, i.e. the inner edge of the putative torus (Gravity Collaboration et al. 2020b, left panel of Fig. 2.2.2.3). Surprisingly, we found a **thin, clumpy, ring-like structure** of emission with a radius r = 0.24 pc and an inclination i = 70 deg, which we associate with the dust sublimation region. **The observed morphology is inconsistent with the expected signatures of a geometrically and optically thick torus.** Instead, the infrared emission shows a striking resemblance to the 22 GHz maser disc, which suggests they share a common region of origin. The dust structure and photometry are consistent with a simple model of hot dust at T ~ 1500 K that is behind A_K ~ 5.5 (A_V ≈ 90) mag of foreground extinction. This amount of screen extinction could be provided by the dense and turbulent molecular gas distribution observed (e.g. by ALMA) on scales of 1-10 pc.

NGC 3783 is the second object where we have exceptionally resolved the hot dust. The non-zero closure phases allowed us to reconstruct an interferometric image of the dust sublimation region using the exact same dataset as the one to resolve the BLR. The reconstructed image of the hot dust (see right panel of Fig. 2.2.2.3) reveals a faint (5% of the total flux) offset cloud, which we interpret as an accreting or outflowing cloud heated by the central AGN.

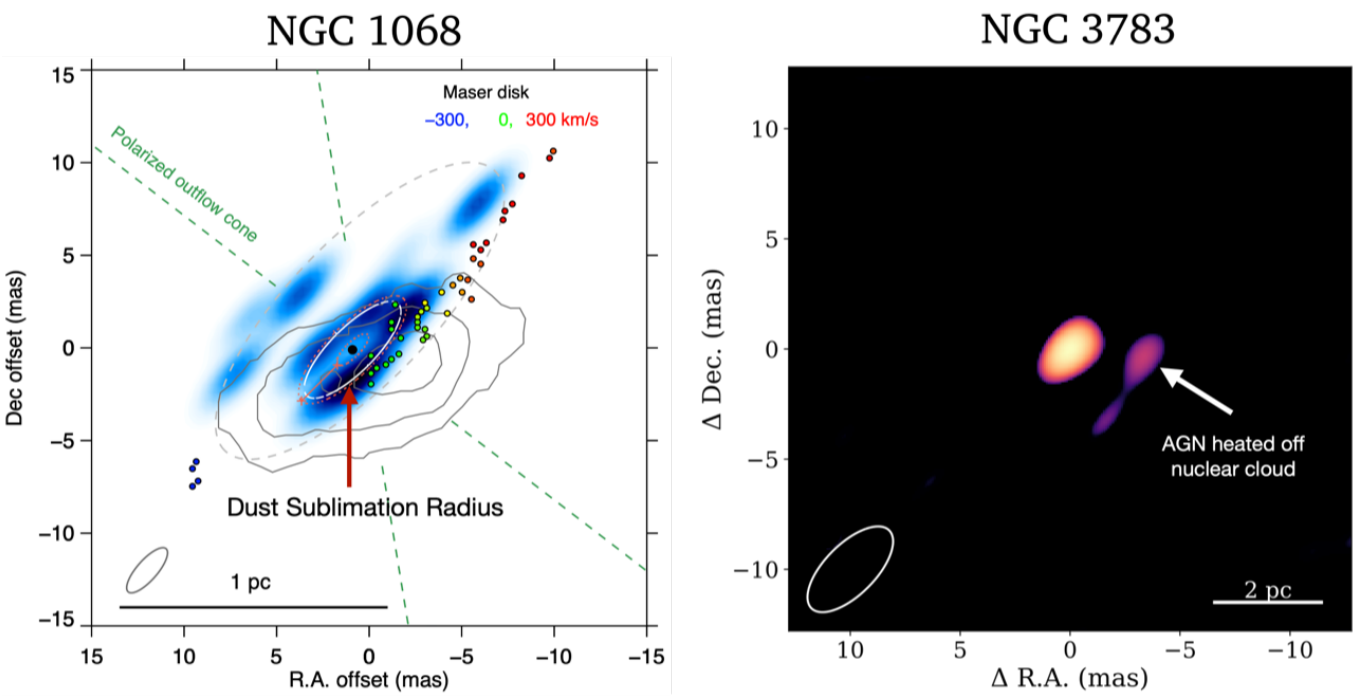

Fig. 2.2.2.3 Left: *Reconstructed hot dust image of NGC 1068. GRAVITY observes primarily a thin clumpy ring at the expected dust sublimation radius given NGC 1068's AGN luminosity. The bright near side of the ring is cospatial to the megamaser disc indicating a common origin.* ***Right:*** *Reconstructed hot dust continuum image of NGC 3783 showcasing the offset cloud 0.6 pc away from the central hot dust at the dust sublimation radius.*

Even in cases where the hot dust cannot be directly resolved, the interferometric technique allows us to derive at least the size of the emitting region. We now have tantalizing results about the size of the hot dust structure in 8 AGN, which suggest that **the 2.2 μm continuum does not follow the expected size-luminosity relation:** continuum reverberation experiments find correlated variability between the optical and near-infrared (NIR) emission with a lag that is consistent with reprocessing. The inferred emission radius scales with luminosity as $R \propto L^{0.5}$ as expected if hot dust radiation peaks near the dust sublimation radius. Using our robust size measurements, the bottom middle panel of Fig. 2.2.2.2 shows that the data for 8 AGN yield a rather flatter $R \propto L^{0.40}$ relation at slightly over 2σ significance. There are two important conclusions: (i) the scatter between objects seems to be larger than the uncertainties, potentially indicating real physical differences between objects, and (ii) the sizes derived are larger for lower luminosity AGN, suggesting a systematic effect in terms of dust emissivity or perhaps related to Eddington ratio, or even an inclination bias at high luminosity. At the same time, new results from reverberation mapping also show that the relation is flatter than previously thought (at about 2σ significance). We have recently been awarded more time on GRAVITY to measure the dust sizes for a further 16 AGN which we will use to fill out our dust R-L relation. All of this data will allow us to explore possible scenarios for the underlying physical cause of the flattening using state-of-the-art models of dust structures around AGN.

Geometric Distances to AGN

Combined spectro-astrometry and RM and geometric distances: While our previous focus with spectro-astrometry (SA) was to use it as a test of RM, we have now also developed the methods necessary for a combined SA+RM analysis of the BLR structure. The joint analysis provides new opportunities to study the BLR structure, with improved accuracies, in particular of BH masses. It is also a promising new and direct method to measure the geometric distance to AGNs. The distances to even nearby AGNs are remarkably uncertain: the measured redshift is strongly affected by peculiar motions, but other methods often do not agree. Therefore, distance becomes the dominant source of error in estimating properties such as size, luminosity, and mass. **By combining the angular size from SA with the linear size from RM, geometric distances can be derived directly via simple trigonometry.** The spectro-astrometry+RM method provides as good of a distance measurement for NGC 3783 (GRAVITY Collaboration et al. 2021b) as other more standard methods such as the Tully-Fisher relation. With an increased sample of AGN in the future with GRAVITY+, it could even be possible to apply this method to independently measure the Hubble Constant.

2.2.2.2 GRAVITY+: Evolution of Supermassive Black Holes and their Host Galaxies over Cosmic Time

As part of GRAVITY+'s Phase A study, we developed the AGN science case to demonstrate the great potential of near-infrared interferometry in the study of supermassive black holes and their immediate environments. Observational and theoretical work indicate that SMBHs play an important role in the early evolution of their host galaxies. The M_{BH}-sigma relation over six orders of magnitudes (Ferrarese et al. 2006), the similar integrated star formation rate and BH growth over cosmic time (Madau & Dickinson 2014) as well as the correlation of star formation history and BH mass seen in individual galaxies (Martin-Navarro et al. 2018) are likely the result of AGN regulated gas feeding and quenching. In order to bring the most active phase of BH growth at redshift 1-3 into reach and to be able to probe the coevolution of high redshift galaxies and their SMBHs, GRAVITY+ with its significant upgrades to both sensitivity and sky coverage is needed.

In particular, high redshift AGN science will be made possible through GRAVITY+'s (1) upgraded adaptive optics (AO) system with state-of-the-art wavefront sensors and laser guide stars (LGS) on all UTs, (2) wide angle off-axis fringe tracking (FT) on guide stars up to 30" away from the science target, and (3) a fainter fringe tracking magnitude limit. The new AO system will significantly improve the Strehl ratio on faint targets, which increases the flux injection into GRAVITY's fibers. This will have a multiplicative effect because not only the science flux but also the fringe tracking accuracy will be improved thus reducing coherence loss. Wide angle off-axis fringe tracking is necessary to increase the probability of finding a suitable FT guide star that enables long integration times needed for the faint targets. Also increasing this probability will be the fainter FT magnitude limit which is expected to be increased from m_K~10.5 to m_K~13 and largely made possible through the upgraded AO system. Fig. 2.2.2.4 shows selected AGN with suitable guide stars of different redshifts and their expected differential phase signal. With the upgrades of GRAVITY+, we will be able to obtain accurate BH masses for a thousand local AGN, a thousand AGN at z~0.6-1.3, 700 AGN at z~2-2.8, and ~100 AGN at z~3 effectively covering the most active phase of black hole growth.

With this large sample of black hole masses up to high redshift, a key planned project would be to trace redshift evolution of the local MBH scaling relations (i.e. M_{BH}-sigma, M_{BH}-M_{bulge}, M_{BH}-$M_{stellar}$). These scaling relations form the basis of SMBH-galaxy co-evolution yet little is known how they evolved over cosmic time. The difficulty is measuring SMBH masses at high redshift where RM is inefficient. Single epoch masses are calibrated based on the local scaling relations and so do not provide an independent measure of the scaling relation evolution. Importantly, the exact evolution of these relations can greatly distinguish between competing models of AGN feedback. Large scale cosmological simulations can match the z=0 galaxy and SMBH population but differ significantly in the evolution of the scaling relations due to different AGN feedback prescriptions (Habouzit et al. 2020). Synergy between GRAVITY+ measured SMBH masses and ELT (such as MICADO) measured host galaxy properties would therefore result in a large leap in understanding SMBH-galaxy co-evolution. In December 2021, the first phase of GRAVITY+ was installed which allowed for wide angle off-axis fringe tracking. As part of commissioning, we observed with GRAVITY for the first time, a z=2.3 QSO (see inset in Fig. 2.2.2.4), and detected fringes across the Hα line, and recently measured differential phases for a z~2.5 QSO (Fig. 2.2.6.4). These are remarkable achievements and give an exciting glimpse into what will be possible with the full power of GRAVITY+.

AGN science with GRAVITY+ is certainly not limited to this one project. We expect GRAVITY+ to make significant contributions to other sub-fields including detecting SMBH binaries, resolving the dust continuum and emission line-emitting gas around tidal disruption events, probing super-Eddington accretion, and further understanding in detail the BLR structure and kinematics over a large range of luminosity.

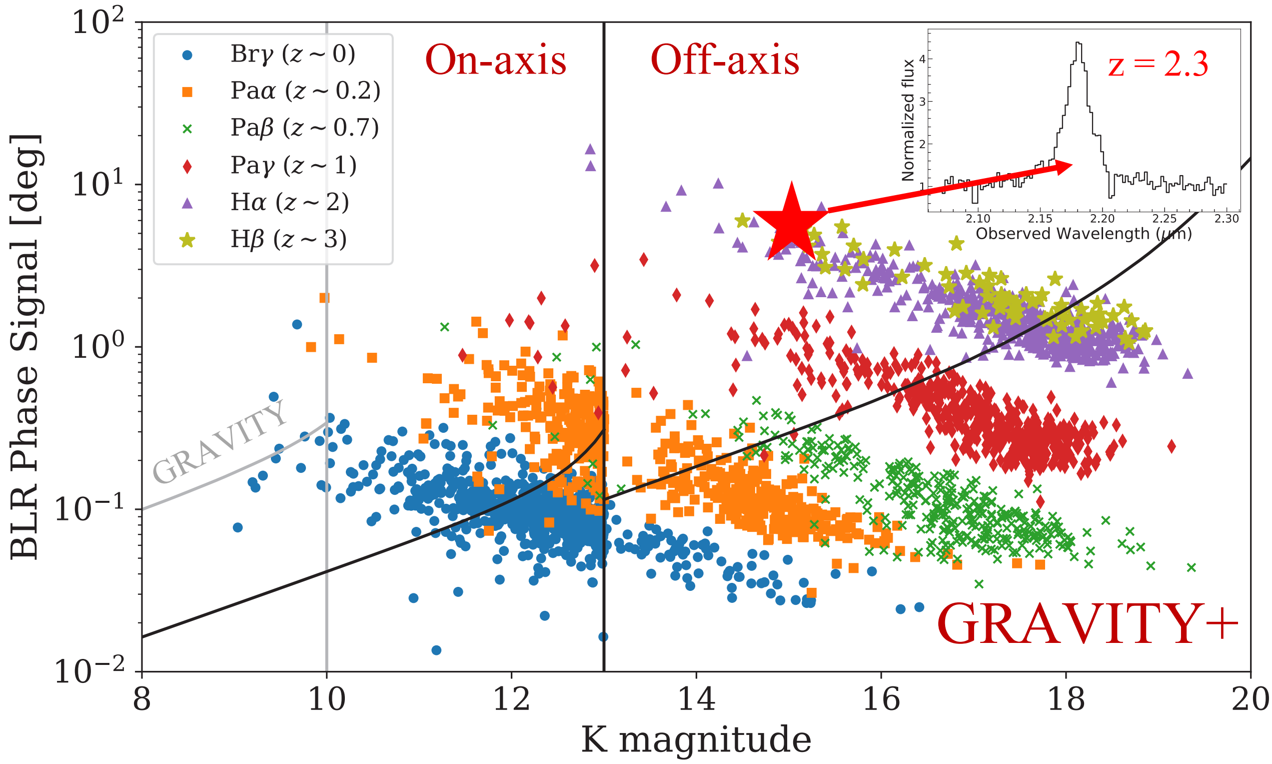

Fig.2.2.2.4 *Extrapolated astrometric phase signal of type I AGNs and QSOs at different redshifts with a suitable guide star within 30”. The colours and symbols indicate the redshift and the BLR line shifted into the observable K-band. The grey lines indicate the current GRAVITY detection limit for a 10h exposure. The black lines show the detection limit for GRAVITY+. Left of the vertical black line indicates on-axis observations without the need for a guide star while targets to the right indicate off-axis observations. Thousands of AGN up to redshift 3.8 will be in reach with GRAVITY+. The large red star and inset figure show the first observation of a z=2.3 QSO with wide angle off-axis fringe tracking.*

Selected References:

Ferrarese et al. 2006, ApJ, 644, L21
GRAVITY Collaboration et al. 2018, Nature, 563, 657
GRAVITY Collaboration et al. 2020a, A&A, 643, A154
GRAVITY Collaboration et al. 2020, A&A, 634, A1
GRAVITY Collaboration et al. 2020, A&A, 635, A92
GRAVITY Collaboration et al. 2021, A&A, 648, A117
GRAVITY Collaboration et al. 2021, A&A, 654, A85
Habouzit et al. 2021, MNRAS, 503, 1940
López-Gonzaga et al. 2016, A&A, 591, 47L
Madau & Dickinson 2014, ARAA, 52, 415
Martin-Navarro et al. 2018, Nature, 553, 307

Eckhard Sturm

Taro Shimizu

(Other team members currently at MPE include R. Davies, F. Eisenhauer, N.M. Förster Schreiber, R. Genzel, S. Gillessen, D. Lutz, T. Ott, D. Santos, J. Shangguan, A. Sternberg, L. J. Tacconi, F. Widmann, T. de Zeeuw)

2.2.3 The Galactic Center: Physics in the Sky

The Galactic Center's role as a truly unique astrophysical laboratory was recognized with the 2020 Nobel Prize in physics. Over 40 years our MPE-IR team has carried out ever sharper and better high-resolution, near-infrared observations of the central parsec of the Milky Way in 1992, discovering O(1000 km/s) velocities of a half a dozen of moderately bright stars orbiting the compact radio source Sgr A* on scales of the outer solar system, very unexpected in terms of how they ever got there. The enormous progress in the last three decades has been driven very much by our team developing and employing novel instrumental techniques, the most important ones being adaptive optics, integral-field spectroscopy and near-infrared interferometry at the 8 m telescopes at ESO's VLT in Chile. In the past years, our Galactic Center science projects have exploited the images with 3 mas resolution and the astrometry with 30 μas precision, which the VLTI instrument GRAVITY since 2017 routinely delivers, outperforming single-telescope imaging by large factors.

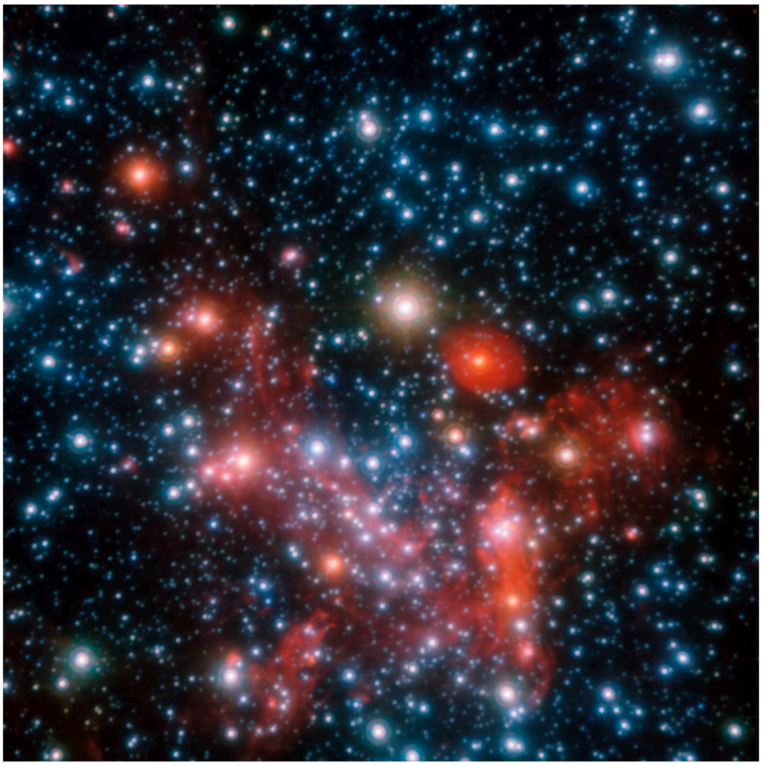

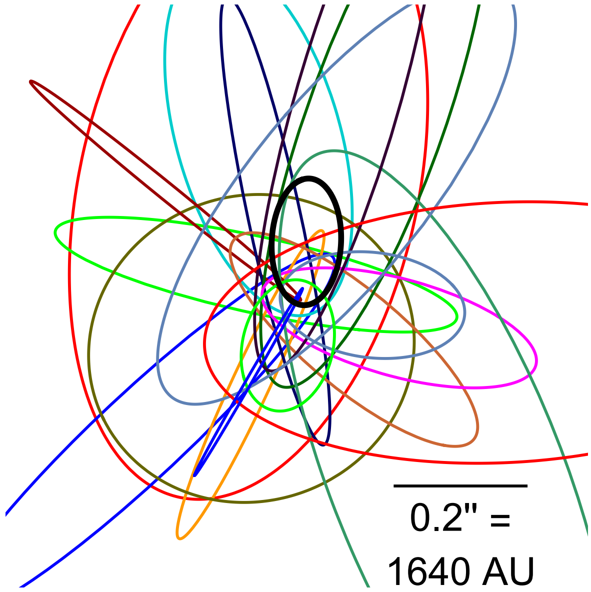

Fig. 2.2.3.1 **Left:** *Pseudo-color, near-infrared image of the Galactic Center, obtained with the adaptive optics imager NACO at ESO's VLT.* ***Top:*** *Stellar orbits in the central arcsecond.*

Located at a distance of 8.3 kpc, the Galactic Center harbors the closest massive black hole (MBH). Its vicinity allows for observations with unparalleled detail. Using adaptive optics at an 8m telescope, one can fully resolve the nuclear star cluster (Fig. 2.2.3.1) and track the motions of individual stars, both in the plane of sky with imaging systems as well as in radial velocity using spectroscopy. This allowed discovering individual stellar orbits (Fig. 2.2.3.1, Schödel et al. 2002, Eisenhauer et al. 2005, Gillessen et al. 2009, 2017) and yielded convincing evidence that the radio source Sgr A* indeed is an MBH.

Yet, the astrometric precision achievable is limited by the crowded environment: Fainter (mK > 19), unseen stars passing close to brighter (mK = 14-17) stars perturb the position measurements of the latter; and the unavoidable seeing halos of very bright cluster stars (mK = 10) create an additional astrometric noise for the stars in the central arcsecond. To overcome these limitations our team has developed GRAVITY, enabling us to obtain even higher resolution data, and taking advantage of the layout of the four 8m telescopes of the VLT as an interferometer. The project schedule was very much driven by the 2018 pericenter passage of the star S2 on a highly elliptical, 16-year orbit (see Fig. 2.2.3.2), an opportunity to map out quickly the gravitational potential over a large radial range.

The combination of high precision astrometry (measured in angular units) and radial velocity data (measured in physical units, km/s) allows for a geometric determination of the proportionality constant between angular and absolute velocities, the distance to the system. The accuracy of the measurement has reached now an astonishing 0.3%, a result of the ultra-precise GRAVITY astrometry and SINFONI spectroscopy obtained during the pericenter passage (Fig. 2.2.3.2 and 2.2.3.3, GRAVITY coll. 2019, 2021).

Already a few weeks after the 2018 pericenter passage, our data set delivered also a significant detection of

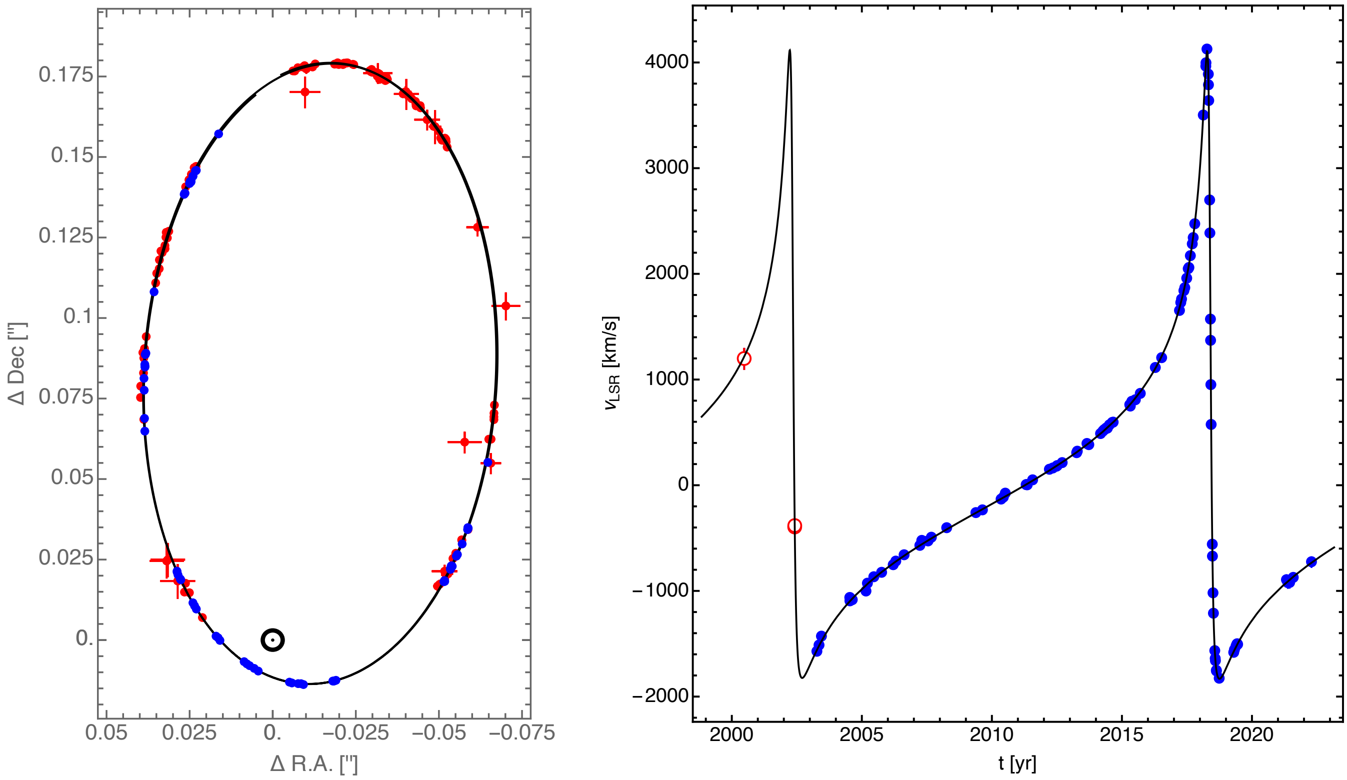

***Fig. 2.2.3.2** The orbit of S2. **Left:** Astrometric data (red points: Speckle and adaptive optics based, blue points from GRAVITY interferometry) and best-fit orbit (black line) plotted in the mass rest frame. **Right:** Radial velocity data (blue points from 2003 – 2019 based on SINFONI and NACO at the VLT, red points from the Keck data set, 2021 data from GNIRS at Gemini North, and 2022 data from the ongoing ERIS commissioning).*

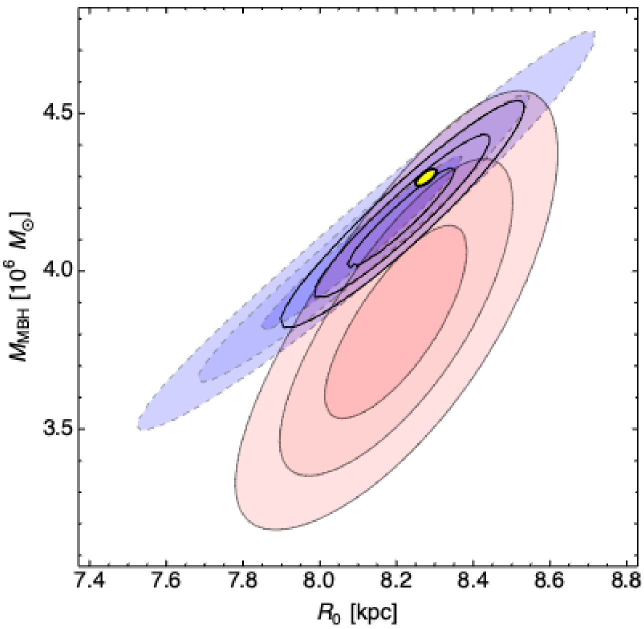

***Fig. 2.2.3.3 Left:** Mass of Sgr A* (M_{MBH}) and distance to the Galactic Center (R_0). The blue shaded area gives the uncertainty contours from adaptive optics data of S2 as of end 2016. The red shaded area is an independent measurement from dynamical modeling of the nuclear cluster. The small yellow ellipse is the result when one includes the GRAVITY data up to end 2021, indicative of the statistical uncertainty below 10pc in R_0.*

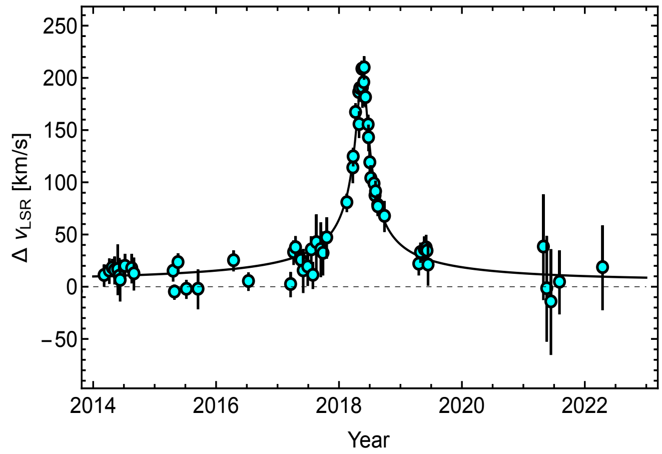

***Fig. 2.2.3.4** The gravitational redshift signal of the S2 orbit. The black line is the best-fit, relativistic orbit minus the same orbit without relativistic effects. The 2021 spectroscopic data carry larger error bars, as they have been obtained with the long-slit spectrograph of GNIRS as Gemini North, whereas the other data are from the integral field spectrograph SINFONI at the VLT, which was dismounted at the end of 2019. The 2022 data point is from the first radial velocity measurement with the newly installed ERIS instrument in April 2022, with a conservative error bar.*

the gravitational redshift affecting the light as it travels from S2 outwards against the gravitational field of the MBH. The combined effect of the redshift and the relativistic Doppler formula leads to an apparent change in the radial velocity data of 200 km/s, well above the spectroscopic measurement precision, which reaches in good data sets 7 km/s. Yet, the measurement is more difficult than what these numbers suggest. Besides the parameter describing the relativistic effect, one needs to determine simultaneously from the same data set 13 more parameters: The position and velocity of the massive black hole (six numbers), its mass, and the six orbital elements of S2. There are significant degen-

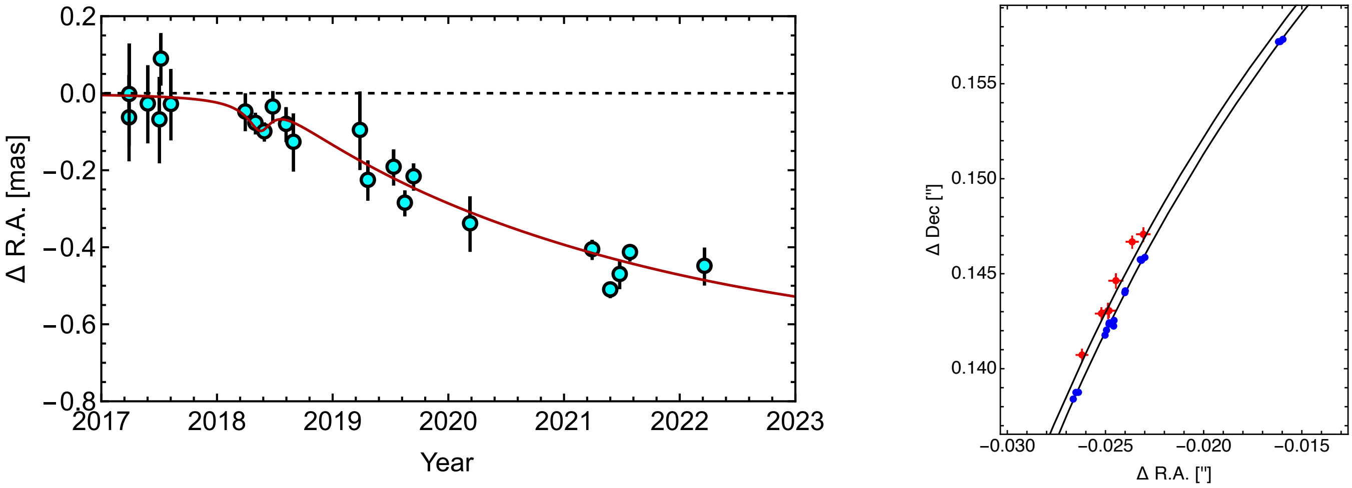

Fig. 2.2.3.5 *Relativistic prograde precession of S2.* ***Left:*** *Residual in x between relativistic orbit (red line) and Keplerian orbit (gray line at 0). The GRAVITY data (red, cyan and blue circles) clearly favor the relativistic model.* ***Right:*** *Plotting the S2 orbit in the mass rest frame and zooming into the 2005 / 2022-part, one can see that the data from the two revolutions do not line up anymore, differing by a few hundred micro arc seconds., as predicted by GR over two revolutions.*

eracies in the 14-parameter fit, and thus the quick detection of the purely spectroscopic effect actually was also a result of the high-precision GRAVITY astrometry, which reduced the degeneracies far enough that the redshift signal became discoverable at the 6σ level by June 2018 (GRAVITY Coll. 2018a). As of today, with the inclusion of data up to early 2022, the significance has increased to around 25σ (see Fig. 2.2.3.4).

While the gravitational redshift is an effect solely altering the light emitted by S2, we also have been able to detect the relativistic nature of the gravitational field in the motion of S2 itself at the end of 2019 with a significance of initially 5σ, where again the challenge is the large number of parameters (GRAVITY Coll. 2020b). The S2 orbit precesses by 12 arc minutes per revolution of 16 years due to the Schwarzschild nature of the metric, like Mercury precesses in the Sun's gravitational field. Since the S2 orbit is highly elliptic (e = 0.88) the precession manifests as an almost instantaneous change of orientation of the orbital ellipse in its plane at pericenter. Therefore, it is measured best with data pre- and post-pericenter. Our latest data covering up to the first 2022 epochs has increased the significance to 7-8σ (Fig. 2.2.3.5, GRAVITY Coll. 2022a).

After 2018, S2 moved away from the MBH, Sgr A*, and has left the central field of view of GRAVITY. While observations were not possible in 2020 due to the global pandemic, we have for the first time in 2021 obtained multi-epoch deep interferometric images of the central 100 mas (Fig. 2.2.3.6). This has allowed us tracking a

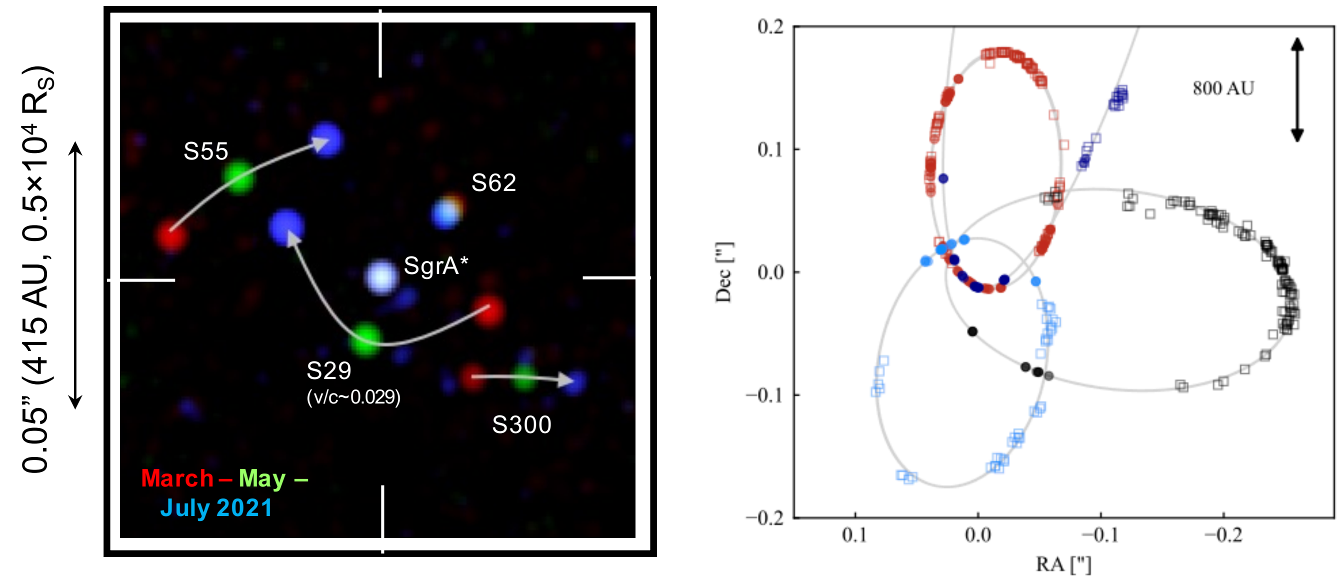

Fig. 2.2.3.6 *Multiple stellar orbits with interferometric data in the central 100 mas observed in 2021. Left: Montage of three images obtained in the months March, May and July, illustrating the quick stellar motions. Right: Data and orbits of the combined orbit fit using the stars S2 (red), S20 (violet), S38 (black) and S55 (cyan), including also the first 2022 epoch.*

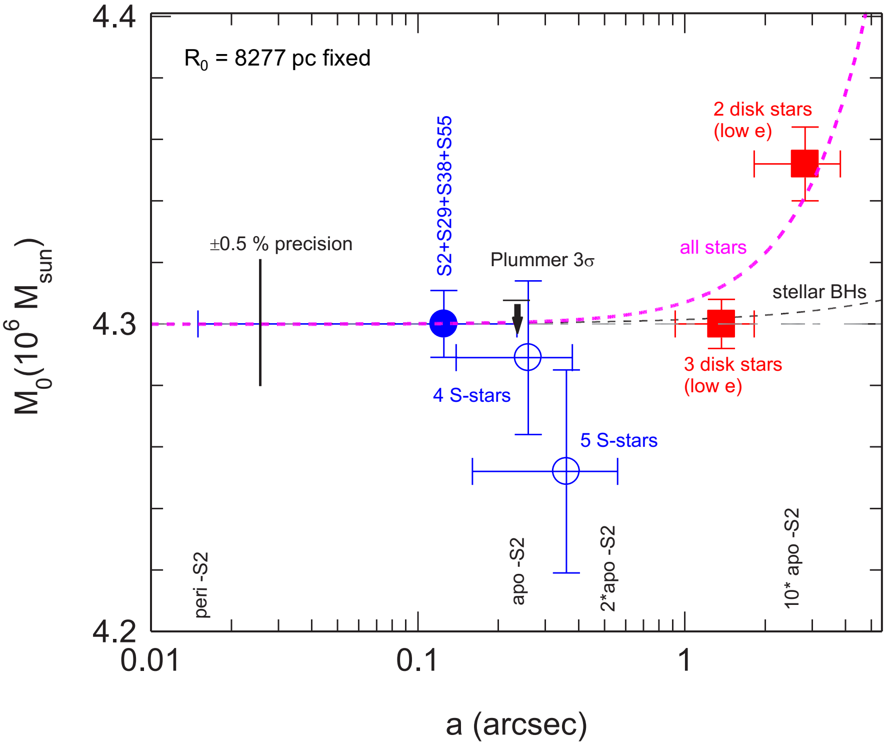

Fig. 2.2.3.7 *Mass distribution in the Galactic Center. The filled blue circle is the central mass, which our four-star fitting has established to lie within the 100 AU pericenter of S29. The black arrow denotes the 3σ upper limit of any extended Plummer mass of assumed scale radius 0.3”. The two open blue circles and two red filled squares show averages of enclosed masses within the semi-major axes of other S-stars and clock-wise disk stars. The magenta dashed line is the sum of the central point mass and the expected, extended stellar mass distribution from the literature.*

number of fainter stars known before (S29, S38, S55, S62) and not known before (S300), at least three of which pass the pericenters of their orbits in 2021 or 2022 (GRAVITY Coll. 2020a, 2022a,b). Notably, S29 dives even deeper into the gravitational potential than S2, reaching a mere 100 AU in May 2021. Using multiple stars with interferometric data in the orbit fit actually is one of the reasons why we are able to improve the significance of the Schwarzschild precession term.

Further, the data set stringent constraints on any potential extended mass configuration around Sgr A*. We can set an upper limit of 0.1% of the mass of Sgr A* (i.e. 4000 solar masses) that possibly could reside inside the apocenter of the S2 orbit. In other words, 99.9% of the mass need to be concentrated within the 100 AU pericenter of S29. Only at radii > 3 arc second, much further out than the S2 apocenter, we might see an increase of the enclosed mass beyond that of Sgr A* alone (Fig. 2.2.3.7).

One key advantage of the interferometric data compared to the adaptive optics imaging is the fact, that in each individual exposure of 300 seconds we can detect the near-infrared counterpart of Sgr A*. This means that one can reference in a direct way the stellar positions to the mass, removing the need to construct a reference frame, which is the main source of systematic error for the adaptive optics data.

Being able to detect Sgr A* at all times in the near-infrared also means that we were able to derive its flux distribution down to the faintest state, covering 100% of the flux states occurring (Fig 2.2.3.8). For the first time, we can report a characteristic near-infrared flux of Sgr A* of around 1 mJy. At the high flux end, we see a distinct power-law tail. This supports the picture that Sgr A* is a continuously variable source, which on top exhibits from time to time radiative outbursts. Such a two-state picture is a natural consequence, if these flares are coming from single emission regions, dominating then the total system emission.

The interpretation of flares as originating from compact emission zones (“hot spots”) has already been brought forward by analysis of adaptive optics data, invoking also time scales and the spectral energy distribution. With GRAVITY, we have obtained in 2018 much more direct evidence for this picture: We have seen in three occasions flares revolve in a clockwise manner around the mean flare position (Fig 2.2.3.9). The astrometric signature was accompanied also by polarimetric changes, which taken together constrain the Sgr A* system to be seen almost face-on and the accretion disk’s magnetic field needs to be poloidal (GRAVITY Coll. 2018b).

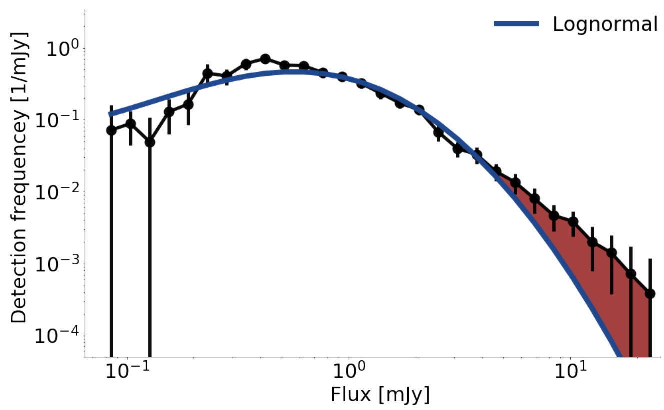

Fig. 2.2.3.8 *Flux distribution of Sgr A*. The peak at around 1 mJy is determined here for the first time, defining a characteristic near-infrared flux of Sgr A*. A lognormal distribution is not sufficient to describe the high-flux end of the distribution, but a tail towards a higher flux is observed (red shaded area).*

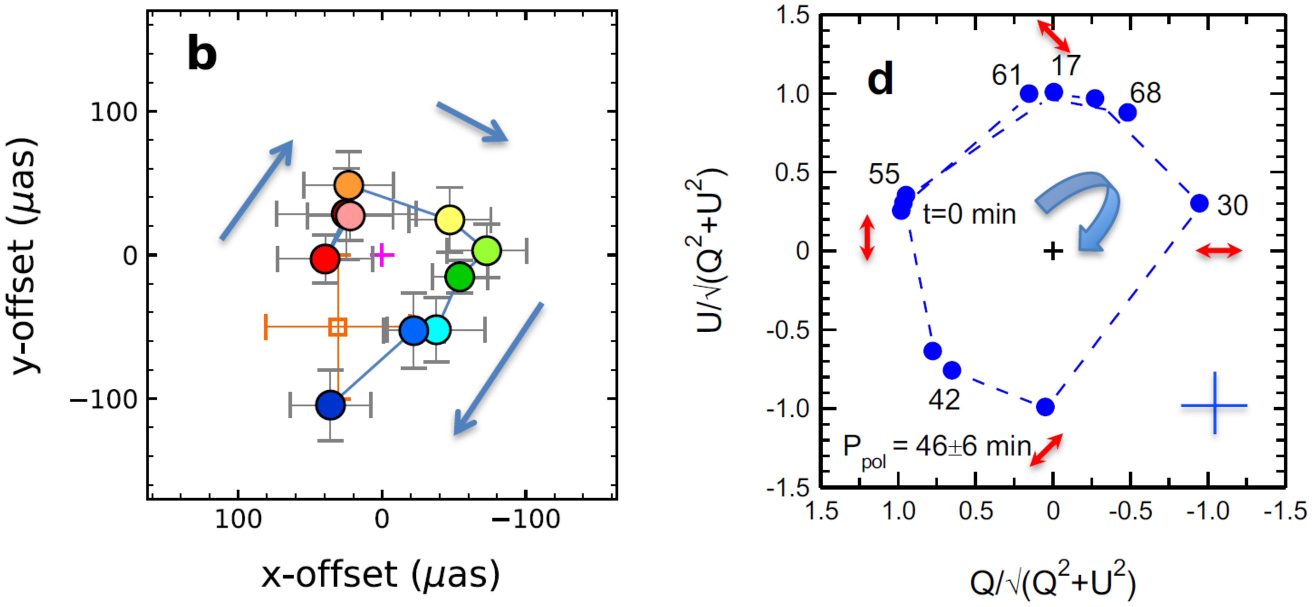

Fig. 2.2.3.9 *Observation of a Sgr A* flare with GRAVITY from 2018.* ***Left:*** *Astrometric data of the emission centroid in steps of 320 seconds, showing a clockwise loop over 70 minutes.* ***Right:*** *The polarimetric Q and U components of the Stokes vector also evolve in a loop over the course of the flare.*

In 2019, we have observed a flare with interesting multi-wavelength coverage: GRAVITY's acquisition camera delivered a 1.5µm light curve, the interferometric data one at 2.2µm. In parallel, Spitzer obtained 5µm data, while Chandra and Nustar covered the X-ray regime from 2 – 70 keV. The data allowed measuring the fluxes and spectral slopes in both the near-infrared and the X-ray bands, and even following their evolution (Fig. 2.2.3.10). Modeling the emission yielded the yet strongest observational evidence that both the near-infrared and the X-ray emission are due to synchrotron emission of transiently heated electrons. While the nature of the near-infrared emission was undisputed, there were several competing models for the X-ray emission, which can be rejected at least for this particular flare.

GRAVITY has opened many new doors in Galactic Center science. But where are we heading next? One key goal for the future is measuring the spin of Sgr A*. There are a few potential routes to this aim:

- The cleanest way is to employ stellar orbits and measuring their Lense-Thirring precession. This requires observing yet unknown stars on even smaller orbits, and tracking them astrometrically with interferometric precision and spectroscopically with an uncertainty in the 1 km/s regime. The spectroscopy will need the large aperture of the ELT, and we are currently increasing GRAVITY's sensitivity in the GRAVITY+ project, such that tracking mK = 20 stars seems feasible. This goal has found recent support in GRAVITY's 2021/2022 astrometric imagery to mK = 20, which shows many more faint stars on 100 AU scales around Sgr A* than we anticipated from earlier AO observations with VLT and Keck.
- A second way might be the precise astrometry of one or a few suitable flares. Flares have the advantage of being probes right at the event horizon. However, since gas physics is used here, such a measurement is less clean, and there are theoretical hints, that the inflowing gas does not align with the spin of Sgr A*, but rather carries only the angular momentum from the stars which expelled the gas.
- A third way could be to derive a distribution of radii at which flares are observed. If there is an inner truncation radius, that might well mark the innermost circular orbit, which in turn is a sensitive probe for the spin. Obviously, it will be a large observational challenge to collect a sufficient number of flares.

Since an astrophysical black hole is fully characterized by its mass and spin, any higher order effects can be predicted once mass and spin are measured. Comparing for instance the experimental quadrupole moment to the value predicted by general relativity would thus constitute a test of the no-hair theorem.

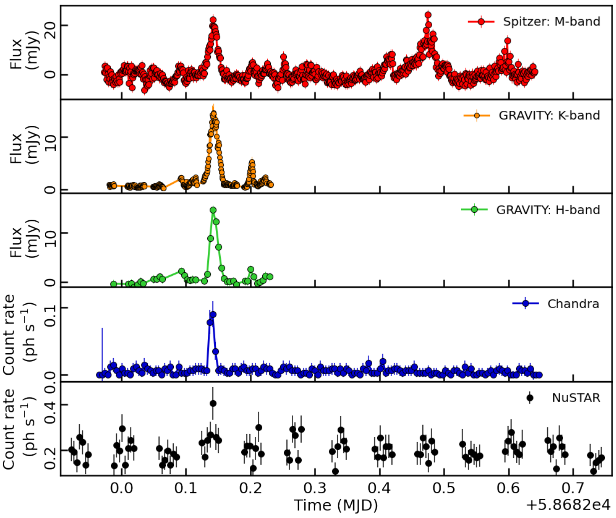

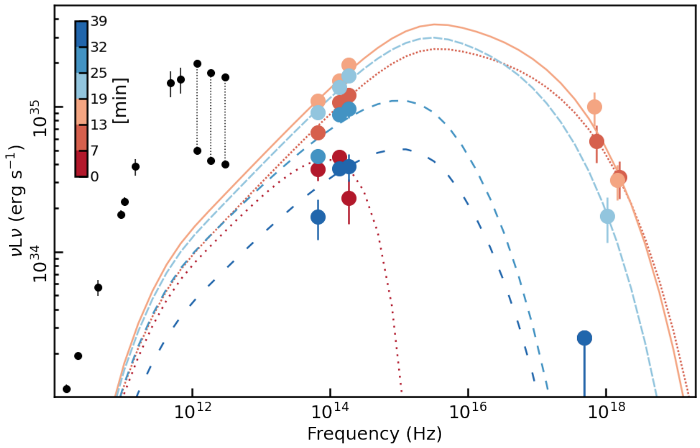

***Fig. 2.2.3.10** Simultaneous observation of a flare with Spitzer, GRAVITY, Chandra and NuSTAR on 2019-07-17. **Left:** Observed light curves of the Sgr A* flare. **Right:** Temporal evolution of the spectral energy distribution. The lines show the emission from a one zone model in which the emission is created by synchrotron emission of a power-law distribution of accelerated electrons with a cooling break in the (unobservable) UV regime.*

Selected References:

Eisenhauer et al. 2005, ApJ, 628, 246
Gillessen et al. 2009, ApJ, 692, 1075
Gillessen et al. 2017, ApJ, 837, 30
Schödel et al. 2002, Nature, 419, 694
GRAVITY Coll. 2018a, A&A, 615, L15
GRAVITY Coll. 2018b, A&A, 618, L10
GRAVITY Coll. 2019, A&A, 625, L10
GRAVITY Coll. 2020a, A&A, 645, A127
GRAVITY Coll. 2020a, A&A, 636, L5
GRAVITY Coll. 2021, A&A, 647, A59
GRAVITY Coll. 2022a, A&A, 657, L12
GRAVITY Coll. 2022b, A&A, 657, A82

Reinhard Genzel

Stefan Gillessen

(Other Galactic Center team members include: P. Amaro-Seoane, G. Bourdarot, P.T. de Zeeuw, A. Drescher, F. Eisenhauer, F. Mang, T. Ott, J. Shangguan, F. Widmann)

2.2.4 ERIS: New Life for Adaptive Optics on the VLT

ERIS saw its first light in February 2022, a major milestone that followed an intensive period of integration and testing at MPE. Replacing two retired instruments that have been central to our scientific programme, ERIS will enhance and transform the fundamental adaptive optics imaging and integral field spectroscopic capability for the VLT through the next decade. By exploiting the full potential of the Adaptive Optics Facility with a new wavefront sensing module, ERIS will achieve superior sensitivity and resolution for more targets than has previously been possible. The imager will provide astrometry for the Galactic Center, while the higher spectral resolution now possible with the integral field spectrometer will enable the next steps in galaxy evolution.

2.2.4.1 From Conception to Commissioning

For one and a half decades, the fundamental near-infrared adaptive optics capability for the VLT was provided by SINFONI and NACO. But with these instruments working beyond their design lifetimes, and the start of science operations for JWST looming, a renewal and enhancement of the performance offered by those instruments was needed. ERIS, the Enhanced Resolution Imaging Spectrometer, fulfils this need. The instrument, built by a consortium of partners from Germany, Italy, the UK, Switzerland, and the Netherlands, and led by MPE, is now mounted at the Cassegrain focus of UT4. It combines a new imaging 1-5 µm camera which also provides high contrast imaging at 3-5 µm, with a full refurbishment and upgrade of the 1-2.5 µm integral field spectrometer SPIFFI, and a new wavefront sensing system that works with the laser guide stars and adaptive secondary mirror already installed on the telescope.

In achieving this, the team has experienced a number of important events during the last 3 years, culminating in the granting of Preliminary Acceptance in Europe by ESO. The work to reach this was carried out under particularly difficult conditions caused by the pandemic: limited travel so that the sub-system acceptance tests had to be done remotely and the reviews held by videoconference, restrictions on the number of people allowed in the integration hall, interruptions due to quarantining and home office. Despite the continuation of this situation during the installation and verification phase at Paranal Observatory in December 2021, commissioning of the instrument has now begun. **This marks a key milestone for our science programmes** as well as for the observatory, as the first major instrument to be installed and commissioned since the start of the pandemic.

Fig. 2.2.4.1 *The ERIS team re-integrating and testing the instrument in the New Integration Hall of the Paranal Observatory. This requires a rigorous set of checks similar to those done at the European Acceptance, to ensure that after shipping the full functionality and performance can still be achieved.*

2.2.4.2 A Forward Look to ERIS Science

ERIS was conceived so that the science performed by the IR/Submm Group would be able to exploit its capabilities in ways that make it competitive to JWST.

Observationally, our galaxy evolution project aims to detect signatures of the physical processes driving mass assembly and structural transformations of galaxies at redshifts z ~ 1-3, which includes the peak of cosmic star formation density and the subsequent shutdown of star formation. **ERIS will reveal these processes by resolving their imprint on galaxy kinematics.** Its adaptive optics will provide high spatial resolution corresponding to 0.5 kpc; and new gratings, especially a higher resolution grating with R ~10500, will facilitate tracing the kinematics on 10-40 km/s. This resolution is needed due to the decline over cosmic time of the characteristic intrinsic velocity dispersion of disks (setting their vertical thickness), and also to probe efficiently between the bright OH skylines. In this context, a particularly important aspect of the SPIFFI refurbishment was to fully remove the aberrations in the line spectral profile, by replacement of the mirrors (to correct diamond-turning effects) as well as the gratings (to correct the 'egg-box' effect caused by light-weighting). ERIS stands out for this science because no other current or planned space-based instrumentation will provide the necessary spectral resolution for kinematics studies of galaxies. Indeed, JWST has a single IFU with only R < 3000; and its focus will be on multi-object spectroscopy of faint galaxies, measuring multi-line diagnostics for a census of galaxy populations up to the highest redshifts. With a sensitivity, as shown in Fig 2.1.4, that is better than other ground-based instruments, and with its higher resolution and wavelength coverage to the J-band, ERIS will surpass JWST in terms of probing physical mechanisms of galaxy evolution and star formation shutdown.

Many of the discoveries in the Galactic Center have come about via capabilities that lie at the core of ERIS. These include the differing spatial distributions of late-type stars, early-type stars, and Wolf-Rayet stars, as well as the various 3D orbital structures they trace. And while the most exquisite monitoring of the orbits of stars closest to Sgr A* is now furnished by GRAVITY, the astrometry that ERIS enables over a wider field will

__Fig. 2.2.4.2__ The integration team after successfully mounting ERIS to the Cassegrain focus of UT4 at the VLT. Adhering to the restrictions associated with pandemic, both for travel and while at the observatory, makes the whole process of integration and testing much more arduous than in normal times. Back row, left to right: A. Puglisi (INAF-Arcetri), P. Grani (INAF-Arcetri), K. Kravchenko (MPE), D. Schuppe (MPE), M. Deysenroth (MPE), Y. Dallilar (MPE). Front row, left to right: A. Riccardi (INAF-Arcetri), D. Barr (ESO), H. Feuchtgruber (MPE).

link this to stars further out as well as providing a reference frame. In the Galactic Center, the key science topics – dynamics of the various stellar populations, the radiative behavior of Sgr A*, flares and gas streamers, and continued monitoring of faint stars around SRG A* are those where **ERIS will be highly competitive with respect to JWST.** Indeed, since sensitivity in this field is limited by crowding, the lower background of JWST yields little advantage. Instead, the regular and long-term monitoring possible from a ground-based observatory combined with the higher resolution due to the larger aperture is essential for future studies of this ever-changing region.

The start of commissioning has opened a new phase in the project that will enable the next exciting steps in our science projects.

Helmut Feuchtgruber

Ric Davies

Eckhard Sturm

(Other ERIS team members include: A. Agudo Berbel, Y. Dallilar, M. Deysenroth, D. Lutz, F. Eisenhauer, N. Förster Schreiber, H. Gemperlein, R. Genzel, S. Gillessen, M. Hartl, J. Hartwig, D. Huber, H. Huber, K. Kravchenko, P. Langer, H. Özdemir, C. Rau, D. Schuppe, L. Tacconi, E. Wiezorrek)

2.2.5 MICADO: the First Light Instrument for the First ELT

MICADO, the adaptive optics camera for the ELT that is being designed and built under MPE leadership, is nearing the end of its Final Design Review. ESO are now planning that it should be available in 2027 for both the first technical light of the telescope and the first science observations. The simple and robust design will enable MICADO to exploit the unique features of the ELT early on, yielding an unprecedented combination of resolution and sensitivity. It will lead to new insights about galaxy evolution at high redshift by directly resolving small galaxies and sub-structures of larger galaxies on scales < 100 pc, and providing star formation histories over cosmic time by spatially resolving the relic stellar populations of local galaxies. In the Galactic Center, it will lead to the characterization of main sequence stars with masses < 1 M_{sun}, trace orbits that lie within light hours of Sgr A*, and measure the spin of the black hole.

2.2.5.1 Project Status

MICADO will equip the ELT with a diffraction-limited capability for imaging, astrometry, coronography, and slit spectroscopy at near-infrared wavelengths – and open new observational windows with exciting opportunities for new and unexpected discoveries. It will work with the laser guide star multi-conjugate adaptive optics system MAORY; and also has its own single-conjugate adaptive optics (SCAO) system that uses just a single natural guide star. The project will begin its Manufacturing, Assembly, Integration, and Test phase in the second half of 2022. ESO's schedule shows that MICADO, with its SCAO system, will be the only instrument installed on the telescope's Nasmyth Platform in time for the ELT first technical light in 2027. Following a period of commissioning, **it will be the first instrument available for science operations.**

Fig. 2.2.5.1 *The ELT, rendered as it will look when completed, on the summit of Cerro Armazones (credit: ESO) and MICADO as it might appear when first installed on the Nasmyth Platform of the ELT. The whole instrument stands a little over 6m high in order to reach the optical axis provided by the telescope's Pre-Focal Station (not shown).*

2.2.5.2 Observing Modes and Science Outlook

The instrument's most basic mode will obtain **diffraction-limited images** with a resolution of 4-12 mas at 0.8-2.4 μm using an array of 3×3 H4RG detectors. The multiplex advantage of the 50.5 arcsecond wide field is complemented by a 19 arcsecond field that provides the fine sampling for shorter wavelengths and to deblend crowded fields. With a point source sensitivity comparable to that of JWST, and a resolution a factor 6 better, **this mode is well suited to studying galaxy evolution.** We now have a fairly robust outline, in terms of global properties, of how galaxies assembled and transformed into the present-day Hubble sequence. MICADO will enable us to resolve faint distant galaxies and assess the sub-galactic components at sensitivities better than any other facility (see Figure 2.1.4) and at spatial scales < 100 pc – equivalent to the seeing limit for the nearby Virgo Cluster galaxies. Poorly explored regimes include lower mass galaxies, which comprise the bulk of the galaxy population, and galaxies at early cosmic time when they were forming their first stars.

Performing **astrometry at better than 50 μas precision** – for example to track relativistically moving stars in the Galactic Center or to determine unambiguously whether there are intermediate mass black holes in globular clusters – is one of the more challenging requirements, and can be achieved through stability and calibration.

The rationale for **spectroscopy** in MICADO is to achieve a simultaneous wide wavelength coverage at high spectral resolution, with a focus on faint compact or unresolved objects. A fixed configuration cross-dispersing spectrograph will provide R~20000 and cover the full near-infrared waveband in just two settings, 0.82-1.55 μm and 1.49-2.45 μm. **In the Galactic Center, an exciting opportunity is to measure the spin of the massive black hole,** a goal that is more tractable via spectroscopy than astrometry. And one that is a step nearer now that GRAVITY imaging to K~20 has shown

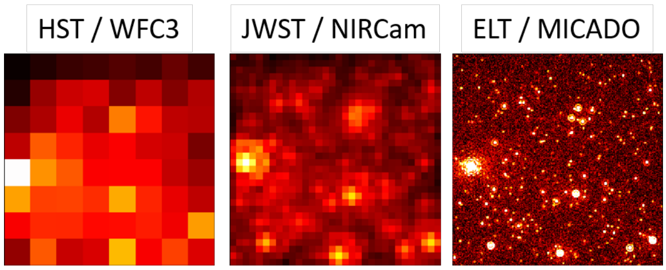

***Fig. 2.2.5.2** Simulation of a highly crowded 1 arcsecond stellar field, as it might appear with the HST, JWST, and MICADO on the ELT. The high resolution of MICADO probes several magnitudes deeper in such fields than any other facility.*

there are many more faint stars on 100 AU scales around Sgr A* than anticipated from earlier AO observations with VLT and Keck (GRAVITY Collaboration et al. 2021, 2022). This goal can be achieved by tracking a late-type star whose entire orbit lies within ~10 mas (0.5 light days, about 1/10 of the S2 orbit) so that it is spatially indistinguishable from Sgr A*. Measuring the radial velocity of the star to better than 1 km s^{-1} enables one to discern in the stellar orbit the impact of the black hole's quadrupole moment, which according to general relativity is fully determined by the spin. With MICADO, sufficient accuracy can be reached via internal referencing between the stellar absorption features and the atmospheric absorption features imprinted into the observed continuum.

The **coronography mode** is a pathfinder in the study of planets around other stars, which is one of the fundamental science drivers for the ELT. Now that a large number of exoplanets are known, we are entering a phase driven by the need to characterize these planets, in particular the atmospheres of giant exoplanets. MICADO will use pupil and focal plane masks, exploiting the large aperture of the ELT to achieve a meaningful contrast at very small inner working angles.

2.2.5.3 Technical Achievements

Fig. 2.2.5.3 *Lothar Barl (an MPE senior engineer), in the integration hall, between tests of MICADO's Focal Plane Mechanism, which uses the new magnetically coupled drive.*

In addition to its responsibilities for system engineering and leading the project, MPE is contributing several major sub-systems that form the core of the instrument. Notably, contracts have been placed already for the cold optics modules with the Fraunhofer Institute for Applied Optics and Precision Engineering in Jena, and for the cryostat and cooling system with Cryo-Vac Low Temperature Technology near Köln. We have worked with these companies to provide the necessary review documentation so that they are ready to begin manufacturing in the near future. Once delivered, these components will be mounted on the rotator bearing, one of the main sub-systems that MPE is providing. The others, which will be manufactured and assembled in-house by our workshops, are the detector positioning system and the focal plane mask mechanism. These too are novel, and in particular, the latter will avoid wear in the drive using a magnetically coupled gear system that has been developed at MPE (and patented) for this purpose. In the coming years, we will begin integrating all these pieces at MPE to make what will become the first instrument on the first of the ELTs.

Ric Davies

Sebastian Rabien

Eckhard Sturm

(Other MICADO team members include: L. Barl, F. Biondi, Y. Cao, F. Eisenhauer A. Emslander, N. Förster Schreiber, N. Geis, H. Gemperlein, R. Genzel, S. Gillessen, M. Hartl, F. Haußmann, V. Hörmann, H. Huber, K. Kravchenko, D. Lutz, L. Neumeier, A. Pflüger, J. Schubert, L. Tacconi, J. Ziegleder)

2.2.6 New Era of Interferometry with GRAVITY+

GRAVITY and the Very Large Telescope Interferometer have transformed high angular resolution astronomy with ground-breaking results on the Galactic Center, active galactic nuclei, young stellar objects, and exoplanets (§2.1). The GRAVITY+ project will soon boost optical interferometry to the next level, opening up the extragalactic sky for milliarcsecond resolution interferometric imaging, giving access to targets as faint as K = 22 mag, and providing ever higher contrast for the observation of exoplanets. This is made possible with the implementation of wide-field fringe-tracking, new state-of-the-art adaptive optics, laser guide stars for all 8m telescopes of the VLT, and performance improvements of GRAVITY and the VLTI.

At the occasion of the last visiting committee in 2019, we reported on the gravitational redshift in the orbit of the star S2, and on the orbital motion of gas close to the innermost stable orbit, around the **Galactic Center** black hole. Since then, GRAVITY observations continued with equally outstanding results on the Galactic Center (§2.4), e.g., the detection of the **Schwarzschild precession** in the orbit of S2 (now at 7-8 σ). Of great astrophysics importance also for future gravitational wave research is the finding that the orbits of the innermost stars now constrain the extended mass component inside the S2 apocenter to ≤ 0.1% of the black hole mass. At the same time, GRAVITY opened up new observing windows for a wide range of astrophysics, most prominently with the detection and characterization of exoplanets, and resolving of the gas and dust around supermassive black holes in **Active Galactic Nuclei** (§2.3). As in earlier technology-driven revolutions – for example, adaptive optics – it was the emergence of a new observational parameter space, which made the difference between gradual progress and large leaps. For GRAVITY, this leap was milliarcsecond angular resolution for objects more than 1000 times fainter than what was possible before.

However, the current GRAVITY/VLTI sensitivity is still a factor of a **few hundred to thousands away from the fundamental quantum limit.** The worst offenders are throughput (limited by the performance of the current adaptive optics, and light losses along the optical train towards the detector), photon noise contamination from the laser metrology, and coherence loss from vibrations at the telescope level.

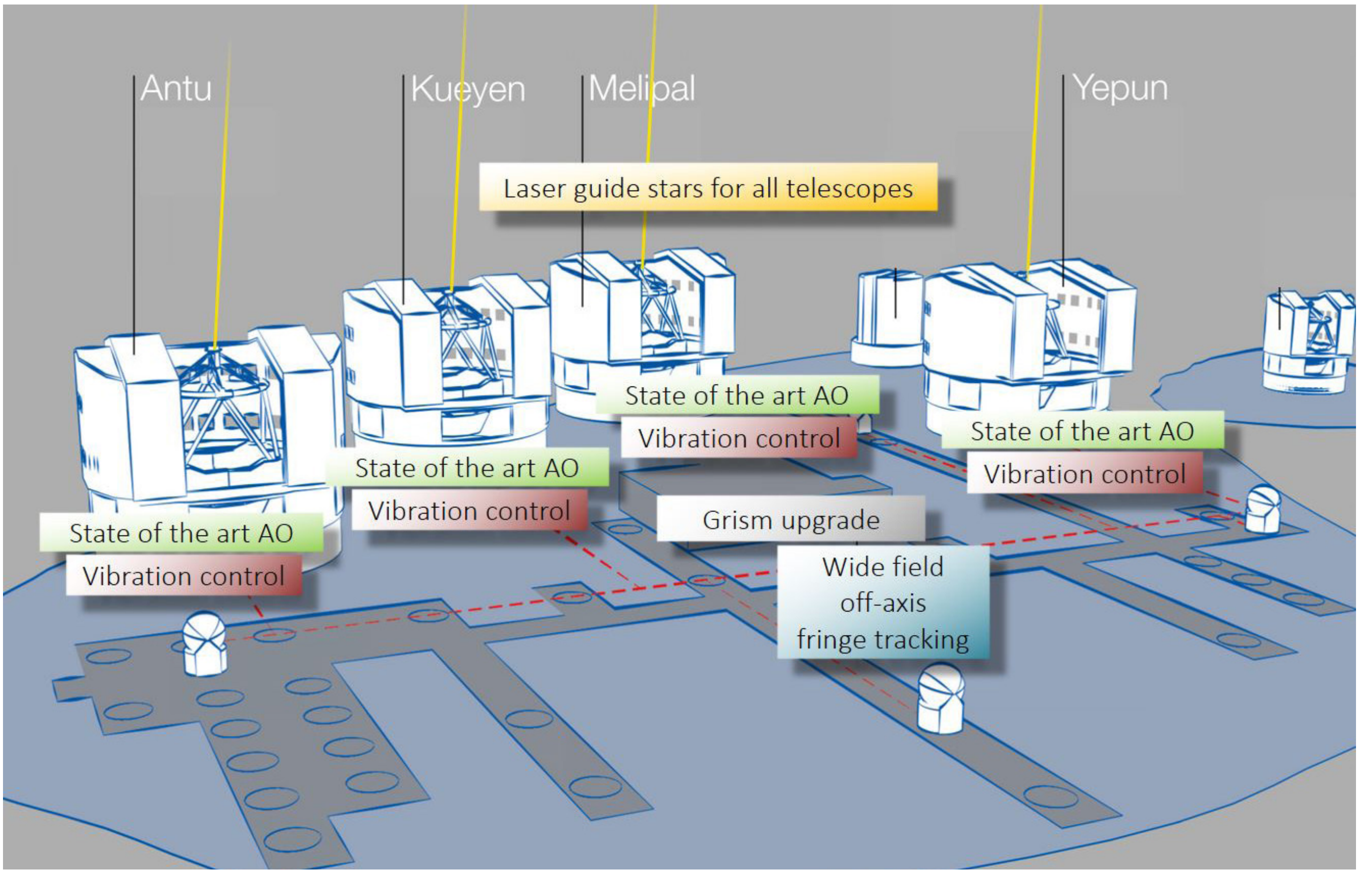

Fig. 2.2.6.1 *Upgrades of the GRAVITY instrument and the VLT interferometer to GRAVITY+ for faint science, all-sky, high-contrast, milliarcsecond interferometric imaging. The key elements are state of the art adaptive optics, laser guide stars for all telescopes, improved instrument throughput and vibration control, wide-field off-axis fringe tracking, reduced noise contamination from the laser metrology, and the development of a noise free science detector.*

The GRAVITY+ upgrade under the lead of MPE will overcome these limitations by implementing a **laser guide star** assisted state-of-the art **adaptive optics** and **off-axis fringe tracking** out to the maximal off-axis angles permitted by atmospheric properties. The proposal **"towards faint science, all-sky milliarcsecond optical interferometric imaging"** was first presented at the ESO Very Large Telescope in 2030 conference in June 2019. Following the successful phase-A study, and the recommendation and approval by the ESO governing bodies, the agreement for the implementation of GRAVITY+ was signed in early 2022. The new state-of-the-art GRAVITY+ adaptive optics will be installed 2024, and laser guide stars will follow in 2025.

GRAVITY+ will start **yet another revolution in high angular resolution astronomy**: It will bring fundamental contributions to the study of black holes, across the full range of masses. It will open up the possibility to measure the spin of Sgr A*, study supermassive black hole growth and coevolution with galaxies over cosmic time, identify intermediate mass black holes (if they exist), detect isolated stellar mass black holes, and possibly uncover a new class of primordial, low mass black holes that might contribute to 'dark matter'. GRAVITY+ will characterize a hundred **active galactic nuclei out to high redshifts** and look-back times of ~10 Gyr. In addition to dynamical mass measurements of black holes, this greatly expanded set of targets will make it possible to directly detect supermassive black hole binaries and probe the cosmic expansion. The increased sensitivity and off-axis tracking will even allow for tracing the gaseous phase of tidal disruption events. GRAVITY+ will directly detect and do spectroscopy of **exoplanets that are out of reach for traditional coronagraphs**. It will provide the first measurement of the mass-luminosity relation of young planets, determine their atmospheric composition and orbital architecture to unprecedented precision, reveal the youngest planets in the process of forming, and confirm the nature of free-floating planets. Finally, GRAVITY+ will spatially resolve newly born stars, the formation of planetary systems, and stars at the end of their life, giving access to objects never observed before in this detail.

The first step towards GRAVITY+, the off-axis fringe tracking – nick-named **GRAVITY Wide** – was implemented end of 2021, and adds yet another worldwide unique capability to the VLTI array. The highlight from the first observations was the detection of **fringes and differential phase signatures from a redshift z~2.5 quasar**. This new mode will be offered in the next observing period, and will be the starting point for the direct measurement of black hole masses at the peak of cosmic galaxy formation and black hole growth.

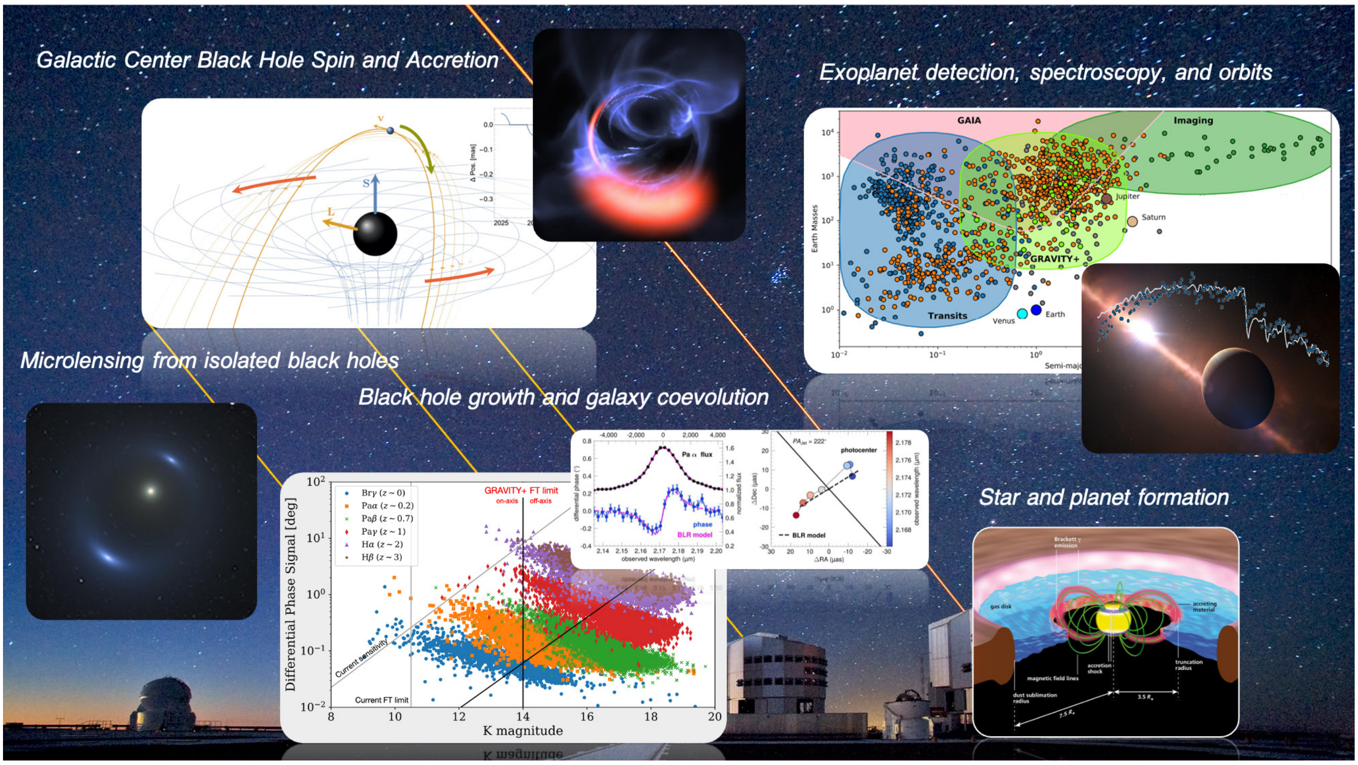

Fig. 2.2.6.2 *GRAVITY+ will bring another revolution in high angular resolution astronomy with direct detection, spectroscopy and orbits of a large sample of exoplanets out of reach for single telescopes (**top right**), fundamental contributions to black hole physics including the spin of the Galactic Center black hole (**top left**), characterization of hundreds of active galactic nuclei out to high redshifts (**lower middle**), detection of isolated black holes and verification of free-floating exoplanets by microlensing (**lower left**), and spatially resolved observations of newly born stars, the formation of planetary systems, and stars at the end of their life (**lower right**).*

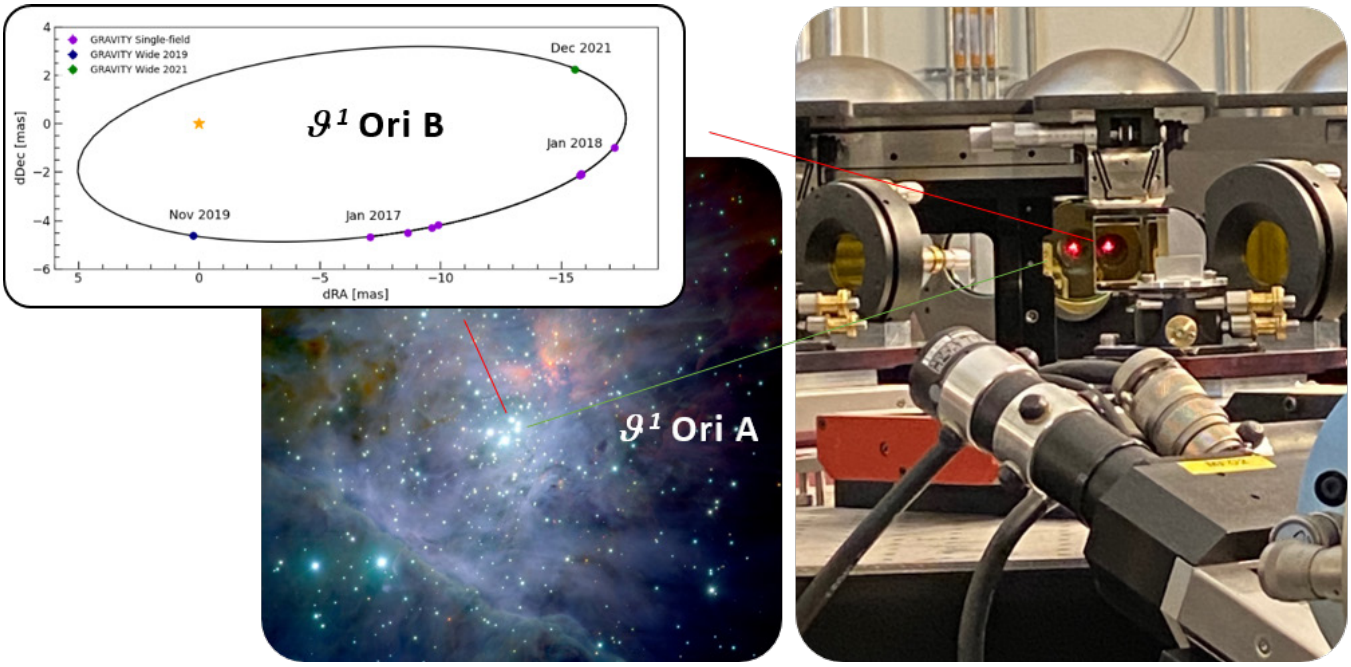

Fig. 2.2.6.3 *First light for GRAVITY Wide: picture of the newly installed periscope optics to feed two widely separated stars to GRAVITY (**right**, with the Nasmyth light source used for alignment). The binary star ϑ 1 Ori B (**left**) was one of the first objects observed with GRAVITY wide.*

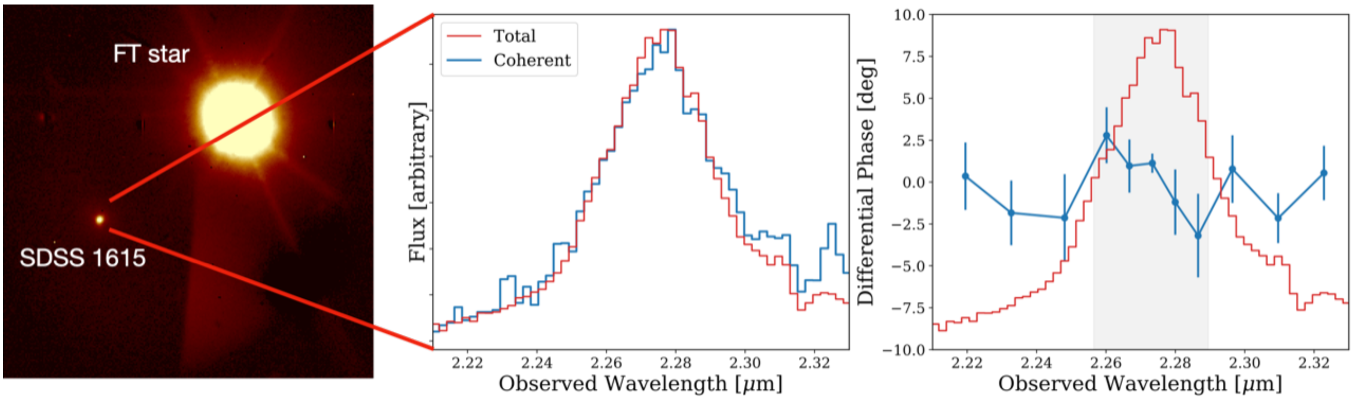

Fig. 2.2.6.4 *World's first Optical/IR interferometric observations of objects at cosmological distances with GRAVITY Wide: Acquisition image of the z=2.46 quasar SDSS 1615 (**left**). The fringes were stabilized on the nearby, bright fringe-tracking reference star. The mid panel shows the spectrum (red) and correlated flux (blue) of the broad Hα line at 2.28 μm. The right panel shows the spectral differential phase (blue) with indications for the differential phase signal of a rotating broad-line region. Upcoming observations will provide a dynamical mass of the supermassive black hole.*

Frank Eisenhauer

Stefan Gillessen

Taro Shimizu

Dieter Lutz

(Other GRAVITY team members include Reinhard Genzel, Thomas Ott, Eckhard Sturm, Max Fabricius, Tim de Zeeuw, Linda Tacconi, Ric Davies, Natascha Förster Schreiber, Felix Widmann, Guillaume Bourdarot, Jinyi Shangguan, Antonia Drescher, Daryl Santos, Felix Mang, Jonas Sauter, Nikhil More, Senol Yazici, Frank Haussmann, Christian Rau, Michael Hartl, Ekkehard Wieprecht, Erich Wiezorrek, Josef Schubert, Susanne Dengler, Jasmin Zanker-Smith)

2.2.7 Star and Planet Formation

The overarching goal of our program is to constrain the physics and chemistry of star- and planet-forming regions and follow the evolution of molecules from clouds to disks and planets, using combined observations (ALMA, VLT/VLTI, *Herschel*, NOEMA and soon JWST) and models. Highlights over the past 3 years include (a) studying and quantifying the origin of substructures and kinematical perturbations in disks; (b) determining disk demographics with ALMA, showing that the dust mass distribution is remarkably similar between low- and high-mass regions and that only young disks have high enough dust masses to be consistent with the observed exoplanet population; (c) inner vs outer disk structure as probed with IR; (d) following the trail of water and complex organic molecules from collapsing cores to disks and comets, (e) modeling the ISM in star-forming galaxies with unprecedented resolution and showing how X_{CO} depends on metallicity and beam size. Interactions with the IR group center on the galactic-extragalactic relation and VLTI-Gravity studies of disks and exoplanets, and with CAS on astrochemistry, i.p. water.

Substructures and their origin in disks

High-angular-resolution ALMA and scattered light observations, including by our team, reveal that disks around young stars appear in a variety of shapes with (sub-) structures being ubiquitous but their origin is still debated. Besides direct imaging, one of the most promising methods to distinguish different mechanisms is to study the gas kinematics. In particular, deviations from Keplerian velocity can be used to probe perturbations in the gas pressure profile that may be caused by embedded (proto-)planets. Wölfer et al. analyzed the CO gas brightness temperature and kinematics of the CQ Tau transitional disk, which shows bent and twisted iso-velocity curves, caused by spiral structures between ~10 and 180 au. Together with deep gas and dust cavities, these structures point to a massive embedded companion. A survey of archival data on ~30 transitional disks by Wölfer shows that such spiral structures are however not common. With Izquierdo (ESO/Leiden) and Testi, a new statistical framework to detect and quantify kinematical perturbations driven by young planets has been developed which can locate them not only in radius but also in azimuth, the *Disc Miner* package. Application to the HD163296 disk reveals two planets, one of them not seen before. With Paneque (ESO/Leiden) and Miotello, similar techniques are being applied to derive the vertical structure of disks, clearly revealing the layered structure of different molecules predicted by models.

ALMA survey of disk demographics

Following our pioneering ALMA survey of ~100 Class II (1-3 Myr) disks in the Lupus star-forming region (Ansdell et al. 2016, 2018), similar demographic studies have been performed for other star-forming clouds by our team, most notably Corona Australis, σ and λ Orionis, and NGC 2024. Just before the Covid shutdown, a record 873 disks were observed in Orion A by van Terwisga et al., the largest such survey yet, allowing to study trends within a single cloud as function of position and cluster membership. The disk mass distribution of the full sample in this high-mass star-forming region is remarkably similar to that of low-mass clouds like Lupus and shows no significant trends with position. This implies that initial disk masses are essentially constant at scales of 100 pc, with only age and proximity to a bright UV source lowering disk masses significantly. These surveys also confirm that at 1-3 Myr, the medium dust disk mass is only that of Neptune, with only a few disks having enough mass to form a giant planet core. In contrast, comparison with disks in the embedded stage of star formation (≤0.5 Myr) by Tychoniec et al. shows that they have sufficient solids to explain the observed exoplanet systems with efficiencies of 15-30% that are acceptable by planet formation models. Gas emission is found to be univer-

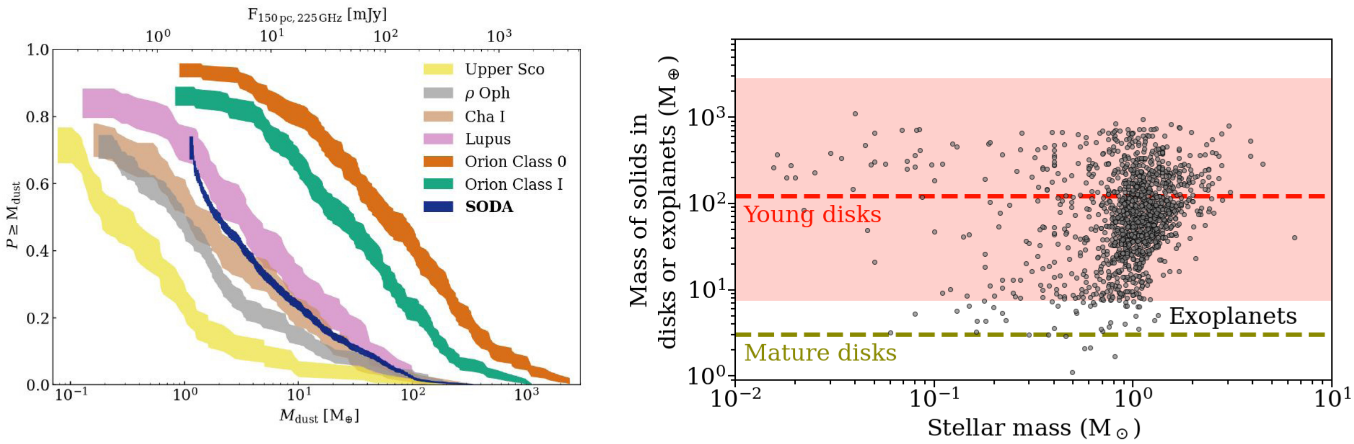

Fig. 2.2.7.1 Left: *Disk mass distribution in Orion A (SODA) compared with that of young disks in Orion (Class 0, I) and with other star-forming regions (van Terwisga et al. 2022). Upper Sco is the oldest region at 5-10 Myr.* ***Right:*** *Comparison of mass in solids in disks with that in mature exoplanets. Only young disks have enough solid mass to build the observed exoplanets (Tychoniec et al. 2020).*

sally weak for T Tauri disks, implying either more rapid disk evolution than predicted by standard models, and/or volatile carbon being locked up in other species than CO, scenarios that have been modeled in detail with the Leiden part of the group. The CO data also allow sizes of gas disks to be determined, a further test of viscous evolution. Recent attention has shifted to the structure and evolution of higher-mass disks around Herbig Ae/Be stars, co-led by Grant with the Leiden group.

The fact that Class II disks do not have enough dust mass to form exoplanets suggests that some form of planet formation begins early when the disk and young star are still embedded in a surrounding envelope. Cridland et al. model the gravitational collapse of a dusty gas cloud to investigate whether the collapse could drive the production of a first generation of planetesimals - 10-100 km sized objects. Dust and gas are indeed found to fall in at sufficiently different rates that the dust could coalesce quickly in the embedded disk to drive the production of at least 7-35 M_{Earth} of planetesimals in the midplane where the dust-to-gas ratio can be raised to near unity for sufficiently large grains (a few 10s of microns).

Inner disks

The inner 10 au of disks is a key region for forming planets. It contains warm, dense gas and dust which is best characterized in the near- and mid-infrared. The coming years will see a revival of infrared spectroscopy by at least three facilities that complement each other: (1) JWST (high sensitivity, unhindered by atmosphere); (2) VLTI-GRAVITY(+) (high spatial resolution for bright sources) and (3) VLT-CRIRES+ (high spectral resolution). As a result, the group is shifting expertise and projects to the infrared. Grant, Bettoni et al. analyzed CRIRES+ Science Verification data of full L- and M-band spectra of the young binary system S CrA (Fig. 2.2.7.2). Many lines are seen, most notably the CO ro-vibrational lines at 4.7 μm that can be used to determine the CO emitting radius, excitation temperature, and gas surface density. Such velocity resolved data are vital inputs to thermo-chemical disk models, notably our in-house DALI model, and will be critical for the interpretation of lower resolution data from JWST-MIRI and NIRSPEC. EvD's group is leading/involved in a dozen JWST GTO, ERS and GO programs.

The inner (few au) disk is also probed in dust and gas with VLTI-Gravity. Bohn, Wölfer et al. investigated the misalignments of inner dust disks with those of the outer disks measured through ALMA CO Keplerian fits. Six out of the 20 transitional disks (including CQ Tau) show significant misalignments that also cause shadows in scattered light and could point to embedded planets. On small scales of <1 au, a VLTI-Gravity survey of 44 Herbig and T Tauri disks (0.4-10 $L_{\odot}$) led by Perraut shows that the $R \propto L^{1/2}$ trend line for the inner rim is no longer valid at low-luminosities, and that the K-band sizes are larger than those predicted from dust sublimation computation. Magnetospheric accretion does not appear to be the process governing the location of the half-flux radius either, but scattering could play a role.

Water trail from clouds to habitable worlds

Van Dishoeck et al., including Caselli, finalized the synthesis paper on Herschel observations of water throughout the star formation process, from clouds to disks and comets, including intermediate stages, which, until now, had received less attention. Combined observational, modeling and laboratory work shows that most of the water is formed as ice on tiny dust particles in cold and tenuous interstellar clouds prior to star formation. When a cloud collapses into new stars and planets, this water is largely preserved and quickly anchored into pebble-sized dust particles, already in the embedded disk stage, where these pebbles then form the building blocks for new planets. Combined analyses of water gas and ice show that up to 50% of the oxygen budget may be missing. In cold clouds, an elegant solution is that this apparently missing oxygen is locked up in larger μm-sized grains that do not contribute to infrared ice absorption. The fact

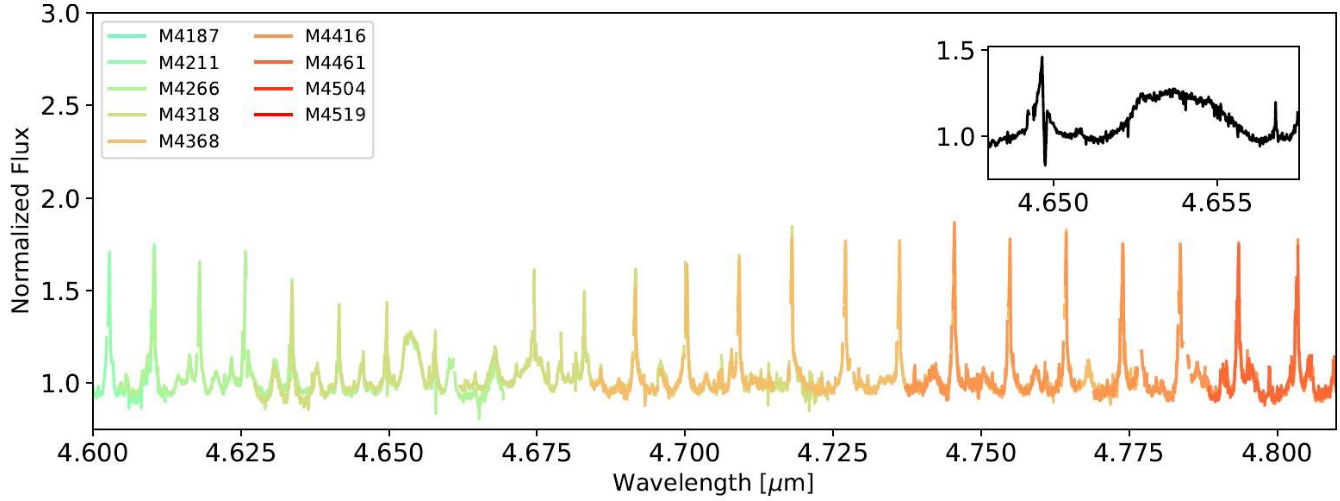

__Fig. 2.2.7.2__ M-band CRIRES+ SV observations taken in September 2021 illustrating the broad wavelength coverage including regions not observed before. Many CO ro-vibrational lines arising from the inner 10 au are clearly detected.

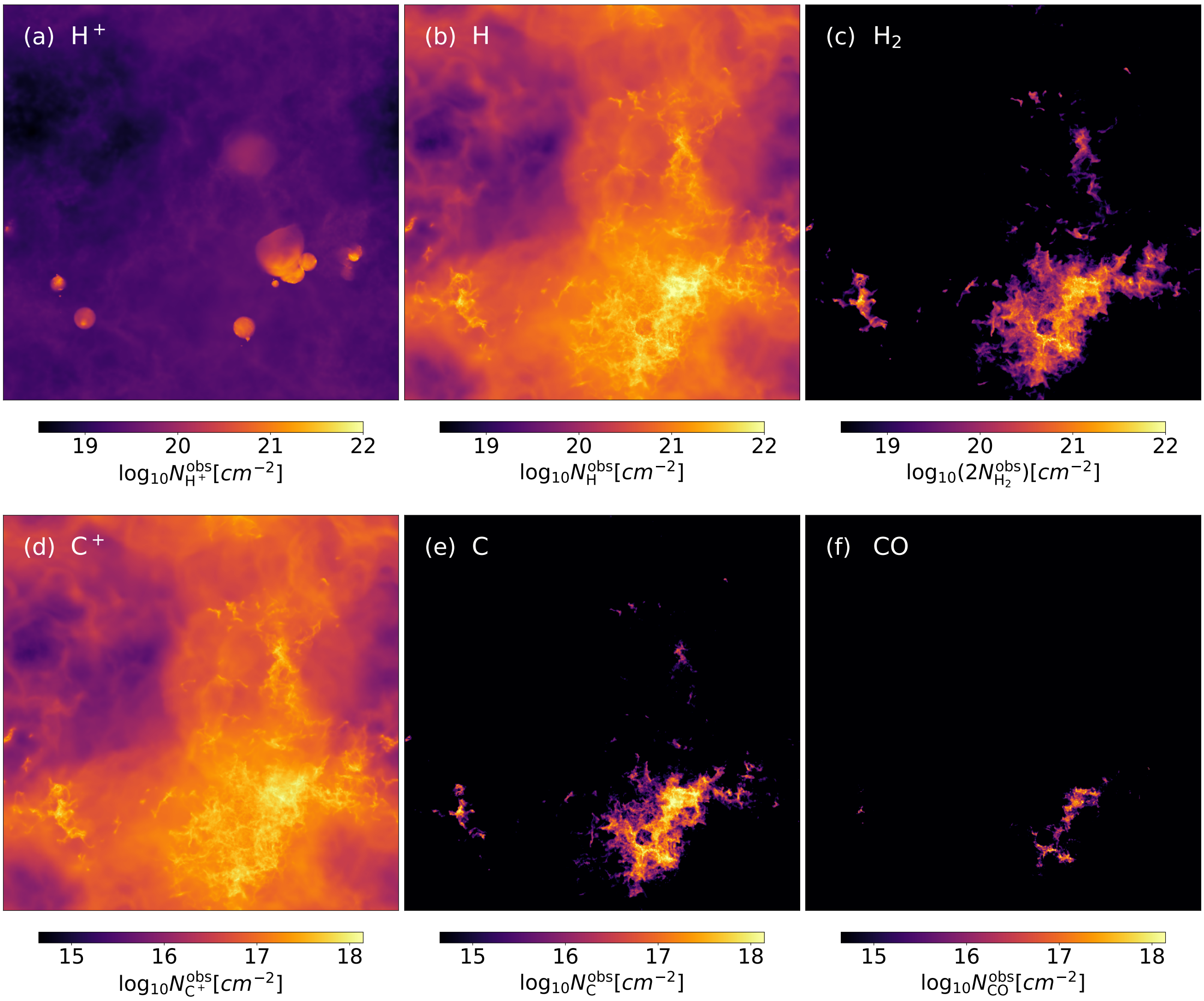

Fig. 2.2.7.3 *Column densities of H^+, H, H_2, C^+, C and CO in a stellar feedback-regulated ISM at solar metallicity from hydrodynamical simulations. The complicated structure of the ISM on kpc scale is properly captured by the sub-parsec resolution. H_2 is spatially more extended than both C and CO due to radiation shielding (Hu, Sternberg & van Dishoeck 2021).*

that even warm outflows and hot cores do not show H_2O at full oxygen abundance points to an unidentified more refractory component as well.

Connecting disk chemistry with exoplanets

Cridland et al. developed a series of models that connect disk chemistry with that of planets that form in them, with a focus on the processes that affect C/O and C/N ratios. Such models are key to interpreting the exoplanet compositions that are now being measured by VLTI-Gravity as part of the exoGRAVITY programs. A unique case is formed by the PDS 70 system, the only system with two currently accreting giant planets and for which the disk has been imaged by ALMA in dust continuum and molecular lines. Fitting of the observed radial profiles of CO and C_2H confirms the assertion of Facchini et al. that the disk is slightly carbon rich (with C/O ~ 1.01). Computing the subsequent formation of giant planets in such a disk shows that their atmospheres should then also be carbon rich. This result does not agree with the current observational findings of exoGRAVITY, who find C/O of no more than 0.7 for PDS 70b. This suggests that whatever chemical process led to the disk's current C/O > 1, likely occurred on a slower timescale than the giant planets' formation.

Other projects

Studies of complex organic molecules (COM) on solar-system scales in embedded sources are continuing with ALMA. Following the ALMA PILS 345 line survey of IRAS16293-2422 led by Jørgensen (~20 papers), focus is now shifting to other low mass protostars that will also be observed with JWST for ice features, to directly compare gas and ice abundances and pinpoint their origin: gas or ice. Also, rather than single sources, larger samples are being studied, both low- and high mass, with COM abundance ratios surprisingly constant. Deep ALMA observations of the IRS48 disk show that its spectacular dust trap is also an ice trap revealing several COMs that are usually invisible in Class II disks.

ISM and gas-star cycle in galaxies at molecular cloud scale

Systematic multi-wavelength observations of the ISM and stellar population are now becoming available that resolve individual molecular clouds for entire nearby galaxies, essential for understanding galaxy evolution. Surveys such as PHANGS involving Schruba reveal large variations between a cloud's star formation activity and gas mass, indicative of capturing clouds at different evolutionary stages. With Kruijssen, a model has been developed that links the observed de-correlation of gas and star formation tracers. Application to ALMA observations of the nearby spiral NGC 300 indicates that star formation in molecular clouds is fast (~10 Myr) and inefficient (Kruijssen et al.). The slow conversion of gas into stars on galactic scales thus stems from the repeated cycling of gas between a diffuse, non-star-forming and a dense, star-forming state.

To obtain a deeper understanding of the underlying physics and chemistry, Hu, Sternberg and vD have conducted high-resolution hydro-dynamical simulations coupled with a time-dependent H_2 network of a feedback-regulated ISM resolving the detailed structure of molecular clouds down to sub-parsec scales (0.2 pc). The results are then post-processed with an accurate chemistry network to model the associated C^+/C/CO abundances, based on non-steady-state ("non-equilibrium") H_2 abundances. A wide range of metallicities (0.1 < $Z/Z_\odot$< 3) is being studied to connect with observations of high-redshift galaxies. In typical star-forming galaxies with solar metallicity, CO emission is a robust tracer for the invisible H_2 gas where star formation occurs. However, at low metallicities where dust shielding becomes inefficient, the UV penetrates deeper into the clouds and photodissociates CO, making it a poorer tracer, with CO gas only surviving in dense compact regions. A steady-state ("equilibrium") model substantially over-produces H_2 but not CO because H_2 is limited by its available time to form in the dynamic ISM. This helps explain the observed relationship between H_2 and CO column densities in galactic clouds and shows that the mass fraction of CO-dark H_2 gas is significantly lower than what a fully steady-state model predicts. In a follow-up study, Hu, Schruba, Sternberg, and vD have conducted radiative transfer calculations to generate synthetic maps of CO emission and show that the CO-to-H_2 conversion factor, X_{CO}, is a multi-variate function of CO intensity, metallicity and beam size. Taking all three variables into account allows observers to more accurately infer the underlying H_2 mass.

Ewine van Dishoeck

(Other MPE team members 2019-2021 include PhD students L. Wölfer (Oct. 2019- Oct. 2021) and G. Bettoni (start Oct 2021, DFG funded) and postdocs Y. Liu (Jan 2019 to Jan 2020), A. Cridland (Oct 2020 to Oct 2021), and S. Grant (start Sept 2021). For the extragalactic projects, A. Schruba (up to Oct 2019) and Ch.-Y. Hu (start Oct 2019) were appointed on the DIP DFG grant with A. Sternberg. About 100 refereed papers with MPE affiliation have been published in this period)

Selected References:

Bohn, A. et al. (including Wölfer, van Dishoeck) 2021, A&A in press arXiv:2112.00123

Cridland, A.J., van Dishoeck, E.F., Alessi, M., Pudritz R.E. 2020, A&A 642, A229

Cridland, A.J., Rosotti, G., Tabone, B., Tychoniec, L., McClure, M., van Dishoeck E.F. 2021, A&A in press arXiv:2112.06734

Hu, C.-Y., Sternberg, A., van Dishoeck, E.F. 2021, ApJ 920, 44

Hu, C.-Y., Schruba, A., Sternberg, A., van Dishoeck, E.F. 2022, ApJ, submitted

Izquierdo, A.F., Testi, L., Facchini, S., Rosotti, G., van Dishoeck, E.F. 2021, A&A 650, A179

Kruijssen, Schruba et al. (including van Dishoeck, Tacconi) 2019, Nature 569, 519

Van Dishoeck, E.F., Bergin, E.A. 2021, in ExoFrontiers, ed. N. Madhusudhan, IOP ebooks

Van Dishoeck, E.F. et al. 2021, A&A 648, A24

Wölfer, L., Facchini, S. et al. (including van Dishoeck) 2021, A&A 648, A19

3 Optical and Interpretative Astronomy

Cut-out of the Coma-Cluster with NGC 4889 (a Brightest Cluster Galaxy) at the bottom right. Color-composite based on u', g', r' images taken with the Wide-Field-Imager of the Wendelstein 2m Fraunhofer-Telescope.

3. Optical and Interpretative Astronomy (OPINAS)

3.1 Overview

OPINAS research is focused on (mostly) massive galaxies and their relation to the dark, non-baryonic components of the universe, namely Black Holes, Dark Matter and Dark Energy. We strive to analyse the structure, stellar populations and formation of massive galaxies at unprecedented levels of precision and, in doing so, improve our understanding of how these properties are related to the galaxies' central black holes and their Dark Halos. By using galaxies as tracers of large-scale structure and as agents in gravitational lensing, we derive tighter constraints on the nature of Dark Matter and Dark Energy and on cosmological parameters. In order to achieve our goals we also built state-of-the art instruments for ground and space.

The OPINAS group is a joint group of the MPE and the University Observatory Munich (USM). Ralf Bender is full professor at the University of Munich and Director at MPE. About 2/3 of the group is located at MPE, the other 1/3 at the Observatory. Most of our scientific projects have participants from both places providing cohesion across the group. Instrument development is separated: the development of space hardware and software (ESA Euclid) is located at MPE, ground-based instrumentation (ELT MICADO) at the Observatory (out of tradition and for funding reasons). Several group members (Bender, Fabricius, Gerhard, Saglia, Sanchez, Seitz, Thomas) are also involved in undergraduate teaching.

Ortwin Gerhard's Milky Way and Nearby Galaxies Group is an independent MPE group associated with OPINAS and we have collaborated on various projects over many years. His separate report can be found at the end of the OPINAS Group Report, while his highlights are included in this overview.

The OPINAS highlights of the past three years have been:

- We developed a new, non-parametric deprojection method (de Nicola et al. 2020*) that allows the recovery of triaxial density distributions with minimal assumptions. This enabled us to derive the shapes of **Brightest Cluster Galaxies** (BCG) on an object by object basis for the first time. Based on a sample of 42 objects with extremely deep imaging data (Kluge et al. 2020) we showed that the flattening and triaxiality of the BCGs' outer parts are compatible with the shapes of Dark Matter halos from ΛCDM simulations (de Nicola et al. 2022, submitted). This is consistent with the finding that the BCGs' outer light is aligned with the Dark-Matter dominated cluster potential (Kluge et al. 2021). Interestingly, the BCGs' inner parts are rounder and more triaxial than even the most modern and comprehensive hydrodynamic simulations of galaxy formation (Illustris/TNG and others) predict (de Nicola et al. 2022, submitted).
- To accurately measure the mass of **supermassive Black Holes and the Dark Matter halo properties** of massive triaxial ellipticals we have developed a new fully 3-dimensional Schwarzschild orbit-superposition code (SMART, Neureiter et al. 2021). An essential improvement is the unbiased model selection taking into account for the first time the true degrees of freedom of the orbit models (Lipka & Thomas 2021). In combination with the new triaxial deprojection code (de Nicola et al 2020, see above) we demonstrated with N-body simulations that we can not only recover the 3D shape of the galaxies but also their Black Hole masses and stellar mass-to-light ratios with 10% precision. As one of the first applications we have modelled NGC 5419, an elliptical galaxy with two nuclei which probably each contain a supermassive Black Hole (Neureiter, 2022, in prep.). We are currently analysing BCGs with extremely diffuse cores promising to contain even more massive Black Holes than the most massive one we have discovered so far (Mehrgan et al. 2019).
- The **stellar initial mass function** (IMF) of massive ellipticals has been much debated in recent years and results from dynamical modelling, gravitational lensing and stellar population analysis are often contradictory. We have compared our dynamically derived stellar mass-to-light ratio profiles with results from stellar population fitting for the same objects and found that, while radial M/L trends seem consistent, the M/L of stellar population models are systematically higher by up to a factor 2 (see posters by Parikh, Mehrgan, Thomas). This is a large discrepancy which indicates a still substantial lack of understanding of the IMF problem. We also analysed abundances of various elements which elucidates formation and enrichment histories and yields insights into the IMF enigma (Parikh et al. 2019, 2021).
- The **stellar halos of early-type galaxies** (ETGs) show diverse kinematics; massive fast rotators (FR) often have halo rotation similar to slow rotators (SR), due to the fading of the rapidly rotating inner component in the surrounding halo. To understand the implications for their accretion history, **Ortwin Gerhard's group** compared observed ETGs with simulated ETGs from the Illustris TNG100 project which have a similar diversity in halo rotation and shapes (Pulsoni et al. 2020). Low mass ETGs

**complete references to our publications cited here can be found in the sections following this overview.*

are completely dominated by in situ stars, while the most massive ETGs are dominated by stars accreted in mergers. Mergers tend to erase the disk-within-halo rotation of the in situ component, and generate spherical-triaxial shapes. In their halo properties, simulated massive FR and SR show a continuity along which SR concentrate towards slow rotation and high accretion fraction, despite the clear bi-modality of the central regions (Pulsoni et al. 2021).

- The **Galactic boxy/peanut bulge and bar** has complicated abundance structure: the inner bulge is a mostly old, alpha-overabundant, early component of the Galaxy but APOGEE data have shown a steep gradient of increasing metallicity and decreasing stellar ages towards the ends of the bar. **Ortwin Gerhard's group** found that the bulge's metallicity map is more pinched than the density, a clear signature predicted by bar formation models (Wylie et al. 2021). The out- and upward metallicity gradients likely imply that co-existing thin high- and thick low-metallicity disks became unstable, forming the bar and then b/p bulge. Integrating ~30 000 inner Milky Way APOGEE stars with 6d phase-space data in one of our best previous bar models, and constructing density, [Fe/H], and age maps from their orbits, we additionally found that the Galactic bar is encircled by a [Fe/H]-rich, ~7 Gyr-old, broad stellar inner ring (Wylie et al. 2022). Simulations predict that this would be built over time by stars formed from infalling gas. The peak of its inferred age distribution (~7 Gyr) then also sets a lower limit on the bar's formation time.
- We played a major role in the final analysis of the completed SDSS **'extended Baryon Oscillation Spectroscopic Survey'** (eBOSS) with the analysis of the quasar two-point correlation function (Hou, Sanchez et al. 2021) and the derivation of the consensus constraints on cosmological parameters (Alam et al. 2021). We investigated the full shape of anisotropic clustering in the combined eBOSS and BOSS data set which suggests a slightly higher local Dark Energy density (by 1.7σ) than the one preferred by the Planck data set. Moreover, we showed that the tension seen between some local data sets and Planck is the result of the differences in the constraints on the Hubble constant and not of a discrepancy in the amplitude of density fluctuations derived from these datasets (Sanchez 2020, Semenaite, Sanchez et al. 2022).
- The **Hobby-Eberly-Telescope Dark Energy Survey** (HETDEX) is now 50% done. HETDEX is the first blind spectroscopic survey of Lyman α emitting galaxies (LAEs) at $1.8<z<3.5$. When completed it will have detected close to 1 million LAEs. Their large-scale distribution will allow us to put unrivalled constraints on cosmological parameters and Dark Energy at $z>2$, a redshift range not accessible to any current or planned galaxy clustering mission. We have contributed to the HETDEX hardware and software, participated at all levels in the analysis and, in particular, have led the crucial modelling of the separation of LAEs and foreground [OII] line galaxies (Farrow et al. 2021). We are also leading the work on the first LAE clustering measurement of HETDEX (Farrow et al. 2022, in prep.).
- - As partners in the **Dark Energy Survey** (DES) we participated in checking the consistency of weak-lensing signals across different surveys (Amon et al. 2022, with T. Varga as a 'tier 1' author) and contributed significantly to the DES-Year1 cluster cosmology work (Abbott et al. 2020 with substantial contributions by T. Varga). In Pereira, Palmese and Varga et al. 2020 we calibrated an alternative stellar-mass based galaxy cluster mass proxy which promises to be robust against a variety of projection and selection biases. Also, as a key tool for future surveys, and in particular Euclid, we developed a novel unsupervised machine learning algorithm to create synthetic galaxy cluster observation scenarios, which are trained directly from a combination of observational datasets (Varga et al. 2021).
- We delivered the MPE-developed **optics for the Near-Infrared Photometer and Spectrograph** (NISP) of the ESA Dark Energy Mission **Euclid** to LAM Marseille. There, we supported the integration of the optics into NISP and completed the analysis of the NISP overall optical performance. Thanks to the near diffraction limit quality of the MPE-developed Camera and Collimator system, we created margins for the telescope and the overall alignment. As a result, the 50% encircled energy radius at the PLM test proved to be 20% smaller than the specifications required.
- OPINAS operates the German **Euclid Science Data Center** (SDC) as one of 9 Europe-wide SDCs which share the workload of the Euclid data analysis. Besides our participation in the shared processing of Euclid data, we are in charge of making ground-based data available to Euclid. These are needed to derive reliable photometric redshifts and are thus essential for the success of the mission. During the last data challenge before launch, the German SDC provided a major fraction for the SGS computing bandwidth, with a 25% contribution to the total data processing effort. As part of the crucial photometric redshift calibration effort, we also obtained NIR spectroscopy at the VLT and LBT to fill critical holes in the color-redshift space.
- The OPINAS group is one of the major partners of the **MICADO** Consortium, the first light instrument for the ESO ELT. We are responsible for the development of the instrument control electronics, the control and preparation software and the cryogenic Main Selection Mechanism (MSM) which enables switching between different instrument modes. During the past three years, we concentrated our efforts on detailing the approved design to bring it to the level necessary for the Final Design Review (FDR), which by now is near successful completion.

Our strategy for the next years is as follows:
We will apply our powerful new deprojection and Schwarzschild 3D methods to a high S/N and high resolution set of massive galaxies from VLT-MUSE, VLT-SINFONI, LBT-MODS and HST (most of these data are already or will soon become available). In parallel, we will extend the code to enable the study of barred disk galaxies. Our goals are to (a) analyse systematic uncertainties of previous more simplified modeling (e.g. with axisymmetric models) and (b) obtain much tighter and more reliable constraints on Black Hole masses and Dark Matter halo parameters over the full range of galaxy masses. Moreover, we will study the stellar mass-to-light ratios of massive galaxies (including their gradients), using both improved dynamical modeling, spectral synthesis and the analysis of abundance patterns with the aim to resolve the IMF enigma. On a time-scale of 5+ years, ELT-MICADO will deliver data of unprecedented quality and resolution on the structure of galaxies, their central regions and their stellar populations, enabling us to extend our analyses both to low mass objects (and lower mass black holes) and to higher redshifts. With our continuously improving methods we will be ready to fully exploit this fantastic new opportunity.

Concerning Dark Matter and Dark Energy on large scales, our immediate next goal is to fully understand and exploit the HETDEX data set and to derive first constraints on Dark Energy and cosmological parameters at redshifts above 2. In parallel, we will prepare for the massive data sets from Euclid and further large cosmology surveys (DESI, PFS, LSST/Rubin). Beyond our already deep involvement in Euclid at various levels (hardware, data processing, Science Working Groups, Euclid Board etc) we are currently stepping up our efforts in Euclid data modelling and in the generation of higher accuracy cosmological predictions (e.g. Sanchez et al. 2021, Lippich and Sanchez 2022, Halder et al. 2021, Varga et al. 2021).

Ralf Bender

A Selection of OPINAS Key Science Papers of the Last Ten Years
(first author papers or papers with leading contributions)

Paper	*Title*	*Comment*	*Cites*
S. Alam et al. 2021, PRD, 103, 083533) (alphabetical author list)	*Completed SDSS-IV eBOSS: Cosmological implications from two decades of spectro-scopic surveys at the Apache Point Observ.*	*Joint analysis of the final BOSS and eBOSS data, which includes the BAO and full-shape results produced in our group over the last 10 years.*	*309*
J. Hou, A. Sanchez et al. 2021, MNRAS, 500, 1201	*The completed SDSS-IV eBOSS: BAO and RSD measurements from anisotropic clustering analysis of the quasar sample in configuration space between z=0.8 and 2.2*	*Analysis of the final eBOSS QSO sample, including the derivation of the consensus constraints for this sample, with J. Hou (OPINAS PhD student) and A. Sanchez as OPINAS first authors.*	*83*
A. Sanchez 2021, PRD,102, 123511	*Arguments against using h-1Mpc units in observational cosmology,*	*The normalization of the matter power spectrum with σ8 has caused misconceptions for both the σ8 tension and the way in which growth-rate estimates inferred from redshift-space distortions are commonly expressed.*	*31*
H. Flewelling et al. 2020, ApJS, 251,7	*The Pan-STARRS1 Database and Data Products.*	*With essential contributions from D. Farrow and R. Saglia. R. Saglia has led the testing and debugging of the Pan-STARRS database over 10 years.*	*404*
Euclid Collaboration, A. Blanchard et al. 2020, A&A, 642, 191	*Euclid preparation. VII. Forecast validation for Euclid cosmological probes.*	*A. Sánchez is one of the corresponding authors and coordinated the group charged with producing updated cosmological forecasts for Euclid.*	*135*
M. Kluge et al. 2020 ApJS 247, 43	*Structure of Brightest Cluster Galaxies and Intracluster Light.*	*Largest ultradeep local cluster survey (170 clusters) to date, with surface brightness limit of 30 g' mag/arcsec2.*	*33*
T. McClintock, T. Varga, D. Grün et al. 2019, MNRAS 482, 1352	*Dark Energy Survey Year 1 results: weak lensing mass calibration of redMaPPer galaxy clusters.*	*Most accurate mass-observable calibration so far with T. Varga (OPINAS PhD student) as one of two corresponding authors.*	*117*
K. Mehrgan et al. 2019, ApJ 887, 195	*A 40 Billion Solar-mass black hole in the extreme core of Holm15A, the central galaxy of Abell 85.*	*The largest supermassive black hole ever detected stellar-dynamically in the local universe.*	*36*
Khoperskov et al. 2019, A&A 622, L6	*The echo of the bar buckling: Phase-space spirals in Gaia Data Release 2.*	*Bending waves propagating in simulated barred galaxy can cause similar disk phase-space patterns as seen by Gaia.*	*65*
B. Hoyle et al. 2018, MNRAS 472, 592	*Dark Energy Survey Year 1 Results: redshift distributions of the weak-lensing source galaxies.*	*Derivation and critical validation of the redshift distribution of weak-lensing source galaxies in the Dark Energy Survey.*	*140*
T. Parikh et al. 2018, MNRAS, 477, 3954	*SDSS-IV MaNGA: the spatially resolved stellar initial mass function in~400 early-type galaxies.*	*An important step forward towards understanding the stellar IMF enigma in massive elliptical galaxies.*	*71*
S. Alam et al. 2017, MNRAS 470, 2617 (alphabetical author list)	*The clustering of galaxies in the completed SDSS-III Baryon Oscillation Spectroscopic Survey: cosmological analysis of the DR12 galaxy sample.*	*Central result of the entire BOSS project. A. Sánchez was main contributor and derived BAO and full-shape measurements and developed a method to optimally combine all results into a set of consensus constraints.*	*1550*
A. Sanchez et al. 2017, MNRAS, 464, 1640	*The clustering of galaxies in the completed SDSS-III BOSS: Cosmological implications of configuration-space clustering wedges.*	*Full-shape analysis of the final BOSS clustering measurements that led to the most accurate cosmological constraints from this sample.*	*124*
Portail et al. 2017, MNRAS 465, 1621	*Dynamical modelling of the galactic bulge and bar: the Milky Way's pattern speed, stellar and dark matter mass distribution.*	*Fitted to a variety of star count and kinematic data these are arguably still the best dynamical models for the Milky Way's bar.*	*189*
K. Chambers et al. 2016, astroph/161205560	*The Pan-STARRS1 Surveys.*	*With R. Saglia, J. Koppenhöfer and D. Farrow as tier 1 authors. R. Saglia has led the testing and debugging of the Pan-STARRS database over 10 years*	*1592*
J. Bland-Hawthorn, O. Gerhard 2016, ARAA 54, 529	*The Galaxy in Context: Structural, Kinematic, and Integrated Properties.*	*Comprehensive review of pre-Gaia Milky Way structure.*	*837*
J. Thomas et al. 2016, Nature 532, 340	*A 17-billion-solar-mass black hole in a group galaxy with a diffuse core.*	*One of the biggest black holes yet in an almost isolated galaxy: possible descendants of very luminous quasars can be found outside of modern-day rich clusters*	*81*
R. Saglia et al. 2016, ApJ, 818, 47	*The SINFONI Black Hole Survey: The black hole Fundamental Plane revisited and the paths of (co) evolution of supermassive black holes and bulges.*	*The largest sample of stellar-dynamically determined black hole masses of the last 10 years, based on VLT-AO Observations with SINFONI.*	*145*
C. Wegg et al. 2015, MNRAS 450, 4050	*The structure of the Milky Way's bar outside the bulge.*	*Unparalleled red clump star count data and analysis for the Galactic bar from multiple NIR surveys.*	*210*
D. Gruen, S. Seitz et al. 2014, MNRAS 442, 1507	*Weak lensing analysis of SZ-selected clusters of galaxies from the SPT and Planck surveys.*	*Developed important methodology which is now a standard for individual weak lensing cluster mass estimates.*	*90*
J. Thomas et al. 2014, ApJ 782, 39	*The Dynamical Fingerprint of Core Scouring in Massive Elliptical Galaxies.*	*Massive elliptical galaxies lack stars on radial orbits in their centers - the proof of core formation via binary black holes.*	*53*
J. Kormendy & R. Bender 2012, ApJS 198, 2	*A Revised Parallel-sequence Morphological Classification of Galaxies: Structure and Formation of S0 and Spheroidal Galaxies.*	*Demonstration that Spheroidals and S0 galaxies form a parallel sequence to Spiral and Irregular galaxies, connected with them via stripping and harassment.*	*263*
A. Sánchez et al. 2012, MNRAS, 425, 415	*The clustering of galaxies in the SDSS-III BOSS: cosmological implications of the large-scale two-point correlation function.*	*The paper goes beyond the analysis of the BAO peak alone and exploits the full shape of clustering measurements from the first data release of BOSS.*	*197*
R. Laureijs et al. 2011, arXiv:1110.3193	*Euclid Definition Study Report.*	*Key contributions from R. Bender and F. Grupp, both have Euclid Founder status.*	*2233*

OPINAS Personnel Structure
(f=female, i=international)

- 1 director (Bender), 1 independent group leader (Gerhard, retired March 2022)
- 4 (0f, 2i) tenured senior scientists at MPE (Saglia, Fabricius, Sanchez, Thomas)
- 2 (1f, 0i) tenured senior scientists at USM (Grupp, Seitz)
- 11 (5f, 9i) non-tenured scientists and postdocs (6 MPE, 5 USM)
- 13 (4f, 8i) PhD students (9 MPE, 4 USM)
- 5 (2f, 2i) Master students
- 1.5 (0f, 0i) tenured IT staff (MPE)
- 14 (3f, 3i) technical staff (7 MPE, 7 USM) of which 12 non-tenured 3rd-party funded (DLR-Euclid, BMBF-Micado)

OPINAS 3rd-Party Funding Since 2016

- ESA-Euclid: ~11 million Euro for Euclid NISP NIR optics and Euclid German Science Data Center (SDC) from German Space Agency (DLR)
- ELT-Micado: ~4 million Euro from the Federal Ministry for Research (BMBF)
- other projects: ~1.5 million Euro from German Science Foundation (DFG) and others

OPINAS publication and citation statistics (as of March 2022)

- ~640 refereed publications since 2011 with ~42000 citations, h=95 (~13 authors per paper)
- ~405 refereed publications since 2016 with ~19800 citations, h=63 (~14 authors per paper)
- ~250 refereed publications since 2019 with ~6100 citations, h=38 (~19 authors per paper)

(not including general data release papers from SDSS, BOSS etc.)

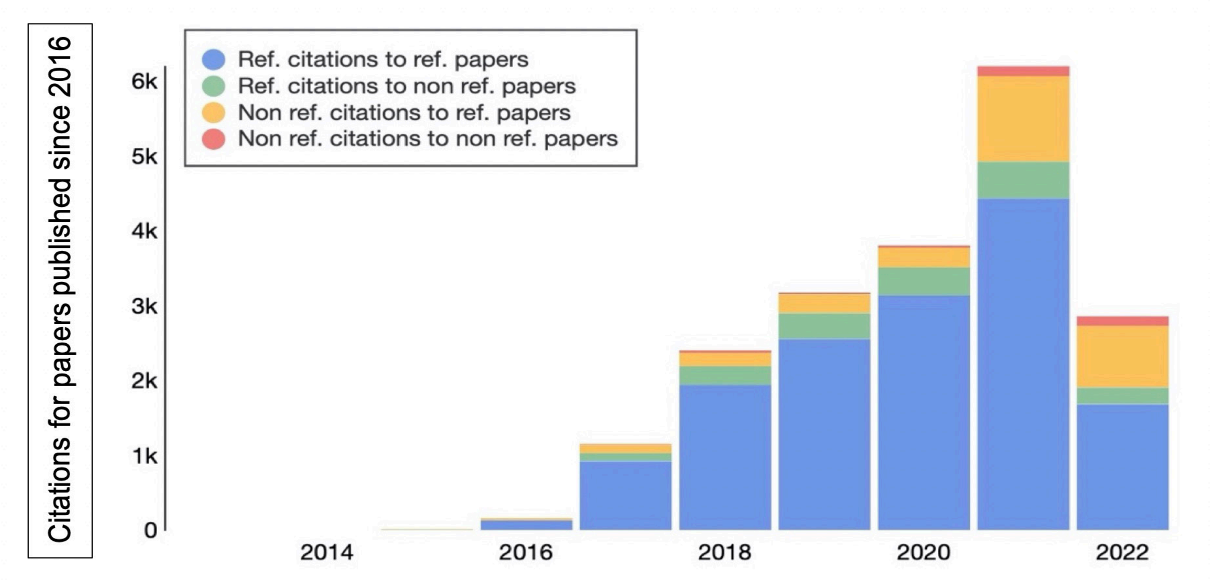

3.2 Structure, Dynamics and Stellar Population of Galaxies

Over the last years we have developed new methodology and machinery to take the analysis of the dynamics of elliptical galaxies, bulges and bars onto a new and unprecedented level of accuracy. Key elements are a new versatile deprojection code for triaxial objects, a new 3D orbit superposition Schwarzschild code (SMART) and improvements in data analysis. We demonstrated the power and reliability of the new tools by applying them to realistic N-body simulations of elliptical galaxies with black holes. Average accuracies of black hole masses and mass-to-light ratios of 10% were achieved over all projections. Together with our unique combination of deep MUSE data and adaptive-optics assisted SINFONI spectroscopy our goal for the next years is to take stellar dynamical studies onto a new level of precision. Using data from the MaNGA survey, we concluded that the initial mass function (IMF) becomes similar to that of the Milky Way at the half-light radius while bottom-heavy IMFs in galaxy centers lead to a mass excess factor of 1.5. In our sample of MUSE-observed cuspy/cored elliptical galaxies we confirmed this trend to higher mass galaxies. Moreover, we show that with an appropriate scaling factor the dynamically determined stellar mass-to-light ratio profiles agree well with state-of-the-art stellar population synthesis models. Using our new 3D deprojection code, we measured the radially resolved intrinsic triaxial shapes of brightest cluster galaxies (BCGs) from very deep photometric data, for the first time on an object-by-object basis (i.e. not just statistically). We showed that, beyond ~30kpc, the outer light of BCGs is better aligned with their clusters than with the actual central BCG body. It amounts to ~69+/-17% of the light of the main body of the BCGs. The outer triaxial shape properties of BCGs resemble those of simulated dark-matter halos, i.e. they are strongly triaxial and consistent with a formation from accretion of smaller galaxies and galactic debris. Exploiting the same very deep photometric data, we detect tens of thousands potential ultra-diffuse galaxies (UDGs) in the Coma and Abell 262 clusters. We show that UDGs do not form a distinct population, rather they overlap with non-UDG dwarf galaxies in terms of their effective radius, surface brightness and total luminosity. We apply our improved dynamical modelling tools to a sample of dwarf ellipticals of the Virgo cluster observed with our VIRUS-W spectrograph. Contrary to the expectations of ΛCDM models, we find that these galaxies have cored halos.

The morphology of most galaxies is shaped by the physics of dissipation, for example by quiescent star formation building up galaxy disks or by bursty, merger-induced star-formation leading to classical bulges or to power-law elliptical galaxies with bright centers. In contrast, the structure of the most massive galaxies is mainly the result of collisionless processes. Once the reservoir of cool gas suitable for star formation has been used up further mass growth happens via dissipationless mergers or via accretion (with reduced or no star formation). Collisions between galaxies of roughly equal mass and without significant amounts of gas leave triaxial remnant galaxies behind. Frequent kinematic misalignements or isophotal twists in massive ellipticals are the observational signs of triaxiality in their stellar body and, presumably, also in their surrounding dark-matter halos. Massive elliptical galaxies hold clues regarding many important astrophysical questions. For example, they are thought to host the most dwarf-star-dominated stellar populations (at least in their centers). Also, the properties of supermassive black-hole (SMBH) scaling relations among high-mass galaxies (both the scatter and the slope) depend on – and hence reflect – different growth mechanisms of SMBHs and their hosts.

Triaxial dynamical modelling of massive elliptical galaxies

To accurately measure the mass components of such triaxial ellipticals we have developed the new fully 3-dimensional Schwarzschild orbit-superposition code SMART (Neureiter et al. 2021) together with a triaxial deprojection code (see below). We have tested the triaxial dynamical modelling extensively on a realistic, high-resolution N-body merger simulation of two elliptical galaxies with SMBHs. High-quality observational data were created for five different viewing angles. We showed that SMART allows recovery of the stellar mass-to-light ratio and the mass of the central SMBH with a typical accuracy of 10% (Fig. 3.2.1, *see poster by B. Neureiter*). Such an accuracy is required to understand the shape of the initial-stellar-mass function (IMF) or the evolution of SMBHs and their hosts. To achieve this level of accuracy it was necessary to maximise the information content of the kinematical data and to optimise their usage. Two important aspects here are the exploration of the entire line-of-sight velocity distributions of the stars and the optimisation of the regularisation in the models. The innovative new approaches that we developed for this purpose are described below.

A particularly interesting example for a massive triaxial elliptical galaxy with a depleted stellar core is NGC 5419. This galaxy has a non-axisymmetric rotation field with a kinematically distinct core (KDC), see Fig. 3.2.2, left. Our new SMART models describe the galaxy's rotation field very well (Fig. 3.2.2, right). What is the origin of the KDC in NGC 5419 and other similar core galaxies? The triaxial models uncover that a surprisingly simple *intrinsic* rotation structure can explain the complexity that we see in projection on the sky. In-

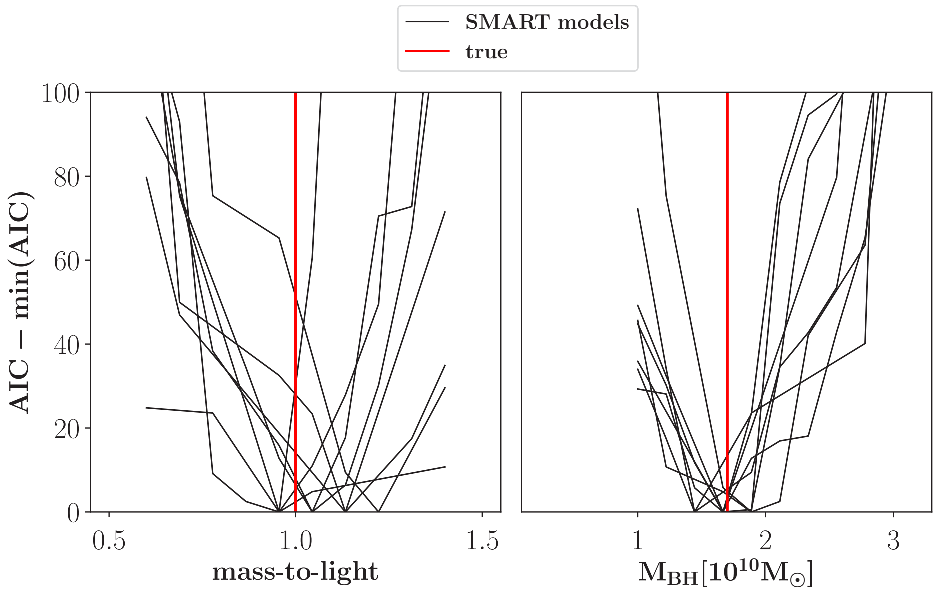

***Fig. 3.2.1** Recovery of the stellar mass-to-light ratio **(left)** and black-hole mass **(right)** of an N-body merger simulation of two elliptical galaxies with black holes. The red lines locate the true values of the merger. Black lines correspond to fits of noisy mock data for various viewing angles. The triaxial code SMART minimises a generalised form of the Akaike Information Criterion (AIC; y-axis) to find the best-fitting viewing angles, stellar M/L, black hole mass and five dark-halo parameters.*

side 8 arcsec the stars seem to populate all tube orbits in the opposite rotation direction as outside this radius (*see poster by B. Neureiter*). Recent numerical N-body simulations (Rantala, […],Thomas et al, 2019, ApJL, 872, 17) provide a stellar dynamical explanation for such a rotation reversal: Core galaxies like NGC 5419 form in dissipationless mergers. On their way to the center, the SMBHs experience a reversal of their orbits after each pericenter passage. In major mergers such a reversal leaves a footprint in the stellar remnant: the gravitational pull of the SMBHs causes a respective rotation reversal of the surrounding stars. A stellar dynamical origin of KDCs in massive elliptical core galaxies could explain why the stellar populations in KDCs and their hosts are similar.

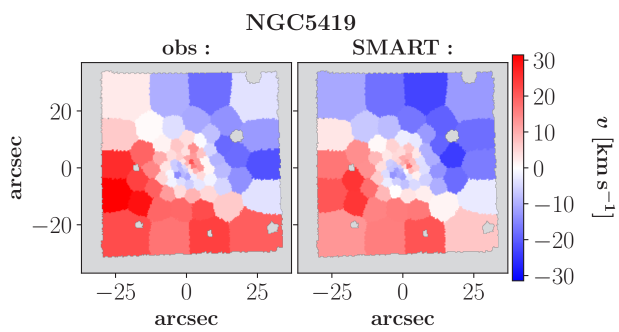

***Fig. 3.2.2** Observed rotation field of the galaxy NGC 5419 **(left)**. The galaxy has a kinematically distinct core. However, the areas on the sky with prograde motion are connected and the same holds for the areas with retrograde motion. This apparent ‚inspiral' pattern can be well explained by triaxial orbits as the SMART model on the right shows.*

Brightest Cluster Galaxies (BCGs)

Brightest Cluster Galaxies (BCGs) appear similar to massive elliptical galaxies, yet have distinct properties. BCGs are located at the centers of the most massive structures of the universe and transition into the surrounding intracluster light (ICL). We continued our study on the very deep photometric sample of local BCGs of Kluge et al. (2020, ApJS, 247, 34). Using new precise measurements of galaxy structural parameters and stellar velocity dispersions we find that the fundamental plane of regular ellipticals is different from that of BCGs. Accretion of less massive cluster galaxies increases BCG sizes but the stars in their inner regions do not "feel" this outer growth and retain their original velocity dispersion, which leads to the offset in the fundamental plane. The fact that the structural properties of the initial BCG seed or core – prior to the main outer accretion – are still imprinted in the central stellar kinematics allows an independent estimate of the accreted extra light in the outer parts. It amounts to ~69 +/- 17% of the light of the BCG, in good agreement with estimates based on photometric decomposition and with predictions from numerical simulations (*see posters by M Kluge*). This faint outer stellar light – the ICL -- grows with cluster mass, velocity dispersion and size as well as with the integrated satellite galaxy brightness. Moreover it is better aligned with the orientation of the host cluster than the BCG itself and is therefore a potential tracer of dark matter (Kluge et al. 2021, *see poster by M. Kluge*).

Previous studies have tried to determine the average intrinsic shape of massive elliptical galaxies and BCGs, mostly using statistical approaches to deproject the distribution of the observed mean galaxy ellipticities as a whole. With our newly developed non-parametric triaxial deprojection code (de Nicola et al. 2020) we could show that the viewing angles of a triaxial galaxy can be constrained purely photometrically via the deprojection. This exploits the fact that galaxies are roughly ellipsoidal and many mathematically possible viewing angles are ruled out since the implied luminosity density is unrealistically far from the observed shapes of real galaxies. By deprojecting a subsample of the Kluge et al. BCGs we measured for the first time the radially resolved intrinsic shape parameters p=b/a and q=c/a (where a,b,c are the long, intermediate and short axes) and the triaxiality parameter $T=(1-p^2)/(1-q^2)$ of massive galaxies purely from photometric data.

Most BCGs in the Kluge sample are almost maximally triaxial. While they become flatter in the outer parts, the triaxiality does not change significantly with radius. The recovered 3-dimensional intrinsic shapes of real BCGs at large radii agree well with simulated dark-matter halos in the TNG100 simulation, in fact the real galaxies are even more triaxial than the simulations. (Fig. 3.2.3, *see poster by S. de Nicola*, paper submitted). This supports the idea that the ICL is a tracer of dark-matter.

Many of the Kluge et al. BCGs have large depleted stellar cores with sizes above ~1kpc. Such large cores suggest that many of them host ultramassive black holes (UMBHs) with a mass of 10^{10} $M_\odot$ or larger. However, so far only a handful of UMBHs have been observed. We are currently using the MODS spectrographs at the LBT to collect long-slit optical spectra along the major, minor and intermediate axes BCGs galaxies where we detect a core large enough to imply the existence of a SMBH with mass 10^{10} $M_\odot$ or larger (Mehrgan et al. 2019, ApJ, 887, 195). For the subsample of BCGs lacking HST imaging we are also performing Adaptive Optics imaging in the H- and K-bands with the NIR LUCI instrument at the LBT. This sample is augmented by 8 BCGs from an ongoing MUSE follow-up program of BCGs in the Kluge et al. sample ("The search for ultramassive black holes in BCGs – Black holes with tens of billions of solar masses", PI K. Mehrgan).

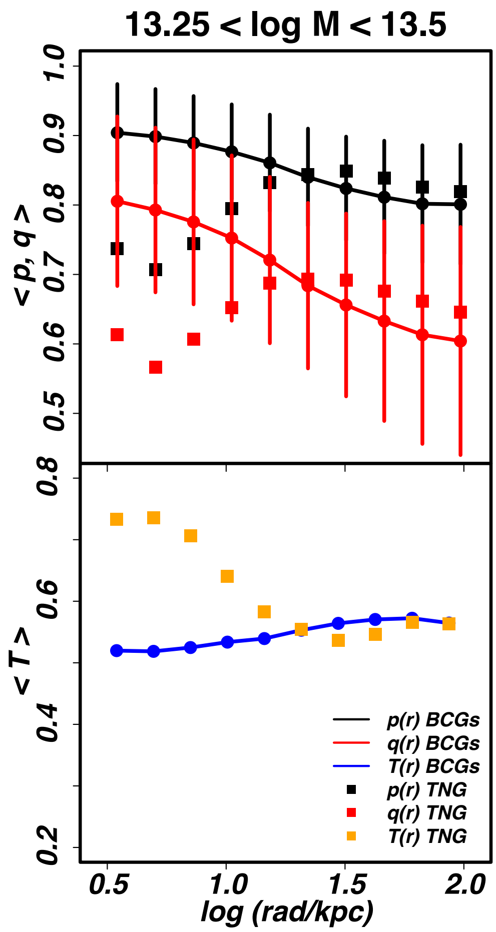

Fig. 3.2.3 Top: *Comparison between the stellar shape parameters p and q of BCGs and dark matter halos in the TNG simulation. For the BCGs we also compute the RMS in each radial bin (shown as error bar).* ***Bottom:*** *Same comparison but for the triaxiality parameter T.*

Stellar populations and the initial-stellar-mass function (IMF)

A topic highly debated in recent years is the question concerning the universality of the IMF. Original claims based on a comparison of stellar-population predictions assuming a Milky-Way-like (Kroupa) IMF with dynamical or lensing results indicated that the IMF becomes progressively more dwarf-dominated (or bottom heavy) with increasing galaxy mass or velocity dispersion. However, the mechanism driving this variation remains to be understood and these results are in tension with lensing mass estimates for nearby massive ellipticals obtaining Milky-Way-like IMFs. More recently the evidence for radial variations of the IMF within galaxies has been growing with current observations suggesting that dwarf-star dominated stellar populations are mostly confined to galaxy centers. Using data from the MaNGA survey, Parikh et al. (2018) concluded that the IMF becomes similar to that of the Milky Way at the half-light radius while bottom-heavy IMFs in galaxy centres lead to a typical mass excess factor of 1.5. In fact, the IMF within galaxies correlates with the stellar velocity dispersion, but this local IMF-σ relation within galaxies is

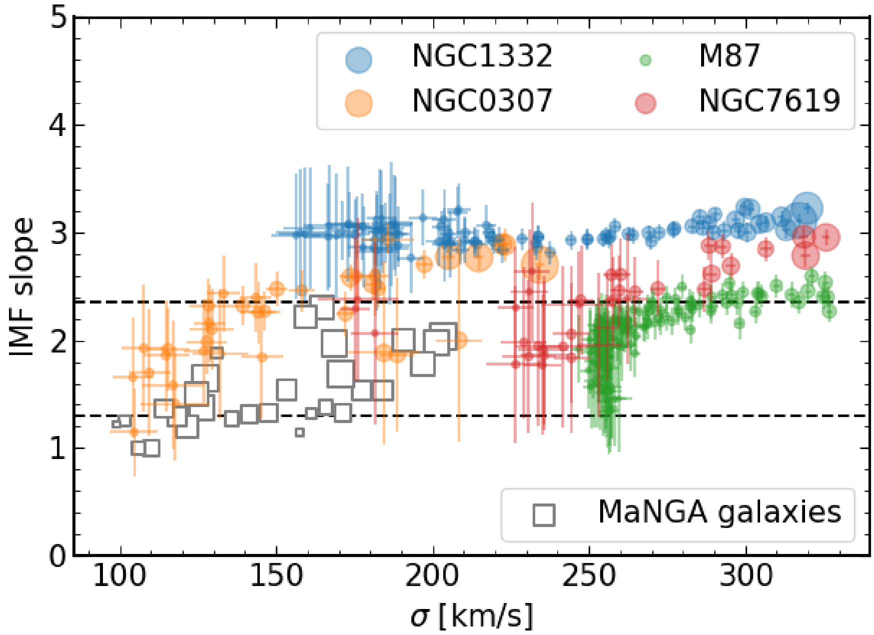

Fig. 3.2.4 *The low mass IMF slope, between 0.1 - 0.5 $M_\odot$, is shown against the velocity dispersion. New MUSE galaxies are shown in color, grey symbols show three different mass bins of MaNGA galaxies. The symbol size decreases with radii, large symbols represent galaxy centres. The dashed lines mark the Salpeter (2.35) and Kroupa (1.3) IMF.*

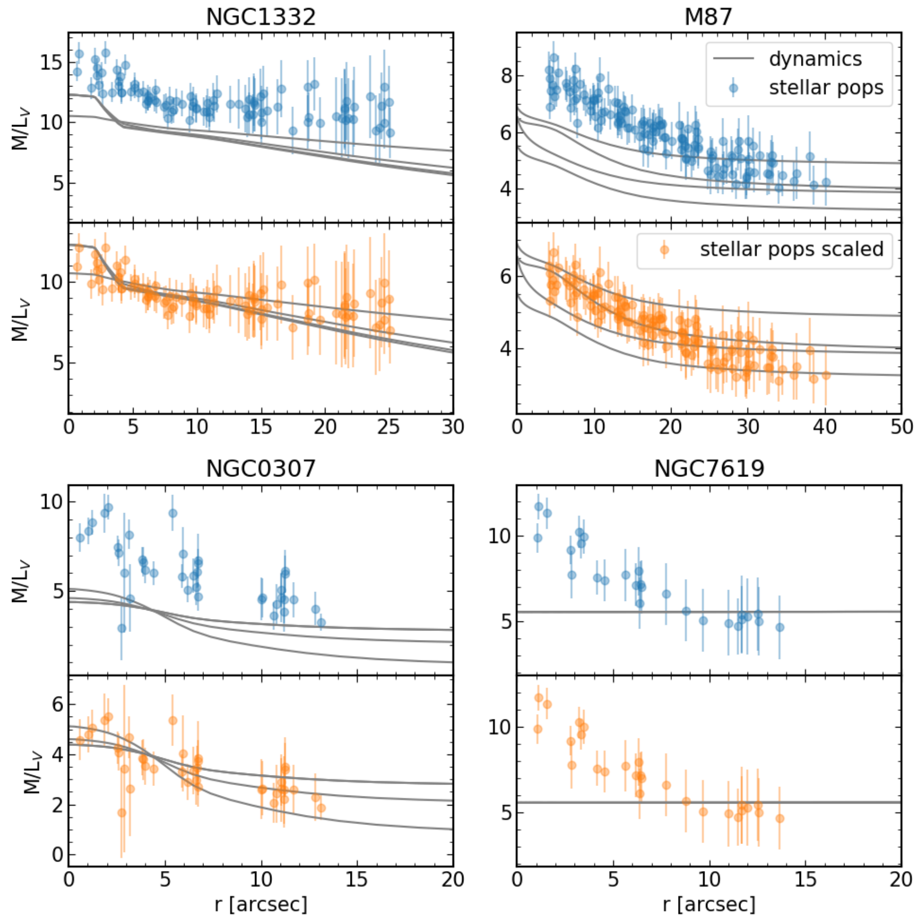

Fig. 3.2.5 *M/L ratios in the V band are shown for four galaxies as a function of radius. Blue symbols with 1-sigma error bars show the results from stellar population modelling of the Voronoi-binned spectra, while grey lines show the dynamical results (projected along the line-of-sight) for the galaxies split into quadrants. The bottom panel for each galaxy shows the result after rescaling the M/L ratios (orange symbols) to match the dynamical profiles.*

steeper than the global relation with galaxy mass. The MaNGA analysis (grey squares in Fig. 3.2.4) was based on stacked spectra and while the IMF radial gradient was independent of the stellar population model used, the absolute value of the IMF slope differed. To remove the ambiguities in current IMF studies a detailed comparison of independent constraints on the IMF (e.g. from stellar population synthesis (SSP) models and via mass constraints from stellar dynamics) needs to be performed on an object-by-object basis. Furthermore, we can now measure radially resolved IMF variations from SSP models in individual galaxies. Our advanced dynamical models also allow us to measure non-parametric stellar M/L gradients from kinematical data. Detailed agreement between both methods is required to settle the question about the universality of the IMF and to understand its physical origin.

In our MUSE program 'Constraining the initial-stellar-mass function in massive galaxies' (PI J. Thomas) we have observed a sample of nearby massive galaxies split into fast-rotating power-law galaxies and slowly-rotating core galaxies. Power-law ellipticals form through dissipative merges probably giving rise to strong population gradients. Core galaxies form in gas-poor mergers which tend to wash out gradients. On the stellar population side we make optimum use of the available information via full spectral fitting with Conroy et al. 2017 models. Our new results (colored points in Fig. 3.2.4; *see poster by T. Parikh*) show a continuation of the trend found by Parikh et al. 2018, and also offer a detailed look into higher mass galaxies. The correlation between the IMF slope and the velocity dispersion is seen, while individual galaxies might represent the true scatter in this relation. On the dynamical side, using advanced analysis techniques we find gradients in the two power-law galaxies NGC1332 and NGC0307 (Fig. 3.2.5, *see poster by K. Mehrgan*). Of the two core galaxies NGC7619 and M87 only the latter shows a significant gradient (Fig. 3.2.5; for M87 we use archival MUSE data, *see poster by J. Thomas*). We find that while gradients between the two methods agree, there is a systematic offset such that the stellar population M/L is biased to larger values. We calculate scaling factors for each galaxy (M87 – 0.77, NGC1332 – 0.77, NGC0307 – 0.57) which when applied to the stellar-population values, eliminate this offset. Possible systematics in the stellar population results could arise due to incompleteness of the underlying stellar library, partially unaccounted broadening effects and inaccurate correction for the atmospheric telluric absorption. For the dynamical models, uncertainties in M/L can arise from systematics in the dark-matter halo models or from triaxiality. With additional high quality data and our advanced dynamical modelling techniques we are now in a position to systematically address these questions in the near future.

Precise measurements of element abundances are necessary since any uncertainty in these parameters translates to an uncertainty in the IMF. Moreover, they constrain galaxy formation and evolution and provide clues regarding the nucleosynthetic production pathways of elements. Parikh et al. 2019, 2021 derived individual chemical element abundances of C, N, Mg, Na, Ca, and Ti from stacked MaNGA spectra. The elements C, Mg, and Ti were found to trace each other both as a function of galaxy radius and galaxy mass, suggesting constant star formation timescales. Conversely, N and

Ca are generally offset to lower abundances. The under-abundance of Ca compared to Mg implies delayed enrichment of Ca through Type Ia supernovae, whereas the correlated behaviour of Ti and the lighter α elements, suggest contributions to Ti from Type II supernovae. Strong negative radial gradients for [Na/Fe] correlated with the total metallicity, suggest a metallicity-dependent Na enrichment. The abundances of elements show similar gradients with the local velocity dispersion, independent of morphology, hence these relations appear to be driven by galaxy mass or velocity dispersion rather than galaxy type.

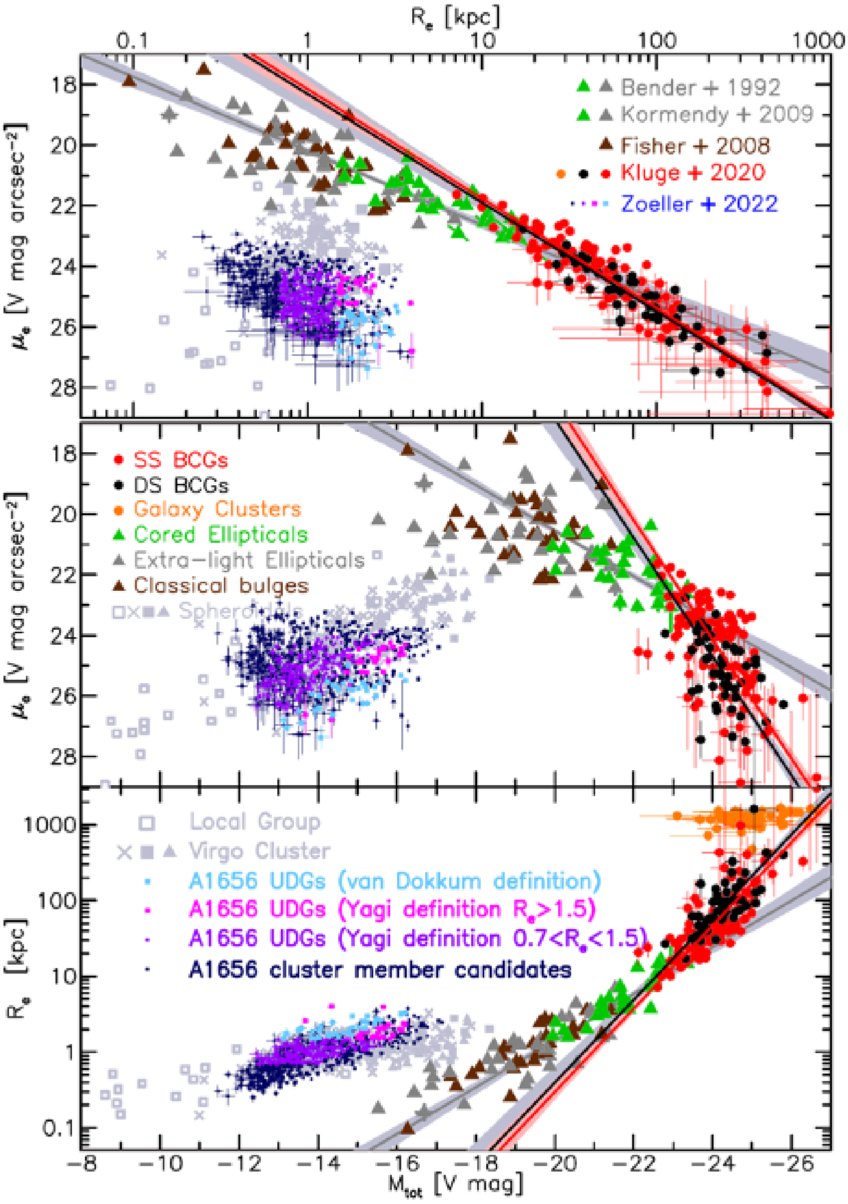

Fig. 3.2.6 *The structural properties of the Wendelstein sample of dwarf galaxies in Abell1656 (Coma cluster) in comparison to spheroidals, ellipticals, BCGs and galaxy clusters from the literature. UDGs are not distinct from non-UDG dwarf galaxies. The Figure also shows how BCGs (DS=double Sersic, SS=single Sersic) bridge the gap between regular elliptical galaxies and the properties of galaxy clusters.*

Advances in Data Analysis

For the kinematical analysis of our MUSE and MODS samples we use a newly developed spectral fitting code WINGFIT to measure LOSVDs non-parametrically (*see poster of J. Thomas*). An extension of the classical Akaike Information Criterion (AIC) of model selection has been derived and implemented to optimise the smoothing (*see posters by M. Lipka, J. Thomas*, paper submitted). This novel approach can be applied to any non-parametric or parametric model with potentially many astrophysical applications. We have implemented the extended model selection based on effective number of parameters also in SMART and in our 2-dimensional axisymmetric Schwarzschild code. We have shown that accounting for the varying number of effective parameters in these complex orbit models is crucial to obtain unbiased results for the various mass components and, also, for the viewing angles (Lipka 2020, Lipka and Thomas 2021, *see poster by M. Lipka*). The combination of robust LOSVD shapes and the improved constraining power from the advanced model selection opens the door to precision dynamics at the 10% level that we are aiming at (*see posters by M. Lipka, B. Neureiter*).

Advanced methods and unique data – achieving the next level of precision in stellar dynamics

Our approach of pushing the limits in accuracy and precision of dynamical models is particularly matched to our VLT-MUSE sample of massive early-type galaxies. In comparison to triaxial models of larger statistical samples like SAMI, MaNGA or CALIFA our data and analysis stand out in terms of

- **High Spatial Resolution.** Existing adaptive-optics assisted VLT-SINFONI observations allow us to include SMBHs in the analysis.
- **Very deep MUSE data** – designed to yield a spatially resolved S/N of >200 per Å for IMF studies – allow us to extract 10x more kinematical constraints at a S/N level that is still 10x higher than in existing samples. For the first time, we can measure the central density slope and triaxiality of DM halos as well as mass-to-light-ratio gradients.
- **Next Generation Data Analysis.** Non-parametric deprojections, non-parametric LOSVDs and the advanced unbiased model selection technique overcome the limitations of currently used parametric Multi-Gaussian luminosity models and Gauss-Hermite LOSVDs as well as biases in the traditional χ2-based mass determination.

- **N-body Verification.** Based on realistic, independent N-body merger simulations we have optimised and verified our triaxial modelling setup. Using an up to 10x higher orbital resolution than typically adopted in the analysis of larger samples we can reach the accuracy required to probe the scatter in SMBH scaling relations and the IMF variation in massive galaxies.

Dwarf galaxies

Recently, the class of ultra-diffuse galaxies (UDGs) has been introduced based on their very low central surface brightness and yet comparably large sizes. We systematically surveyed the Coma cluster and Abell 262 with the Wendelstein Wide Field Imager to investigate how UDG structural parameters relate to other non-UDG dwarf galaxies. Tens of thousands of potential UDGs were analysed. We show that UDGs do not to form a distinct population. In terms of their effective radius, surface brightness and total luminosity they overlap with non-UDG dwarf galaxies. The original UDG definition of van Dokkum or the extended one by Yagi identify dwarf galaxies with the largest effective radius R_e and lowest effective surface brightness μ_e at a given luminosity M_{tot} (Fig. 3.2.6; *see poster by R. Zöller*).

Dwarf galaxies are important laboratories to study the inner properties of dark matter (DM) halos. The cold dark matter picture predicts steep central logarithmic DM density slopes around -1 (or even steeper through baryonic contraction). With our advanced dynamical modelling methods we are now in the position to measure unbiased dark-matter density slopes. Our current models favour dark matter halos with flat cores (*see poster by M. Lipka*). This not only holds for the dwarf ellipticals but also for the more massive galaxies in our MUSE sample.

As for the massive galaxies we complement the dynamical analysis with an investigation of the stellar populations. Our dwarf galaxies are metal poor with high abundances and some age gradients (*see poster by A. Jouili*).

Galaxies with bars

A galaxy population that – apart from the Milky Way and M31 -- remains rather unexplored in terms of dynamical modelling and for which we know comparably little about the orbital structure, SMBHs and stellar masses are barred galaxies. Roughly half of all disk galaxies have bars, with some possessing additional inner bars and inner cold disks. Other, tri-dimensional components sticking out the disk structure can be a classical bulge (possibly originating from merger events) or a pseudo- or boxy/peanut (B/P) bulge (generated during the buckling phase of bars). Within the HST and VLT-MUSE program "Determining the kinematic and stellar population nature of composite bulges in the local universe", P.I. P. Erwin, we are studying a representative sample of disk galaxies to understand the properties of their substructures. First results are published by Erwin et al. (2021) and Blumhoff (2021), *see poster by M. Blumhoff*. Comparing the stellar populations of an un-barred and barred galaxy, the former shows a clear gradient in stellar populations whereas the latter appears more uniform. The barred galaxy has recent star formation and young stars at all radii, whereas the un-barred galaxy has mostly an old centre, and younger metal-poor stars in the outer regions (*see poster by T. Parikh*). Triaxial modeling with an upgraded version of SMART is in preparation.

Selected References:

Blumhoff, M., 2021, Master Thesis, LMU
de Nicola et al. 2020, MNRAS, 496, 3076
Erwin, P. et al. 2021, MNRAS, 502, 2446
Kluge, M. et al. 2020, ApJS, 247, 43
Kluge, M. et al. 2021, ApJS, 252, 27
Lipka, M, 2020, Master Thesis, LMU
Lipka, M., Thomas, J., 2021, MNRAS, 504, 4599
Neureiter, B. et al. 2021, MNRAS, 500, 1437, 5
Parikh, T. et al. 2018, MNRAS, 477, 395
Parikh, T. et al. 2019, MNRAS, 483, 3420
Parikh, T. et al. 2021, MNRAS, 502, 5508


Jens Thomas


Taniya Parikh


Roberto Saglia

(Other OPINAS team members include R. Bender, M. Fabricius, A. Jouili, M. Lipka, M. Kluge, K. Mehrgan, B. Neureiter, S. de Nicola, R. Zöller. Former team members include M. Blumhoff, P. Erwin, G. Pentaris)

3.3 Large Scale Structure and Cosmology

The dramatic progress in the accuracy of cosmological observations in the last decades has transformed cosmology into a data-driven field. These new data have revolutionised our view of the Universe, allowing us to build a clear picture of its evolution, and that of the structures within it. However, this picture presents us with some of the most profound puzzles in contemporary physics. Galaxy clustering measurements are amongst the most powerful tools to shed light on these outstanding problems. The activities of the OPINAS group at MPE cover all aspects of the analysis of galaxy redshift surveys. The overarching goal of these studies is to maximise the scientific return from studies of the large-scale structure (LSS) of the Universe to reach the goal of genuine precision cosmology in the analysis of present and future surveys.

Galaxy redshift surveys

Thanks to galaxy redshift surveys such as the Baryon Oscillation Spectroscopic Survey (BOSS, Dawson et al., 2013) and the extended Baryon Oscillation Spectroscopic Survey (eBOSS, Dawson et al., 2016), clustering analyses have become one of the most powerful cosmological probes. New surveys such as the Hobby-Eberly Telescope Dark Energy Experiment (HETDEX, Gebhardt et al 2021, Hill et al 2021), the Dark Energy Spectroscopic Instrument (DESI, DESI Collaboration 2016), the Prime Focus Spectrograph survey (PFS, Takada et al., 2014), and the ESA space mission Euclid (Laureijs et al. 2011) offer us a unique opportunity for precision cosmology. At the same time, these datasets demand an urgent revision of traditional analysis methods. OPINAS members are actively developing the tools required to fully exploit the bounty of survey data that will soon be available.

Data analysis: from observations to galaxy clustering statistics

After playing a major role in the analysis of data from BOSS, OPINAS members continued contributing to the analysis of the quasar sample from eBOSS Data Release 16 (DR16), which contains 343,708 spectroscopically confirmed quasars between redshift $0.8 < z < 2.2$. In comparison with our previous analyses using DR14, the final sample doubled the number of objects as well as the survey area. We led the clustering analysis in configuration space by measuring the two-point correlation function and decomposing it using the Legendre polynomials (Hou et al., 2021). We also performed detailed analyses of the observational systematic errors that could affect these measurements, and contributed to the construction of the final set of weights that are applied in all clustering analyses of this sample.
After the completion of eBOSS, our data analysis activities are now centred on the ongoing HETDEX project. HETDEX is a spectroscopic survey conducted from the McDonald Observatory in Texas. The survey uses an array of 74 integral field units (Hill et al. 2021) attached to the 10 m Hobby-Eberly telescope to take spectroscopic measurements over two regions with areas of 390 deg^2 and 150 deg^2. Each shot results in spectra measured from 33k fibres, which are searched for emission line galaxies (ELGs). We expect to detect a sample of 10^6 high-redshift ($1.9 < z < 3.5$) Lyman-alpha emitting galaxies (LAEs) and a comparable number of

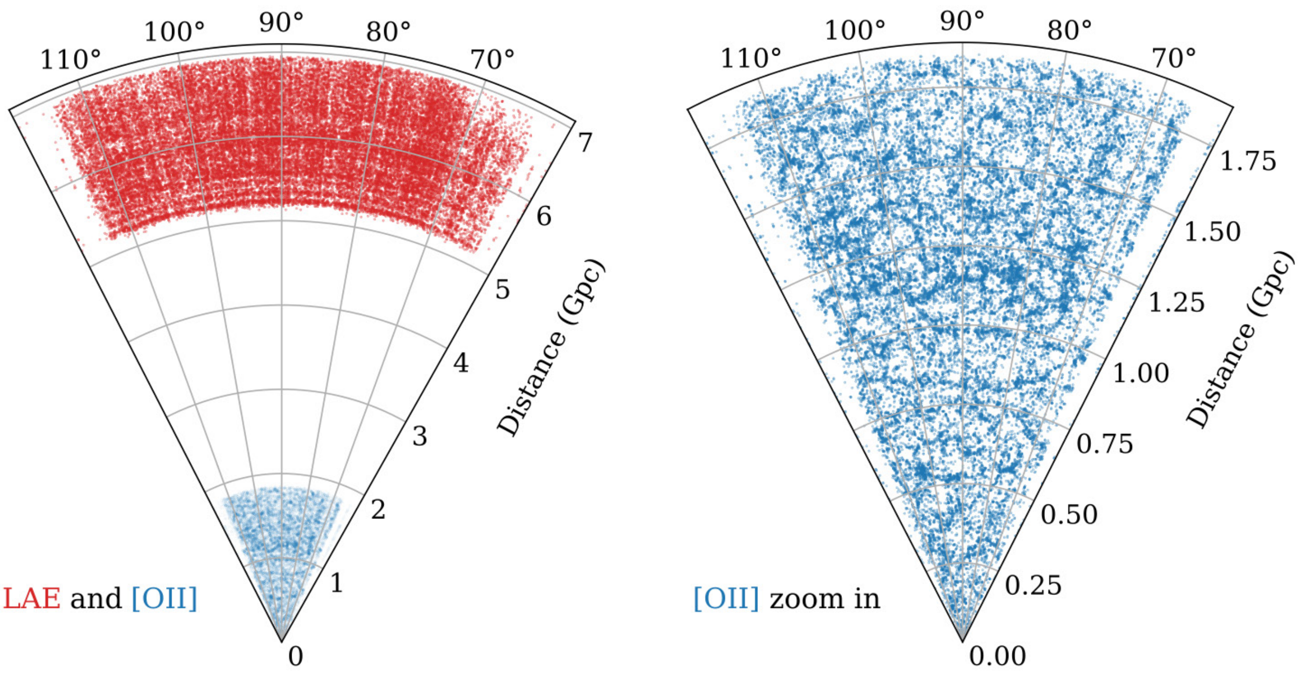

Fig. 3.3.1 Left: *cone plots of HETDEX detections of LAEs (red) and [OII] emitting galaxies (blue) on an early catalogue.* ***Right:*** *zoom in on the [OII] emitters, where the cosmic web is clearly visible.*

low redshift (z < 0.5) [OII] emitting galaxies, without the target preselection used in traditional spectroscopic surveys. The LAE sample from HETDEX will be the largest of its type by orders of magnitude. The survey is roughly 50% complete, and about 30% of the data has been processed. Figure 3.3.1 shows cone plots of ELGs detected in the survey.

The primary goal of HETDEX is to use the clustering statistics of the ELGs to probe the expansion and growth of structure rates of the Universe (see Gebhardt et al. 2021 for details). The constraints from the LAE sample will nicely complement upcoming and existing surveys, which focus on lower redshifts. OPINAS is a major partner in HETDEX and we have made vital contributions to the project. On the infrastructure side, we have developed observation scheduling and quality control software used in the observatory. We have also made large contributions to the data reduction by, e.g., visually classifying detections, testing methods of sky subtraction, carrying out quality control on data products and contributing to the astrometry pipeline. Several of our members have been awarded science architect status. OPINAS is also heavily involved in high-end science. We used simulations of HETDEX to study the impact of [OII]-emitter misclassification on the clustering statistics of the LAE sample (Farrow et al. 2021). This work involved developing a significant part of the source classification pipeline of HETDEX (Davis et al., in prep). We are also leading the work on the first clustering measurements of HETDEX ELGs (Farrow et al., in prep) and working closely with collaborators on measurements of the faint LAE luminosity function (Jeong et al., in prep). We contributed forecasts to the scientific requirements document of HETDEX, and intend to use realistic HETDEX simulations to forecast the final constraints from the survey (Farrow et al. in prep.). Finally, we lead the studies of the selection function of HETDEX, the probability a galaxy will be detected as a function of position, wavelength and source properties. The selection function is a key ingredient to nearly all statistical studies and will be vital for the primary science goals. We added Python modules that return completeness estimates from an input sky position and wavelength to the application programming interface of HETDEX, and an early version has already been used in studies of the luminosity function of bright LAEs (Zhang et al. 2021).

Future HETDEX work will reap the benefits of our contributions. Concrete plans relying on LSS include constraining cosmological parameters with the LAE and [OII] samples, direct imaging of the cosmic web via intensity mapping, and estimating the ELG halo-occupation distribution. The unique insights we have from our contributions to both technical and higher-end aspects of the survey place us in an excellent position to lead some of the key cosmological and large-scale structure studies of the HETDEX survey.

Modelling clustering statistics

Accessing the cosmological information encoded in LSS observations requires accurate theoretical models. The main problem in galaxy clustering analyses is the modelling of scales in the non-linear regime, where the growth of density fluctuations is extremely difficult to predict. Two additional obstacles are the relation between the galaxy and matter distributions, known as galaxy bias, and the impact of the redshift-space distortions (RSD) caused by the peculiar velocities of the galaxies. We have contributed to developing and testing state-of-the-art models of non-linearities, bias,

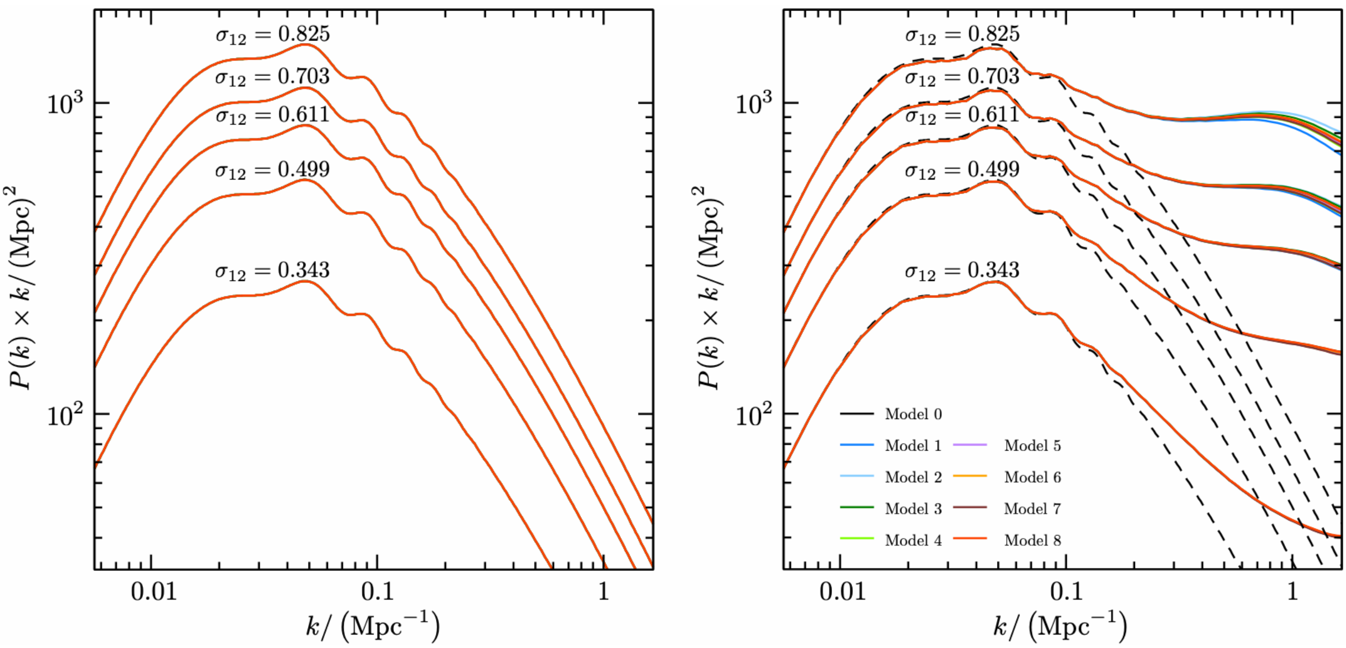

Fig. 3.3.2 Left: *linear matter power spectra of different cosmologies covering a wide range of evolution parameters evaluated at the redshifts at which their values of σ_{12} match the values indicated by the labels.* ***Right:*** *matter power spectra of the same models measured from N-body simulations (solid lines) compared against their linear-theory predictions (dashed lines).*

and RSD (e.g., Sánchez et al. 2017, Hou et al. 2021). These models were validated by a series of non-blind and blind analyses of mock BOSS and eBOSS samples, and were found to provide unbiased constraints.

Future datasets such as DESI and Euclid will require higher accuracy in our cosmological predictions. A key ingredient to extend our models further into non-linear scales is to test the regime of validity of our description of galaxy bias. In Eggemeier et al. (2020) and Pezzotta et al. (2021), we tested the commonly used one-loop bias expansion for the power spectrum using a variety of synthetic galaxy samples. We found that a four-parameter model (linear, quadratic, cubic non-local bias, and constant shot noise) provides a robust modelling up to k_{max} = 0.35 h/Mpc. In Eggemeier et al. (2021), we extended these tests by performing a joint analysis of the real-space power spectrum and bispectrum. We included non-linear triangle configurations for the bispectrum, thanks to a complete one-loop description of galaxy bias consistent with what is commonly used for the power spectrum. The comparison of this extended model against the leading order ("tree-level") bispectrum shows that the one-loop corrections roughly double the applicable range of scales of the bispectrum (from k_{max} = 0.17 h/Mpc at tree level to k_{max} = 0.3 h/Mpc), leading to a 1.5 - 2x improvement on parameter constraints.

Alternative statistics that encode compressed higher-order information can complement the standard two-point measurements. These include the Minkowski functionals (MFs), which describe the geometry and topology of the cosmic density field. In Lippich & Sánchez (2021) we developed MEDUSA, an accurate method for estimating the MFs of three-dimensional point distributions based on their Delaunay tessellation. These measurements are complementary probes of non-linearities in the density field. Another route to access cosmological information beyond the global two-point statistics is to perform a density-split analysis. In Paillas et al. (2021), we suggested splitting the galaxy density field according to the local density, and cross-correlating those densities with the entire galaxy field. The combination of a series of cross-correlation functions from split densities can capture the non-Gaussianity of the density field, leading to improved cosmological constraints over those of standard analyses.

Despite steady progress in the modelling of non-linearities, the perturbation theory approaches commonly used in clustering analyses are bound to break down in the highly non-linear regime. Accessing the rich information content of non-linear scales requires completely overhauling current LSS methods. High-resolution cosmological simulations are an ideal tool for this task. In recent years, emulators based on N-body simulations have become a common tool to describe the non-linear power spectrum (e.g., Euclid Collaboration et al., 2021). Due to their high computational cost, the number of simulations used in the emulator design must be kept to a minimum. This makes it difficult to explore a high-dimensional cosmological parameter space while maintaining accurate predictions.

In Sánchez et al. (2021), we presented a new approach to describe statistics of the non-linear density field that can help with this task. We classified cosmological parameters into two groups, shape parameters, which determine the shape of the linear matter power spectrum, $P_L(k)$, and evolution parameters, which only affect its amplitude at any given redshift. We showed that the time evolution of $P_L(k)$ in models with identical shape parameters but different evolution parameters can be mapped from one to the other by relabelling the redshifts corresponding to the same values of σ_{12}, which is defined as the RMS linear mass variance in spheres of radius 12 Mpc (Sánchez 2020). Fig. 3.3.2 illustrates this relation. The left panel shows $P_L(k)$ for nine cosmologies with the same shape parameters and a wide range of evolution parameters (including non-flat universes and different dynamical dark energy models). When they are evaluated at the redshifts that correspond to the same values of σ_{12}, their linear power spectra are indistinguishable. Using N-body simulations, we showed that the same evolution mapping relation can be applied to the non-linear density field with high accuracy (right panel of Fig. 3.3.2). The deviations seen in the highly non-linear regime can be described in terms of the different structure formation histories experienced by each model to reach the same value of σ_{12}. This relation drastically reduces the number of parameters required to describe the non-linear power spectrum.

Sánchez et al. (2021) also showed how this relation can be exploited to build an emulator of the non-linear P(k) whose predictions can be applied to an arbitrary choice of evolution parameters and redshift. The smaller number of parameters involved in the emulation, and the fact that no explicit sampling of z is required, results in more accurate predictions. We are currently producing an emulator, which we call *Cassandra*, that will serve as a proof of concept of this design. The same approach can be applied to alternative statistics such as, e.g., the mass function, or density-split clustering measurements, opening up the possibility to perform a battery of cosmological tests based on a consistent theoretical description.

Cosmological parameter constraints

The final step in galaxy clustering analyses is to link theory and observations to obtain cosmological constraints. In Hou et al. (2021), we derived distance and growth rate measurements from the QSO sample from eBOSS DR16. We also combined our results with those of the Fourier-space analysis into a set of consensus constraints, whose cosmological implications were explored in Alam et al. (2021).

In Tröster et al. (2020), we revisited our analysis of the final BOSS (Sánchez et al., 2017) and showed that

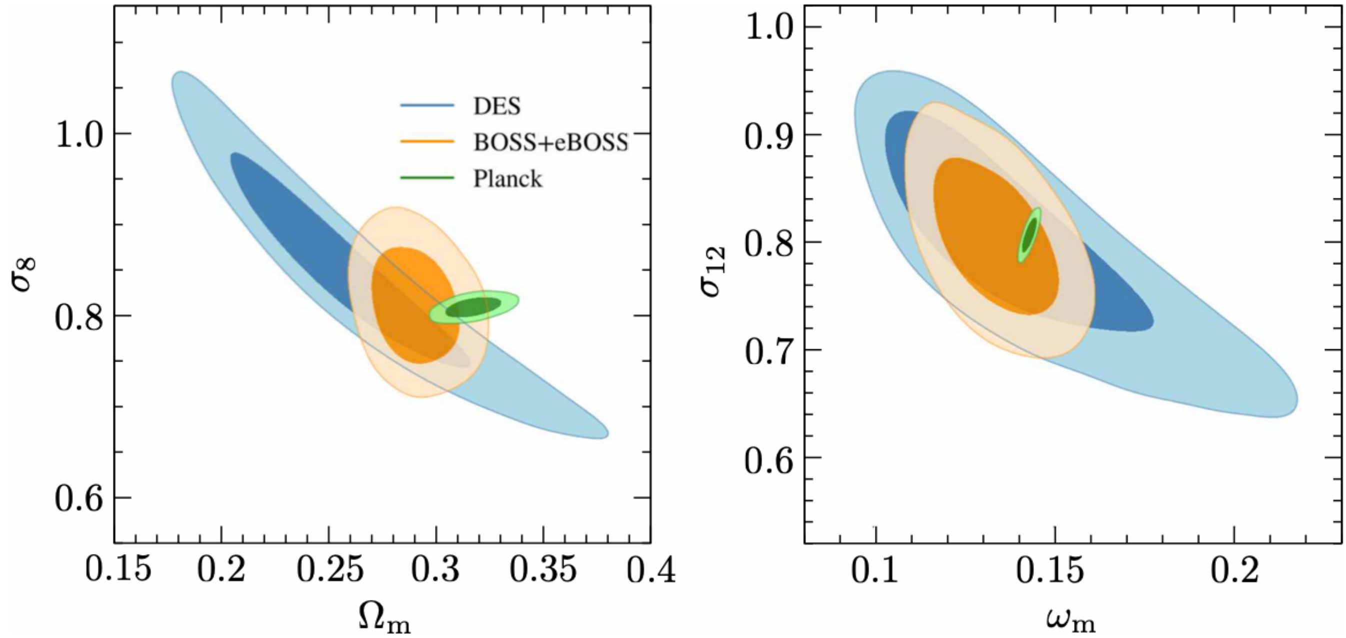

***Fig. 3.3.3** Constraints recovered from Planck (green), DES (blue), and BOSS + eBOSS (orange) under the assumption of a ΛCDM cosmology on the parameters $\Omega_m - \sigma_8$ (**left**), and $\omega_m - \sigma_{12}$ (**right**). While DES prefers lower values of σ_8 than Planck, they are in excellent agreement when considering σ_{12}.*

these measurements can constrain flat ΛCDM parameters without relying on other data sets. Additionally, Tröster et al. (2020) combined BOSS data with cosmic shear measurements from KiDS (Hildebrandt et al., 2020). This study served as a pathfinder for the joint analysis of the same BOSS data and the latest KiDS dataset (KiDS-1000, Kuijken et al., 2019), which more than doubles the survey area from previous KiDS samples (Heymans et al., 2021; Joachimi et al., 2021; Tröster et al., 2021).

Intriguingly, all weak lensing measurements to date yield lower values of σ_8, the linear-theory RMS mass fluctuation in spheres of radius 8 Mpc/*h*, than what is predicted from the best-fitting ΛCDM model to the cosmic microwave background (CMB) data from Planck (e.g., Hikage et al., 2019; Abbot et al. 2021; Heymans et al., 2021). This discrepancy is commonly known as the "σ_8 tension". Interestingly, the value of σ_8 recovered from BOSS by Tröster et al. (2020) is also 2.1σ low compared to Planck's prediction, with the difference increasing to 3.4σ when the KiDS measurements are added.

The σ_8 tension is usually described as a difference in the amplitude of density fluctuations preferred by Planck and that recovered from low-redshift probes. However, this interpretation is incorrect. In Sánchez (2020), we reviewed some of the complications that originate from the common practice of expressing cosmological measurements and theoretical predictions in units of Mpc/*h*. A crucial problem caused by these units is related to the normalisation of the power spectrum in terms of σ_8. The drawback of using σ_8 is that the reference scale R = 8 Mpc/*h* depends on *h*. For datasets with different posterior distributions on *h*, the obtained constraints on σ_8 represent an average of σ(R) over different scales, leading to different, not necessarily consistent, results. This issue can be avoided by normalising *P(k)* using a reference scale in Mpc. Sánchez (2020) proposed to use σ_{12} = σ(R = 12 Mpc). For models with *h* ~ 0.67 as suggested by Planck data, σ_{12} has a similar value to σ_8, but they differ for other values of h.

In Semenaite et al. (2021), we performed a joint analysis of our measurements from the final BOSS and eBOSS. We focused on ΛCDM parameters that are independent of *h*. The left panel of Figure 3.3.3 shows the constraints in the $\Omega_m - \sigma_8$ plane derived from Planck, the Dark Energy Survey (DES), and the combination of BOSS and eBOSS. For the values of Ω_m selected by Planck, DES data prefers lower values of σ_8. However, these results are sensitive to the differences in the posterior of h, which is much wider in the case of DES than for Planck. The right panel of Fig. 3.3.3 shows that, when this difference is eliminated using the physical matter density, ω_m, and σ_{12}, all these probes are in good agreement. This indicates that the tension seen in the left panel is the result of the differences in the constraints on h and not of a discrepancy in the amplitude of density fluctuations perceived by these datasets.

In the coming years, Euclid will allow for joint analyses of accurate clustering and weak lensing measurements. OPINAS is heavily involved in Euclid and we have made key contributions to the project and are set up to participate efficiently in its science exploitation (see the specific section on Euclid for more details).

Outlook

Building upon our leading contributions to the cosmological interpretation of galaxy surveys, we are developing novel techniques by combining analytic models with high-resolution numerical simulations to unlock access to a wealth of cosmological information out of reach of present-day methods. These tools will allow OPINAS to have a leading role in the scientific exploitation of some of the most exciting datasets of the coming years, which have the potential to transform our understanding of the properties of dark energy, enable novel tests of general relativity, or accurately estimate the total neutrino mass.

Ariel Sánchez

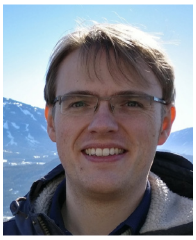

Daniel Farrow

(Additional collaborators from the OPINAS group: R. Bender, J. Graciá Carpio, M. Esposito, M. Fabricius, F. Grupp, U. Hopp, M. Lippich, A. Pezzotta, R. Saglia, A. Semenaite, J. Snigula, and J. Weller. Former team members include: J. Hou)

Selected References:

Abbott T.M.C., et al., 2021, Phys. Rev. D., 105, 023520
Alam S., et al., 2021, Phys. Rev. D, 103, 083533
Dawson K. S., et al., 2013, AJ, 145, 10
Dawson K. S., et al., 2016, AJ, 151, 44
DESI Collaboration et al., 2016, arXiv:1611.00036
Eggemeier A., et al., 2020, Phys. Rev. D, 102, 103530
Eggemeier A., et al., 2021, Phys. Rev. D, 103, 123550
Euclid Collaboration, Knabenhans M., et al., 2021, MNRAS, 505, 2840
Farrow D., et al, 2021, MNRAS, 507, 3187
Gebhardt K., et al 2021, ApJ, 923, 217
Heymans C., et al., 2021, A&A, 646, A140
Hill G. J., et al., 2021, AJ, 162, 298
Hikage C., et al., 2019, PASJ, 71, 43
Hou J., et al., 2021, MNRAS, 500, 1201
Joachimi B., et al., 2021, A&A, 646, A129
Kuijken K., et al., 2019, A&A, 625, A2
Laureijs R., et al., 2011, arXiv e-prints, p. arXiv:1110.3193
Lippich M., Sánchez A.G., 2021, MNRAS, 508, 3771
Paillas E., et al., 2021, MNRAS, 505, 4
Pezzotta A., et al., 2021, Phys. Rev. D, 104, 043531
Sánchez A. G., et al., 2017, MNRAS, 464, 1640
Sánchez A. G., 2020, Phys. Rev. D, 102, 123511
Sánchez A. G., et al., 2021, MNRAS submitted, arXiv:2108.12710
Takada M., et al., 2014, PASJ, 66, 1
Tröster T., et al., 2020, A&A, 633, L10
Tröster T., et al., 2021, A&A, 649, A88
Zhang Y., et al, 2021, ApJ in press, arXiv:2105.11497

Additional selected publications on LSS by the OPINAS group during the past three years:

Euclid Collaboration, Blanchard A., et al., 2020, A&A, 642, 191

3.4 Gravitational Lensing and Dark Matter

In recent years, low redshift, large scale structure clustering and weak lensing (WL) LCDM constraints have reached – for the density fluctuation amplitude σ_8 and the matter content Ω of the Universe – similar precision as high redshift LCDM-CMB constraints (see, Abbott et al. 2021, Phys. Rev. D., 105, 023520, for the Dark Energy Survey (DES) collaboration and Aghanim et al. 2020, A&A, 641, A6, for the Planck collaboration). While KiDS-survey analyses reported tensions between these constraints at the 2–3 sigma level (Heymans et al. 2021, A&A, 646, A140), the Abbott et al 2021 results are lower than but consistent with the Planck fluctuation amplitude. At the same time, present day Hubble constant (H_0) predictions based on CMB and LCDM seem to be in conflict with measurements in the local and low redshift universe (Freedman et al. 2021, ApJ, 919, 16 and references therein). Taken together, this raises speculations whether LCDM has to be ruled out as a valid description of our Universe.

Therefore, in order to further probe and constrain LCDM or alternative models, we a) participated in collaborations which investigated the consistency of WL signals across different surveys, b) were significantly contributing to the DES-Year1 cluster cosmology work, c) led the creation of a cluster weak lensing simulation tool that allows to study biases in cluster weak lensing analysis methods, d) developed more sophisticated analysis methods which extract higher signal to noise constraints from weak lensing data and are sensitive to nuisance parameters of previous analyses, e) using the LMU/USM Wendelstein observatory, we monitored two strong lensing systems and carried out time delay analyses to increase the sample with lensing based Hubble constant estimates and, f) prepared for the future larger data sets which come available to us from the Rubin (LSST) and Euclid surveys.

Are weak lensing cosmic shear surveys consistent?
In “Lensing without borders”, DES, KiDS, HSC, SDSS and CFHTLenS survey members have studied together whether the “excess surface density” signal for galaxies selected by the same photometric criteria (red galaxies) are consistent for the different surveys (Leauthaud et al. 2021). Since this quantity involves measuring the redshifts and shapes of the lensed galaxies, it is sensitive to the most relevant weak lensing measurement biases, which also enter the shear correlation functions. The estimates from the different survey teams are compatible over various radial ranges and foreground galaxy redshifts, the two higher redshift bins indicate biases depending on survey depths and potentially stellar density, but the errors are covered by the systematic budgets of the survey analyses. The follow up analysis by Amon et al. 2022 (submitted to MNRAS) updates the above measurements with the

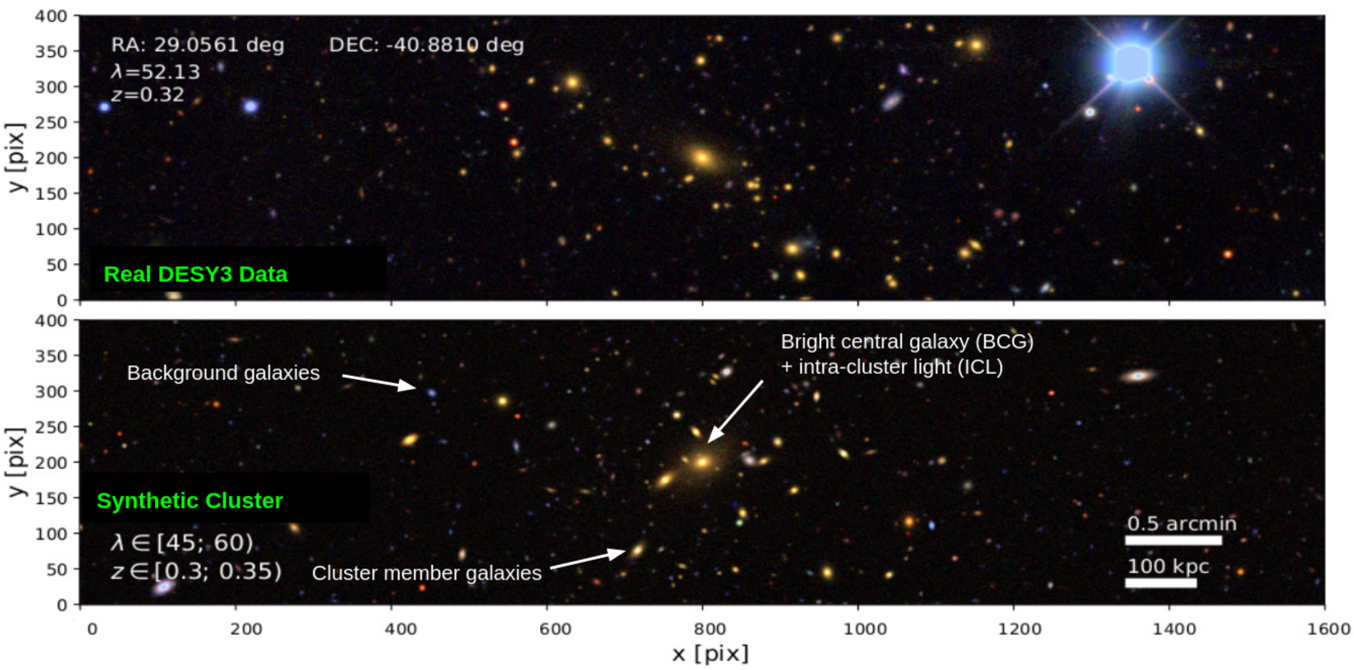

Fig. 3.4.1 *Real and synthetic galaxy cluster side by side.* ***Top:*** *gri color composite image of a real redMaPPer galaxy cluster in the DES Y3 footprint.* ***Bottom:*** *gri color composite image of a synthetic galaxy cluster representative of $\lambda \in [45; 60)$, $z \in [0.3; 0.35)$. This cluster image is generated according to the statistical learning method of Varga et al. 2021.*

most recent data releases of current weak lensing surveys. It demonstrates consistency between the galaxy mass profiles measured from lensing and the profiles predicted from galaxy clustering (from spectroscopic surveys) and a halo occupation distribution model, based on cosmological models with values preferred by both, either the Planck satellite or most recent weak lensing surveys constraints. T. N. Varga is a tier 1 author in these two DES publications and was in charge of measuring "excess surface density" for the galaxies for the DES Y1 and Y3 data releases.

Cluster weak lensing: cosmological constraints and systematic uncertainties

With the publication of the first year cosmology results from the masses and abundances of galaxy clusters from the DES by Abbott et al. 2020 (alphabetical author list, including substantial contribution from T. N. Varga), it has been revealed that optically detected galaxy cluster based cosmology studies reached a systematic uncertainty-dominated regime and hence cosmological constraints based on abundances and masses of such samples are biased. The efforts of our group have thus been oriented to address and overcome the challenges of this new systematic uncertainty frontier. As part of this, in Pereira, Palmese and Varga et al. 2020 we performed the calibration of an alternative, stellar mass based galaxy cluster mass proxy, which holds the promise of potentially being more robust against a variety of projection and selection biases.

While weak gravitational lensing provides a practical method to study the mass properties of galaxy clusters, it involves a unique challenge for validating these measurements for a multitude of reasons: Cluster lines of sights deviate from the cosmic median line-of-sight in terms of the abundance and properties of (cluster member) galaxies resulting in increased blending among light sources, they host a diffuse intra-cluster light (ICL) component influencing photometry, and induce characteristically stronger gravitational shears at small scales. The impact of the above effects can be best characterised in end-to-end tests going from mock observations to recovered cluster masses.

We developed a novel unsupervised machine learning algorithm to create synthetic galaxy cluster observation scenarios, which are trained directly from a combination of observational datasets (Varga et al. 2021, Fig. 3.4.1): We measure and model the photometric properties of galaxy clusters and their sky environments from the Dark Energy Survey Year 3 (DES Y3) data in two bins of cluster richness $\lambda \in [30; 45)$, $\lambda \in [45; 60)$ and three bins in cluster redshift ($z \in [0.3; 0.35)$, $z \in [0.45; 0.5)$ and $z \in [0.6; 0.65)$. This wide field data is augmented with deep-field imaging data, which is used to extrapolate galaxy populations beyond the limiting magnitude of DES Y3 and calculate the properties of cluster member galaxies via statistical background subtraction. New independent realisations of mock galaxy clusters are created as random draws from a distribution function, which are then rendered into synthetic images in the same format as actual survey observations. Synthetic galaxy cluster images are generated from real observational data, and thus are independent from the assumptions inherent to cosmological simulations with "ad-hoc" description of the galaxy-halo connections and photometric properties of the galaxies. Our algorithm is however designed to be trivially adaptable for extra information that could come from numerical simulations of galaxy and galaxy cluster formation, or from spectroscopic or multi-wavelength observations, and to correct for survey incompleteness. New realisations of synthetic clusters are then created at minimal cost, which will enable upcoming cluster weak lensing analyses to generate the large number of images needed to characterise systematic uncertainties in cluster mass measurements.

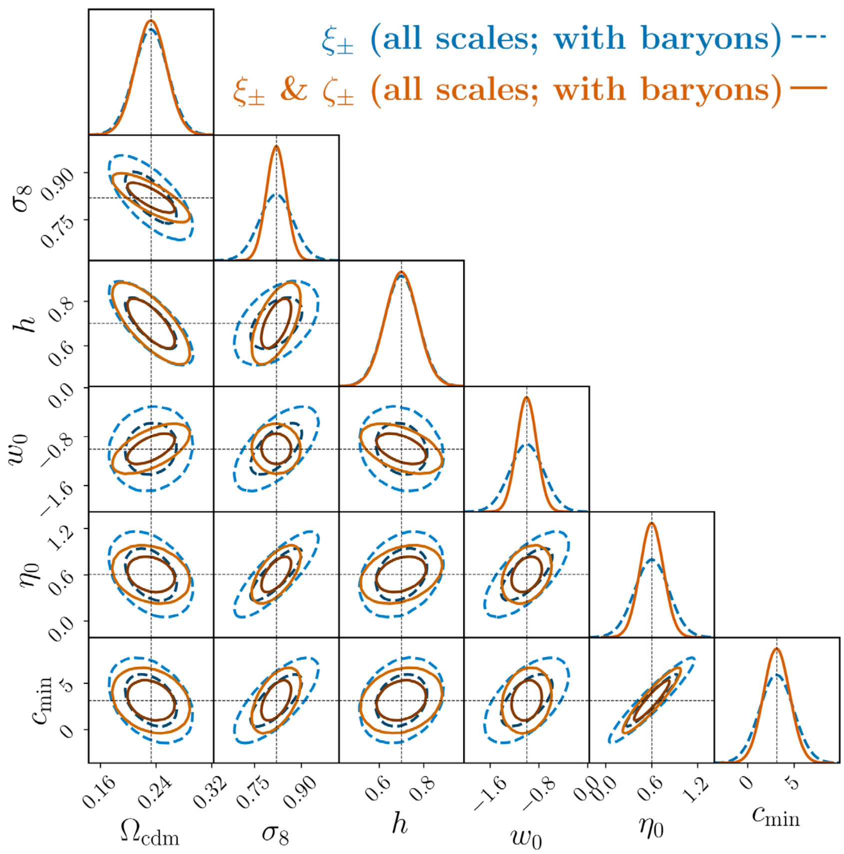

Fig. 3.4.2 Marginalised 1- and 2-dimensional Fisher constraints for four cosmological parameters Ω_{cdm}, σ_8, h, w_0 and two baryonic feedback parameters η_0, c_{min} for a Dark Energy Survey like weak lensing mission. The results are shown in dashed blue and solid orange ellipses for the $\xi_\pm$ and combined $\xi_\pm$ & $\zeta_\pm$ analyses, respectively; the black dotted lines mark the fiducial values. It is clear that the addition of $\zeta_\pm$ leads to improved constraints on all the parameters compared to $\xi_\pm$ analysis alone. Adapted from Figure 8 of Halder & Barreira 2022.

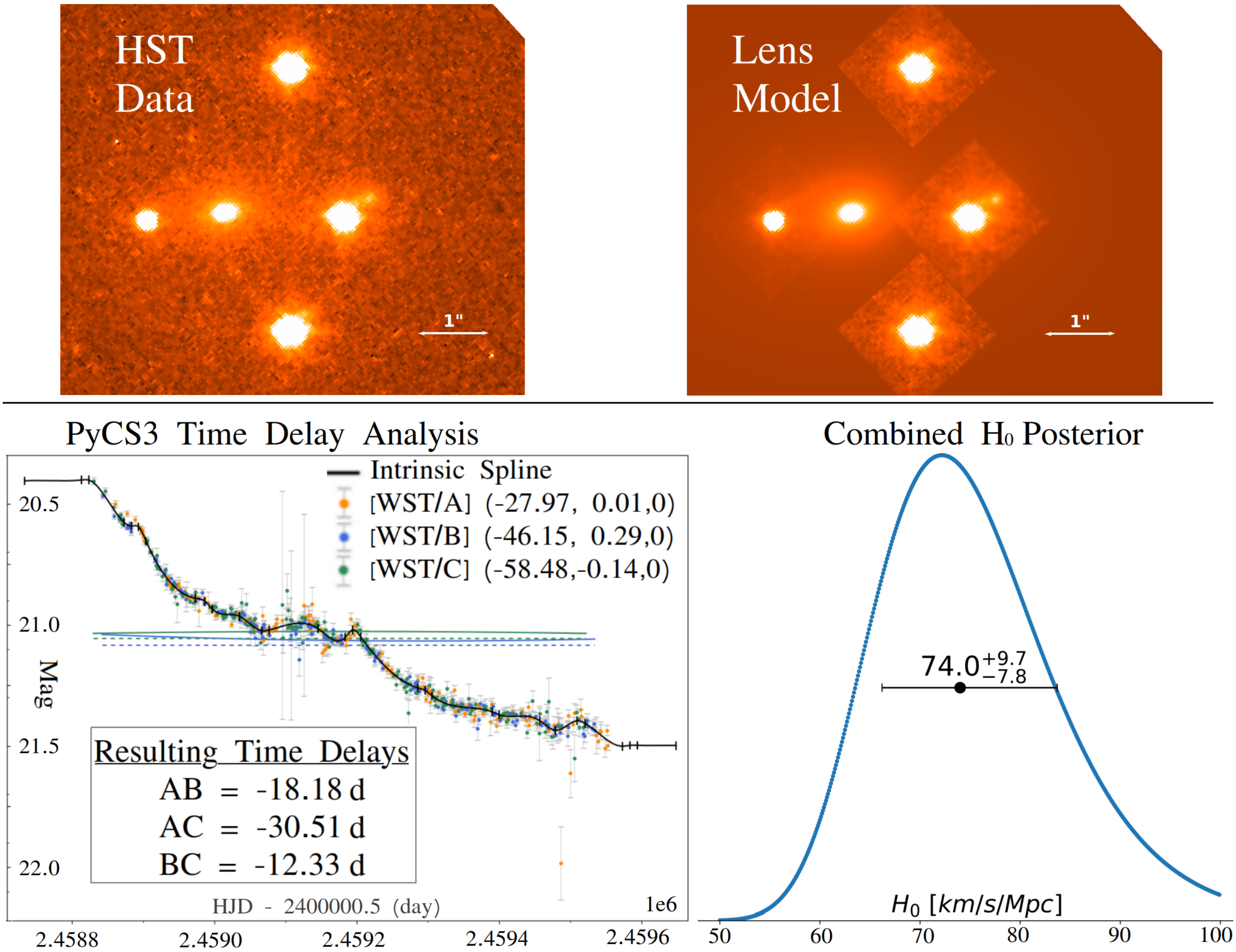

Fig. 3.4.3 ***Top left:*** *HST observation in the F475X filter;* ***Top right:*** *our lenstronomy model for the lensing system in the F475X filter.* ***Bottom left:*** *black line: spline fit to the QSO intrinsic light curve in g' filter; colored points: all light curve data points of the three brightest images, shifted by their time delays and lensing magnifications; colored lines: best fit spline fits for the slowly varying part of the microlensing effect towards each of the 3 images.* ***Bottom Right:*** *Combined posterior for the Hubble constant.*

The synthetic cluster images can then be analysed in the same way as observations to quantify errors and biases. This algorithm will also be important for the interpretation of Euclid data. The method of Varga et al. 2021 allowed Stella Seitz (as PI) and her postdocs and students to join the LSST Dark Energy Science Consortium of Rubin through an accepted in-kind contribution. We will adapt and incorporate the above approach into the data processing pipelines of LSST DESC.

Novel statistical methods to extract more information from LSS weak lensing surveys

Statistical analyses of weak lensing data allow us to directly probe the large-scale structure in our Universe and enable us to address key questions about the nature of dark matter, dark energy, gravity and complex astrophysical baryonic processes. The majority of cosmic shear analyses performed to date are based on the shear 2-point correlation functions (PCFs) ($\xi_\pm$). However, the cosmic shear field is non-Gaussian distributed, and therefore, there is additional, independent, information stored in its higher-order moments. Hence, the need for exploring methods which probe the higher-order information in the vast amounts of observed data obtained by weak lensing surveys is of paramount importance. However, the measurement and modelling of higher-order lensing statistics remains a challenging enterprise. Recently, in Halder et al. 2021 and Halder & Barreira 2022, we have proposed a particularly promising higher-order statistic — the integrated shear 3-point correlation function ($\zeta_\pm$) — which can be measured directly from cosmic shear data by correlating 1-point aperture mass statistics with 2-point shear correlation functions measured within apertures distributed across a survey footprint. Both the ingredients can be measured easily using existing, well-tested numerical algorithms which are routinely employed for the calculation of the 2PCF $\xi_\pm$. Having developed a rigorous theoretical model for $\zeta_\pm$ we have found through simple Fisher matrix forecast analyses that already for a Stage-III weak lensing mission such as the DES, the data combination of $\xi_\pm$ & $\zeta_\pm$ can lead to substantial improvements in parameter constraints on both cosmological and astrophysical (e.g. baryonic processes which affect the distribution of dark matter on small scales) parameters, compared to standard analyses with $\xi_\pm$ alone (see Fig. 3.4.2). With the Master thesis of Gong we have also prepared the analysis framework for extending the $\zeta_\pm$ analysis towards constraining the sum of neutrino masses from cosmic shear data. In general, our works underline the importance of cosmic shear studies beyond the conventional 2PCF and the investigation of $\zeta_\pm$ in particular for current and upcoming weak lensing surveys.

Are Hubble constant estimates at low and high redshift conflicting LCDM? – Increasing the number of strong lensing systems with local H_0 estimates by monitoring them with the 2m Wendelstein telescope

For intrinsically varying sources like QSOs, strong gravitational lens systems allow to measure the gravitational time delays and thus the Hubble constant. Precisions for individual systems depend on the modelling of lens features, source variability, photometric precision and cadence of the monitoring and can vary, in the best cases, between 2.5 and ~10%. A combination of 7 such systems yielded a formal Hubble constant error of 2% (Millon et al. 2020, A&A, 639) and a value of 73.3km/s/Mpc. However, Birrer et al. 2020 (A&A 643, 165) showed that this holds only when assuming that density profiles of lens galaxies are power law-like: if one allows for a degeneracy mimicking cored profiles the above precision reduces to an accuracy of 8% for the combined sample. Hubble constant estimates can be made more accurate if profiles of elliptical galaxies (fulfilling the selection function of strong lensing systems) are known more precisely and if the numbers of such systems with precise time delays can be increased.

For about 2 years we have therefore been monitoring SDSJ1433+6007 and PSJ1721+8842 with the 2m telescope of our Wendelstein Observatory in the Bavarian Alps. Both systems are quadruply lensed QSOs. We show results for the first system below (Queirolo et al. in prep.). Data have been obtained in the g'-band with an average cadence of 4 days and a median PSF of 1.07", and, using our data reduction (Kluge et al. 2020, APJS, 247) and difference imaging pipelines (Gössl and Riffeser, 2002, A&A, 381) we obtained light curves which were then analysed with PyCS3 of the CosmoGRail collaboration (Millon et al., 2020, JOSS, 5(53)). For the strong lensing model we have analysed archival HST data in several optical and NIR-filters using Lenstronomy (Birrer and Amara, 2018, PDU, 22) and modelling the density profile of the lensing galaxy as a power law.

Combining the posteriors for the Fermat potential differences and the light curve time delay measurements, we were able to constrain the Hubble constant to 74.0 km/s/Mpc with a precision of 12% (see Fig. 3.4.3). A more precise measurement will be possible once the QSO's intrinsic light curve shows more features relative to the currently very strong, but almost power law-like decline (altered by microlensing).

Selected References:

Abbott, T.M.C. et al., 2020, Phys. Rev. D, 102, 023509, (https://arxiv.org/pdf/2002.11124.pdf), (DES Y1 Cluster mass and abundance cosmology)
Amon, A. et al. 2022, MNRAS, submitted (https://arxiv.org/abs/2202.07440) (with Varga, T. N. as Tier 1 author)
Gong, Z., 2021, Master Thesis, LMU
Halder, A., 2020, Master Thesis, LMU
Halder, A., Friedrich, O., Seitz, S., Varga, T.N., 2021, MNRAS, 506, 2, (https://arxiv.org/pdf/2102.10177.pdf)
Halder, A. & Barreira, A., 2022, MNRAS, submitted (https://arxiv.org/pdf/2201.05607.pdf)
Leauthaud, A. et al., 2022, MNRAS, 510, 4, (https://arxiv.org/pdf/2111.13805.pdf) ("Lensing Without Borders", with Varga, T.N. as 8th co-author).
Pereira M. E. S, Palmese A., Varga T. N., et al., 2020, MNRAS, 498, 4, (https://arxiv.org/abs/2006.ers10162)
Queirolo G., Seitz, S., Riffeser, A., Kluge, M. et al. 2022, in prep.
Varga, T.N., Gruen, D., Seitz, S. et al., 2021, MNRAS, 504, 4, (https://arxiv.org/pdf/2102.10414.pdf)


Stella Seitz


Tamas Varga


Anik Halder


Giacomo Queirolo

Other OPINAS team members include: L.Z. Gong (PhD student), A. Riffeser (senior USM staff), M. Kluge (PD), R. Bender, U. Hopp, A. Barthelemy (PD, joined in 2022), D. Rufer (master student)

3.5 EUCLID

With its launch in 2023 Euclid (ESA) will be transformational to modern cosmology. It will probe the structure of the universe by both, the largest ever study of the distance-redshift relationship of galaxies and through a weak lensing survey that directly measures the gravitational distortions on the images of galaxies as their light traverses the matter distribution in the universe. For this Euclid will observe over 6 years the entire extragalactic sky and obtain optical and near infrared images and spectroscopic information over 14.000 square degrees. OPINAS played a key role in the design of the telescope and led the construction of the near infrared channel. The latter will host some of the largest refractive optics every launched to space for any civil space mission. OPINAS also operates the German Euclid science data center that will analyze about a tenth of the data stream from the space probe itself but is also responsible for validating and coadding the ground-based imaging data for the mission. Also, by conducting a significant effort to obtain spectroscopy at the VLT and LBT telescopes we play a significant role in calibrating photometric redshifts, which are crucial for the weak lensing science. Further, we contribute significantly to the preparation of the scientific exploitation of the Euclid dataset through participation in several science working groups and task forces that address the control of systematics.

NISP Instrument

Optical design and system engineering as well as the near infrared optical channel imaging optics of the ESA/Euclid mission are in the responsibility of MPE. Since the hardware has been delivered and integrated at the system prime LAM Marseille in late 2019 test campaigns at instrument level (2020) and on pay-load-module level (2021) have been completed successfully. Tests have shown excellent performance of both the spectroscopic and the photometric channel of the NISP near infrared spectrometer and photometer. An issue with one of the four gratings can be resolved by slightly adapting the survey strategy. Actually, the well above specification performance of our NISP optics helps mitigating this issue as well and generates space to have a well above specification PLM performance expectation. Fig. 3.5.2 shows the measured spot quality in relation to the requirement for the Y, J H photometric bands of EUCLID NISP. The shaded data represents the instrument, the bold data the instrument plus telescope performance. The MPE developed method of combining computer generated holograms (CGH) with accurate tactile coordinate measuring technology (CMM) has proven extremely successful in the alignment of optical systems to single micron accuracy, leading to close to diffraction limited performance of the MPE built optics.

Fig. 3.5.1 The integrated Euclid Structural and Thermal Model (STM) ready for test

Currently the as-built model and the in-flight prediction model for NISP are built up and correlated with measured data at MPE. Goal of these models is to allow in flight debugging in case we see any non-expected behaviour and to allow for detailed simulations prior to the first data coming from the spacecraft. In addition the correlated model will provide a more detailed insight in the PSF as it is not bound to the finite detector sampling of 0.3 arc seconds in the near-infrared instrument.

German Science Data Center

MPE hosts the German Science Data centre (SDC-DE) for the Euclid space mission. As one of nine data centres that are distributed across Europe and the US it will store and analyse data from the space probe itself but also carries the additional responsibility of making ground-based data available to the project. The latter is crucial as Euclid's weak lensing science requires very precise photometric redshifts for lensing sources. For this, data from the DES, Rubin, and the UNIONS survey are ingested, coadded and uploaded into the Euclid science archive resulting in what will likely be the single largest collection of ground-based imaging data. Particular emphasis is given to the validation of the stringent Euclid requirements with regard to the data quality, in particular the photometric accuracy. The Science Ground Segment (SGS) conducted a series of so-called scientific challenges over the past years.

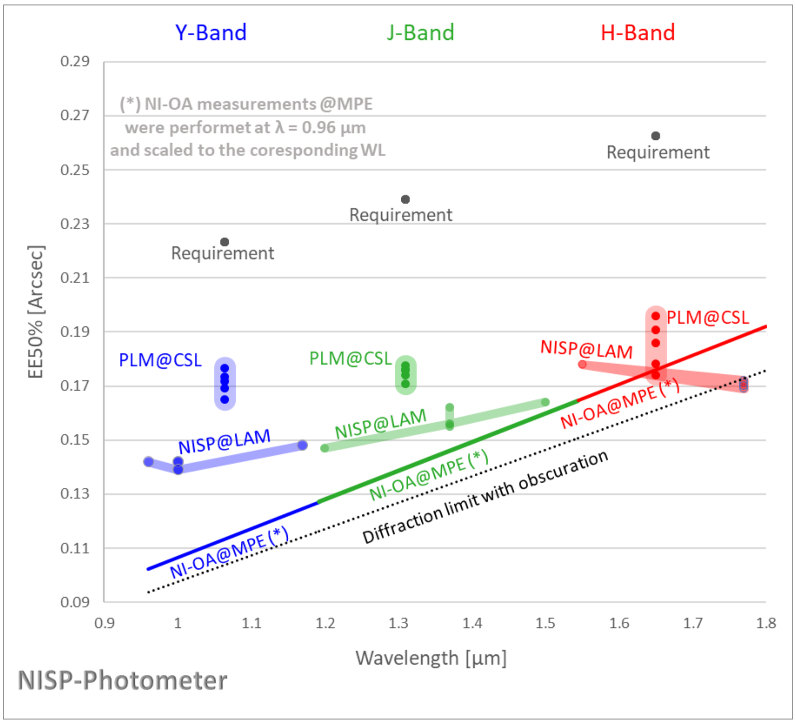

Fig. 3.5.2 *Instrument and pay-load-module test results compared to the requirment for the NISP photometer channel. Tests on optics level at MPE, on instrument level at LAM Marseille and on PLM level at CSL Liège are shown.*

With increasingly larger simulated sky coverage these initially targeted the integration of the various different Euclid processing functions into the central orchestration of Euclid, but have with the 7th and 8th challenge in 2020 and 2021 started to increasingly address the scientific integrity of the participating pipelines. SC8 simulated 150 sq. degrees on the sky starting from the Euclid flagship cosmological simulation which were projected into images and spectra for all Euclid space and ground based channels. SDC-DE contributed 25% of the overall computing resources to the SGS during this challenge. In 2022 the SGS pipelines and infrastructure will undergo the Operational Rehearsal and the Readiness Review which will address the fitness of the SGS for operations of Euclid after launch in 2023.

Towards Meeting the Photometric Redshift Requirements

Our activities for OU-PHZ focused on the spectroscopic calibration of photometric redshifts. In Guglielmo, Saglia et al. 2020 we published the results of the KMOS part of the dedicated ESO Large Program. We continued these efforts using the LUCI spectrographs at the LBT. We measured new high-quality spectroscopic redshifts for 251 galaxies, filling 41 SOM (self-organizing map) cells without calibration and almost doubling the spectroscopic redshifts for 153 cells; a related paper has been submitted to A&A. For further details refer to the poster by Saglia et al. R. Saglia and S. Kruk continued the assessing of the spectra of the Geneva spectroscopic database that will provide the final calibration of the Euclid photometric redshifts. Furthermore, S. Kruk has been active in the Euclid galaxy morphology working group, see Poster by Kruk et al.

Scientific Groundwork

OPINAS is also heavily involved in the preparation for the scientific exploitation of Euclid data. We have a strong presence in the Galaxy Clustering Science Working Group of, where in recent years we have led several teams such as the Likelihood Work Package or the Systematic Errors Tiger Team (2017). We also coordinated the Inter Science Working Group Task Force for Forecasting (IST:F), which produced updated cosmological forecasts for the mission, based on galaxy clustering, weak lensing, and their combination (Euclid Collaboration et al., 2020). The Fisher forecasts codes produced within this group were instrumental as part of the internal Science Performance Verification 2 exercise. We also led the IST for the Likelihood (IST:L) until April 2021, when we completed a milestone with the internal release of the first version of the Cosmology Likelihood for Observables in Euclid (CLOE), the likelihood modules that will be used for the joint analysis of all Euclid probes. Besides contributing to the next release of CLOE, we are also leading a key paper focused on the construction of the covariance matrices for galaxy clustering two-point statistics, which is the main potential source of systematic errors in the likelihood function (see the specific section on LSS and cosmology for more details).

Selected References:

Guglielmo, V., Saglia, R.P. et al. 2020, A&A, 642, A192
Saglia, R.P. et al. 2022, submitted to A&A
Euclid Collaboration, Blanchard A., et al., 2020, A&A, 642, 191

Frank Grupp

Max Fabricius

Roberto Saglia

Ariel Sánchez

(Other OPINAS team members include R. Bender, S. Kruk, S. Seitz, T. Varga, R. Zöller. Former team members include Postdocs A. Galametz and V. Guglielmo)

3.6 MICADO – Multi AO Imaging Camera for Deep Observations

OPINAS Work Packages

MICADO is the first light instrument for the ESO Extremely Large Telescope (ELT). Combined with the Multi-Conjugate Adaptive Optics Relay MAORY, MICADO will deliver diffraction-limited images in the infrared wavelength range. It will equip the ELT with a high (1.5 mas/px) and low resolution (4 mas/px) imager, a medium resolution spectrograph (R~10000) covering a broad wavelength range (J-K Band) and a high contrast imaging mode. The OPINAS group is one of the partners of the MICADO Consortium and is responsible for the development of the instrument control electronics, control and preparation software and the cryogenic Main Selection Mechanism (MSM). During the past three years, we concentrated our efforts in detailing the approved design to bring it to the level necessary for the Final Design Review (FDR). Because of the complexity of the MICADO instrument and limited resources on ESO side, FDR has been split into 4 parts. The project will begin its Manufacturing, Assembly, Integration, and Test phase in the second half of 2022.

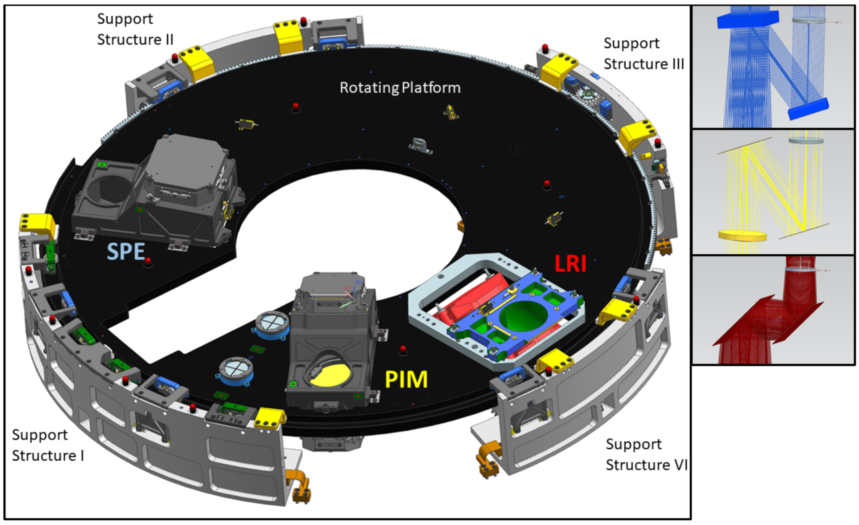

Fig. 3.6.1 Final Design of the Main Selection Mechanism (MSM)*: The MSM consists of four independent support structures that host several small bearings to guide the precise movement of the rotating platform with its optical modules. The supports also host all necessary sensors, a passive indent mechanism and the drive unit with the cryogenic stepper motor. The operating temperature of the MSM is 82K.*

In the MICADO Project the OPINAS/USM group is responsible for the Control Electronics, Control Software and a cryogenic mechanism, the so-called Main Selection Mechanism (Fig. 3.6.1). The MSM is located inside the MICADO cryostat and enables the instrument to switch between its operational modes (Low/High Resolution Imaging -LRI/HRI-, Pupil Imaging -PIM- and Spectroscopy -SPE-). The MSM is located between the fixed collimator and camera optics. The operating temperature inside the cryostat is 82K. The rotating platform with an outer diameter of 1300 mm, is driven by a cryogenic stepper motor. To reduce friction inside the mechanism and because of space constraints, several small ball bearings guide the movement and leave only the rotational freedom. Three optical modules are mounted on this platform and we will use a passive indent mechanism to achieve the repeatability and precision necessary in positioning the optical components inside the science beam. **Table 1** shows the tight tolerances for the LRI module. The given numbers reflect the total wave-front error (WFE) budget, but also the split between manufacturing, Alignment/Integration/Test (AIT) and cooldown. The re-positioning accuracy of the module when switching between the different modes in operational state is less critical for the optical performance, but for a mechanism of this size still very challenging.

The control electronics under responsibility of the OPINAS/USM group is shown in Fig. 3.6.2 and highlighted in magenta. In total we will deliver four cabinets hosting all necessary components to control the cryogenic mechanisms, the MICADO cryostat, the Co-Rotating Platform and the De-Rotator. All control functionality will be implemented by using Programmable Logic Controllers (PLCs). The cabinets will be located either on the so-called intermediate Nasmyth Platform or on the Co-Rotating Platform. One of the most complex systems to control in our work-package is the cryostat. Fig. 3.6.3 gives an overview of the cryogenic, Fig. 3.6.4 of the vacuum components that

	Total [nm]	MSF [nm]	LSF [nm]								
LRI module	35	10	33.5								
			Defocus [nm]			Zernike 2–4 [nm]			4< Zernike<36 [nm]		
Per mirror	16.8	7.1	7.5			13			7.5		
			M	AIT	CD	M	AIT	CD	M	AIT	CD
			6	4	4	6	9	6	7	0	0

Table 1 *Total WFE budget for the complete LRI module and split in mid and low spatial frequencies (MSF, LSF). The single mirror values are in addition split in manufacturing (M), AIT defaults and cooldown (CD). All values are given in nm.*

are needed for the control. Because of its complexity the implementation of the electronics and especially the software in a safe way to not damage the internal expensive parts is a challenging task.

The MICADO control software is based on a customisable ESO framework and will be distributed between an Instrument Workstation and the PLCs. The observation preparation software is organised as an ESO web application with instrument-specific microservices. Fig. 3.6.6 shows the top-level MICADO software architecture with its main components and dependencies in the ELT control system context. Those under full or partial OPINAS/USM responsibility are colored again in magenta. In total the MICADO instrument has ~40 software controllable functions. These are for example devices like the high-precision De-Rotator that will be delivered with the MICADO Instrument. To test the software prototype for this challenging system, a functional hardware model has been developed at

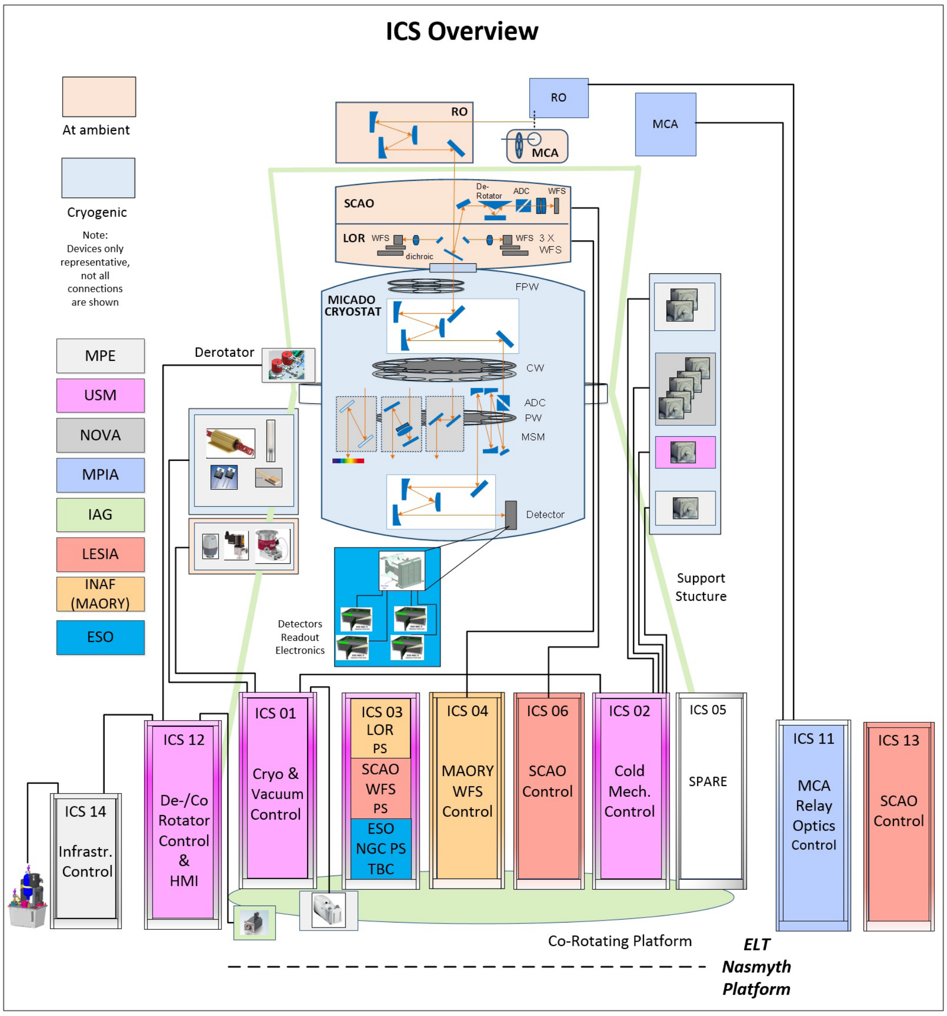

__Fig. 3.6.2 Overall control system__: Overview of the MICADO control electronics components, indicating their purpose, how they are linked, and where they are located. OPINAS/USM components are highlighted in magenta

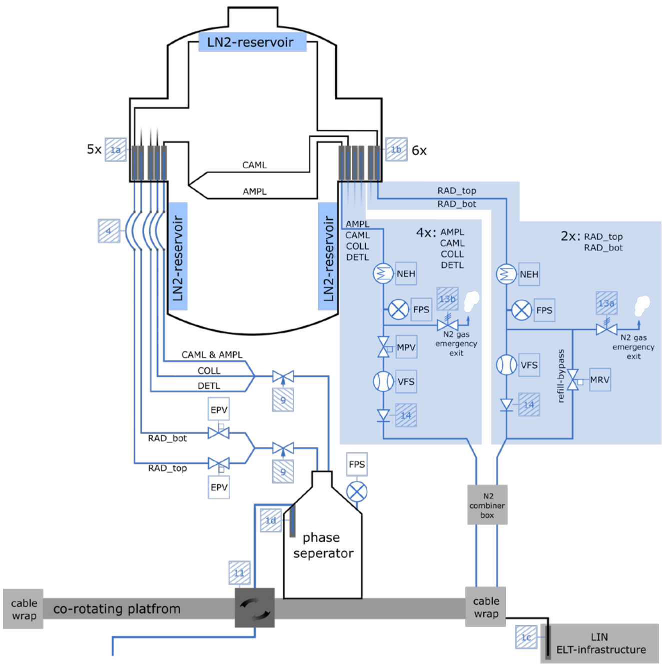

Fig. 3.6.3 Overview cryogenic components: *Overview of the cryo components that need to be implemented in the Cryostat Control Software.*

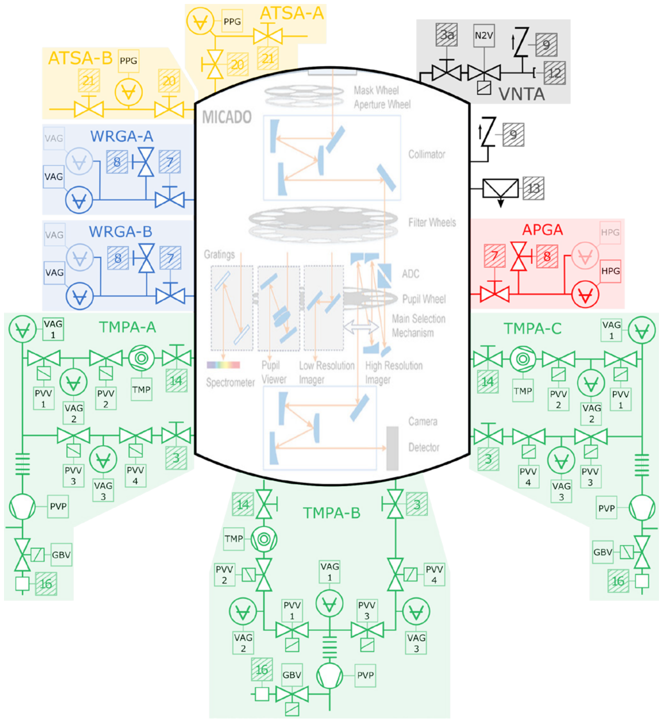

Fig. 3.6.4 Overview vacuum components: *Overview of the vacuum components that need to be implemented in the Cryostat Control Software.*

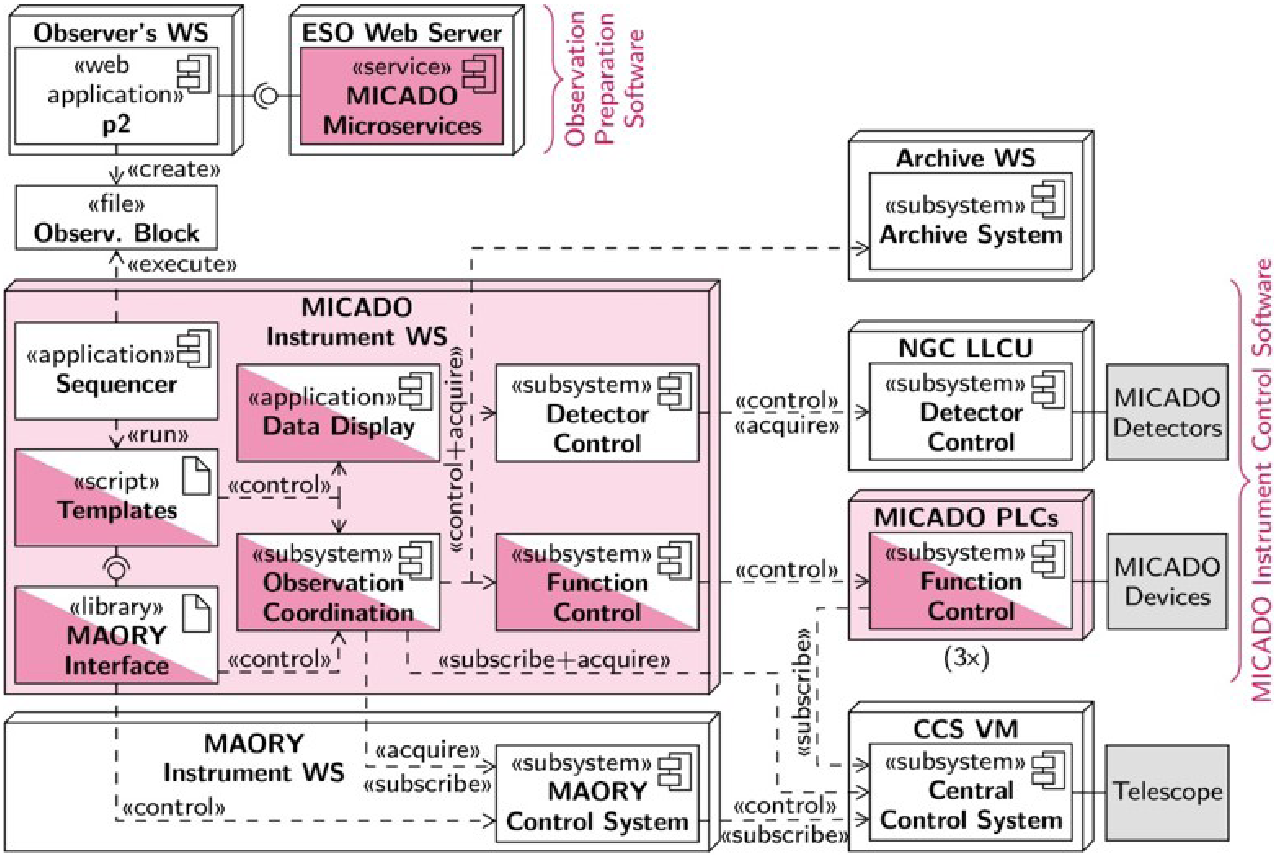

***Fig. 3.6.6 Software architecture**: Top-level MICADO software architecture (particularly important here: Template scripts and Function Control) with main components and dependencies in the ELT control system context. Those under full or partial OPINAS/USM responsibility are coloured magenta.*

USM (see Fig. 3.6.5). Measurements performed with this test setup showed that all MICADO accuracy requirements can be fulfilled. The tests will be repeated with the real MICADO de-rotator as soon as a prototype is available. In addition, several cold devices like filter-wheels, the Atmospheric Dispersion Corrector (ADC) or other rotating mechanisms inside the cryostat need to be implemented.

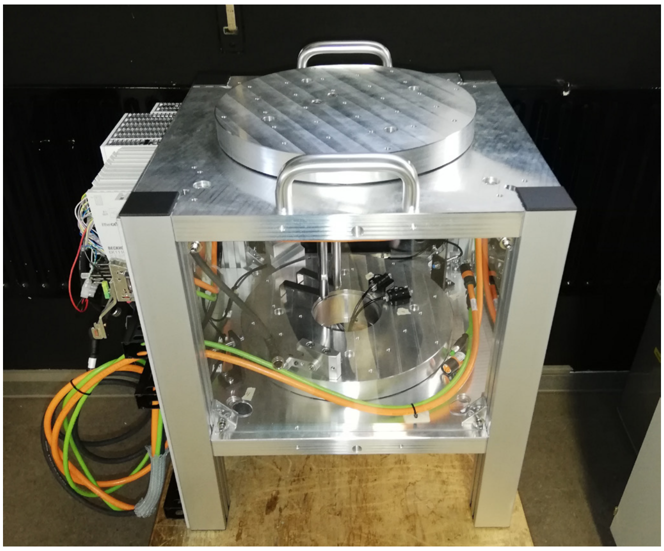

***Fig. 3.6.5 Functional model of the derotator / corotator system:** The control architecture of the model is very similar to the one of the final system and allows for realistic test scenarios.*

Selected References:

MPE infrared group science report, Davies, R. et al. 2022
Wegner M. et al., Proc. SPIE Volume 11452, 114522M (2020) https://doi.org/10.1117/12.2560788
Haeuser M. et al., Proc. SPIE 10702, 107028Z (27 July 2018); doi: 10.1117/12.2312048
Wegner M. et al., Proc. SPIE 9913, 99133M (26 July 2016); doi: 10.1117/12.2231332
Lang-Bardl F. et al., Proc. SPIE 10702, 107028Y (11 July 2018); doi: 10.1117/12.2311959
Monna A.. et al., Proc. SPIE 10702, 1070295 (11 July 2018); doi: 10.1117/12.2312492

Florian Lang-Bardl

Frank Grupp

(Other OPINAS team members include R. Bender, S. Annadevara, M. Fabricius, H. Kellermann, H.-J., Hess, H. Kravcar, F. Kummer, A. Monna, J. Schlichter, J. Thomas, M. Wegner, V. Ziel)

3.7 Dynamics Group – Milky Way and Nearby Galaxies

3.7.1 Structure, Dynamics, and Origin of the Milky Way Galaxy

The Milky Way as a galaxy has low specific star formation rate, signalling a fairly advanced stage of evolution, a large (~5 kpc) bar, a mostly old barred (B/P) bulge containing ~30% of the stellar mass, and a short disk scale-length (Bland-Hawthorn & Gerhard 2016 ARAA). The unique astrometric data from the Gaia mission combined with ground-based surveys result in large samples of Milky Way (MW) stars with 6-dimensional phase-space information, abundances, and estimated stellar ages, providing a fossil record of MW formation and evolution. The disk is seen to be dynamically perturbed, with non-equilibrium signatures related to the bar and spiral arms as well as to vertical oscillations in the disk. Much of the low-mass stellar halo was likely built by an ancient massive merger.

Dynamics of the MW's bulge/bar, and inner dark matter cusp
Using red clump star counts and bulge stellar kinematics together with made-to-measure (M2M) modelling, we previously reconstructed the mass distribution and dynamics of the inner Galaxy, including the bulge, long bar, inner disk and dark halo (Portail et al. 2017, P17). These models, arguably still the best dynamical models of the MW bar region, found a slow bar pattern rotation speed placing corotation near R~6kpc, a large (~2/3) fraction of the total stellar mass in the bar region, and a likely core or mild cusp in the central dark matter halo density.

More recently we have been working on the next generation of models, aiming to better constrain the dark matter cusp in the bulge region. We completed an analysis of infrared proper motions (PM) from the VIRAC-1 survey, cross-matched to the Gaia absolute astrometric reference frame. 40 million giant star PM all across the bulge clearly show the kinematics of a barred boxy/peanut bulge (Clarke et al. 2019). These newer data are also very well described by the best models from P17. With a careful analysis of (mostly systematic) errors and an outlier-tolerant method we used this fact to accurately constrain the bar pattern speed (Ωp=33.3+-1.8 km/s/kpc, Clarke & Gerhard 2022). The result is in excellent agreement with recent resonance analysis of disk orbits. We have now upgraded the data to VIRAC-2, included all of APOGEE DR17 and a new nuclear disk mass value (Sormani et al. 2022), implemented a new method to determine the dark matter cusp from these data, and are currently running a new sequence of dynamical models (Clarke et al., in prep.).

Chemo-dynamics of the MW's bulge/bar and a newly discovered inner stellar ring
The inner Galactic bulge is a mostly old, alpha-over-abundant, early component of the Galaxy (Barbuy et al. 2018) but APOGEE data have shown a steep gradient of increasing metallicity and decreasing stellar ages towards the ends of the bar. In Wylie et al. (2021) we recalibrated the ARGOS bulge survey to the APOGEE [Fe/H], [Mg/Fe], Teff and log g parameter scales using the Cannon data driven method. We combined the resulting A2A and APOGEE surveys, and with the combined data for ~40 000 giants we investigated the bulge abundance structure. We found that the bulge's metallicity map is more pinched than the density, a clear signature predicted by bar formation models. The inner bulge is more metal-poor than the outer bar, and while the vertical gradient in the bulge flattens near the plane, that in the bar remains steep. The most likely formation scenario for this configuration is that co-existing high- and low-metallicity disks became unstable, forming the bar and then b/p bulge.

However, some ingredient still seemed to be missing. By integrating ~30 000 inner MW APOGEE stars in one of the best potentials of P17 and constructing density, [Fe/H], and age maps from their orbits, we found that the bar is encircled by a [Fe/H]-rich, ~7 Gyr-old, broad stellar inner ring (Fig.3.7.1, Wylie et al. 2022). Thin star-forming inner rings are seen in barred galaxies, and often related to the bar's 4:1 resonance. A parallel gas-dynamical study indicates that the MW may also pos-

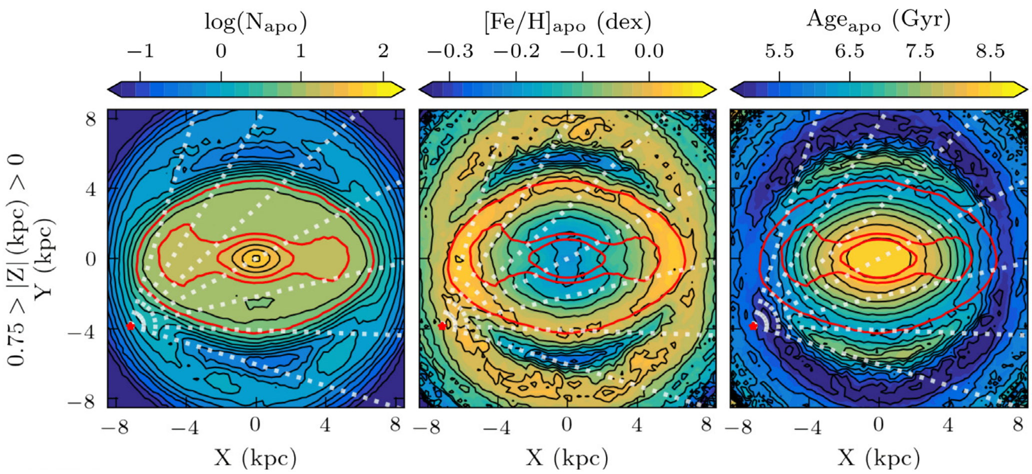

*Fig. 3.7.1 The Milky Way's stellar ring in orbital density of APOGEE stars (**left**), mean [Fe/H] (**centre**) and mean stellar age (AstroNN, **right**). A few density contours are highlighted in red, sun's position: red star (Wylie et al. 2022).*

sess a gaseous inner ring, consisting of the 3 kpc and Norma arms (Li et al. 2022). The stars formed in this ring would over time build the stellar ring. The peak of its inferred age distribution (~7 Gyr) then also sets a lower limit on the bar's formation time.

Disk and solar neighbourhood dynamics
With a corotation (CR) radius just over 2 kpc inside the sun, the Galactic bar has importance for the kinematics of the solar neighbourhood (SNd), e.g., generating the Hercules stream as reported previously. Monari et al. (2019a,b) used a model from P17 to study this further, finding that no fewer than six of the ridges in local velocity and action space can be associated to bar resonances, including Hercules and a high-velocity arch corresponding to the outer Lindblad resonance (OLR). Laporte et al. (2020) combined the phase-space information with isochrone ages, and found that these ridges stand out by slightly younger ages (predicted by some cosmological simulations) and also that some very low velocity ridges show similar age residuals, i.e. could signal relic disk perturbations. The importance of heated spiral arm stars in the SNd was emphasized by Khoperskov et al. (2020, 2022) who used N-body simulations to show that spirals could be found in angular momentum space, and argued that several of the angular momentum structures in Gaia-RVS data correspond to spiral-like real-space structures, of which three are spatially coincident with maser sources well-known to trace the Galactic spiral arms. This led them to identify many of the SNd velocity substructures – some with bar CR and OLR and others with the Sagittarius, Local, and Perseus arms.

3.7.2 Nearby Barred Disk Galaxies

Barred bulge thickening and modelling
In Sellwood & Gerhard (2020) we studied the mechanisms by which bars thicken into box/peanut bulges, analysing N-body simulations. Besides the well-known buckling instability, the main mechanism is the vertical heating of bar orbits by passage through the 2:1 vertical resonance. As the bar slows down by dynamical friction, the resonance moves outwards and the barred bulge grows in radius (Fig. 3.7.2). With a group at Shanghai Astronomical Observatory, we have been working on the dynamical modelling of barred galaxies. The goals are to constrain the balance between luminous and dark matter through modelling the dynamics of stars and gas, as well as the correlations between the orbit distributions and stellar populations. Tahmasebzadeh et al. (2022) devised a method for deprojecting barred galaxies and verified it by computing orbit distributions; Gajda (unpublished) constructed M2M dynamical models.

Contrasting the MW - the Andromeda galaxy M31
Our neighbour galaxy M31 has similar mass as the MW but appears to represent the opposite end of the spiral galaxy distribution in terms of its rich stellar halo and recent accretion history. With N-body models of Spitzer photometry we found that its bulge consists of a classical bulge with 1/3 of the total bulge mass, and a rotating barred bulge with 2/3 of the mass. Full dynamical models with the M2M particle method including VIRUS-W IFU kinematics confirmed this but also show only weak evidence for the part of the bar in the disk plane (Blana et al. 2018). Following published Lick index analysis which showed that the bar in M31 stands out in metallicity, but not in age or [alpha/Fe], recent M2M stellar population models also find an X-shaped edge-on metallicity structure, a property predicted for barred bulges (Fig. 3.7.2, Gajda et al. 2021).

With a new large sample of planetary nebulae (PN) we studied the kinematics of the large-scale disk in M31, and constructed an age-velocity dispersion relation in three age bins (Fig. 3.7.2, Bhattacharya et al. 2019). Surprisingly, the old disk is dynamically very hot (dispersion ~100-120km/s) which can be explained only by a relatively massive, ~1:5 merger, that heated and thoroughly scrambled the disk ~2.5-4.5 Gyr ago, before the cooler 2.5 Gyr-old disk formed. PN populations in the M31 substructures have properties consistent with this scenario (Bhattacharya et al. 2021).

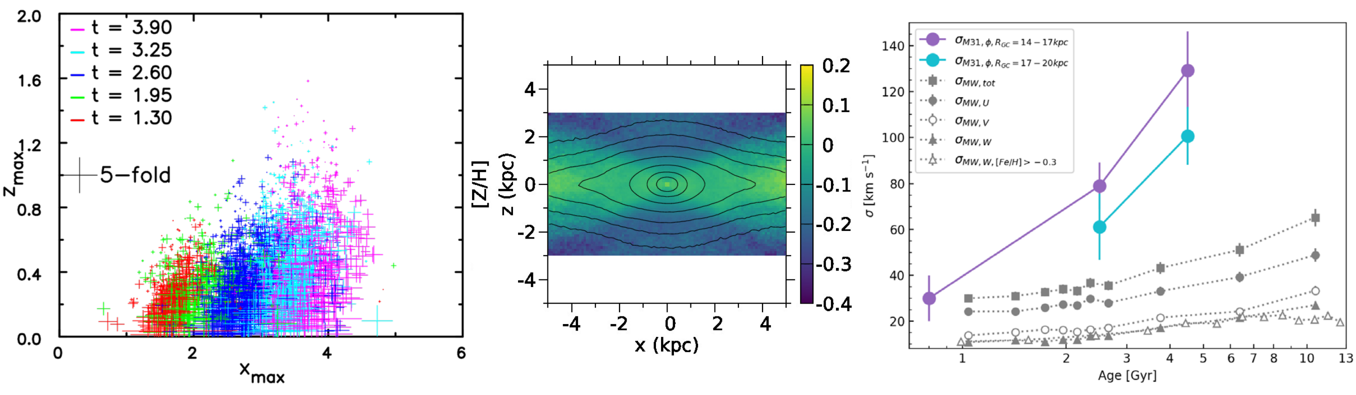

Fig.3.7.2 ***Left:*** *2:1 resonant orbits in an N-body bar moving outwards in xmax [kpc] with time [Gyr] (Sellwood & Gerhard 2020).* ***Center:*** *M2M model for metallicity finds X-shaped [Z/H] map in M31 bulge (Gajda et al. 2021).* ***Right:*** *age-dispersion relation in the M31 disk is much steeper than in the MW (Bhattacharya et al. 2019)*

3.7.3 Stellar Halos and Accretion in Early-Type Galaxies (ETGs)

Dynamical structure and origin of stellar halos in early-type galaxies (ETGs)
PN are excellent kinematic tracers for studying the faint outer halos of ETGs, because of their bright [OIII] emission lines. The ePN.S survey of 33 ETGs (Pulsoni et al. 2018) showed diverse halo kinematics, with a major fraction of massive fast rotators (FR) having halo rotation similar to slow rotators (SR), due to the fading of the rapidly rotating central components in the surrounding halo. This is consistent with a two-phase model where an early, dissipative merger-collapse forming a dense centre of in situ stars is followed by a prolonged phase of growth through mergers and accretion. Simulated ETGs from the Illustris TNG100 project have a similar diversity in halo rotation and shapes as the observed ETGs, and their halos show no clear bimodality between FR and SR (Pulsoni et al. 2020). Accretion history strongly depends on mass: low mass ETGs are completely dominated by in situ stars (Fig. 3.7.3), while the most massive ETGs are dominated by stars accreted in mergers. Mergers tend to erase the disk-within-halo rotation of the in situ component, and generate spherical-triaxial shapes (Pulsoni et al. 2021). Thus in their halo properties, simulated massive FR and SR show a continuity along which SR concentrate towards slow rotation and high accretion fraction, despite the clear bi-modality of their central regions (Fig. 3.7.3). This is consistent with the trends observed for the ePN.S sample.

Outermost halos transiting to the intragroup environment
An earlier study of photometry, velocity distribution and specific frequency of PN in the halo of the Virgo group-central galaxy M49 indicated that this galaxy transits into a higher velocity dispersion intragroup halo, consisting of blue stars accreted from a population of low-mass galaxies with inferred metallicity of about 0.1 solar. More recent work on the halo of M105 (Hartke et al. 2020, 2022) found a similarly PN-rich exponential envelope that coincides with a population of resolved stars with metallicity [M/H] < -1, has moderate rotation and increased velocity dispersion, and traces the transition to the intragroup light. The low metallicity requires significant accretion of systems with masses of $10^7 - 10^8$ solar masses, in tension with current cosmological simulations which predict that accretion from mergers with mass ratios less than 1% is negligible.

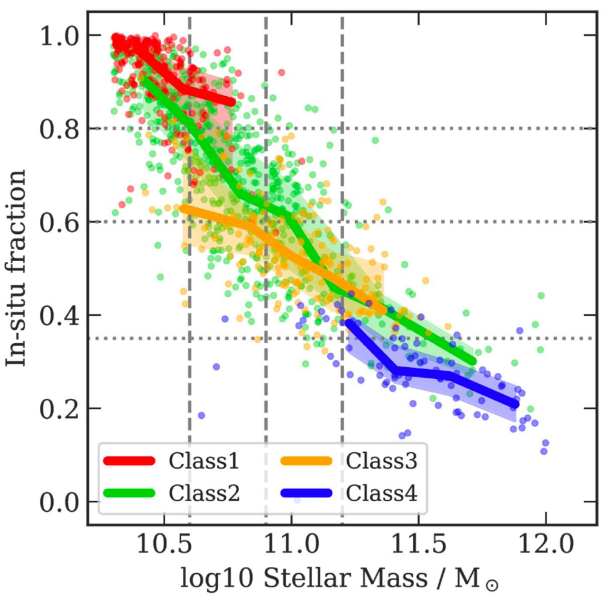

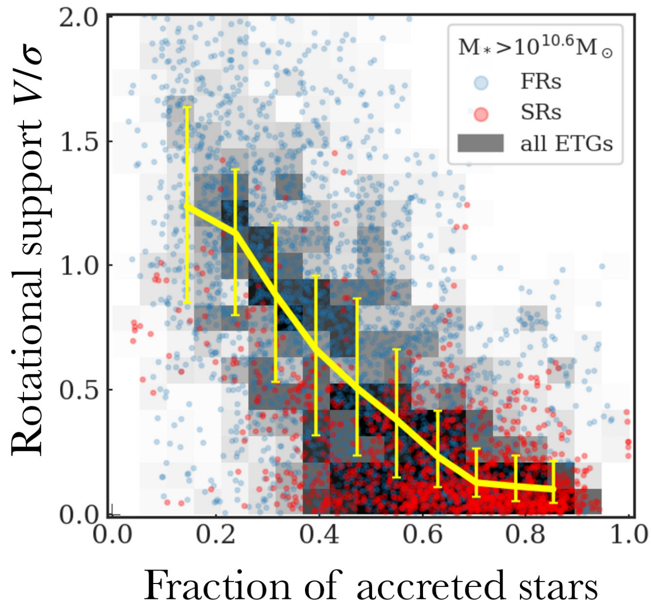

Fig. 3.7.3 ***Left:*** *In-situ fraction in ETGs decreases strongly with stellar mass.* ***Right:*** *Local rotational support decreases strongly with local fraction of accreted stars. From Pulsoni et al. (2021)*

Selected References:
Barbuy, Chiappini, Gerhard, 2018, ARAA 56, 223.
Bhattacharya et al., A&A 2019a, 624, A132.
Bhattarcharya et al. 2019b, A&A 631, A56.
Bhattarcharya et al. 2021, A&A 647, A130.
Blana Diaz et al. 2018, MNRAS, 481, 3210.
Bland-Hawthorn & Gerhard 2016, ARAA 54, 529.
Clarke et al. 2019, MNRAS, 489, 3519.
Clarke & Gerhard 2022, MNRAS, 512, 2171.
Gajda et al. 2021, A&A 647, A131.
Hartke et al. 2020 A&A 642, A46.
Hartke et al. 2022, A&A, in press.
Khoperskov et al. A&A. 2020, 634, L8.
Khoperskov et al. A&A. 2022, in press.
Laporte et al. 2020, A643, L3.
Li, Shen, Gerhard, Clarke 2022, ApJ 925, 71.
Monari et al. 2019a, MNRAS, 632, A107.
Monari et al. 2019, A&A 626, A41.
Portail, Gerhard, Wegg, Ness 2017, MNRAS, 465, 1621.
Pulsoni et al. 2018, A&A 618, A94.
Pulsoni et al. 2020, A&A 641, A60.
Pulsoni et al. 2021, A&A 647, A95.
Sellwood & Gerhard 2020, MNRAS 495, 3175.
Sormani et al. MNRAS, 2022, in press.
Tahmasebzadeh et al. 2022, MNRAS 508, 6209.
Wylie et al. 2021, A&A 653, A143.
Wylie, Clarke, Gerhard 2022, A&A 659, A80.

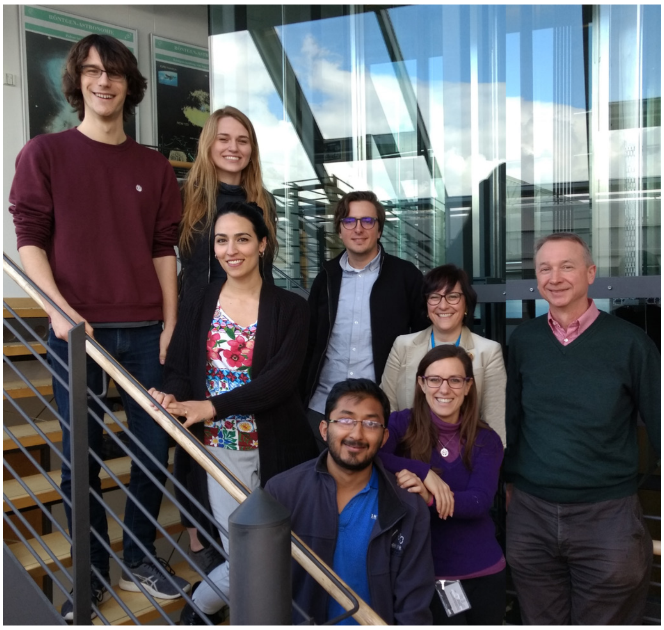

Dynamics Group: From left to right and top to bottom: J. Clarke, S. Wylie, C. Pulsoni, S. Khoperskov (MPE), S. Bhattacharya, M. Arnaboldi, C. Spiniello (ESO), O. Gerhard.

The MPE group consisted of the author, 2-3 PhD students and a post-doc, often augmented by an externally funded post-doc or PhD student. We collaborated with scientists at MPE, MPA, and ESO, the PN.S team, and other international collaborators. Between 01-2019 and 02-2022, we coauthored about 15 first author and 15 non-first author refereed papers.

4 High-Energy Astrophysics

eROSITA was launched to L2 aboard the SRG spacecraft on July 13th 2019 from the Baikonur cosmodrome. It has now completed the fourth of its planned eight all-sky surveys. The resulting skymaps and unprecedented samples of cosmic X-ray sources are set to revolutionise our view of the high energy universe.

4. High-Energy Astrophysics

4.1 Introduction and Overview

On July 13th 2019 eROSITA was launched aboard the SRG spacecraft from Baikonur, Kazakhstan, representing the culmination of almost 2 decades of work by the High Energy (HE) group. The instrument is performing superbly in space and recently completed the first 4 of its planned 8 all-sky surveys. eROSITA is yielding major new insights into all of the strategic research areas of the group: clusters and cosmology, supermassive black hole evolution, compact objects, transients and galactic diffuse hot emission. eROSITA-related science is by far the major focus of the group, along with follow-up from supporting large-area ground-based surveys, and operating high energy missions such as XMM-Newton, Chandra, Swift and NICER. Our hardware program, anchored by the PANTER X-ray optics facility and the detector development collaboration with the MPG Semiconductor Laboratory (HLL) provides a clear future perspective, with Athena WFI being the main activity, along with several smaller project contributions.

A decade after the signature of the agreement that formalized the Spectrum-RG mission, eROSITA was launched in July 2019 (Fig. 4.1.1). The first science data were received in late August that year, and the formal "first light" with all seven telescope was achieved 13th October. The subsequent calibration and performance verification (CalPV) phase saw the first serious science observations, along with the first major publications. eROSITA has now completed the first four of its planned eight all-sky surveys, with the exploitation of the early all-sky survey data already well under way. While we have barely scratched the surface of what the incredibly rich eROSITA dataset can yield in terms of science, breakthrough results have already been obtained.

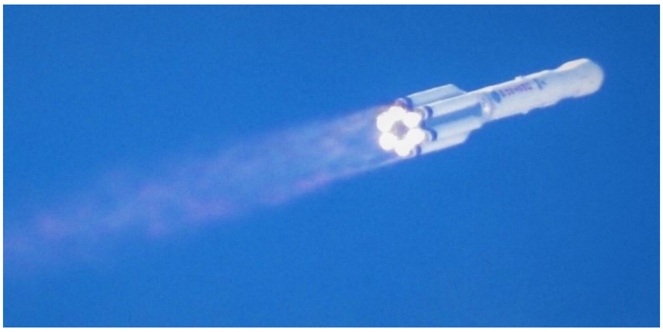

Fig. 4.1.1 *Spectrum RG was launched from Baikonur cosmodrome in July 2019 using a proton rocket* ***(left)****, captured spectacularly in mid-flight by MPE's Vadim Burwitz* ***(right)****.*

Science Highlights from eROSITA led by MPE:

- Discovery of the eROSITA bubbles, vast hot gas structures extending more than 10kpc above and below the Galactic plane and presumably powered by energetic processes in the Galactic centre via star formation or activity of the central black hole (Predehl et al. 2020).
- X-ray detection of high redshift (z>5.5) luminous AGN, with implications for black hole growth and the accretion luminosity density into the epoch of reionization (Wolf et al. 2021, 2022)
- Breakthroughs in time domain science, including the discovery of Quasi-Periodic Eruptions of the central back holes in formerly quiescent galaxies for the first time (Arcodia et al. 2021, 2022), as well as other novel transient phenomena (Malyali et al. 2022)
- Stacked detection of the hot circumgalactic medium gas in quiescent galaxies at z=0.05-0.3, with potentially major implications for galaxy evolution (Comparat et al. 2022)
- Population analysis of the first large samples of X-ray selected clusters of galaxies (A. Liu et al. 2021; Bulbul et al. 2021; Bahar et al. 2021; Ghirardini et al. 2021) and AGN (T. Liu et al. 2021; Nandra et al. 2022). These demonstrate that in the 4-year all-sky survey eROSITA will fulfil or even exceed its design goals in terms of the expected data quality and sample sizes.
- Public release of the eROSITA CalPV data, along with catalogues of the X-ray sources, their multiwavelength identifications and redshifts, X-ray variability and X-ray spectral properties (Brunner et al. 2021, Salvato et al. 2021, Boller et al. 2021, T. Liu et al. 2021)

Many of these results have been presented in a special issue of A&A devoted to the first eROSITA data release, with 16 MPE first author papers of 30 in total, many of which were based on the 130 deg^2 eFEDS survey. The group is now heavily focused on catalogue production and science analysis of the first all-sky survey, with the data release and accompanying science papers due in early 2023.

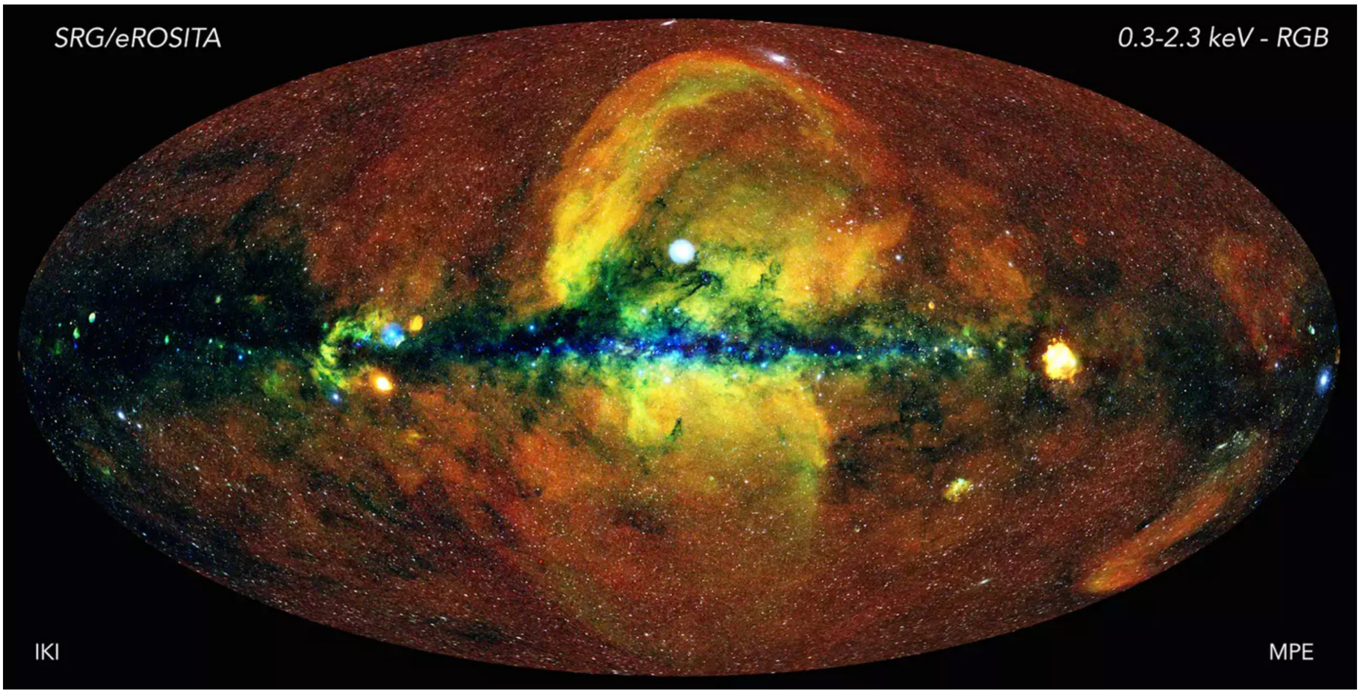

Fig. 4.1.2 *eROSITA's "breathtaking" all-sky map* will be an enduring and iconic image for X-ray astronomy. Exploiting the wealth and breadth of science from these data will dominate our activities for the next decade.*

At the time of writing eROSITA is in safe-mode pending clarification of the implications of the sanctions against Russia, which is obviously a major concern. We hope to return to normal operations as soon as possible, to ensure that the full potential of this unique instrument can be realized. Either way we expect eROSITA to dominate science activity for the group for the next decade. When the X-ray dataset is completed, the harvest will continue with new supporting data from SDSS-V, 4MOST and Rubin/LSST, in which the HE group has secured participation, and Euclid via collaboration with the OPINAS group.

Overall, the scientific output of the group during the 2019-21 reporting period has been very strong, with over 400 refereed papers, 106 of which feature an MPE first author. This is now, of course, being given a significant boost with eROSITA. A selection of the highest impact papers of the group can be found in Table 4.1.1 and cover the breadth of science within the group, covering black hole evolution, galaxy clusters, compact objects and transients. Our leadership in missions and instruments, as well as the development of new techniques, is also well represented. Further external recognition of the achievements of the group and its members include: the Institutional Marcel Grossmann award, accepted by Peter Predehl on behalf to MPE for the development of eROSITA; honorary membership of the Germany Physical Society (DPG) awarded to Emeritus Director Joachim Trümper; an ERC consolidator grant awarded to Esra Bulbul for work on eROSITA cluster surveys and Clarivate highly-cited researcher status awarded to Mara Salvato in 2019 and 2020.

** https://www.bbc.co.uk/news/science-environment-53102718*

Title	Authors	Year	Citations	Rate/yr
X-ray spectral modelling of the AGN obscuring region in the CDFS: Bayesian model selection and catalogue	**Buchner, J.; Georgakakis, A.; Nandra, K.;** et al.	2014	666	83
eROSITA Science Book: Mapping the Structure of the Energetic Universe	**Merloni, A.; Predehl, P.; Becker, W.;** et al.	2012	632	66
The Hot and Energetic Universe: A White Paper presenting the science theme motivating the Athena+ mission	**Nandra, K.;** Barret, D.; Barcons, X.; et al.	2013	471	53
A kilonova as the electromagnetic counterpart to a gravitational-wave source	Smartt, S.J.; **Chen, T.-W.;** Jerkstrand, A.; et al.	2017	467	106
The Fermi GBM Gamma-Ray Burst Spectral Catalog: Four Years of Data	**Gruber, D.;** Goldstein, A.; Weller von Ahlefeld, V.	2014	245	31
Second ROSAT all-sky survey (2RXS) source catalogue	**Boller, Th.; Freyberg, M.J.; Trümper, J.; et al.**	2016	244	41
A very luminous magnetar-powered supernova associated with an ultra-long gamma-ray burst	**Greiner, J.;** Mazzali, P.A.; Kann, D.A.; et al.	2015	201	30
The eROSITA X-ray telescope on SRG	**Predehl, P.; Andritschke, R.;** Arefiev, V.; et. al.	2021	190	175
The nine lives of Cosmic Rays in Galaxies	Grenier, I.A.; Black, J.H.; **Strong, A.W.; et al.**	2015	186	28
Accreting supermassive black holes in the COSMOS field and the connection to their host galaxies	**Bongiorno, A.; Merloni, A.; Brusa, M.;** et al.	2012	183	20
The incidence of obscuration in Active Galactic Nuclei	**Merloni, A.; Bongiorno, A.; Brusa, M.; et al.**	2014	178	22
Obscuration-dependent Evolution of Active Galactic Nuclei	**Buchner, J.; Georgakakia, A.; Nandra, K.; at al.**	2015	175	25
The Third Fermi GBM Gamma-Ray Burst Catalog: The First Six Years	Narayana Bhat, P.; Meegan, C.A.; **von Kienlin, A.;** et al.	2016	163	28
Discover of pulsations from NGC 300 ULX1 and its fast period evolution	Carpano, S; Haberl, F.; Maitra **et al.**	2018	162	40
The Second Fermi GBM Gamma-Ray Burst Catalog: The First Four Years	**von Kienlin, A.;** Meegan, C.A.; Paciesas, W.S.; et al.	2014	151	19
A statistical relation between the X-ray spectral index and Eddington ratio of active galactic nuclei in deep surveys	**Brightman, M.;** Silverman, J.D.; Mainieri, V.; et al.	2013	125	15
Glactic synchrotron emission with cosmic ray propagation models	Orlando, E.; **Strong, A.;**	2013	115	14
CANDELS/GOODS-S, CDFS and eCDFS: Photometric Redshifts for Normal and X-ray detected galaxies	**Hsu, L.T.; Salvato, M.; Nandra, K.; et al.**	2014	114	14
Cosmic evolution and metal aversion in superluminous supernova host galaxies	Schulze, S.; **Krühler, T.;** Leloudas, G.; et al.	2018	107	28
The XXL Survey II. The bright cluster sample; catalogue and luminosity function	Pacoud, F.; **Clerc, N.;** Giles, P.A.; Adami, C.; et al.	2016	106	20
Are Compton-thick AGNs the missing link between mergers and black hole growth	Kocevski, D.D.; Brightman, M.; Nandra, K.; et al.	2015	100	16
The many flavours of photometric redshifts	**Salvato, M.;** Ilbert, O.; **Hoyle, B.;**	2019	97	34
Cyclotron lines in highly magnetized neutron stars	Staubert, R.; **Trümper, J.;** Kendziorra, E.; et al.	2019	88	35
Universal thermodynamic properties of the intracluster medium over two decades in radius in the X-COP sample	Ghirardini, V.; **Eckert, D.;** Ettori, S.; et al.	2019	84	28
Gamma-ray bursts as cool synchrotron sources	**Burgess, J.M.; Bégué, D.; Greiner, J.;** et al.	2020	60	34
Detection of large-scale X-ray bubbles in the Milky Way halo	**Predehl, P.;** Sunyaev, R.; **Becker, W.;** et al.	2020	57	29
UltraNest - a robust, general purpose Bayesian inference engine	**Buchner, J.**	2021	31	27

Table 4.1.1 *A selection of the highest impact publications since 2012 led by HE group members (shown in bold) or with an enabling contribution from one or more group members. Papers with >100 total citations or more recent work with a high citation rate (>25/year) are shown.*

Project Highlights

- Athena WFI has recently gone through its system requirements review (SRR), the second major review of the instrument. The first full-size 512x512 DEPFET detector have been manufactured at HLL, and successfully tested at MPE. Additional key technologies, notably the detector electronics and thin optical blocking filter, have been demonstrated.
- The HE group has manufactured, tested and delivered the flight detector modules for the CCD cameras for the FXT instrument aboard the Einstein Probe (EP) mission to our partners at IHEP in China. Under contract with ESA, and together with Media Lario, we have also delivered the FXT flight mirrors.
- MPE has provided the flight CCDs and custom readout ASICs for the SVOM MXT instrument to our partners at CEA, FR.
- Silicon drift detectors for the SFA instrument aboard eXTP project have been manufactured by HLL and the required performance demonstrated in the lab setup at MPE.
- In our PANTER facility, we have performed calibration and testing for EP, SVOM, Athena and numerous optics technology developments, including technologies for future missions such as Arcus and AXIS. PANTER continues to be a centre of excellence for X-ray optics calibration and testing, and a key facility In Europe.

Beyond eROSITA, the group strategy remains to leverage our hardware development program to ensure a bright future scientifically. Athena is the largest future project, with MPE contributing the WFI instrument. Athena successfully passed through Phase A at the end of 2019. Mission adoption is currently scheduled for mid-2023 for a launch in 2034. The WFI instrument team just recently completed its system requirements review with ESA, with a technology readiness assessment planned for later this year in advance of adoption. WFI technology development is making excellent progress, along with maturation of the instrument design. The current major concern for the project is the performance ESA's Silicon Pore Optics (SPO), particularly the angular resolution. Our contribution to the Athena optics development centres around SPO testing at MPE PANTER facility, where the optics are tested and validated.

Given the extended timescale for Athena, our smaller mid-term projects take on a new prominence. We have secured a significant involvement in the Einstein Probe (EP) project (launch 2023), in collaboration with the Chinese Academy of Science (CAS) and ESA. High energy transients are EPs main targets, with a wide-field X-ray telescope (WXT) and two eROSITA-like modules compromising the follow-up X-ray telescope (FXT). MPE is providing the FXT detector modules and the eROSITA flight spare for the mission, in return for 10% of the scientific exploitation. Our pnCCD and ASIC contribution to SVOM, through CEA (FR), has recently been concluded, in preparation for launch in 2023. With HLL, we are also developing Silicon Drift detectors for the Chinese eXTP project, which will perform high throughput spectral-timing studies of AGN and binaries. Finally, we continue to keep a close eye on developments at NASA, being involved in the Arcus MIDEX proposal and with potential participation in X-ray Probes.

Kirpal Nandra for the MPE High Energy Group

4.2 Astrophysics Research

4.2.1 Supermassive Black Hole Demographics and Evolution

Black holes of millions to billions of solar masses inhabit the cores of virtually all massive galaxies. These SMBH contain approximately 0.1% of a galaxy's mass. However, it is still unclear how these black holes formed and became so massive and how the SMBH feeding impacts the host galaxy. eROSITA is in the process of revealing unprecedented samples of luminous quasars which rapidly accumulate black hole mass. Much of the high-energy group's focus has been focussed on transforming the X-ray and multi-wavelength data products towards scientific insights, the first of which have already arrived.

Billion solar mass black holes shining brightly in the optical have been identified as early as 1 billion years after the Big Bang. This implies an efficient growth mechanism, or a black hole formation mechanism that starts already at dozens of solar masses. However, the identification of such quasars is plagued by selection biases. For example, heavily enshrouded galactic cores are missing in the selection that is most sensitive to direct observations of the hot accretion flow. X-rays, in contrast, can penetrate even thick columns of dust and gas, and thus provide the most efficient and pure selection of quasars. However, due to instrumentation limitations, sufficiently deep X-ray surveys have been limited to small areas on the sky.

Prior to the launch of eROSITA our work on SMBH demographics had a strong focus large-scale spectroscopic followup of XMM-samples with SDSS (Comparat et al. 2020), yielding physical quantities such as black hole mass measurements (Coffey et al. 2019), which were used to explore the diversity in quasar properties (Wolf et al. 2022). An XMM survey of the SDSS reverberation mapping field was also undertaken (Liu et al. 2020), yielding a sample of X-ray emitting quasars with very precise black hole mass estimates. Using a variety of Chandra fields, we also expanded our previous work on constraining black hole spins via X-ray spectroscopy (Baronchelli et al. 2020).

The subsequent launch of eROSITA has the potential to revolutionise this field. In an early tour de force, eROSITA surveyed the largest contiguous area on the sky in only four days. This survey field, eFEDS, identified 22,000 quasars across cosmic time (Brunner et al. 2021; Salvato et al. 2021; T. Liu et al. 2022). An exciting new development based on these data has been the identification of the first very high redshift (z=5.81) AGN from eROSITA (Fig. 4.2.1; Wolf et al. 2021). The detection of even this single objects hints potentially at a large population of luminous, X-ray bright sources in the early Universe than previously thought. The tentative detection of a further z=6.56 AGN in eFEDS corroborates this, and high-z searches in the eRASS data are ongoing (Wolf et al. 2022).

To achieve such science results requires reliable estimation of cosmological distances. MPE, as co-founding member of 4MOST, the Sloan Digital Sky Survey (SDSS) V and member of SDSS-IV, is leading an extensive optical spectroscopy follow-up program for spectral identification of eROSITA sources (SPIDERS, PI: Andrea Merloni). To position the spectrograph, the optical positions corresponding to the X-ray detections

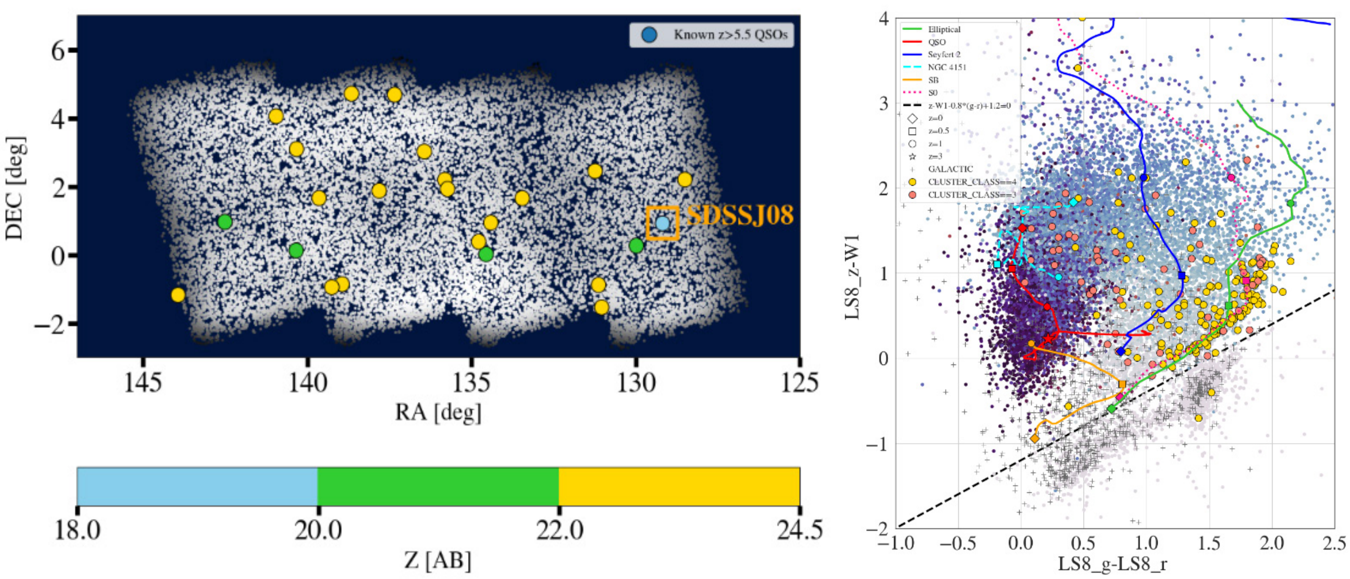

Fig. 4.2.1 (left) *Detected point sources in the 140 deg² eFEDS pilot survey executed during the CalPV Phase, the largest contiguous X-ray survey at this depth performed prior to eRASS. Amonst the almost 30,000 point sources in this image, the orange square highlights a detected z=5.81 quasar.* ***(right)*** *The eFEDS sources are classified by their optical and infrared colours. Below the dashed line lie stars, just above are ellipticals as commonly found in the centers of galaxies clusters. To the upper left are Seyfert galaxies and quasars.*

first need to be identified. This is challenging, because the fast X-ray surveying capabilities imply large point spread functions, which contain many optical counterparts. Secondly, for scientific studies quasars also need to be distinguished from other sources, such as stars. Thirdly, where sources are too faint to be reached by spectrographs, the redshift needs to be estimated based on source extent and photometric colours. These three tasks can only be achieved with extensive multi-wavelength data compilations and sophisticated data analysis techniques.

The high-energy group at MPE has contributed to extensive photometry campaigns of the sky surveyed for the German eROSITA collaboration. This corresponds mostly to the southern sky. Examples includes the completion of deep g, r and i band photometry for declinations below zero by the Dark Energy Camera. Recently, the Vista telescope has also completed deep near-infrared observations of the southern sky. These data are combined with sophisticated analysis techniques for merging multi-wavelength catalogs and inferring photometric redshifts, for which the high-energy group has world-leading expertise (Salvato et al 2019).

To understand the population picked up by eROSITA, sophisticated end-to-end simulations have been performed, led by Dr. Johan Comparat. Starting from state-of-the-art models of how galaxies and SMBH populate dark matter halos and light up as AGN, these generate realistic data products down to X-ray photon events as picked up by the eROSITA detectors as they survey the sky. The X-ray detection capabilities were extensively tested in Liu et al. (2021), providing a careful assessment of the selection biases, an important prerequisite for inferring the underlying population and testing evolutionary models.

Over the next few years, the high energy group will be able to harvest the fruits of these investments, and learn about the drivers of extreme SMBH accretion from redshift 6 down to the local Universe, which eROSITA surveys with unprecedented numbers.

Johannes Buchner

Kirpal Nandra

(Other HEG members include: T. Boller, H. Brunner, J. Comparat, T. Dwelly, Z. Igo, T. Liu, A. Merloni, M. Salvato, S. Waddell, J. Wolf. Former members: L. Baronchelli, D. Coffey)

Selected References:

Baronchelli L., et al. 2020, MNRAS, 499, 4768
Brunner H. et al. 2021, A&A, in press
Coffey D. et al. 2019, A&A, 625
Comparat J. et al. 2019, MNRAS, 487, 2005
Comparat J. et al. 2020a, 636, 97
Comparat J., 2020b, OJAp, 3, 13
Salvato M. et al. 2019, NatAs, 3, 212
Salvato et al. 2021, A&A, in press
Liu T. et al., 2020, ApJS, 250, 32
Liu T. et al., 2021a, A&A, in press
Liu T. et al., 2021b, A&A, in press
Wolf J., et al. 2020, MNRAS, 492, 3580
Wolf J., et al., 2021, A&A, 647, 5

4.2.2 Clusters of Galaxies: Large-scale Structure and Cosmology

Galaxy clusters are the most massive gravitationally-bound regions of the large-scale structure. The space between the galaxy members is filled with a hot dilute plasma, a.k.a. intra-cluster medium (ICM) that has been heated to extreme temperatures (>107 K) due to the gravitational collapse. The ICM predominantly emits in the X-ray band through thermal bremsstrahlung. Understanding the characteristics and astrophysics of clusters of galaxies using the multi-wavelength observations and using their observations for constraining the cosmological parameters are among the major foci of the clusters and cosmology group. With the availability of eROSITA calibration and PV observations, the group has mostly focused its activities on characterizing the population of clusters using multi-wavelength surveys..

Cluster Microphysics and AGN feedback

AGN feedback is not only important for its impact on clusters and groups of galaxies, where it can prevent the rapid cooling that would otherwise be taking place, but is also important for our understanding of the evolution of galaxies. However, our understanding of feedback is incomplete. For example, we have few measurements of the turbulence in the ICM, which is affected by feedback and mergers. With the large samples of clusters that eROSITA is detecting, we will make progress in understanding feedback across a range of wavelengths. Detailed studies of individual systems also have great power in studying the microphysics of the ICM and feedback. Sanders et al. (2020) developed a novel new technique to use background detector lines to help determine the energy scale of the EPIC-pn instrument on XMM in order to measure the redshift of iron lines emitted by clusters. Using this technique the velocities within the ICM of the Perseus and Coma clusters were mapped, examining sloshing and subcluster motions. This technique was also applied to the Virgo cluster (Gatuzz et al. 2021). eROSITA with its wide field of view and well-determined background enables our understanding of complex cluster systems. Sanders et al. (2021) studied the calibration observations of the A3266 cluster, finding a complex system of likely four subclusters merging, as seen by striped material and shocks.

Constraining Cosmology and Large scale structure with eROSITA

eROSITA is designed as a Stage-IV Cosmology experiment and its main scientific goal is to constrain cosmological parameters by detecting ~100,000 galaxy clusters. The cluster number counts as a function of redshift and their mass is a powerful cosmological probe that is orthogonal and complementary to the other cosmological geometrical experiments. The eFEDS observations are designed to give a sneak preview of the cluster number counts that will be detected at the final survey depth. In the area of 140 deg^2 covered by eFEDS, 542 candidate clusters and groups of galaxies in the redshift range of 0.01 <z<1.2 are detected as extended X-ray sources down to a flux limit of ~10^{-14} erg s^{-1} cm^{-2} in the soft 0.5-2 keV band (Liu et al. 2021). The X-ray properties of these clusters, e.g. X-ray luminosity, gas mass, number density, and ICM temperatures, out to R$_{500}$ are presented in Bahar et al. (2021). Additionally, we find 346 additional clusters hiding in the plain sight misclassified as point sources (Bulbul et al. 2021). These two studies demonstrate that the predictions of cluster number counts are on target and we will be able to measure ICM emission out to R$_{500}$ at the final sur-

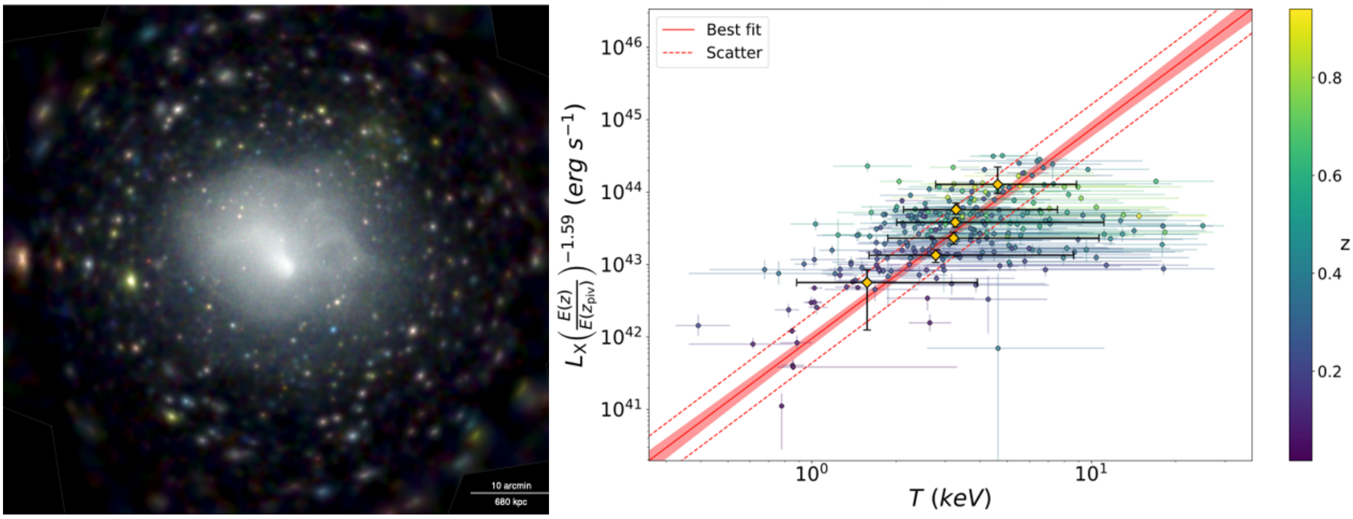

***Fig. 4.2.2 (left)** RGB image of A3266 using the 0.3–0.8, 0.8–1.3, and 1.3–2.3 keV bands. A location-dependent Gaussian smoothing has been applied to the count, exposure and background maps (Sanders et al. 2021). **(right)** Lx-T scaling relations of the eFEDS clusters (Bahar et al. 2021). The eFEDS sample extends the scaling relations to low mass, low luminosity galaxy cluster and group regime.*

vey-depthThe galaxy clusters and groups detected in eFEDS provide an ideal sample for studying the redshift and luminosity evolution of the morphological parameters and characterization of the underlying dynamical state of the sample. Based on a number of estimators (concentration, central density, cuspiness, ellipticity, power-ratios, photon asymmetry, and Gini coefficient), we construct a new dynamical indicator, relaxation score, for all the clusters in the eFEDS sample in Ghirardini et al. (2021). We find no evidence for bimodality in the distribution of morphological parameters of our clusters, rather we observe a smooth transition from the cool-core to non-cool-core and from relaxed to disturbed states. A significant evolution in redshift and luminosity is also observed in the morphological parameters examined in this study after carefully taking into account the selection effects. Surprisingly, we find that an X-ray selected eFEDS cluster sample is not biased towards relaxed clusters as has been suggested in the literature. These results and our morphology estimator will be used for the future eROSITA All-Sky surveys to reduce the scatter in cluster scaling relations. Seppi et al. (2021) created a method to account for the dynamical state of the halo when measuring the halo mass function. It offers a connection with dynamical selection effects (e.g. cool core bias) in galaxy cluster observations. This is key toward precision cosmology using cluster counts as a probe. The morphology of clusters, affected by cool cores associated with feedback, impacts how clusters are selected in X-ray surveys. Käfer et al. (2019, 2020) studied the distribution of morphologies of observed clusters and then put this to use to develop a low-scatter method for the selection of clusters in the eROSITA survey through simulations.

Using a sample of HSC shear-selected clusters catalog, in Ramos-Ceja et al. (2021), we investigated the effects of cluster selection methods by comparing the eFEDS X-ray- and the HSC shear-selected galaxy cluster samples. The relation between X-ray bolometric luminosity and weak-lensing mass reveals that the normalization of the bolometric luminosity and mass relation of the X-ray selected and shear-selected samples is consistent within 1σ. Moreover, we found that the dynamical state and merger fraction of the shear-selected clusters is not different from the X-ray selected ones. Four shear-selected clusters are undetected in X-rays: one is the result of projection effects, while the other three have an X-ray flux below the ultimate eROSITA detection limit. Our results indicate that there is no significant population of X-ray underluminous clusters and X-ray selected cluster samples are complete and can be used as accurate cosmological probes.

Well-established scaling relations between cluster observables and the mass provide a way forward for estimating cluster masses, therefore for cosmological studies. In Bahar et al. (2021), we investigate the scaling relations between X-ray observables of the clusters (L_x-T, L_x-M_{gas}, Y_x- L_x) detected in the eFEDS field taking into account the selection effects. Using Bayesian population modeling, we find that both the slopes and normalizations are in good agreement with the simulations including non-gravitational physics and the recent results in the literature that take into account selection effects. However, our results significantly deviate from the self-similar model that omits the non-gravitational effects.

Cosmic structures evolve hierarchically from high-density peaks in the primordial density field, and form galaxies, galaxy groups, and clusters of galaxies under the action of gravity. In the complex large-scale structure formation scenario, these galaxies, groups, and clusters are connected to each other via filamentary structures called the cosmic web and form large superclusters. In the eFEDS field, we reported a discovery of a supercluster consisting of eight galaxy clusters at z~0.36 (Ghirardini et al. 2021b). We use radio follow-up observations with LOFAR and uGMRT to search for diffuse emission and constrain the dynamic state of the system. We later found 18 additional superclusters in the eFEDS field and provided their properties in Liu et al. (2021).

Optical follow-up with the SDSS-5 and 4MOST infrastructure

The spectroscopic survey SDSS-V and 4MOST will observe the eROSITA sky starting in 2022 and 2024 (until 2026 and 2029). By 2029, one million spectra of AGN and another million of galaxies in clusters will be available through both SDSS-V and 4MOST collaborations. They will enable the accurate measurement of the redshifts of more than 80% of eROSITA extragalactic sources. For the galaxy clusters, the redshift uncertainty will decrease by a factor of ~20 (Clerc et al. 2020) enabling tighter cosmological constraints than with photometric redshifts, as shown by Ider Chitham et al. (2020). First target catalogs are in preparation and will rely on the eRASS:3 survey combined with the legacy survey DR10. Final target catalogs will be constructed combining eRASS:8, legacy survey DR10, LSST and Eudlic imaging.

Simulated eROSITA Sky

To enable precision cosmology measurements using the LSS hosting X-ray emission processes, we have developed state-of-the-art models of the X-ray emission of the LSS. In Comparat et al. (2019), we presented an N-body simulation-based mock catalog creation method for X-ray-selected active galactic nucleus (AGN) samples. The model reproduces the observed hard X-ray AGN luminosity function (XLF) and the soft X-ray logN-logS from redshift 0 to 6. In Comparat et al. (2020), we describe a novel method to predict the X-ray emission of galaxy clusters. Given a set of dark matter halo properties (mass, redshift, ellipticity, offset parameter), we construct an X-ray emissivity profile and image for each halo in the light-cone. We predict scaling relations for the model clusters, which are in good agreement with the literature. The predicted number density of clusters as a function of flux also agrees with previous measurements. Using these models and past light cones, we follow the eROSITA scanning strategy to produce a list of X-ray photons following the eFEDSand the first and eight All-Sky Observations. Liu T. et al. (2022) tested and optimized the eROSITA source detection procedures. Because our simulated data is highly representative of the real eFEDS data, we used the mock catalogs to measure the completeness and purity of the eFEDS catalogs as a function of multiple parameters, such as detection likelihood, flux, and luminosity.

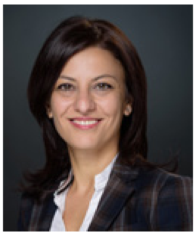

Esra Bulbul

Johan Comparat

Miriam Ramos-Ceja

Jeremy Sanders

(Other members include: E. Bahar, V. Ghirardini, J. Ider-Chitham, A. Liu, R. Seppi, S. Sheereram. Former members: G. Erfanianfar, E. Gatuzz, F. Käfer)

Selected References:

Bahar, Y. E., Bulbul, E., Clerc, N., et al. 2021, A&A in press, arXiv:2110.09534
Bulbul, E., Liu, A., Pasini, T., et al. 2021, A&A in press, arXiv:2110.09544
Clerc, N.et al. 2020 MNRAS.497.3976C
Comparat J., et al., 2019, MNRAS, 487, 2005C
Comparat J., et al., 2020, OJAp, 3E, 13C
Erfanianfar G,m et al., 2019, A&A, 631, 175
Gatuzz E., Sanders J.S., et al., 2021, MNRAS, in press, arXiv:2109.06213
Ghirardini, V., Bahar, E., Bulbul, E., et al. 2021a, A&A in press, arXiv:2106.15086
Ghirardini, V., Bulbul, E., Hoang, D. N., et al. 2021b, A&A, 647, A4
Ider Chitham, J.; Comparat, J. et al. 2020 MNRAS.499.4768
Käfer F., et al., 2019, A&A, 628, A43
Käfer F., et al., 2020, A&A, 634, A8
Liu, A., Bulbul, E., Ghirardini, V., et al. 2021a, A&A in press, arXiv:2106.14518
Liu T., Merloni A. , Comparat J. et al. 2022 submitted to A&A arXiv:2106.14528
Ramos-Ceja, M, Oguri, M., Miyazaki, S., et al. 2021, A&A in press, arXiv:2109.07836
Sanders J.S., et al., 2020, A&A, 628, A43
Sanders J.S., et al., 2021, A&A, in press, arXiv:2106.14534
Seppi, R.; Comparat, J.; Nandra et al. 2021 A&A...652A.155

4.2.3 Compact Objects and Accretion Physics

One of the main research topics of the HE group at MPE deals with compact objects, like white dwarfs, neutron stars, stellar-mass and supermassive black holes, and the physical processes which power their X-ray emission. eROSITA plays an increasingly important role in the discovery of new objects in order to build large samples for the various source classes. For detailed spectral and temporal studies of the X-ray emission from accreting objects, which allow us to investigate the matter flow and its interaction with the radiation, follow-up observations are conducted. Deep X-ray observations with e.g. Chandra, NuSTAR and XMM-Newton completed by multi-wavelength data from radio to Gamma rays are essential for our research.

Detection of extreme flip-flops in an X-ray binary

We performed a detailed investigation of the outburst of the X-ray binary Swift J1658.2-4242, utilising long observations from XMM-Newton, NuSTAR, Astrosat, Swift, Chandra, and HXMT in X-rays, and combining these with observations with INTEGRAL in Gamma-rays, and ATCA in radio. We detected 15 so-called flip-flop transitions, which are top-hat-like, rapid changes between two semi-stable states in the X-ray light curve and the power spectrum. The flip-flops we observed are of a more extreme variety than have ever been seen before, with the bright flip-flop state being 77% brighter than the dim state. We also observed the first direct transitions between quasi-periodic oscillation types A and C, without an intermediate type B, during these extreme flip-flop transitions. The bright state X-ray spectrum was fitted with a higher temperature, and stronger power-law component, compared to the dim state spectrum. The times of flip-flop transitions were found to almost always occur at integer multiples of 2761 s. This potentially indicates the existence of a repeating mechanism that is responsible for causing these observed dramatic transitions.

The Proper Motion of Central Compact Objects in Supernova Remnants

The proper motion of neutron stars encodes information about the physical velocity and origin of these compact stellar remnants, which can be used to constrain the explosion kinematics and age of the parent supernova. For the peculiar class of young, thermally emitting neutron stars deemed Central Compact Objects (CCOs), such measurements can only be performed in X-rays, where they are exclusively detected. For the CCO RX J8022-4300 in the supernova remnant (SNR) Puppis A, we performed the most accurate such measurement to date, by precisely co-aligning a set of Chandra observations using a set of astrometric reference sources from Gaia DR2. This conclusively disproved previous claims of an extremely high neutron star kick velocity of 1600 km/s, as we constrained its value to (760 +/- 70) km/s for an assumed distance of 2 kpc, which is much easier to reconcile with numerical modelling. In combination with an independent estimate of the supernova explosion site, we derived a kinematic age of (4600 +/- 700) yr for Puppis A and its CCO. Following a similar approach applied to sets of archival Chandra data, we performed proper motion measurements for a sample of six further CCOs. This effort almost doubled the number of CCOs with directly constrained kinematics. While we found neither theoretically "problematic" neutron star velocities in excess of ~ 1000 km/s, nor obvious departures from the radio pulsar velocity distribution (Hobbs et al. 2005), our measurements established constraints on likely

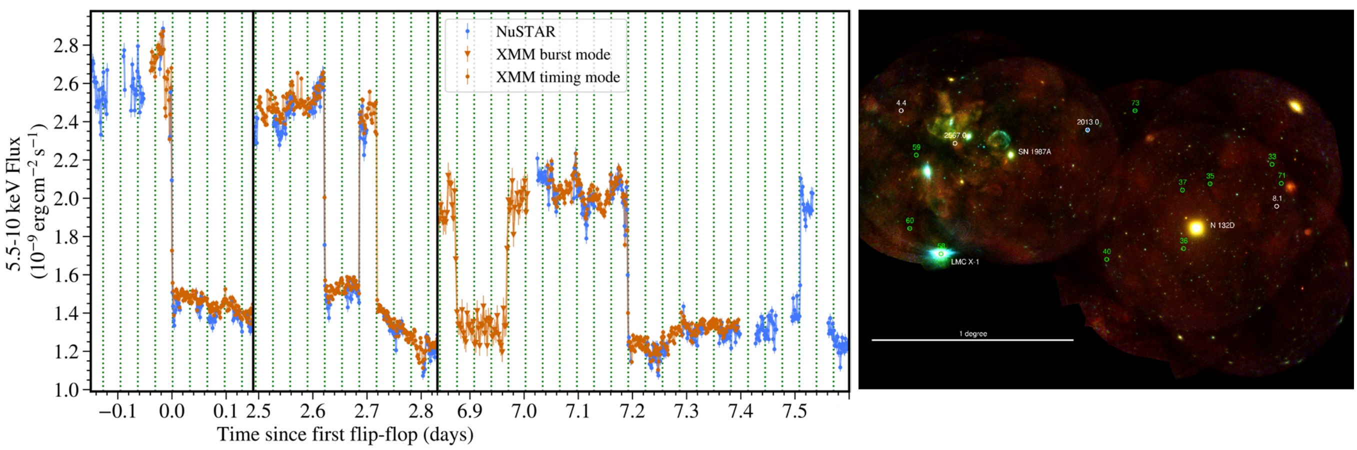

*Fig. 4.2.3 **(Left)** Collection of NuSTAR and XMM-Newton light curves featuring flip-flops. The green lines are plotted every 2761 s since the first observed flip-flop transition. These lines fit through almost all observed flip-flop transitions, possibly indicating that this timescale might guide the flip-flop transitions. The amplitude of flip-flops decreases over time, at a faster rate than the decrease in the average flux. **(Right)** LMC mosaic from eROSITA observations around SN 1987A and N 132D. Red, green, and blue represent X-ray energies in the bands 0.2-1.0 keV, 1.0-2.0 keV, and 2.0-4.5 keV, respectively. The HMXB pulsars are marked with white circles and labelled with their pulse period measured near the time of their discovery. HMXBs and candidates without known pulse period are indicated by green circles. The newly discovered Be/X-ray binary SRGEt J052829.5-690345 is marked as source 73.*

explosion sites of the parent supernovae. For selected cases, this allowed determining fundamental properties of the systems, such as their age or the degree of intrinsic asymmetry in the X-ray emission of the parent SNRs.

The high-mass X-ray binary population in the Magellanic Clouds

With well-known distances, low foreground absorption and a very advantageous visibility for space observatories, the Magellanic Clouds are ideal laboratories for X-ray source population studies. For one of its first-light observations, eROSITA, the soft X-ray instrument on board the Spektrum-Roentgen-Gamma mission, was pointed at SN 1987 A in the Large Magellanic Cloud (LMC). Together with observations from the calibration and performance verification phase a contiguous 4.4 square degree field was covered. Fourteen high-mass X-ray binaries (HMXBs) including candidates were known before in this area and we discovered one new Be/X-ray binary (a HMXB with a Be companion star). Similarly, calibration observations of the supernova remnant 1E 0102.2-7219 in the Small Magellanic Cloud (SMC) covered 23 HMXBs, which includes 16 X-ray pulsars. Five pulsars were sufficiently bright to allow a detailed spectral and temporal analysis and from one Be/X-ray binary the pulsations were discovered in the eROSITA data for the first time. The pulse periods for the two pulsars SXP 726 and SXP 1323 measured from the eROSITA data were ~800 s and ~1006 s, respectively, which is very different from their discovery periods. Including archival XMM-Newton observations, we updated the spin-period history of the two long-period pulsars, which have shown nearly linear trends in their period evolution for more than 15 years. The corresponding average spin-down rate for SXP 726 is 4.3 s/yr, while SXP 1323 has a spin-up rate of -23.2 s/yr. Measuring the spin period derivative over a long time allows to estimate the magnetic field strength of the neutron star and to put constraints on the accretion flow and transfer of angular momentum in these systems.

Discovery of pulsations from the young and energetic rotation-powered pulsar PSR J0058-7218:

The Magellanic Clouds, especially the SMC, host a large population of HMXBs (predominantly Be X-ray binaries), that has been studied extensively in the past. These Be X-ray binary pulsars are typically a few 10 million years old and have spin periods ranging from 1 to 2000 s. On the other hand, of the 'younger' population of isolated neutron stars that constitute the rotation powered pulsars, just a few are known. Only seven such objects have been discovered in the SMC until now from radio surveys and their detection may be prone to several selection effects and observational biases. A breakthrough was made in this regard with the discovery of a 22 ms pulsar, PSR J0058-7218 from the central compact source associated with IKT16, a supernova remnant in the SMC with an age of about 15 kyr. The pulsar is embedded in a soft and symmetric pulsar wind nebula (PWN) surrounding a bright hard X-ray source, a.k.a. PSR J0058-7218. We measured the spin period and spin period derivative of the pulsar at 21.7661076 ms and 2.9×10^{-14} s/s, respectively. Assuming the standard spin-down scenario with magnetic dipole radiation, the spin-down power corresponds to 1.1×10^{38} erg/s implying a Crab-like pulsar. This makes PSR J0058-7218 the most energetic pulsar discovered in the SMC so far and a close analogue of PSR J0537-6910, a Crab-like pulsar in the Large Magellanic Cloud. PSR J0058-7218, like PSR J0537-6910 is a radio and Gamma-ray-quiet pulsar, and is currently only detected in the X-ray regime.

Accretion onto black holes across the mass scale

We have studied the well-known observed correlation between monochromatic X-ray and UV luminosities in AGN, which is a proxy for the accretion disk and X-ray corona emission. In particular, focusing on radiatively-efficient AGN, i.e. the ones that radiate from a few percent to tenths of the Eddington limit. This relation carries important physical insights since it states that for increasingly luminous AGN the coronal emission increases less than the disk emission. However, this rela-

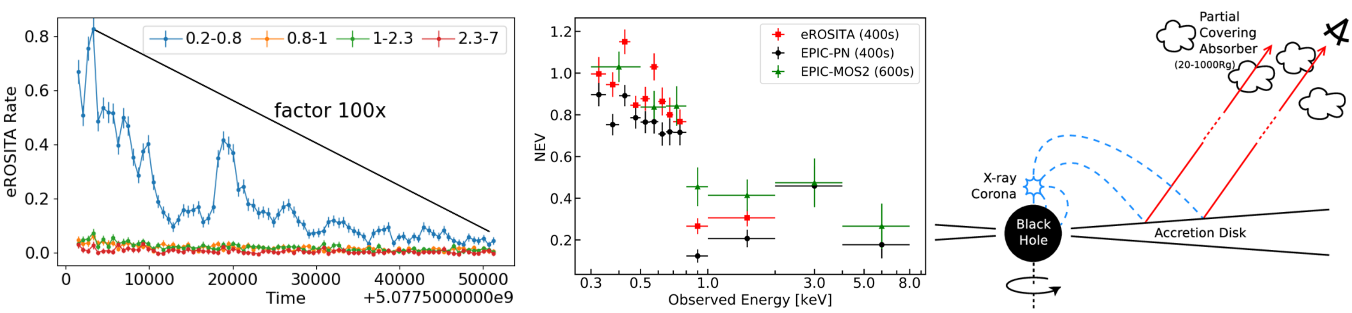

Fig. 4.2.4 Left: *During the eROSITA observations, 1H 0707-495 showed a dramatic flux drop by a factor of 100 in about one day.* ***Middle:*** *Normalized excess variance (NEV) as a function of energy. The NEV spectra reveal dramatic variability below 0.8 keV, with a striking drop off between 0.8 and 2.0 keV. The variability increases slightly from 2 to 4 keV before dropping again from 4 to 8 keV.* ***Right:*** *Illustration of the considered scenario. Above a spinning black hole, X-rays are emitted anisotropically. Because of the compact corona very close to the black hole, the majority of the photons either hit the accretion disc or fall into the black hole. From the high- to the low-flux state, an ionized partial coverer is obscuring an increasing part of the emitted X-ray radiation.*

tion still lacks a clear theoretical explanation despite being used for many applications including. A self-consistently coupled disk-corona model can predict the observed relation, i.e. the observed X-ray and optical-UV luminosities, provided the population of observed AGN is preferentially highly spinning. This is extremely important since high incidence of highly-spinning sources significantly impacts the growth of black holes over cosmic time, as spin makes black holes more efficient and it also impacts the co-evolution between black holes and the galaxies they reside in, since high spins are key to efficiently launch collimated outflows up to galaxy scales. We also connected both phenomenology and physics of accretion onto stellar-mass and supermassive black holes in a mass scale invariant fashion, in particular for the radiatively efficient and non-jetted end of accretion modes. A comparison of the above-mentioned disk-corona relation between AGN and X-ray binaries (XRBs) indicate that a mass-scaling of properties might hold after all and they are consistent with the disk-corona systems in AGNs and XRBs exhibiting the same physical processes, albeit under different conditions for instance in terms of temperature, optical depth and/or electron energy distribution in the X-ray corona, heating-cooling balance, coronal geometry and/or black hole spin. Identifying what is and what is not mass-invariant in accretion flows around black holes allows a correct use of XRBs, notoriously more favourable observationally (they are brighter and evolve on human timescales), to understand how their supermassive analogues grow, evolve and impact the surrounding galaxies.

The nature of extreme ultra-soft X-ray variability in 1H0707-495 first detected by eROSITA

One of the most prominent AGNs, the ultra-soft Narrow-Line Seyfert 1 Galaxy 1H0707-495, has been observed with eROSITA as one of the first CalPV observations on October 13, 2019 for about 60 ks. The 2019 spectrum is drastically different from other AGN spectra observed so far, as it is much more variable at low energies up to only 0.8 keV. The simultaneous XMM-Newton spectra show the same basic shape. We showed that the unusual soft X-ray variability, first detected by eROSITA, is due to a combination of an obscuration event and strong suppression of the variance at 1 keV by photo-ionized emission. An ionized partial coverer and strong relativistic reflection explains the unique X-ray softness. During the eROSITA observations, 1H 0707-495 showed in addition a dramatic flux drop by a factor of about 100 in just one day. This variability is primarily in the soft band, and is much less extreme in the hard band. Such extremely large-amplitude variability has been observed in the past only in a few AGNs such as IRAS 13224-3809, GSN 069, and RX J1301.9+2747. In the combined eROSITA and XMM-Newton observation, 1H 0707-495 was caught in a historically low hard-flux state.

Selected References:

Arcodia et al., A&A, 628, A135 (2019)
Arcodia et al., A&A, 638, A100 (2020)
Bogensberger et al., A&A, 641, A101 (2020) • Boller et al., A&A, 647, A6 (2021)
Carpano et al., A&A, in press, arXiv2106.14536 (2021)
Carpano et al., MNRAS, 490, 4804 (2019)
Haberl et al., A&A, in press, arXiv2108.11517 (2021)
Maitra et al., A&A, 657, A26 (2022)
Maitra et al., MNRAS, 507, L1 (2021)
Maitra et al., MNRAS, 504, 326 (2021)
Maitra et al., A&A, 647, A8 (2021)
Maitra et al., MNRAS, 490, 5494 (2019)
Mayer et al., ApJ, 899, 138 (2020)
Mayer & Becker, A&A, 651, A40 (2021)
Treiber et al., MNRAS, 503, 6187 (2021)

Frank Haberl

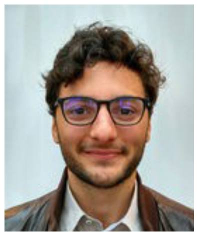

Riccardo Arcodia

David Bogensberger

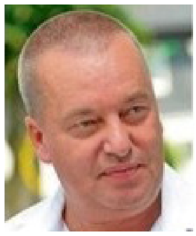

Thomas Boller

Chandreyee Maitra

Martin Mayer

(Other members include: W. Becker, S. Carpano, J. Greiner, D. Kaltenbrunner, A. Rau, R. Willer. Former members: L. Baronchelli, P. Maggi, G. Vasilopoulos)

4.2.4 Transients

The study of transient astronomical events, or short 'transients', in the HE group utilizes predominantly MPE's investments in space- (eROSITA, Fermi/GBM, INTEGRAL-SPI/ACS) and ground-based (GROND) instrumentation. The main scientific focus over the last three years has been on the study of eROSITA detected transients associated to the nuclei of previously inactive galaxies, including Quasi-Periodic Eruptions (QPEs) and Tidal Disruption Events, and on the prompt emission properties of Gamm-Ray Bursts (GRBs). Other topics of exploration included superluminous supernovae, supernovae associated to GRBs, and GRB host galaxies.

X-ray QPEs

Using the SRG/eROSITA all-sky survey data, Arcodia et al. (2021) discovered very-high-amplitude bursts of X-rays recurring every few hours originating near the centre of two previously quiescent galaxies. Follow-up observations with XMM-Newton and NICER determined the period, amplitude and burst profiles of these QPEs) and showed that they are inconsistent with current models of accretion disk instabilities. Instead, they suggest that QPEs might be driven by a secondary orbiting body, with mass much lower than that of the main ~10^5 - few x 10^6 $M_\odot$ black hole. Possibilities include a star or even a white dwarf, which might be partially disrupted by the huge tidal forces close to the black hole at each passage. This scenario could make QPEs viable candidates for the electromagnetic counterparts of extreme mass ratio inspirals, with considerable implications for multi-messenger astrophysics and cosmology. Regardless of their origin, finding more QPEs from the continuing eROSITA survey will help us to understand how black holes are activated in low-mass galaxies.

Nuclear Transients with eROSITA

A PhD thesis led to the development of a pipeline for the identification of transients and large-amplitude variable sources within the eROSITA All-Sky Survey. (Malyali 2021). This has already facilitated the publication of papers by the eROSITA consortium, and has also enabled systematic searches for nuclear transients, such as Tidal Disruption Events (TDEs), to be performed. The eROSITA discovery of the extreme nuclear transient AT 2019avd (Malyali et al. 2021) as an ultra-soft, large amplitude flare from a previously quiescent galaxy, highlighted the difficulty of identifying TDEs using solely the information provided by the X-ray observations. While the X-ray properties alone would have made AT 2019avd a strong TDE candidate, the broader multi-wavelength picture clearly shows a more complex scenario than that which has been seen in all pre-eROSITA TDE candidates. This work implies that the X-ray properties of a nuclear transient alone are not always able to distinguish between different physical origins of the large-amplitude variability seen in galactic nuclei, with more complex variability behaviour possibly present in the multi-wavelength datasets. In addition to AT 2019avd, extensive follow-up campaigns have been conducted for a number of eROSITA-discovered TDE candidates, with detailed studies of these to be produced in the near future.

Gamma-ray Bursts

The fourth Fermi-GBM Gamma-Ray Burst Catalog (von Kienlin et al. 2020) contains the standardized analysis results for 2356 GRBs spanning 10 years of operation. A key result is that about one quarter of the GRBs belong to the short duration class, thought to originate from the mergers of two compact objects. This is significantly larger than the results using previous definitions based on the duration of the prompt emission

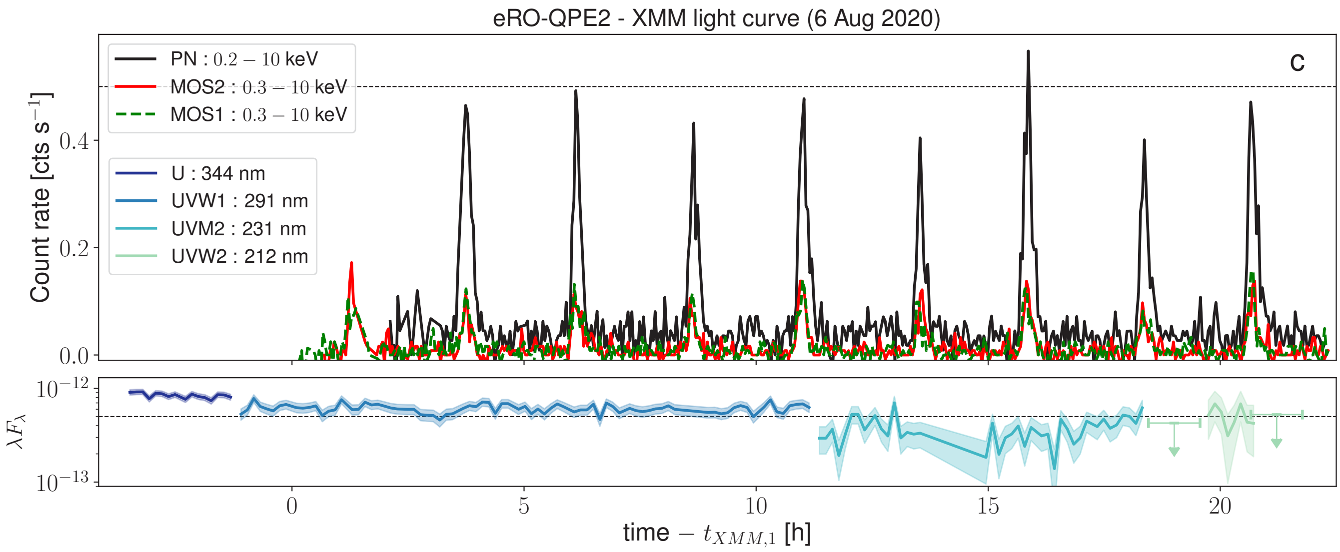

__Fig. 4.2.5__ XMM-Newton X-ray (top) and UV(bottom) light curve of the QPE source eRO-QPE1.

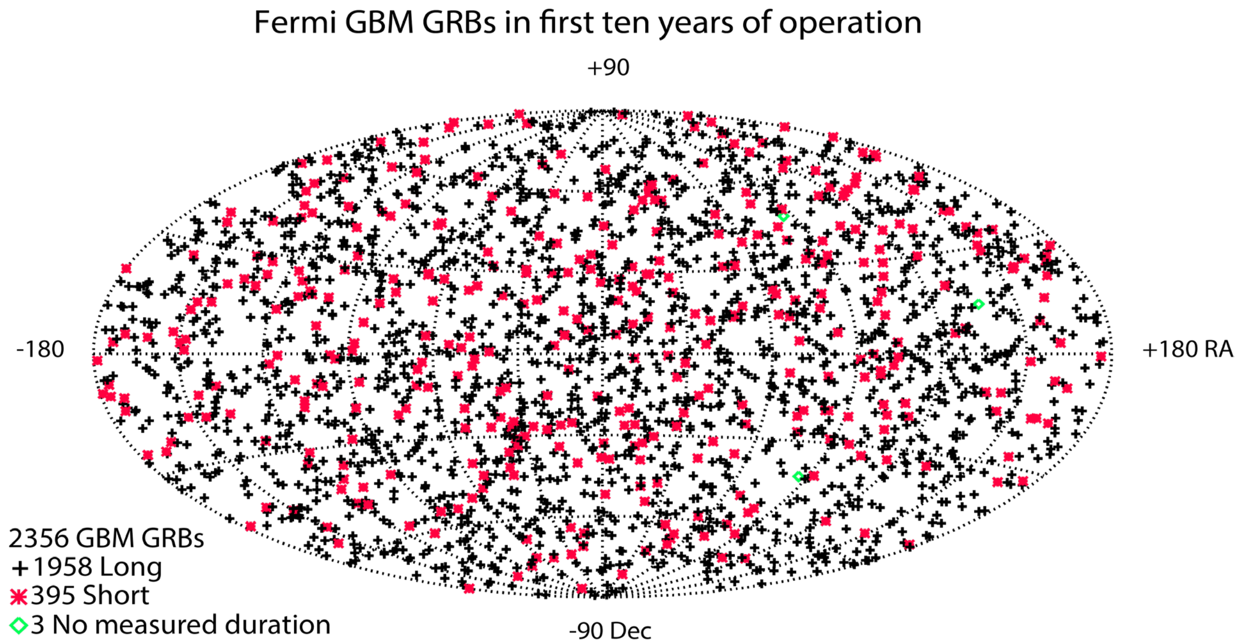

Fig 4.2.6 *Sky distribution of Gamma-ray Bursts detected during the first 10 years of Fermi/GBM.*

(with≤2s). The catalog provides the community a foundation upon which to perform more detailed follow-up analysis, taking advantage of the huge dataset of GBM-detected GRBs. This is already reflected by numerous studies using the 10-year catalog (~70 citation within 2 years). One of the follow-up analyses is the third GBM GRB spectral catalog (Poolakkil et al. 2021) which presents time integrated and peak-time spectral analyses of GRBs detected. From 2297 GRBs, the catalog contains a compendium of over 18,000 spectra and constitutes the largest sample size for comparing the spectral parameters of long and short GRBs.

The longstanding problem in GRB localisation accuracy was addressed by the development of the BALROG code (Berlato et al. 2019) which allows simultaneous fitting for the location and spectrum thereby significantly reducing the remaining systematic error. A statistically robust update to the timing and triangulation algorithm for GRB localization via arrival time triangulations was presented in Burgess et al. (2021). A physical background model for Fermi/GBM was described in Biltzinger (et al. 2020).

Other highlights included addressing the question whether spectral width of the prompt gamma-rays is a reliable measure of GRB emission physics (Burgess 2019). A systematic study of single-pulse GRBs with known redshift showed that the prompt emission can be fit with synchrotron emission when properly incorporating time-dependent cooling of the electrons (Burgess et al. 2020a). While supportive of synchrotron, simultaneous spectral and polarization analysis of time-resolved GRB polarization measurements with POLAR and GBM revealed a rotation of the polarisation angle throughout a GRB (Burgess et al. 2019). Examining the observer-frame parameter space of short GRBs from Fermi/GBM, led to the prediction that the majority of future GW-detections of NS-NS mergers will be accompanied by faint γ-ray emission (Burgess et al. 2020b).

Selected References:

Arcodia. R., et al., 2021, Nature, 592, 704
Berlato, F., et al., 2019, ApJ, 873, 60
Blitzinger, B, et al., 2020, A&A, 640, A8
Burgess, J.M., 2019, A&A, 629, A69
Burgess, J.M., et al., 2019, A&A, 627, A105
Burgess, J.M., et al., 2020a, Nature Astron., 4, 174
Burgess, J.M., et al., 2020b, Frontiers in Astron, & Sp. Sci., 7, 40
Burgess, J.M., et al., 2021, A&A, 654, A26
Mayali, A., et al., 2021, A&A, 647, A9
von Kienlin, A., et al. 20202, ApJ, 893, 46


Arne Rau


Riccardo Arcodia


Jochen Greiner


Andreas von Kienlin


Adam Malyali

(Other members include F. Berlato, B. Biltzinger, J.M. Burgess, F. Kunzweiler, I. Grotova, Z. Liu, A. Merloni, K. Nandra; Former members: J. Chen, T. Schweyer)

4.2.5 Galactic Structure and the ISM

The X-ray sky is rich in extensive, diffuse structures that can be up to half the size of the entire sky. The X-ray emission from these structures is usually caused by hot plasma with temperatures of several million degrees. Most of these emissions can be associated with supernova remnants. In addition, however, there are structures whose causes are not so clear or have been discussed for a long time. In contrast to X-ray observatories like XMM-Newton or Chandra, SRG/eROSITA as an all-sky survey instrument with its practically unlimited field of view is excellently suited to map those large regions with smooth and uniform exposures.

eROSITA Bubbles

The North Polar Spur is the largest and most conspicuous emission structure in the X-ray sky. Its cause has been debated for decades - a nearby supernova remnant or galactic structure emanating from the center of the Milky Way. With the eROSITA discovery of two symmetrical bubbles, of which the North Polar Spur is a part, the Galactic Centre origin was proven. These bubbles extend more than 11 kiloparsec above and below the Galactic Centre and include a structure in the southern sky which resembles the North Polar Spur. These X-ray bubbles are closely related to features seen also in γ-rays, the so-called Fermi-Bubbles. Large energy injections from the Galactic Centre are the most likely cause of both the γ-ray and X-ray bubbles. This could be due to strong shocks during an explosion that happened over 15 million years ago, when the Galactic Centre was 100 million times brighter than it is presently. The total energy of the shock-heated X-ray emitting gas amounts to $\sim 10^{56}$ erg, sufficient to perturb the structure, energy content and chemical enrichment of the circumgalactic medium.

While it is still uncertain whether this energy output was due to AGN activity or a nuclear starburst, these observations could provide important clues for the cosmological evolution of galaxies in general. The halo of the Milky Way provides a laboratory to study the properties of the shocked hot gas predicted by models of galaxy formation. Continuous observation with eROSITA will provide various physical parameters of the shock-heated X-ray gas. In particular, the temperature of the X-ray emitting gas can constrain the expansion velocity of the bubble, which has been roughly estimated to be ~300–500 km s^{-1}. In turn, the metallicity and absorbing column density are crucial for understanding the past activity of Sgr A*, which may have been triggered by either a nuclear starburst or an AGN.

Supernova Remnants

Supernova remnants (SNRs) are observable for about $(6–15) \times 10^4$ years before they fade in the interstellar medium. With a Galactic supernova rate of about two per century, there should be ~1200 SNRs in our Galaxy, but only ~300 are currently known. eROSITA offers a promising opportunity to find new supernova remnants, especially those that are strongly absorbed by the interstellar medium. One recent discovery is G249.5+24.5 ("Hoinga"), the largest SNR found so far at wavelengths other than the radio. This source is located at an unusual high Galactic latitude. The brightest and most prominent structure in the western part of the Milkyway is the Vela complex with at least three prominent remnants: Vela SNR with almost 8° diameter, the bright Puppis A to the northwest, and Vela Junior to the southeast of Vela. All three are at different distances, with Puppis A being the farthest away and Vela the closest. Vela Junior was detected only 23 years ago due to its hard non-thermal spectrum. All three remnants contain a compact object in their centre, two of which are also Pulsars (Vela and Puppis A).

Puppis A shows a strong peak of foreground absorption in the southwest quadrant, which in combination

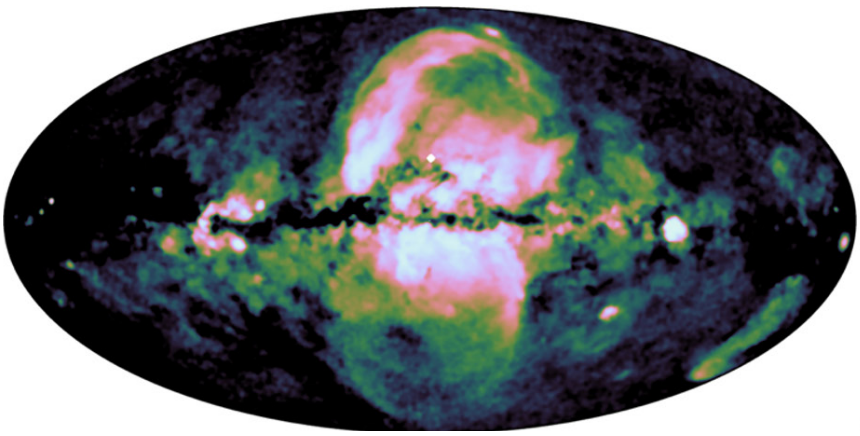

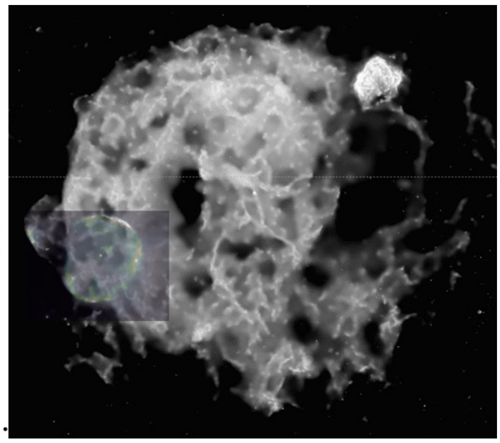

Fig. 4.2.7 (left) *The eROSITA bubbles. In this false-colour map the extended emission at energies of 0.6-1.0 keV is highlighted. The contribution of point sources was removed and the scaling adjusted to enhance the larges-scale structures in our Galaxy.* ***(right)*** *The Vela complex shows the highly dynamical evolution of Vela and Puppis A SNRs while the much younger Vela Junior (overlayed) is dominated by its non-thermal shell.*

with high temperatures at the northeast rim creates the well-known strip of hard emission crossing the remnant. We estimated the age of the shock in the individual regions based on the observed distribution of the ionisation age. We find a fairly recent shock interaction for the prominent northeast filament and ejecta knot, as well as for the outer edge of the bright eastern knot. Finally, elemental abundance maps show only a single distinct enrichment of the plasma with ejecta material, consistent with a previously reported knot, and no obvious ejecta enrichment in the remainder of the SNR. Within this region, we confirm the spatial separation of silicon-rich ejecta from those dominated by lighter elements. The apparent elemental composition of this ejecta-rich region would imply an unrealistically large silicon-to-oxygen ratio for a core collapse supernova. In reality, both the observed composition of the ejecta and their apparent distribution may be biased by the unknown location and strength of the reverse shock.

Solar System

We used the performance verification phase to observe the most promising comet which was visible at that time, comet C/2018 W2 (Africano). Although this comet was visually as faint as 11.4 mag, we succeeded in detecting X-ray emission from this comet, caused by solar wind charge exchange reactions. The observation happened to coincide with the passage of solar wind plasma with enhanced density over the comet, which caused the comet to exhibit an X-ray flare, accompanied by indications of spectral changes. Solar wind charge exchange occurs also with interstellar gas streaming through our solar system and causes it to glow in soft X-rays. The wide field of view, high sensitivity to soft X-rays, high spectral resolution, large distance from the Earth magnetosphere and exosphere, and the possibility to perform repeated all-sky surveys makes eROSITA the perfect instrument to study the properties of this foreground emission, which is inevitably present in any X-ray observation. By comparing the surveys which are now available, we have found already evidence that this component is present and that its flux is correlated with solar activity, as expected.

SRG is the first X-ray mission at Sun-Earth L2. The all-sky survey offers the opportunity to study variations of the solar wind in this region, due to the multiple coverage of the observed sky regions within a day. Variations along a survey great circle compared to an earlier or later scan can then be attributed to non-cosmic, i.e. solar origin. Moreover, the multiple all-sky surveys allow also a discrimination on time scales of half a year. Such enhancements can be caused by solar coronal mass ejections and by strong solar flares. These can be distinguished by the time delay between release from the Sun and arrival at L2 (several days CMEs, less than 1 hour for solar flare particles). Additionally, their response in the eROSITA telescopes also differs in terms of detailed temporal and spatial characteristics.

Werner Becker

Konrad Dennerl

Peter Predehl

Michael Freyberg

(Other members include F. Camilloni, F. Haberl, N. Locatelli, C. Maitra, M. Mayer, A. Strong, Y. Zheng.)

Selected References:

F. Camilloni et al., 2022, A&A submitted
W. Becker et al. 2021, A&A 648, A30
M. Mayer et al. 2022, A&A accepted
P. Predehl et al., 2020, Nature 588, 22

4.3 Projects

4.3.1 eROSITA

eROSITA (extended ROentgen Survey with an Imaging Telescope Array) is a sensitive wide-field X-ray telescope designed to perform a deep all-sky survey, with the primary goal of discovering all massive clusters of galaxies along our past light cone. eROSITA is the primary instrument on the Spectrum-Roentgen-Gamma (SRG) mission, which was successfully launched on July 2019. eROSITA started a survey of the entire sky on December 13, 2019, and has completed its fourth scan in December 2021. At MPE, we are responsible for operating eROSITA, calibrating the instrument, processing the data, archiving and analysing them with an (evolving) in-house developed software. Management of the eROSITA-DE science consortium and organization of the Data Releases fall also under the responsibility of the MPE team.

SRG was launched on July 13, 2019 from Baikonur, Kazakhstan, using a Proton-M rocket and a BLOK DM-03 upper stage. On its three months cruise to the second Lagrangian point (L2) of the Earth-Sun system, 1.5 million km in the anti-sun direction, spacecraft and instruments underwent checkout and commissioning, an early calibration and performance verification (CalPV) program was also executed. Since mid-October 2019 SRG is in a six-month-periodic halo orbit around L2, with a major semiaxis of about 640,000 km within the ecliptic plane and about 490,000 km perpendicular to it (as of Jan 2022). In July 2021 all the observations performed by the German Consortium as part of the CalPV program have been released to the public in the Early Data Release*, accompanied by a series of publications, many of which are highlighted elsewhere in this report. Starting in December 2019, the mission has entered its survey mode, with the spacecraft engaged in a continuous rotation around an axis pointing to the neighborhood of the sun. Since the whole sky is covered every half year, a total of eight scans will be completed after the planned four years of survey-mode operations. At the time of writing, four all-sky surveys have been completed (Fig. 4.3.1). The all-sky survey program will be followed in early 2024 by a phase of pointed observations, including access through regular announcements of opportunity for the worldwide astrophysical community.

eROSITA Operations at MPE

The Mission Control Center of the SRG mission is located in Moscow at NPO Lavochkin (NPOL) premises, where spacecraft control, flight dynamics and ground antenna interfacing take place. From NPOL the instrument telemetry is distributed to the High-Energy Astrophysics Institute of the Russian Academy of Sciences (IKI) and to MPE, where the instrument control and operations are located. Close interfacing between these three institutions occurs on a daily basis, with IKI the pivot between MPE and Mission Control. MPE is fully responsible for the operations of eROSITA, for maintaining its health and functionality, as well as planning periodic maintenance of the instrument and supporting contingency and station keeping operations, when required. This materializes in daily tasks that must be executed in due time, as well as 4 to 6 hours of daily ground contact time, during which the main objectives are:

eROSITA by Numbers (as of 25.02.2022): Major Mission Milestones	
Days in space	957
Days in full ops. Mode	871
eRASS1	100% (187 days)
eRASS2	100% (185 days)
eRASS3	100% (186 days)
eRASS4	100% (188 days)
eRASS5	35% (66 days)
Data downloaded	~410 GB
Avg. camera availability	98%
Avg. total outage time	4.8%
Avg. commands rate	75/day
Avg. data telemetry rate	450 MB/day
Max. power coonsumption	340W<P<360W

**https://erosita.mpe.mpg.de/edr/index.php*

- Get real-time telemetry access to verify the telescope is fully operational and the cameras deliver science data.
- Execute in real time any commands required for changing settings of cameras and diagnostics operations. On average, ~75 eROSITA commands are sent daily.
- Mass memory dump of science and house-keeping data from eROSITA, for approximately 2 hours a day, for a daily data generation of 450MB.

To carry out all these tasks daily a team of 10 people is in place, composed of instrument experts and data analysis experts.

Characterizing eROSITA data

Background and Calibration: SRG/eROSITA is the first X-ray telescope at L2. With its large halo orbit dimensions, it is exposed to the solar wind and to galactic cosmic rays. Minimum ionizing particles (MIPs) are rejected onboard, and this rejection rate is an indicator of the incident high-energy proton flux and its variations with time, which are related to solar cycle (11-yr) and solar rotation (27-d). Fig. 4.10 shows this rate as function of time. The overall variations are quite small: after a maximum at mid-2020 (a few months after solar minimum) the rate has decreased by about 5%, modulated by solar rotation of order 2%, and individual spikes due to solar coronal mass ejections and solar flares (in particular end of October 2021). It is expected that the general level of galactic cosmic rays will continue to decrease with increasing solar activity in the next years, but individual flaring events will become more numerous (see Freyberg et al. 2020 for more details). Over more than a decade, a significant effort of the team at MPE was devoted to calibrate the seven eROSITA telescope modules (TMs). Thanks to the availability of the PANTER test facility, major milestones were achieved well before launch with an extensive on-ground calibration campaign (Predehl et al. 2021 and Dennerl et al. 2020), that allowed the science team to make use of science-quality calibrated data very early on after the end of the CalPV phase. Below, we describe in more details two aspects of the ongoing in-flight calibration effort, to demonstrate the outstanding quality of the instrument calibration.

In-orbit Energy Calibration

A suitable source for testing the quality of the current energy calibration is the Supernova Remnant 1E 0102-7217 in the Small Magellanic Cloud, which provides sharp emission lines at well defined energies. In Fig.3, we combine 10 SRG/eROSITA single pixel spectra of that source, taken in November 2019 and 2021 with the 5 TMs which are not affected by the optical light leak. We applied an empirical spectral model which was developed by the 'International Astronomical Consortium for High-Energy Calibration' (IACHEC), where the emission lines are organized into four groups, corresponding to O VII, OVIII, Ne IX, and Ne X. The normalizations of these groups were treated as free parameters, but coupled to the same value for each spectrum. Only the global normalization was allowed to be adjusted for each spectrum, as well as a shift of the absolute energy scale, which turned out to be correct to an accuracy of a few eV! A comparison of the line widths did

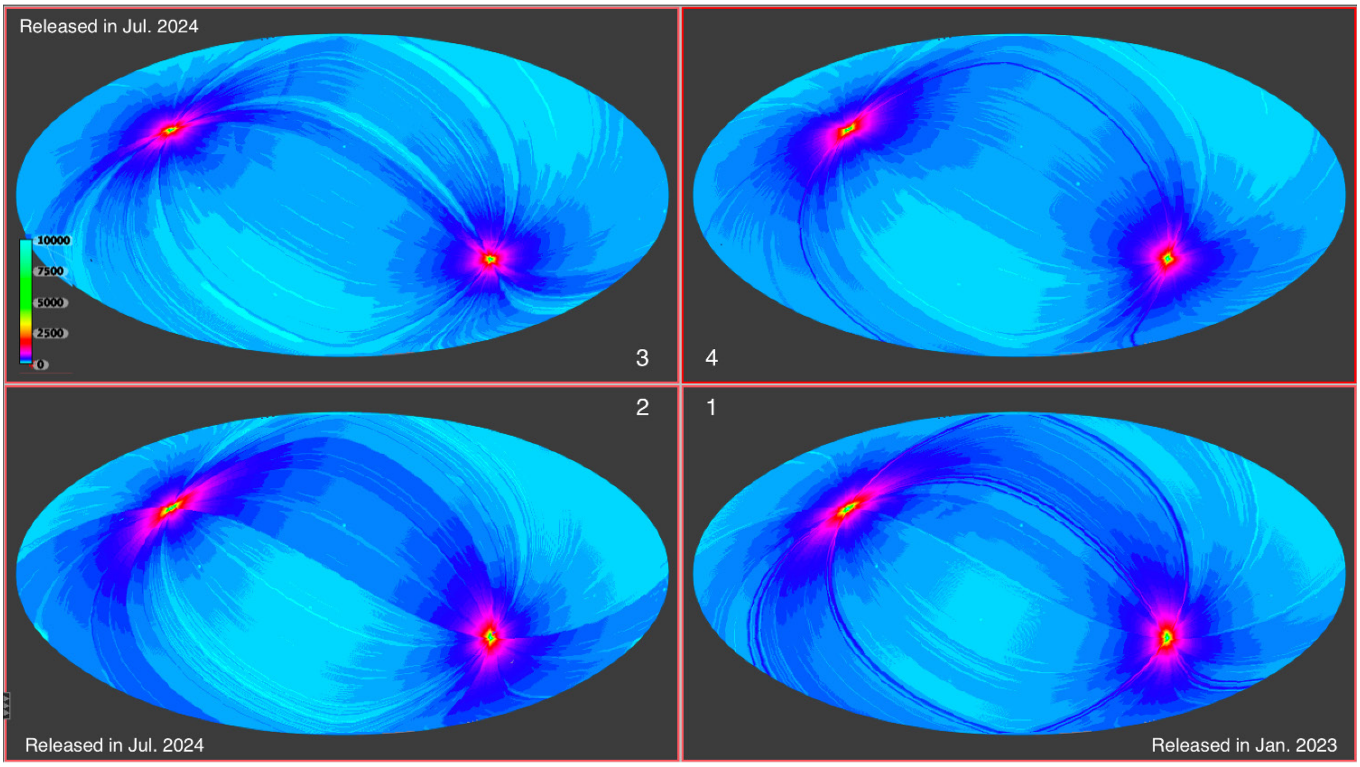

Fig. 4.3.1 *Aitoff projections of the exposure maps (in seconds) in the 0.6-2.3 keV band obtained by eROSITA during the first 4 surveys (from the bottom right, counterclockwise). Over most of the sky, each survey accumulates exposures ranging between 100 (cyan) and 200 (light blue) seconds, corresponding to a flux limit sensitivity of about 3-4x10^{-14} erg/s/cm2 (Predehl et al. 2021).*

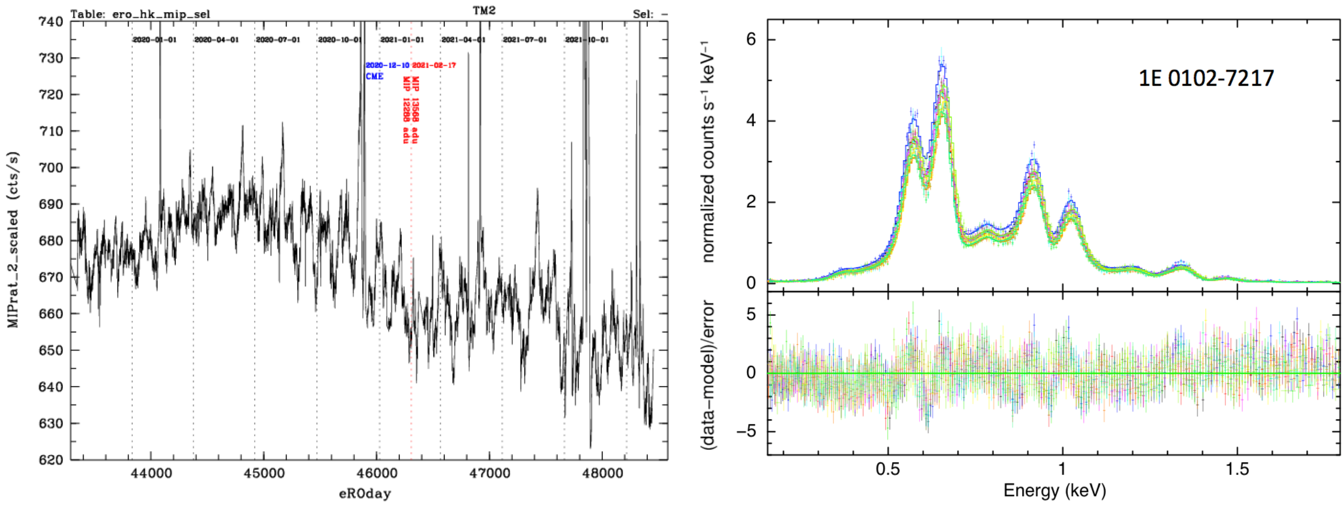

Fig. 4.3.2 (left) *Long-term light-curve of the rate of MIPS on TM2 rejected on-board, a good indicator of the high-energy proton flux hitting eROSITA. Vertical dashed lines are in 3-month intervals, the time unit (eROday) corresponds to a 4-h great circle time of the all-sky survey. Secular evolution of the rate mainly (anti-)correlates with the solar cycle, with small amplitude variations tracking the solar rotation cycle. A few large solar flares are evident. (right) Superposition of 10 SRG/eROSITA single pixel spectra of 1E 0102-7217, taken with the 5 TMs which are not affected by the optical light leak in Nov 2019 and 2021, demonstrating that the energy calibration is accurate to a few eV and that within two years no degradation of the spectral resolution is evident.*

not yield any significant increase during the first two years of the mission.

In-orbit PSF calibration

The depth of the two-year all-sky survey observations enables validation of the on-ground measurements of the point spread function (PSF) using stacked images of point sources detected in the survey. Fig. 4.3.3 shows the survey-averaged PSF of the TM1 telescope created from measurements made at the PANTER facility, compared to equivalents for each telescope module generated from stacked X-ray images of point sources in the detector-frame. Such stacked images can be generated as a function of energy and detector position, similar to what was done at PANTER. The data also help validate the ground-based vignetting measurements of the telescopes. In survey mode, we achieve an average Half-Energy Width (HEW) of ~30”, in line with the pre-launch expectations. This accurate PSF model will be used in future re-processing to improve the image fidelity and source detection and characterization.

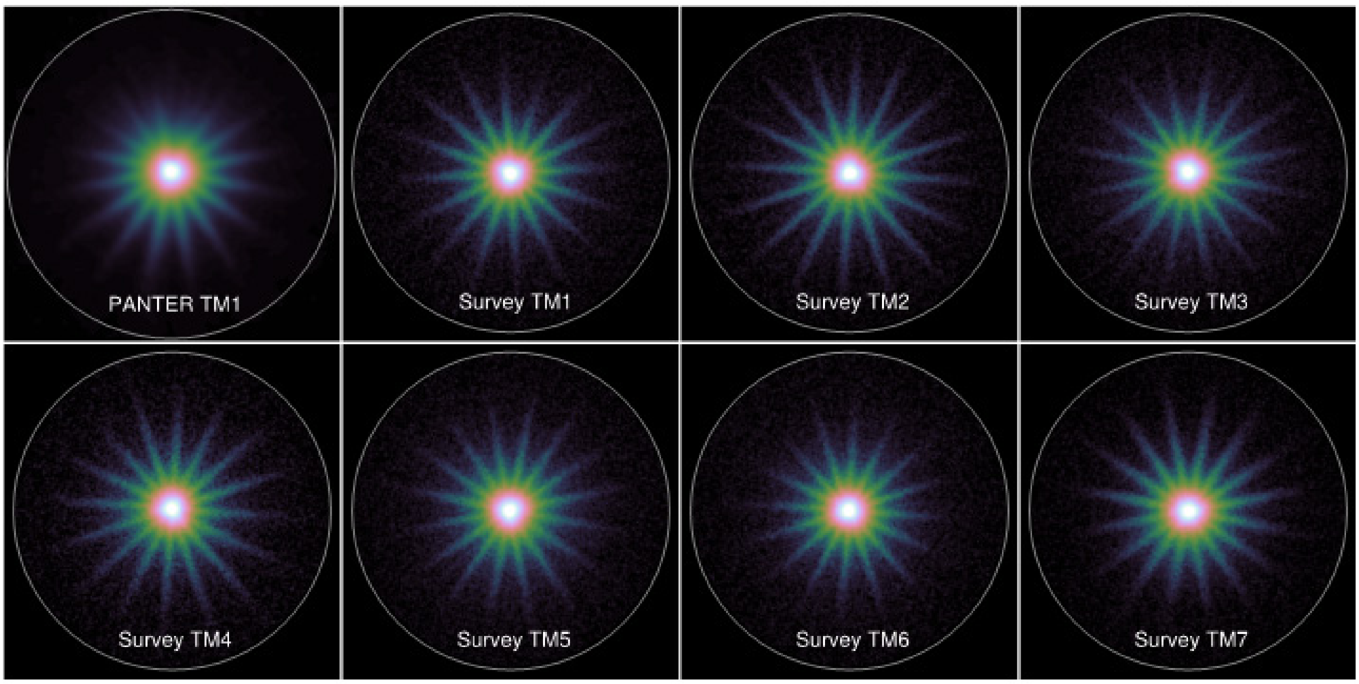

Fig. 4.3.3 *Survey-averaged PSF of the eROSITA TM1 telescope created from measurements made at the PANTER facility at an energy of 0.93 keV, compared to equivalents for each telescope module, generated from stacked X-ray images of point sources in the detector-frame between energies of 0.3 and 2.3 keV. The circle in each panel shows a radius of 4 arcmin.*

eROSITA data analysis, archiving and distribution
The eROSITA data analysis pipeline consists of four main chains, organized into event calibration, image and exposure map creation, source detection, and the creation of source specific products such as spectra and light-curves. A pipeline control environment triggers task chains execution and performs housekeeping activities. The pipeline is designed to process data from each of the three principal observing modes of the SRG spacecraft: all-sky survey observations, pointings at individual targets, and scan-mode observations. All-sky survey processing proceeds on a daily basis, providing the team with the most recent products, including full catalogs of all detected sources, for each eRASS (eROSITA all-sky survey) each week. Periodically (with milestones correlated with major data releases), the full re-processing of all data is performed with the most recent calibration settings and software development. Access to calibrated eROSITA data products and catalogs by eROSITA consortium members is facilitated via a browser-based data access tool. Users may request calibrated data products, such as calibrated X-ray event lists, images and maps, source catalogs and associated source specific data products for sky regions of interest. Requested datasets are retrieved from the archive and made available for password-protected downloading.

Andrea Merloni

Herrmann Brunner

Diogo Couthino

Konrad Dennerl

Michael Freyberg

Peter Predehl

Jeremy Sanders

Selected References:
Coutinho et al. 2020, SPIE 11444, id. 114444S
Dennerl et al. 2020, SPIE 11444, id. 114444Q
Freyberg et al. 2020, SPIE 11444, id. 114441O
Predehl et al. 2021, A&A, 647, 1

(Other HEG team members: W. Bornemann, S. Friedrich, R. Gaida, A. Gueguen, F. Haberl, W. Kink, C. Maitra, S. Mueller, K. Nandra, M. Ramos-Ceja, M. Salvato, I. Stewart)

4.3.2 Other Operating Missions

In addition to eROSITA, several other X-ray and γ-ray observatories with major contributions from the MPE HEG are operational in space, some already for more than two decades. These are still work horses in their respective fields, enabling new science for MPE and the wider scientific community.

XMM-Newton EPIC-pn calibration

To improve the response matrix and the energy-dependent sensitivity for the EPIC-pn instrument, which was designed and built by MPE, we developed a model which uses empirical-mathematical functions. To derive their parameters we carried out new dedicated observations of the standard calibration sources 1E 0102.2-7219 and RX J1856.5-3754. The spectrum of the supernova remnant 1E 0102.2-7219 is dominated by well-separated emission line complexes, which can be used to calibrate energy scale, resolution and redistribution at energies between 0.5 keV and 1.5 keV. In combination with the soft featureless spectrum of the isolated neutron star RX J1856.5-3754, it was possible to optimize the set of time-dependent parameters which successfully describe all spectra of the two sources taken over 16 years.

XMM-Newton Survey Science Centre (SSC)

The SSC collaboration has continued to create and validate serendipituous source catalogues from XMM-Newton pointed observations. A milestone has been the release of the 4XMM catalogue, which is updated on an almost annual basis. The current version DR11 contains more than 600000 unique sources detected in EPIC observations. For more than 319000 sources for the first time source level products like time series and spectra are available, along with variability information. The sky area with an exposure >1 ks is about 1239 deg^2. Moreover, an additional “stacked catalogue” has been built from overlapping observations (current version 4XMM-DR11s) with 275440 sources having several contributing observations. This allows also fainter objects to be detected as well as long-term variablity studies over up to 20 years. MPE still contributes to the maintenance and development of EPIC-pn tasks, mainly due to improved and extended calibraton, with synergetic effects from eROSITA.

Chandra

The Low Energy Transmission Grating (LETG) on Chandra was built by MPE in cooperation with SRON, NL. After 23 years in space, the LETG works perfectly within its original specification. Our benefit is a continued share of the Chandra guaranteed time allocation.

INTEGRAL

INTEGRAL continues its extended mission, now in orbit for more than 19 years. The nominal mission began on December 16, 2002 and lasted 24 months. Since then, INTEGRAL is operated in its extended mission phase, currently approved by the Science Programme Committee (SPC) to last until 31 December 2022. Further extension beyond 2022 is not secure yet. Future AO cycles are continued to be planned to run on an annual basis, if operations are again approved after 2022. A New Astronomy Reviews paper (Kulkers et al. 2021) provides a comprehensive update of the satellite status after more than 18 years of operations. On 22 September 2021, the INTEGRAL spacecraft went into emergency safe mode. One of the spacecraft’s three active ‘reaction wheels’ had turned off and stopped spinning, causing a ripple effect that meant the satellite itself began to rotate. Fortunately, the INTEGRAL Flight Control Teams at ESA's ESOC mission control center were able to rescue the mission that was nearly lost.

Fermi

The Gamma-ray Burst Monitor (GBM) is the MPE HE group contribution to Fermi, and continues successful operation. The GBM team including members of NSSTC in Huntsville, Alabama and the HE group and its European partner institutes monitors the instrument configuration health, validates the data products, and provides quick-look assessment and dissemination of GBM triggers. The role of the GBM Burst Advocate (BA) duty scientist (daily European/ MPE BA shifts from 7 am to 3 pm) supplements the automated RoboBA pipeline. Duties have evolved following the joint detection of GW170817 with GBM and LIGO/Virgo. The GBM BA confirms that RoboBA has run, that event classification is correct, and sends out circulars if needed. GBM also participates in the Inter Planetary Network (IPN), providing improved localizations by triangulating GRB data from spacecrafts in and beyond the low-Earth Orbit. A comparison between the automated Fermi GBM RoboBA localizations of GRBs and the independently developed BALROG algorithm was published by the GBM team in 2020.

Selected References:

N. Webb et al. 2020, A&A 641, A136
I. Traulsen et al. 2020, A&A 641, A137

Michael Freyberg, Frank Haberl (XMM), Peter Predehl (Chandra), Andreas von Kienlin (Integral and Fermi)

(Other HEG team members include K. Dennerl, S. Carpano, V. Burwitz, R.Diehl, T. Siegert, X.-L. Zhang)

4.3.3 ATHENA

Athena – the Advanced Telescope for High-ENergy Astrophysics – is ESA's next large X-ray telescope designed to address the 'The Hot and Energetic Universe' science theme. It is an L-class mission in the Cosmic Vision program with two scientific instruments, the Wide Field Imager (WFI) and X-ray Integral Field Unit (X-IFU). These are complementary interchangeable focal plane cameras behind a novel Silicon Pore Optics mirror system expected to provide unprecedented X-ray survey power and high-resolution spectroscopy, respectively. The WFI is being developed by an international consortium under the leadership of MPE and is the major hardware project of the HE group beyond eROSITA. The group is deeply involved in the Athena mission overall, with K. Nandra being a member of the Athena Science Study Team and several group members chairing scientific and infrastructure working groups and topical panels. MPE is also making a major contribution to the Athena optics development with the PANTER X-ray test facility.

The Wide Field Imager (WFI) is a powerful new X-ray camera for the Athena X-ray observatory, which has been designed to meet the requirements of the 'Hot and Energetic Universe' science theme. The instrument is based on unique Silicon DEPFET technology developed in the Semiconductor Laboratory (HLL) of the Max Planck Society. The DEPFET detectors provide the WFI's large 40'x40' field of view, state-of-the-art energy resolution, low noise, fast readout, and high time resolution, with excellent radiation hardness. These properties, in combination with the unprecedented effective area and wide field of the Athena telescope, are expected to provide breakthrough capabilities in wide-field X-ray imaging spectroscopy (see Table 1 for an overview). The WFI has been designed probe the typical activity of supermassive black holes at z>6; perform a complete and quantitative census of this accretion activity at z=1-4, including the most obscured objects; pinpoint the hot gas occupying the most massive dark matter haloes at z>2 when the first groups and clusters of galaxies formed; measure the temperature and abundances of clusters of galaxies out to their virial radius; perform spectral-timing measurements of bright compact sources to determine the geometry of the innermost accreting regions.

The ambitious WFI science is enabled by a Large Detector Array (LDA) consisting of four large-format (512x512 pixel) DEPFET devices, delivering a field of view of 40'x40'. The pixel size corresponds to 2.3" on

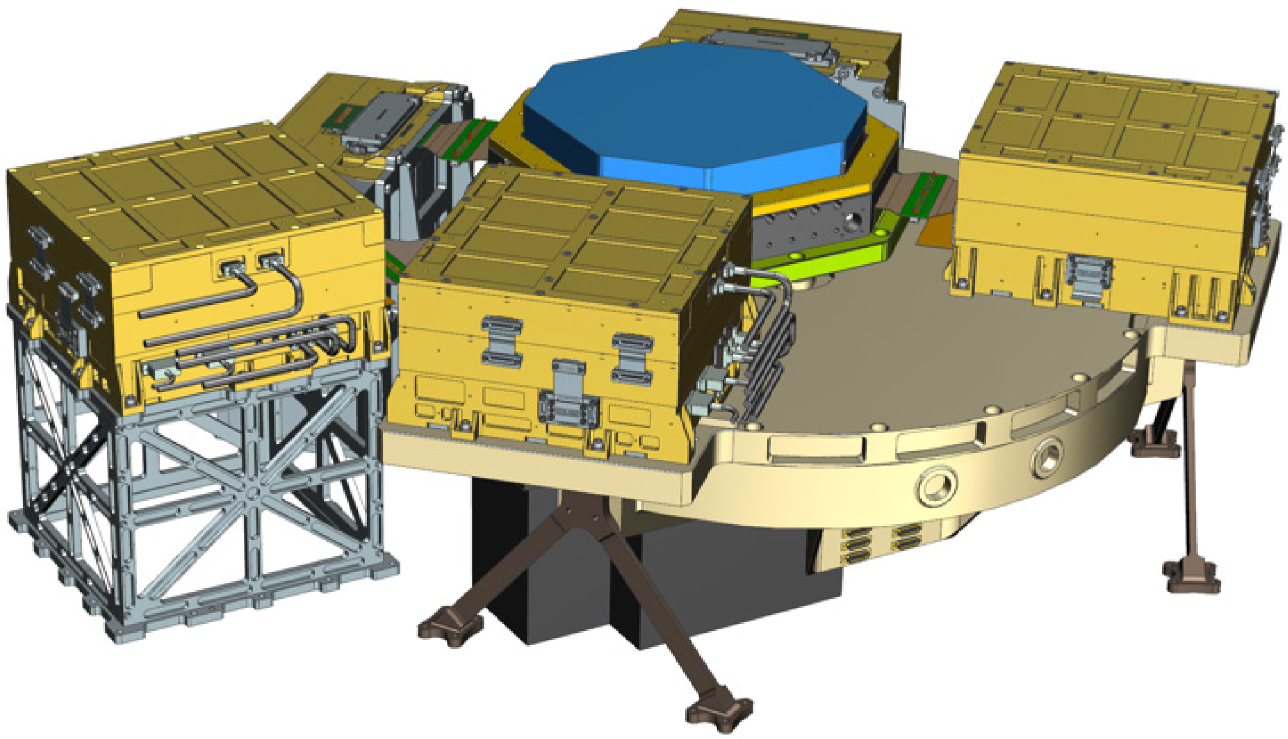

Fig. 4.3.4 Design drawing of the Athena/WFI instrument with its main subsystems; the camera head (centre with blue top) incl. DEPFET detectors is connected via flexible leads to the five detector electronics boxes (yellow). Most subsystems are mounted on the Primary Structure (beige), which is combined with the Filter Wheel assembly and mechanically interfaces with the Science Instrument Module.

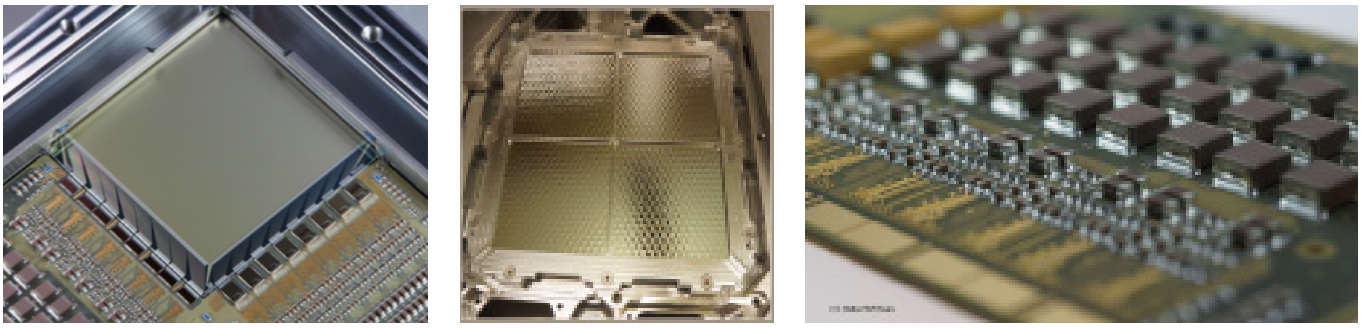

Fig. 4.3.5 (Left) *Full-size 512x512 detector quadrant mounted with its eight VERITAS2 readout ASICs to the left and eight Switcher control ASICs. WFI will use 2x2 of these detectors to deliver the 40'x40' field of view* ***(Middle)*** *Representative model of the WFI filter wheel assembly. Environmental tests have now been performed to prove the flight-worthiness.* ***(Right)*** *The WFI detector have been shorn to be fast enough to process the signals from the DEPFET/VERITAS in real time. A subsection of one of the DE PCBs is shown.*

the sky, oversampling the expected angular resolution of the Athena mirror (5" HEW) to provide accurate imaging and source positioning. A fifth DEPFET is used for the Fast Detector (FD) that is optimized for bright sources and typically used out-of-focus to improve the count rate capability. The DEPFET devices are controlled and read out by custom ASICs, known as Switcher-A and Veritas-2. The latter feed their signals into a total of five Detector Electronics (DE) boxes that perform the on-board frame processing. The output from the DE boxes is combined and fed to the spacecraft by the Instrument Control and Power-distribution Unit (ICPU), which can also perform additional processing. A conceptual design for the WFI instrument has been developed, demonstrating the basic feasibility of the system to (Fig 4.3.3) which is being continuously refined and brought to a more mature level of definition, while respecting the constraints of mass, volume, power and thermal properties required by the project overall.

In parallel a number of key technology developments are being performed (Fig. 4.3.4). These demonstrate a) the performance of the detector system, with a recent milestone being the successful manufacture and testing of a full-size 512x512 DEPFET quadrant, along with its ASICs, b) the design and robustness of the large, ultra-thin optical blocking filter and its assem-

Instrument Performance Parameters

Parameter	Performance			
Energy Range	0.2-15 keV			
	0.2 keV	**1 keV**	**7 keV**	**10 keV**
Instrument Efficiency; w/ external filter	4.2 %	77.9 %	90.6 %	87.6 %
Instrument Efficiency; (w/o) external filter	9.6 %	90.3 %	97.4 %	94.1 %
Eff. Area; on-axis, w/ external filter	0.057 m²	1.08 m²	0.14 m²	0.047 m²
Eff. Area; on-axis, w/o external filter	0.132 m²	1.25 m²	0.15 m²	0.051 m²
Energy Resolution (end-of-life)		<80 eV	<170 eV	
Pixel Size	130µm x 130µm (i.e. 2.24" x 2.24")			
Positional Accuracy	<1" (99.7% confidence)			
	LDA		**FD**	
Field of View	40' x 40' (outer envelope)		2.38' x 2.38'	
Frame time	5 ms		80 µs	
FD Count Rate Capability	1Crab: ~0.3 % pile-up, ~95 % throughput (w/ standard filter) 15Crab: ~1 % pile-up, ~93 % throughput (w/ 100µm Be filter)			
Instrumental Background	~5.5x10⁻³ cnt/s/cm²/keV (2-7 keV)			

bly, for which a breadboard model has been developed and subjected to acoustic noise and vibration testing and c) the the real-time performance of the DE, which has now been demonstrated. The instrument overall has just entered into its systems requirements review, due to be completed in late spring 2022. A dedicated technology readiness assessment to be performed by ESA later in 2022, in advance of the mission adoption expected in 2023. The delivery of the flight instrument to ESA is due in 2030 and for a launch to L1 aboard the Athena satellite in 2034.

The WFI consortium consists of scientific Institutes and universities from ten ESA member states and the USA. The overall project management is performed by the WFI Project Office at MPE. Instrument development work packages, including those for the WFI Instrument Science Center (WISC), have been allocated to a responsible partner, supported by their national funding agency and/or institutional resources. Our own activities are supported by DLR as well as MPG funds, with collaboration with the MPG HLL being absolutely essential for the continuing success of the project. Further details about the WFI instrument development can be found in in a number of articles in the MPE the 'Abstract Booklet'.

Selected References:

Meidinger, N., et al., 2018, Proc. of SPIE, 10699, 1F
Meidinger, N., et al., 2015, JATIS, 1,1, 014006-1
Nandra, K., et al., 2013, arXiV 1306.2307
Rau, A., et al., 2016, SPIE 9905-79

Kirpal Nandra

Norbert Meidinger

Arne Rau

(Other HEG members include: R. Andritschke, A. Behrens, M. Bonholzer, D. Coutinho, J. Eder, V. Emberger, G. Hauser, A. Koch, A. Mayr, J. Müller-Seidlitz, S. Obergassel, S. Ott, D. Pietschner, A. Rau, J. Reiffers, R. Strecker, J. Tran, J. Veredas, A. von Kienlin; former members include: T. Eraerds, B. Köglmeier, A. Lederhuber, W. Treberspurg)

4.3.4 Einstein Probe

Einstein Probe is a mission of the Chinese Academy of Sciences (CAS) due for launch in late 2023. The two instruments comprise the Wide-field X-ray Telescope (WXT), MPE is contributing hardware to the Chinese Einstein Probe (EP) satellite mission for monitoring the X-ray sky. This is done on the one hand as part of a European contribution to Einstein Probe by ESA, which includes the eROSITA-like optic of the FXT (Follow-up X-ray Telescope) and X-ray testing of WXT modules. On the other hand, MPE is independently supplying CCD modules for the FXT focal plane camera and has provided the eROSITA Flight Spare mirror assembly for a second FXT.

Einstein Probe will be a unique and powerful mission to discover high-energy transients and monitor variable objects. The EP science team has defined the observation modes for EP and the EP data policy. Based on the agreement between CAS, ESA, and MPE, MPE will have access to 10 percent of EP observation data, including data from WXT all sky survey, FXT targets of interesting, and EP ToO/follow-up observations. These data will enable MPE members to conduct their own science projects, such as: searching for QPEs in EP data, studying frequency of occultation events in SMBHs, and searching for partial TDEs. At the request of the CAS EP science team, MPE will also contribute

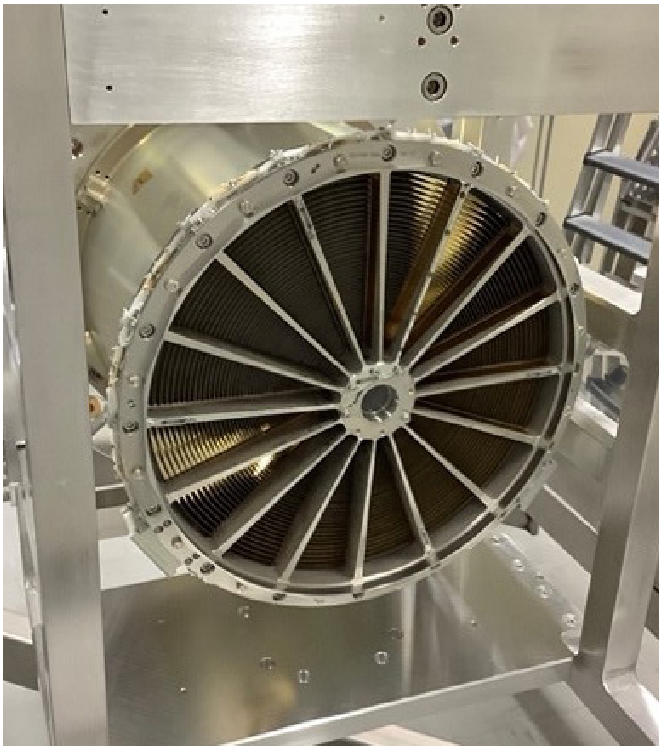

Fig. 4.3.6 *FXT Mirror Module FM* ***(left)*** *and its unification with X-ray baffle under optical control* ***(right)***

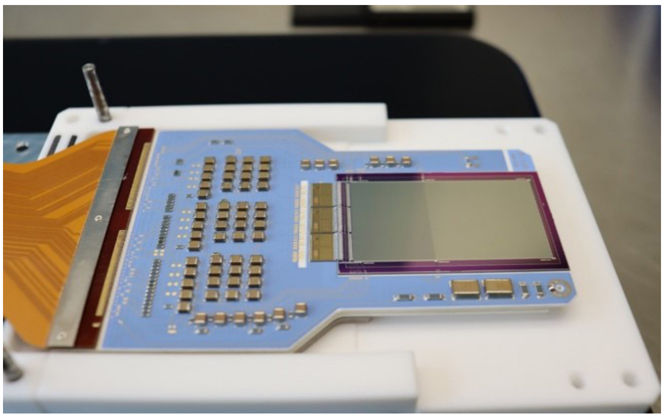

Fig. 4.3.7 *PNCCD detector module of the type delivered to IHEP, Beijing for the FXT focal plane.*

to the EP pre-launch science simulations by providing the eROSITA eRASS1 X-ray catalogue and eRASS1 X-ray diffuse background which match the sensitivity and angular resolution of EP well.

Optics

The FXT design was adopted from eROSITA, i.e. the mirror module consists of 54 nested Wolter mirrors with a focal length of 1600 mm and an effective area of greater than 300 cm2 at 1.5 keV. Together with the X-ray baffle, which suppresses stray-light from single reflection, it forms the mirror assembly. Three of them are to be delivered: structural-thermal model (STM), qualification model (QM), and flight model (FM). Starting in 2019, the mirror modules were manufactured by the Italian company Media Lario, while the corresponding X-ray baffles were made and unified with the mirror modules at MPE. The test and qualification program was carried out specifically for each of the three models: It includes vibration and thermal cycling tests for each model and in total ten X-ray performance tests, where two of them include the X-ray calibration of the QM (which serves as a flight spare) and the FM. In addition, MPE has provided three electron diverters (QM and 2 FMs) that shall prevent electrons from being focused towards the detector. The electron diverters are standalone items with an almost identical design of the eROSITA ones and underwent workmanship tests and a vibration tests at acceptance level. MPE is using its laboratories, cleanrooms and test facilities – in particular the X-ray test facility Panter – for the project. Available equipment and tools from the eROSITA project have being re-used where possible. On behalf of ESA, MPE has already delivered the STM and QM mirror assemblies and all electron diverters to China, the FM mirror assembly shall follow in May 2022.

Detector

The focal plane detectors of the two Einstein Probe FXT telescope are developed at MPE. These PNCCD detector modules are based on those of the eROSITA telescope array. The Einstein Probe FXT detector key performance characteristics are a read noise of 2.6 electrons rms, full frame readout within 9.2ms, an energy resolution of e.g. 150 eV FWHM at 5.9 keV energy, a pixel size of 75 x 75 μm^2 matched to the angular resolution of the Wolter mirror and a high quantum efficiency in the energy band from 0.3 keV to 10 keV by the principle of back-illumination and fully depleted chip thickness. MPE delivered to Einstein Probe FXT first an engineering model detector in 2020, then the qualification model and finally 2 flight detectors in 2021. Next is the flight spare detector module, scheduled for delivery in May 2022.

Peter Friedrich

Arne Rau

Norbert Meidinger

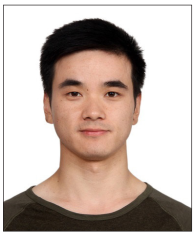

Zhu Liu

(Other members include: J. Eder, K. Hartmann, V. Stieglitz, E. Pfeffermann, R. Gaida, Ch. Rohé, D. Schuppe, V. Burwitz, G. Hartner, S. Rukdee, M. Bradshaw, A. Langmeier, T. Müller, T. Schmidt, B. Budau, F. Soller, K. Dittrich, I. Keil)

4.3.5 SVOM

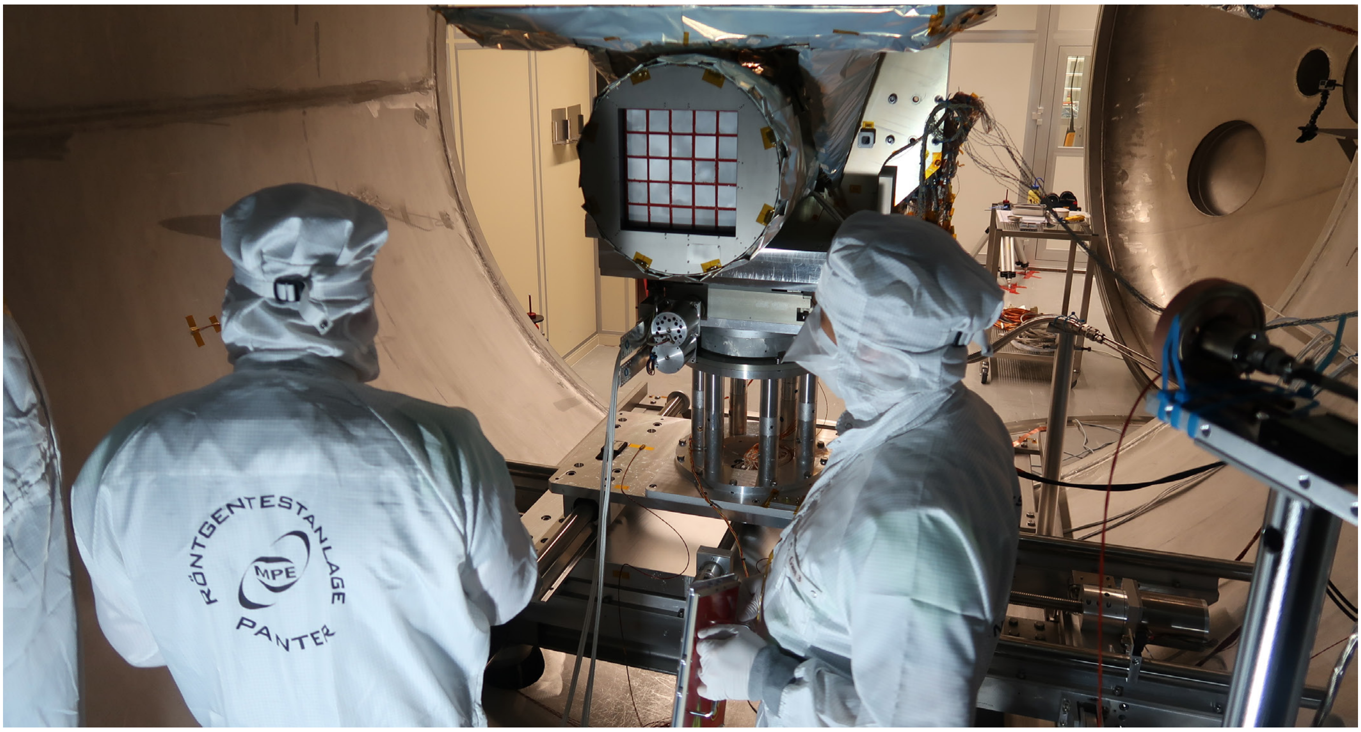

Fig. 4.3.8 *The SVOM-MXT-Flight Model telescope being prepared for the final calibration and performance test in the large vacuum chamber of the PANTER X-ray test facility. Mounted above the telescope is a LN2 shroud used to cool the MXT detector via its radiator to simulate conditions in space.*

MPE collaborates with French partners for the Chinese-French ***SVOM*** (Space Variable Objects Monitor) mission, anticipated to be launched in June 2023. The *SVOM* mission consists of three on board instruments, the French ECLAIRS GRB Monitor, the MXT follow-up soft X-ray telescope, and a Chinese 45cm optical telescope all on a Chinese satellite platform. The mission includes a VHF network for fast transmission of transient alerts to the ground, and two ground-based robotic observatories.

This suite of instruments will allow SVOM to discover Gamma-ray Bursts (GRBs), to study the X-ray and optical afterglow emission in the first minutes after the event, and to obtain early optical spectroscopy with large telescopes to measure the redshifts. SVOM will also play a major role in the search for electromagnetic wave counterparts of gravitational wave sources. MPE will be participating as a co-investigator in the SVOM science.

For the MXT instrument, MPE contributed the key components of the spectroscopic and imaging focal plane detector: the spectroscopic PNCCD sensor chips (frame store CCDs with 256x256 pixels in the image area) and custom 128-channel CAMEX readout ASICs. In the course of the contribution, the silicon chips were integrated in the electro-mechanical structure provided by CEA, France, including wire-bonding of the chips. MPE advised the MXT project team in operation of the spectroscopic X-ray detectors. All PNCCD detectors were assembled and afterwards successfully tested with the flight electronics by the partners at CEA and CNES in 2021.

Furthermore MPE has provided access to the PANTER X-ray test facility for testing and calibrating the MXT light-weight square micro-pore optics as well as for testing the performance and calibrating the complete MXT telescope. During the last 3 years qualification and flight model micro-pore optics tests were done, each respectively followed by a telescope performance model and telescope flight model test. The final end-to-end in Nov 2021 (see Fig 4.3.8) test was successful and the telescope will be delivered to China in Q2 2022 for mounting on the satellite and final testing prior to launch next year. Only the flight spare micro-pore optic remains to be tested at PANTER in spring 2022.

Vadim Burwitz

(Other HEG members include N. Meidinger, A. Rau, K. Nandra)

4.3.6 Future project developments

Arcus

Over the last three years MPE has been supporting the proposal for the NASA MIDEX mission Arcus. The science objectives are to determine how baryons cycle in and out of galaxies including both distant and local systems, probe the feedback power emitted from the dominant ionized outflows in black hole winds and understand how stars, circumstellar disks, and exoplanet atmospheres form and evolve. The heart of the mission is a high-resolution X-ray spectrograph with a spectral resolution of R~3000 (in the 12 Å – 50 Å) and an effective area of 300 cm^2 based on critical angle transmission gratings and silicon pore optics (SPO). MPE has been deeply involved in the technology development for Arcus, procuring the SPOs and testing the optical layout (gratings and SPOs) of the spectrograph on single units to a prototype petal level in the PANTER X-ray test facility. These tests demonstrated the required accuracy for the alignment of the optical elements as well as the spectral resolution necessary to reach the science objectives. In August 2017 the mission was selected for a “phase A” study that was completed in May 2018 with final review (site visit) in September 2018. In February 2019 NASA announced that Arcus was not selected for a “phase B” study, despite impeccable rankings for the science and technology. The team are exploring ways in which this innovative project can be pursued in the future.

Vadim Burwitz

(Other HEG team members include: E. Bulbul, K. Nandra, J. Sanders)

eXTP

A technology development activity on 19-cell silicon drift detectors (SDD) is ongoing with the aim to yield time resolution in the order of a few microseconds together with an energy resolution of better than 180 eV FWHM at 6 keV. The signal readout is performed by multi-channel ASICs developed by the Politecnico di Milano, Italy. Such a fast detector is planned to be used for the SFA (spectroscopic focusing array) instrument of the Chinese eXTP satellite. The enhanced X-ray Timing and Polarimetry mission (eXTP) is a Chinese space science mission with European contributions designed to study fundamental physics under extreme conditions of density, gravity and magnetism.

Thomas Bechteler

Alexander Altmann

(Other HEG team members include: N. Meidinger, K. Nandra, A. Rau.)

4.3.7 Ground-Based

The X-ray data analysis is at the basis of the research in the High Energy (HE) group. However X-ray data alone are often not sufficient to answer our scientific questions and the identification and the follow-up of the X-ray detected sources at other multiwavelength is necessary. Since we are mostly dealing with large sample of sources (e.g., all-sky surveys from eROSITA) we can't rely solely on the access to telescopes via standard proposals, in particular when we are interested in varying sources for which timely observations are necessary. For this reason we continue to invest in ground-based facilities. In addition, because on the involvement of a large number of collaborators that need to access the same massive proprietary data we also invested in a new concept of science platform. We first introduce the platform and then the various ground-based follow-up projects.

SciServer

With the growing amount of data in astronomy there is a clear trend towards science platforms where the astronomers can bring their code to the data instead of the other way around. Collaborative projects are at the same time also getting bigger with many partners from different institutes which all need equal easy access to the collected data and related data sources. For MPE, prime contributor to both the HETDEX (Gebhardt et al. 2021) and eROSITA (Predehl et al. 2021) projects, both large international collaborations, it was a natural decision to pool resources among the OPINAS and HEG groups to set up a science platform together. After few considerations we have opted for cloning SciServer which is currently operating at JHU. SciServer offers user authentication with self-service, interactive and batch computing in private Docker containers, database access through the CasJobs interface, private storage space both in the database and on disk and Python API to access all of the above remotely as well. However the major feature which made the SciServer system the best fit for us was its built-in system of authorisation - any system resource can be assigned in a fine-grained way to a user or a group of users. Users in the eROSITA and HETDEX collaborations should only have access to their own proprietary data and resources, but they also both need access to a large collection of public ancillary data sets such as catalogs and spectral data. On top of that there are typically further subdivisions to consider: in both projects we find numerous working and interest groups which don't necessarily want to share all data, all the time, but do want to have the option to colaborate. SciServer@MPE allows to define private User Volumes that can be shared with other users or user groups. The groups can be set up in an ad-hoc manner by users themselves, so overall this makes it very easy to share files, software and database tables in a flexible manner. SciServer@MPE serves as a private working space for the collaborations while the data still is proprietary and as a development platform for the eventual public data releases.

GROND

The Gamma-Ray Burst Optical Near-ir Detector (GROND) provides simultaneous imaging in seven optical/near-IR filters (g'r'I'z'JH & K). The instrument was developed by the HE group at MPE in collaboration with the Thüringer Landessternwarte Tautenburg and is mounted at the MPG 2.2m telescope at ESO's La Silla observatory. It has been working with a high reliability since mid-2007, albeit with a COVID-related downtimes of 9 and 3 months in 2020 and 2021, respectively. While GROND was initially developed to study the rapidly evolving afterglows of GRBs, in the recent years the powerful concept of simultaneous observations in seven optical/NIR bands has been utilized for studying a much broader range of transient and variable sources and GROND's portfolio now covers nearly all research topics of the HE group. In 2019 the focus of the ToO program was on super-luminous supernovae while since the launch of eROSITA, most of the of time is devoted to the follow-up of X-ray-selected transients, in particular Tidal Disruption Events. The regular observing nights of the last semesters have been successfully used for characterization of a larger sample of eROSITA-selected targets, AGN at z>5.5 (e.g., Wolf et al., 2021), cataclysmic variables, and X-ray binaries. The overall scientific impact of GROND in 2019-2021 is demonstrated by ~26 refereed publications with leadership or contribution from the HE group. This includes two publications 2019 in Nature (Magic collaboration 2021, Izzo et al. 2021), covering the signatures of a jet cocoon in early spectra of a supernova associated with a γ-ray burst and the observation of inverse Compton emission from a long γ-ray burst. The observing time at the 2.2m telescope is shared by the MPE HE group (~16%) with the MPIA Heildelberg (~70%), and the Chilean community (~10%). The HE group allocation is composed of 16 regular observing nights per year and a Target of Opportunity (ToO) override access for 15% of all available nights averaged over the year. The telescope is operated locally by personnel at the La Silla observatory and ToO targets are communicated remotely. Access to the 2.2m telescope is regulated through an agreement with MPIA Heidelberg. The current term is coming to an end in September 2022 but a continued operation is foreseen.

SDSS-IV/V

The next generation of the Sloan Digital Sky Survey (SDSS-V) has started operations in Summer 2020. Unlike the previous SDSS survey incarnations, SDSS-V will be an all-sky, multi-epoch spectroscopic survey of over six million objects, thanks to its dual-hemisphere strategy, that combines identical instruments on the Northern APO and Southern LCO 2.5m telescopes (Kollmeier et al. 2017). Due to the ongoing COVID-19 pandemics, the planned hardware upgrades had to be delayed by

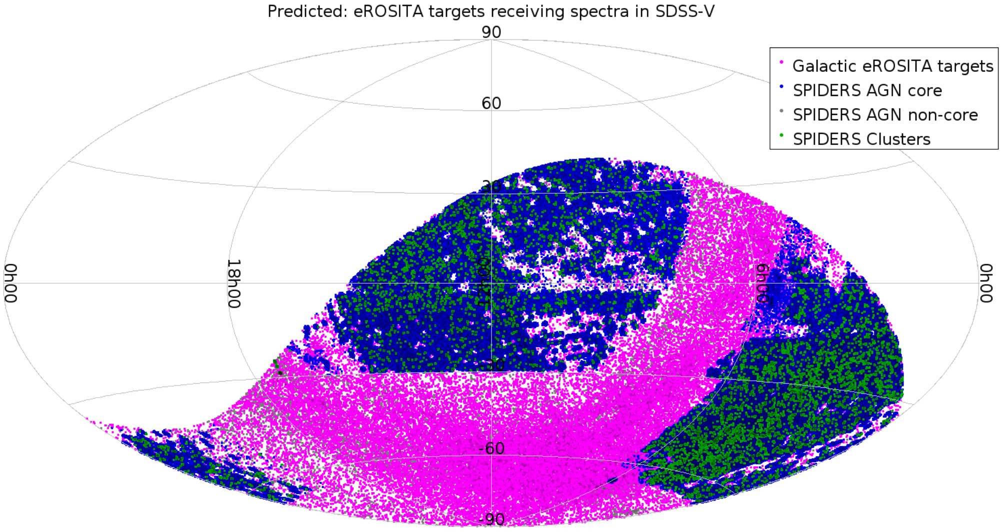

Fig. 4.3.9 A simulation-based sky map of the eROSITA-selected targets to be observed by SDSS-V at the end of the 4.5 years program. Different colors represent different classes of targets (or 'cartons', in the SDSS-V parlance). According to these simulations, SDSS-V will obtain spectra for about 300k X-ray sources.

more than one year. The survey has therefore spent the first 12 months of operations executing an alternative program using the old plug-plate system. As part of this program, eROSITA-selected sources in the eFEDS field (Brunner et al., 2021) were targeted in 39 plates. Finally, the survey commissioning has started in February 2022. By October 2022, both sites should be fully operative in survey mode. SDSS-V will be the first world-class facility to perform systematic, large-scale follow-up of the eROSITA survey as part of the so-called "Black Hole Mapper" and "Milky Way Mapper" programs. Thanks to that effort, MPE scientists will be able to accurately measure redshifts and physical parameters for hundreds of thousands X- ray newly discovered by eROSITA. Figure 1 shows a recent output of a full-survey simulations, highlighting the large number of X-ray selected targets that will be observed by SDSS-V. The final goal is to reach high completeness (>80%) on a sample of X-ray sources from the eRASS:3 catalogue with X-ray flux $F_{0.5\text{-}2keV}>2.5 \times 10^{-14}$ erg/s/cm^2 and r-band optical magnitude r<21.5.

4MOST

The 4MOST consortium has been selected by the European Southern Observatory (ESO) to provide the ESO community with a fiber-fed spectroscopic survey facility on the VISTA telescope, as a complement to several all-sky surveys that will span the electromagnetic spectrum. Starting in 2024, 4MOST (Roelof et al will simultaneously obtain high- and medium-resolution spectra of ~2400 objects distributed over a FoV of ~4 deg2. Its high multiplex, wavelength coverage and spectral resolution will enable detection of chemical and kinematic substructures in the halo, bulge and disc of the Milky Way, and redshift measurements of millions of distant objects, enabling studies of the evolution of galaxies, QSOs and the large-scale structure. 4MOST's capabilities are designed in particular to complement three space-based observatories of prime European interest: Gaia, eROSITA and Euclid. MPE has contributed to the hardware costs of 4MOST, and will also be responsible for its Operations System. In return, MPE will have privileged access to the instrument and data, leading two of the main 4MOST surveys (Clusters, PI: Comparat and AGN, PI: Merloni).

Rubin/LSST

The LSST survey performed at the Rubin Observatory will provide 'ugrizy' photometry for 18k deg2 of sky with a depth of 24.7 and 27.5 magnitude in the r band in single exposure and after 10 years, respectively. This is a long term project (full operation is currently planned for 2024) that will allow us the determine the counterparts of the faintest among the eROSITA sources and later, of the counterparts to Athena survey. It will provide the light curves for the variable sources. We have assured data rights for 5 PIs by proposing (PI Mara Salvato) an in-kind contribution for the software development of a code aimed at computing reliable photometric redshift for AGN via SED fitting, in addition to other small contributions. The proposal has been accepted and we have just now (as at 1/1/22) hired the postdoc that will start to work on the tasks.

Selected References:

Brunner et al. 2021, 2021arXiv210614517B
Gebhart et al. 2021, 2021ApJ...923..217G
Izzo et al. 2019, 2019Natur.565..324I
Kollmeier et al. 2017, arXiv:1711.03234; de Jong, 2019, Nat. Astron., 3, 574
Magic Collaboration 2019Natur.575..459M
Predehl et al. 2021, 2021A&A...647A...1P
Wolf et al. 2021, 2021A&A...647A...5W

Authors: Mara Salvato, Jonas Haase, Andrea Merloni, Arne Rau.

(Other HEG team members include: W. Borneman, J. Comparat, T. Dwelly, J. Ider Chitham, K. Nandra. Former members: J. Chen, P. Schady, T. Schweyer)

4.4 Facilities and Technology Developments

4.4.1 PANTER X-ray Test Facility

During the last 3 years MPE's PANTER X-ray test facility has realised (Fig. 4.4.1), many test campaigns for different X-ray telescope projects with which MPE is involved, all this despite all the challenges that came with the Covid-19 restrictions imposed during the last 2 years. The optics for the Chinese Einstein Probe mission have been calibrated. For the Sino-French SVOM mission the MXT optics as well as the complete X-ray telescope (Detector and optic) have been calibrated. Both missions will be launched in 2023. Optics and coatings developed for ATHENA working towards its Mission Adoption Review (MAR) have also been characterised. More optics and gratings for the Arcus mission, now in NASA MIDEX proposal stage, as well as experimental Kirk-Patrick Baez optics have been successfully measured. In parallel to these campaigns, work on X-ray source characterisation and new beam spectral, spatial, and temporal monitoring capabilities have been implemented and characterised. Thermal testing upgrades to the facility have been tested and verified for testing ATHENA and other optics, even a 1/6th sector of the large Athena mirror is being tested.

The PANTER X-ray test facility was setup in the late 1970s. Its current configuration with the 132m beamline was completed at the beginning of the 1980s to support the *ROSAT* mirror development and its calibration. At the beginning of the 1990s the large Vacuum chamber and clean room in a new building were set up to accommodate and test the f=7.5m mirror modules developed for the *XMM-Newton* Mission (Fig. 4.4.1). Over the years, many upgrades and changes to the facility were implemented to accommodate the new telescopes that were being developed for X-ray astronomy missions, and calibrate them before launch (*EXOSAT, BeppoSAX, JET-X, Chandra (AXAF), XMM-Newton, ABRIXAS, SWIFT, SUZAKU, HXMT, IXPE* prototype detector, the eROSITA mirrors and telescope). The facility currently can be extended to 145 m with a 13m extension (10m beamline and 1.2m diameter 3m long vacuum extension chamber) to measure f=20m segmented IXO type optics.

For the Einstein Probe Mission Follow up X-ray Telescope EP-FXT the engineering model (EM), qualification model (QM) as well as the flight model (FM) optics assemblies have been tested and finally calibrated before delivery to China for integration into the satellite. Also the QM of the Einstein Probe mission Wide-Field X-ray telescope EP-WXT was calibrated in PANTER. (Fig. 4.4.2). For the SVOM missions the MXT QM and FM optics were tested and calibrated. The MXT telescope Performance Model (PM) and as well as Flight Model (FM) have been tested in an end-to end test mode prior to delivery and integration into the satellite in China later this year.

Fig. 4.4.1 *View of MPEs PANTER X-ray test facility in Neuried, in the south west of Munich.*

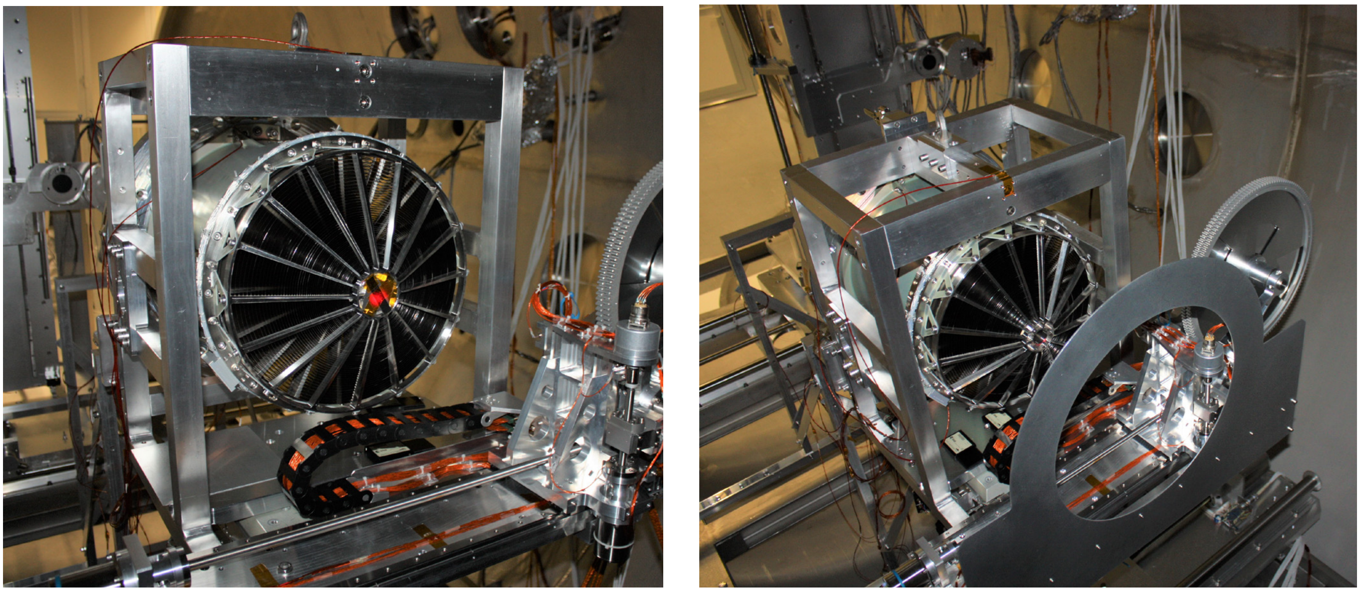

Fig. 4.4.2 *The Einstein probe FXT-QM: The Mirror assembly* ***(left)****, the Mirror Assembly with the "Glücksrad" in front and the PANTER detectors in the back* ***(right)****.*

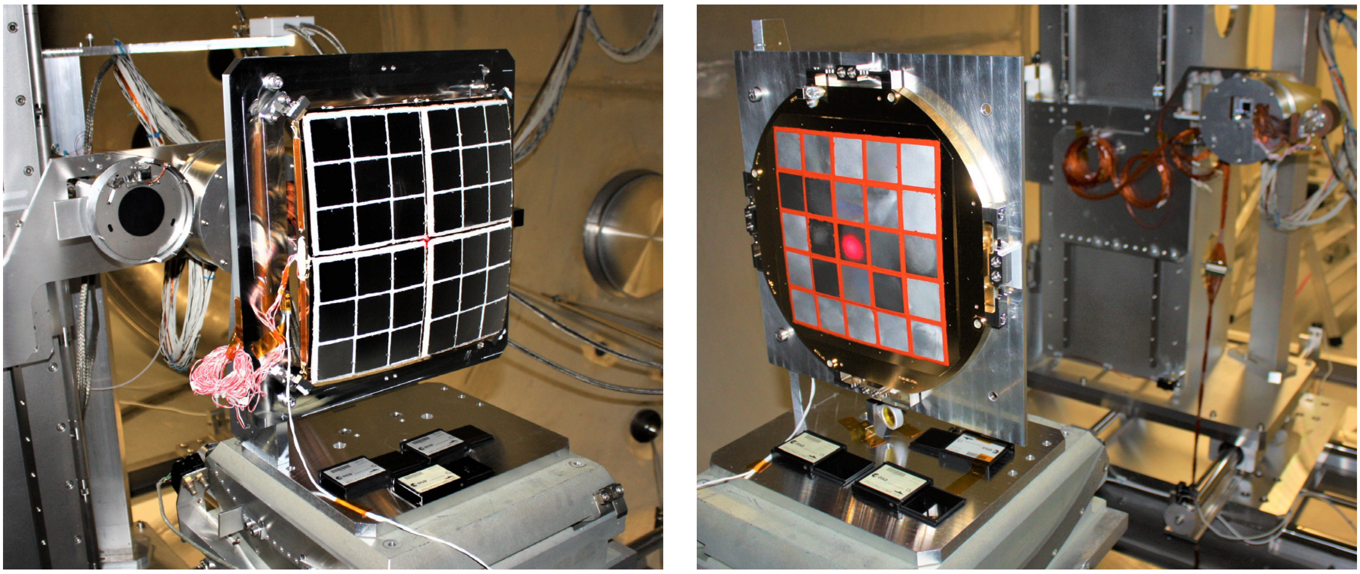

Fig. 4.4.3 *The Einstein Probe WXT-QM optics* ***(left)****, the SVOM MXT-FM optic for calibration in the PANTER vacuum Chamber* ***(right)****.*

Vadim Burwitz

(Other HEG team members include: G. Hartner, T. Mueller, A. Langmeier, S. Rukhdee, T. Schmidt; External Members: E. Breunig, J. Eder ; Former Members: M. Bradshaw, Y. Liao, C. Pelliciari)

4.4.2 X-Ray Optics Development

The PANTER facility gives a unique possibility to study the performance of X-ray optical elements under developments with X-ray illumination, which complements other analyses, metrology and theoretical expectations.

While in the past, mainly X-ray mirror segments made from slumped glass were developed and tested, the focus is now more on silicon-based optics. In particular, there is a collaboration with GSFC, where high resolution Wolter segments are made from cut and polished monocrystalline silicon blocks. As the stacking of these segments without performance degradation is a challenge, the development process at GSFC is iterative, where MPE supports the development by precise X-ray measurements over the full applicable energy range. It is planned to extend the testing also to vibration and thermal tests.

A study for ESA was successfully completed that entailed designing an X-ray test facility that can accommodate and allow the calibration of the large *Athena* mirror. The study showed it is possible but for funding reasons ESA has opted for testing the mirror at the existing XRCF facility in Huntsville, USA. In this context PANTER is still deeply involved in the design of equipment to support the optic in the large chamber at XRCF (see Fig. 4.4.4) as well us to work together with the colleagues at NASA on the complex metrology to ensure the best ground calibration of the Athena Mirror.

Another emphasis in the last years was on multi-layer coatings for enhanced X-ray reflectance. A three-layer Cr/Ir/Cr coating has been studied that theoretically gives high reflectance where pure Iridium or Gold coatings show absorption edges. After an earlier test with flat samples having different chromium layers, a real X-ray telescope was designed as demonstrator: HORUS is composed of two almost identical lobster-eye units (with flat mirrors as approximation to the Kirkpatrick-Baez type mirrors) based on silicon substrate mirrors, which however have different coatings. One of the “HORUS eyes” is coated with 50 nm Gold, while the second is equipped with the new Cr/Ir/Cr coating (6 nm/30 nm/6 nm). The X-ray test covered the band up to ca. 10 keV in order to perform the comparison over the full relevant range. It could be demonstrated that in particular in the soft band a significant improvement of collecting area could be achieved with the new three-layer coating.

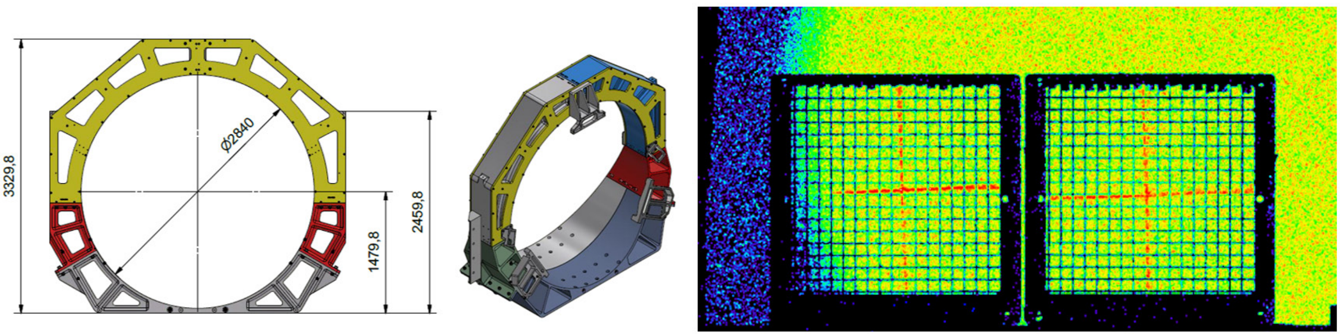

Fig 4.4.4 (Left panels) *The large MGSE support structure CDR design for the ATHENA mirror for XRCF testing (Rightmost panel) HORUS telescope with gold module* ***(left)*** *and iridium module* ***(right)*** *during a low energy continuum beam scan.*

Peter Friedrich

Veronika Stieglitz

Vadim Burwitz

(Other HEG members include: E. Breunig, J. Eder)

4.4.3 X-ray Detector Development

Three different types of spectroscopic and imaging X-ay detectors using CCD, DEPFET and SDD sensors manufactured at HLL have been either developed or commissioned in space during the past three years.

eROSITA camera array

The commissioning of the seven spectroscopic eROSITA PNCCD detectors (0.2 keV – 10 keV) with a time resolution of 50 ms for the image consisting of 384 x 384 pixels was successfully performed after the launch of the SRG satellite in July 2019. All detectors were fully operational and showed a performance similar to that measured on ground, e.g. FWHM(5.9 keV) ≈ 140 eV. The eROSITA detectors are a further development of the EPIC-PN detector aboard of XMM-Newton with improved performance, e.g. significant higher energy resolution at low energies <0.5 keV and minimization of out-of-time events occurrence to 0.2%. The seven eROSITA detectors operate without any major problem till to date.

DEPFET Development (Athena WFI)

First flight-like **DEPFET detectors** were developed, assembled and tested at MPE. The measured performance is very promising and compliant to the project requirements. For the fast detector (FD) (64 x 64 pixels) an energy resolution of 129 eV FWHM at 5.9 keV energy was achieved at time resolution of 80 µs. The measurements of the large detector (LD) (512 x 512 pixels), which is one of four quadrants, yielded an energy resolution of 131 eV FWHM at 5.9 keV energy for a time resolution of 2 ms.

PNCCDs

Detector modules were developed for the two Follow-up X-ray Telescopes (FXT) of the Einstein Probe mission based on the development done for eROSITA. The PNCCD detectors were assembled and afterwards tested at MPE in the GEPARD test facility. The operation instructions were provided together with the individual detector modules to IHEP, Beijing, the Chinese project partner. In total five detectors are delivered to China, started with an engineering model in 2020, followed by the qualification model, and finally two flight detectors (all three in 2021) and a flight spare detector in spring 2022.

SDDs

For high time resolution spectroscopy, a technology development with 19-cell silicon drift detectors (SDDs) is currently performed with potential application for eXTP, a Chinese-European satellite mission. 8-channel ASICs, which were developed by Politecnico Milano are used for the readout of SDD cells.

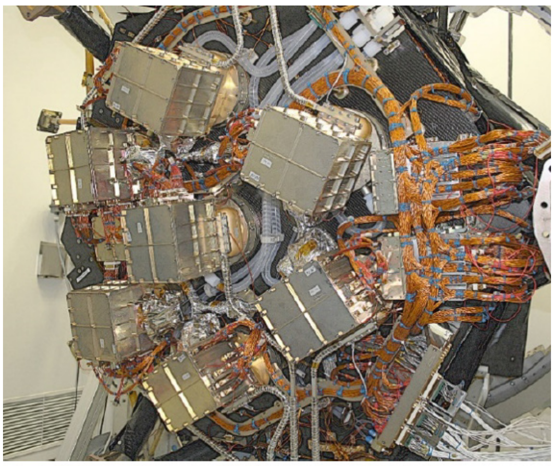

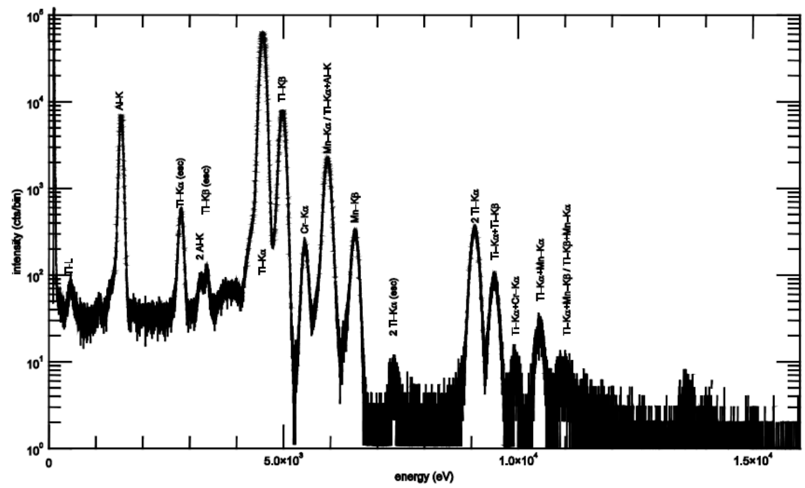

__Fig. 4.4.5 (Left)__ eROSITA camera array (Right) in-flight spectrum of the onboard calibration source.

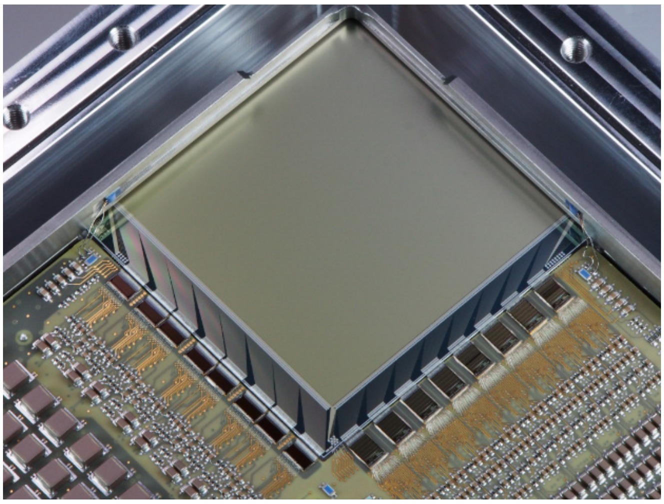

Fig. 4.4.6 *WFI LD prototype detector with the DEPFET sensor (512x512 pixel), 8 custom 64-channel VERITAS ASICs for readout and 8 custom 64-channel Switcher-A ASICs for control.*

All silicon sensors (DEPFET, PNCCD and SDD) were designed and manufactured by the **semiconductor laboratory** (HLL) of **Max Planck Society** based on the individual specifications for each project.

Norbert Meidinger

Kirpal Nandra

Johannes Müller-Seidlitz

5 Center for Astrochemical Studies

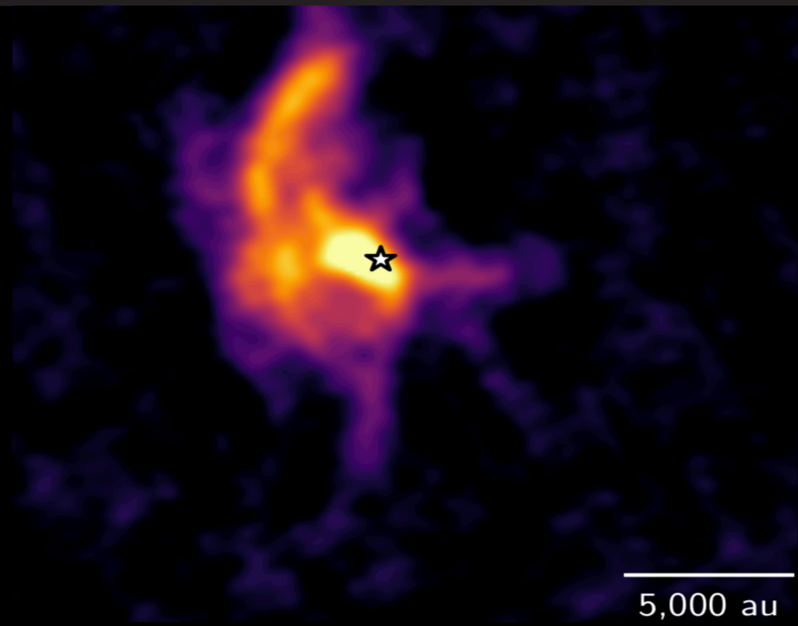

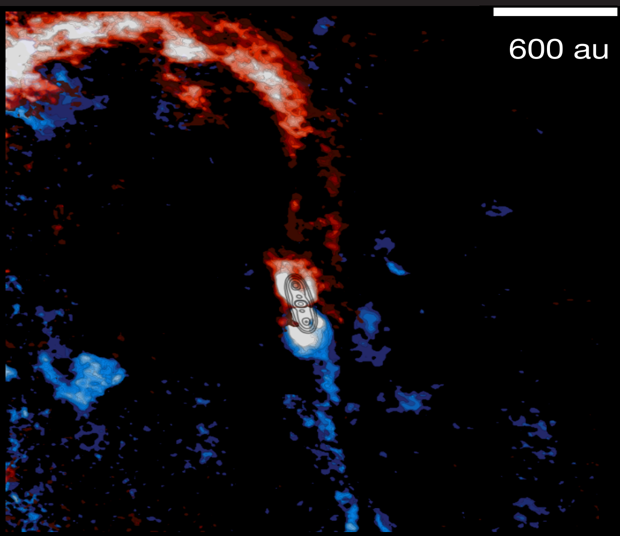

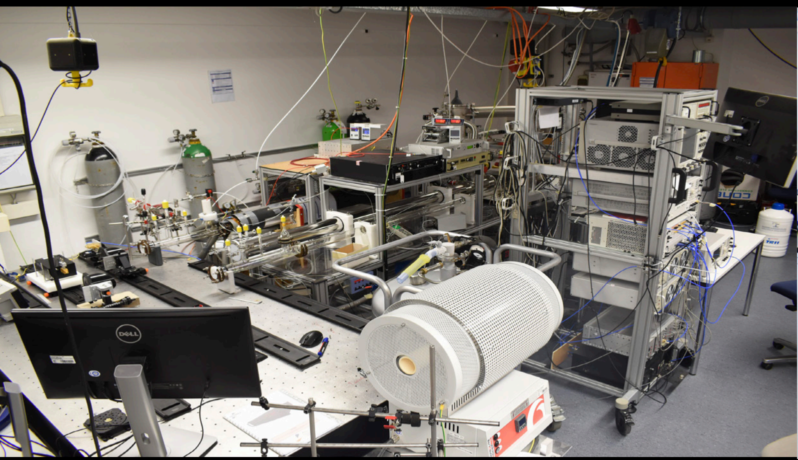

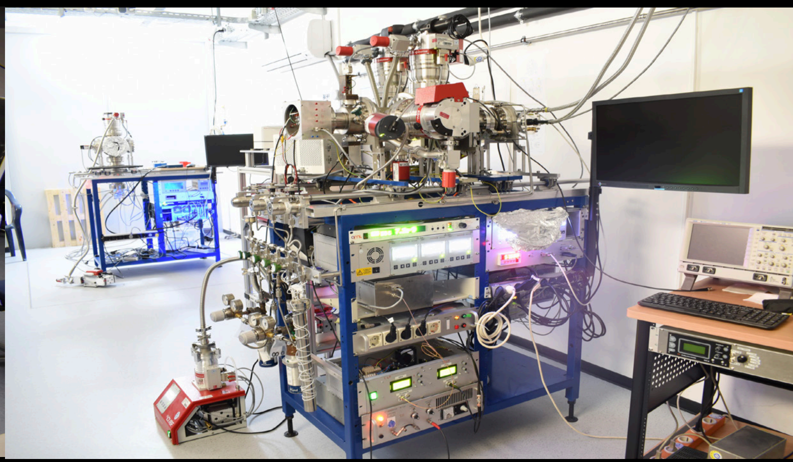

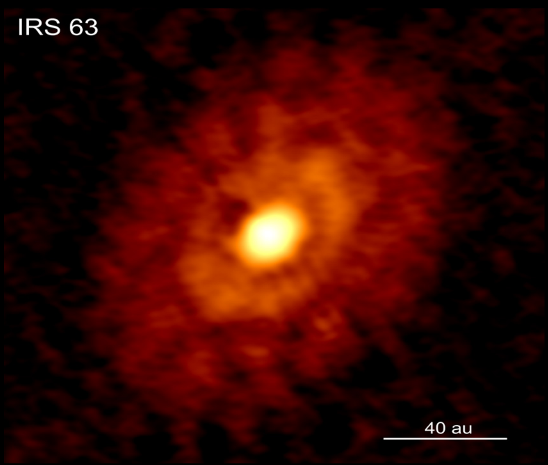

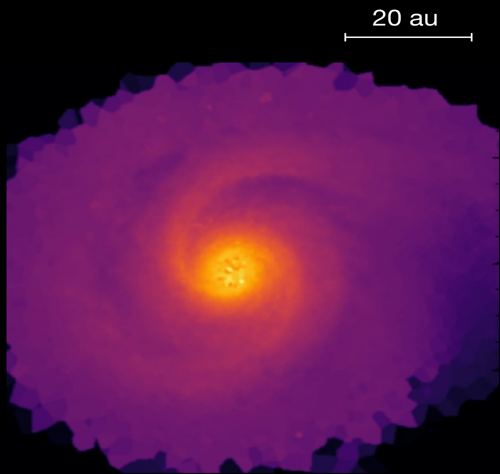

Composite view of important CAS achievements in the past three years. From top left and moving clockwise: the streamer connecting the core outskirts to the protoplanetary disk in a Class 0 source discovered with NOEMA (Pineda et al. 2020, Nature Astronomy, 4, 1158); large streamers connecting a planet forming Class I/II disk to the surrounding cloud (Alves et al. 2020, ApJ, 904, L6); the Ion Trap experiment in operation while measuring the rates of ion-neutral reactions; simulations of a self-gravitating disk that reproduce the dust continuum emission observed at high angular resolution with ALMA (Zamponi et al. 2021, MNRAS, 508, 2583); the youngest protoplanetary disk showing rings and gaps, signature of planet formation (Segura-Cox et al. 2020, Nature, 586, 228); upgrade of the CASAC laboratory (new cell and oven).

5. Center for Astrochemical Studies

5.1 Introduction and Overview

The Centre for Astrochemical Studies combines theory (including astrochemical models, plasma physics and non-ideal magneto-hydrodynamic simulations), observations, and laboratory experiments into a combined approach to tackle questions of star and planet formation and the interstellar medium. Observations with IRAM, ALMA, JVLA, GBT, APEX, SOFIA and other far infrared to millimeter facilities play a key role. Chemical processes are included in dynamical models to follow the ionization fraction and guide observations, which are in turn used to constrain the theory of evolving interstellar clouds and the process of star/planet formation. A concerted program of laboratory spectroscopy is going on at MPE, including different apparatus for the study of reactive species, complex organic molecules and ice and dust. Four complementary approaches are being pursued and they are detailed below.

CASAC (the CAS Absorption Cell) has been built to measure with high precision the frequencies of astrochemically important molecular ions and radicals cooled down to ~80 K, the temperature of liquid nitrogen, used to cool the system. The frequency range for the CASAC (and CASJET) is up to ~ 1.6 THz, overlapping with the available frequency range at NOEMA and ALMA, as well as at the APEX and IRAM telescopes.

CASJET (CAS supersonic free-jet expansion) can measure with high precision the frequencies of astrochemically important molecular ions, radicals and complex organic molecules cooled down to ~10 K, the temperature of interstellar clouds precursors to stellar systems like our own; the frequency range is the same as CASAC, with an extension to lower frequencies where rotational transitions of the heavy molecules reside and which can be reached by the Effelsberg and Green-Bank telescopes and the Jansky Very Large Array interferometer. Measurements with CASAC and CASJET are needed to allow detection in space of astrophysically relevant molecules and then to use these molecules as diagnostic probes of the physical and chemical conditions of interstellar matter.

CASICE (CAS Cryostat) is coupled to a Fourier Transform Infrared (FTIR) spectrometer, a Teraherz Time-Domain Spectrometer (TDS) and a Raman Microscope (RM), to characterize the optical properties of astrophysically-relevant solids and ices, to measure ice spectra, to study atom/radical diffusion within ices and pre-biotic molecule formation and stability. The direct measurements of complex refractive indexes and opacities are needed for the interpretation of dust continuum measurements in cold regions of dense clouds and protoplanetary disks, where dust grains are covered with thick icy mantles; ice spectroscopy, followed by solid feature observations in space, is important to unveil the interstellar ice composition and to test our astrochemical models; studies of atom/radical diffusion are crucial to put constraints on poorly known processes happening on grain surfaces.

The Trap Laboratory is the latest and most challenging experiment. It consists of two setups: the Cold CAS Ion TRAP (CCIT) and the Split-Ring Electrode Trap (SRET). With CCIT, we started to measure rate coefficients of astrophysically relevant ion-molecule reactions, focusing on light species including deuterium. SRET is being assembled and it will be used to study interstellar analogues of dust particles, their physical properties and their interaction with volatile species, mimicking interstellar processes at the base of molecular formation in space, where dust grain particles serve as efficient catalytic surfaces. The ultimate aim is to reproduce interstellar conditions more faithfully than using the macroscopic flat surfaces (called “cold fingers”), as done in laboratories around the world, where kinetics and energetics of astrophysically relevant surface processes are investigated. Rate coefficients of important ion-molecule reactions regulating the deuterium fractionation and the ortho-to-para ratio of H_2 and other light species can also be measured.

In summary, the Center for Astrochemical Studies (CAS) is an interdisciplinary department, where experimentalists, observers and theoreticians work together to unveil the physical and chemical processes of star- and planet-forming regions. Important events happened in the past three years, with Silvia Spezzano being awarded a Max Planck Research Group Leader position in 2020, and Elena Redaelli who started the Minerva Fast Track soon after her PhD defense in 2020 and received the Otto Hahn Medal in 2021. The past years have been very challenging for all of us, due to the many restrictions linked to the COVID-19 pandemic. However, we have acted proactively to allow face-to-face interactions as much as possible, following all the new pandemic-related regulations. For example, we have been able to arrange staff, postdocs and students within the available office space so that everybody could come to the Institute in safety. This was possible by occupying offices typically used for visitors and by organizing shifts so that only single or at most double occupancy in offices was assured. The double occupancy was only allowed in large offices, where plexiglass separations were possible to install, so that no direct contact between occupants was guaranteed. We purchased an air filter in the CAS coffee room, so that a maximum of six people could stay there and have face-to-face discussions or enjoy their lunches and breaks together. Finally, we made ample use of Zoom, especially for meetings with more than two people and for seminars. So, although the pandemic caused some delays, especially in the laboratories, our overall activities have not slowed down significantly and we reached together new important milestones, as reported in the next CAS chapters. Below I briefly summarize some of the achievements.

Laboratory - Section 1

The Trap Laboratory. The trap laboratory has seen the first light of the Cold CAS Ion Trap (CCIT), where rate coefficients of astrophysically relevant ion-molecule reactions can be measured. After tests aimed at reproducing reactions already studied in the past, we have started the study of the $H_2^+ + H_2$ system, and its deuterated forms, important for our chemical models of cold molecular clouds, precursors of stellar systems. The first paper, with the description of the CCIT is in preparation. Significant progress has been made for the other facility in the trap laboratory, the Split-Ring Electrode Trap (SRET), which will allow us to characterize interstellar dust particle analogues and simple chemical processes taking place on their surfaces. For SRET, we expect first light later this year.

Laboratory Characterization of Astrophysical Molecules. With the use of the CAS absorption cell, combined with experiments at the SOLEIL synchrotron in France, it has been possible to characterize two important light hydrates, NHD and ND_2, which have then been detected for the first time in space using archival *Herschel* data. These data allowed us to test our comprehensive chemical models, which include deuteration chemistry. Complex organic molecules (COMs) are also of high interest in CAS, as they are both great diagnostic tools for star-forming regions at various stages of evolution, and they represent an important step toward pre-biotic species. Propargylimine (HC_3HNH) is considered an important precursor for amino acids and we have first characterized the molecule in our laboratories and then detected it in the interstellar medium for the first time.

Interstellar ice analogues. Spectroscopic studies of interstellar analogue ice features have been successfully carried out. After early studies on the O_2 signature in water ices, we have focused on the spectroscopy of CH_3OH in mixed and layered ices and compared the results to our recent observations of solid CH_3OH toward a prestellar core (Goto et al. 2021, A&A, 651, 53). The main result of this comparison was that layered ices best reproduce the observed feature, providing clues on the structure of interstellar icy mantles. More spectroscopic studies have been carried out and they await upcoming JWST observations. Ice optical constants for CO_2 and N_2 ices have also been measured and the THz work of Giuliano et al. (2019, A&A, 629, 112) for CO ice has been extended to the far-IR, crucial for applications to observations of dust continuum emission in star- and planet-forming regions.

Observations - Section 2

The use of IRAM telescopes, ALMA, GBT and JVLA has allowed us to make important contributions in the field of star- and planet-formation from molecular cloud to protoplanetary disk scales.

Dense cores and filamentary structures in molecular clouds. The chemical differentiation found by Spezzano et al. (2016, A&A, 592, L11) toward a pre-stellar core, due to differential illumination by the interstellar radiation field around the core, has been found in other objects, thus highlighting the important role played by the large-scale environment on the chemistry of dense cores. We also accurately measured the difference in velocity dispersion between the lines of a molecular ion (N_2H^+) and neutral species (NH_3) across a dense cloud core and interpret this as evidence of oscillating magnetic fields within the dense gas, connecting the dense material within the core to the more turbulent surrounding cloud.

The role of magnetic fields on the early stages of star formation. Polarization measurements toward the youngest protostar in the Lupus I molecular cloud have allowed us to detect the classical hourglass shape of magnetic field lines predicted by models of star formation in magnetized clouds. We also used high-sensitivity observations of simple molecular ions to measure the cosmic-ray ionization rate across a pre-stellar core, finding a value of a few times 10^{-17} s^{-1}, confirming that cosmic rays are attenuated in their passage from diffuse to dense clouds, as predicted by theory.

From streamers to disks. The first clear evidence of a large-scale streamer of material connecting the mother cloud to a accreting protostars have been reported, based on NOEMA and ALMA observations. This result highlights the importance of asymmetric accretion of material during the evolution of protostars, which can enrich the circumstellar disk chemistry and trigger instabilities within the disk, maybe at the origin of the episodic accretion phenomenon. Asymmetric accretion of material could also be responsible for the formation of rings and gaps unveiled by us within a young protostellar disk. Using ALMA in its most extended configuration, a well-known Class 0 protostar has been found to host a young binary system, where complex substructures, seen in dust continuum emission and complex organic molecules, connect the circumbinary disk to the circumstellar disks.

Theory - Section 3

Cosmic rays in molecular gas. Cosmic rays (CRs) are crucial for the dynamical evolution of magnetized clouds and star-forming regions. Important results have been obtained in the study of CR propagation, with the derivation of analytical expressions of the CR ionization rate ζ as a function of the gas column density N, in cases of diffusive or free-streaming regimes. Comparison with future measurements of $\zeta(N)$ will allow us to determine the mechanism of CR propagation in the interstellar medium. Rigorous calculation of the energy spectrum of electrons produced by CRs in dense clouds have been carried out, crucial for a detailed understanding of gas heating, H_2 dissociation and fluorescence. The interaction of CRs with dust icy mantles has been investigated, finding that desorption mechanisms induced by CRs strongly depend on the dust grain size and on dust location within the cloud.

Magneto-hydrodynamic (MHD) simulations of protoplanetary disks. The dynamical evolution of (magnetized) pre-stellar cores toward the formation of a protostar and protoplanetary disk sensitively depends on the ionization fraction, thus on astrochemistry and dust evolution. The intricate interplay of non-ideal MHD effects, such as ambipolar diffusion and Hall effect, has been studied in detail; we arrived at the conclusion that disk formation is a common process if the cosmic-ray ionization rate is within the observed ranges and very small grains are depleted during the cloud core contraction. Indeed, very small grains have been found to adsorb quickly onto larger grains if ambipolar diffusion is taken into account. Within protoplanetary disks, magnetic fields affect the turbulence spectrum and we found that this leads to faster grain coagulation in the outer regions of protoplanetary disks.

Astrochemical modeling. Once icy mantles are formed in dense and cold clouds, the only external agent that can allow desorption of solid species or alter the ice composition are CRs. A detailed treatment of CR induced desorption has been included in our comprehensive gas-grain chemical models, taking also into account a more realistic dust grain size distribution. This effort showed that the icy mantle composition is very sensitive to the grain size. We also found a possible solution to the long-standing sulfur problem (i.e., in which form is sulfur hiding within dense clouds?): radiation chemistry triggered by CRs transform the bulk of S in H_2S ice into refractory allotropic forms of sulfur, in particular the stable S_8, which then become an important sink of S atoms in regions where S is hydrogenated to H_2S on icy mantles, i.e., in dense clouds.

Publications

20 most cited CAS papers between 2014 and 2021 (CAS members are in bold face and citations are within square brackets at the end of the referenced paper)

Jiménez-Serra, I., **Vasyunin, A., Caselli, P.,** et al. 2016, The Spatial Distribution of Complex Organic Molecules in the L1544 Pre-stellar Core, ApJ, 830, L6 [119]

Vasyunin, A., Caselli, P., Dulieu, F., et al. 2017, Formation of Complex Molecules in Pre-stellar Cores: A Multilayer Approach, ApJ, 842, 33 [113]

Friesen, R., **Pineda, J. E.,** Rosolowsky, E., et al. 2017, The Green Bank Ammonia Survey: First Results of NH_3 Mapping of the Gould Belt, ApJ, 843, 63 [103]

Brünken, S., **Sipilä, O.,** Chambers, E. T., et al., 2014, H_2D+ observations give an age of at least one million years for a cloud core forming Sun-like stars, Nature, 516, 219 [90]

Ceccarelli, C., **Caselli, P.,** Fontani, F., et al., 2017, Seeds of Life In Space (SOLIS): The Organic Composition Diversity at 300-1000 au Scale in Solar-type Star-forming Regions, ApJ, 850, 176 [79]

Zhao, B., Caselli, P., Li, Z.-Y., et al. 2016, Protostellar disc formation enabled by removal of small dust grains, MNRAS 460, 2050 [76]

Bizzocchi, L., Caselli, P., Spezzano, S., et al. 2014, Deuterated methanol in the pre-stellar core L1544, A&A, 569, 27 [67]

Padovani, M., **Ivlev, A.,** Galli, D., **Caselli, P.** 2018, Cosmic-ray ionization in circumstellar discs, A&A, 614, 111 [66]

Zhao, B., Caselli, P., Li, Z.-Y., et al. 2018, Decoupling of magnetic fields in collapsing protostellar envelopes and disc formation and fragmentation, MNRAS, 473, 4868 [66]

Laas, J. C., Caselli, P. 2019, Modeling sulfur depletion in interstellar clouds, A&A, 624, 108 [66]

Ivlev, A., Padovani, M., Galli, D., **Caselli, P.** 2015, Interstellar Dust Charging in Dense Molecular Clouds: Cosmic Ray Effects, ApJ, 812, 135 [61]

Kong, S., **Caselli, P.,** Tan, J.C., et al. 2015, The Deuterium Fractionation Timescale in Dense Cloud Cores: A Parameter Space Exploration, ApJ, 804, 98 [60]

Ivlev, A., Röcker, T.B., **Vasyunin, A., Caselli, P.** 2015, Impulsive Spot Heating and Thermal Explosion of Interstellar Grains Revisited, ApJ, 805, 59 [56]

Kirk, H., Friesen, R. K., **Pineda, J. E.,** et al. 2017, The

Green Bank Ammonia Survey: Dense Cores under Pressure in Orion A, ApJ, 846, 144 [55]

Keto, E., **Caselli, P.,** Rawlings, J. 2015, The dynamics of collapsing cores and star formation, MNRAS, 466, 373 [54]

Alves, F.O., Girart, J.M., Padovani, M. et al. 2018, Magnetic field in a young circumbinary disk, A&A, 616, 56 [49]

Sipilä, O., Caselli, P., Harju, J. 2015, Benchmarking spin-state chemistry in starless core models, A&A, 578, 55 [46]

Henshaw, J.D., **Caselli, P.,** Fontani, F., et al. 2016, Investigating the structure and fragmentation of a highly filamentary IRDC, MNRAS, 463, 146 [46]

Spezzano, S., Bizzocchi, L., Caselli, P., et al. 2016, Chemical differentiation in a prestellar core traces non-uniform illumination, A&A, 592, L11 [43]

Segura-Cox, D.M., Schmiedeke, A., Pineda, J.E., et al. 2020, Four annular structures in a protostellar disk less than 500,000 years old, Nature, 586, 228 [42]

CAS Structure

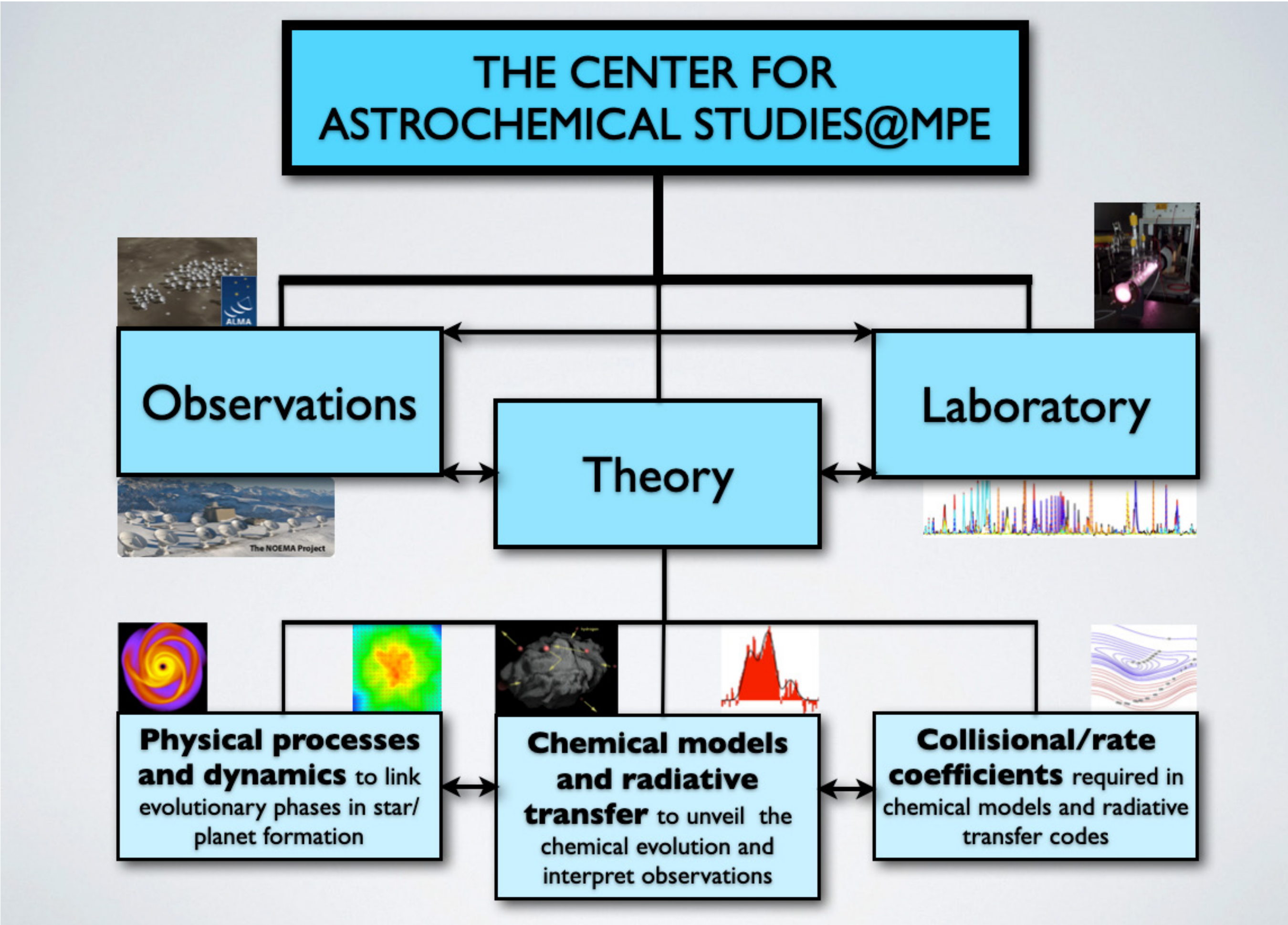

CAS Personnel

CAS PERSONNEL (as of Mar 2022)
(M=Male; F=Female)

- Director: 1F
- W2: 1M
- Max Planck Research Group Leader (W2): 1F
- Staff scientist: 1M
- Tenured scientific service positions (laboratory leaders): 3M, 1F
- Minerva Fast Track: 1F
- Postdoc: 8M, 4F (of which 2 as part of the Max Planck Research Group)
- IT staff (not tenured): 1M
- PhD students: 3M, 6F (of which 2 as part of the Minerva Fast Track and 1 as part of the Max Planck Research Group)

PhD Students graduated since the start of CAS (2014)

Anna Punanova (25.09.2017) – now Permanent Staff at Ural University

Ashley Barnes (01.03.2018) now Postdoc at the Argelander-Institut für Astronomie, Universität Bonn; moving to ESO at the end of 2022 with an ESO Fellowship

Ana Chacón-Tanarro (28.06.2018) – now Permanent Staff at the Observatorio Astronómico Nacional, Madrid, Spain

Vlas Sokolov (27.08.2018) – now Data Scientist at Solita company, Munich

Domenico Prudenzano (27.02.2020) – now Math, Science and Chemistry Teacher at International School of Bologna, Italy

Elena Redaelli (06.03.2020) – now with Minerva Fast Track position at CAS

Johanna Chantzos (19.03.2020) – now Project Leader for microscope system at attocube systems AG, Munich

Carolina Agurto Gangas (22.09.2020) – now FONDECYT Postdoctoral Fellow at Universidad de Chile, Santiago

Birgitta Müller (10.02.2022) – now Postdoctoral Fellow at TUM

Paola Caselli

5.2 Laboratory

5.2.1 The Trap Laboratory

The trap laboratory is the last addition to the laboratories in the CAS group. The instruments being built/ operated in the lab will be (are) used to measure fundamental processes of ions/ large charged particles (dust analogues) grains at temperatures down to 10 K, using trapping techniques employing alternating electric fields without the need for strong bulky magnets. The 22 pole trap instrument is already in operation and first measurements of temperature dependent ion-molecule reaction rates have been conducted. The design phase of the second instrument, the trap for macroscopic particles has been finished and the setup is under construction.

The Trap Laboratory started its journey in 2019, from the ground up. The main topic of the laboratory is closely related to traps and trapping of material of interest in defined surrounding conditions for sufficient time to conduct the desired experiment (see Fig. 5.2.2; left). In order to approach the experi-mental conditions relevant for astronomy/astrochemistry ultra-high vacuum and cryogenic technology are needed. At the same time, it is inherently difficult to restrain neutral particles in a given space in vacuum, therefore, as a most common (best) substitute we restrain the whole laboratory to the processes that involve charged species. The movement and trajectory of ions are predominantly gov-erned by electromagnetism and, under certain conditions, the effect of earth's gravity can be either completely neglected or easily compensated using a static electric field. Under the restriction of neg-ligible gravitational force, the candidates to be studied can be split into two subgroups:

1. Low mass (few *u*) and mostly single charge: The Cold CAS Ion Trap (CCIT)
2. High mass (macroscopic object) and multiply charged: The Split-Ring Electrode Trap (SRET)

The construction of the Cold CAS Ion Trap (CCIT) began in 2019 and all the technical parts, i.e., vacu-um chamber, pumping system, cooling/heating system, gas inlet system, ion source, ion guides and the trap itself were finished in 2020 with acquisition/ control electronics, radio frequency generators and computer control software being fully operational after initial testing and commissioning in 2021 (see Fig. 5.2.1 right). The setup is optimized to investigate interactions of ions (cations or anions) with neutrals in gas form, with a beam of neutral species, and with any kind of photons (from radio-frequency (>20 GHz) up to visible light).

The heart of the CCIT apparatus is a 22 pole rf (radio frequency) ion trap [Ger92] mounted on a cryo-genic cold-head with additional heater able to achieve temperatures from 4 to 300 K. The trap is operated at high frequency of 19 MHz, i.e., optimized for the lower mass range of the spectrum, ions from H^+ to masses of 70-80 *u*. The ions are produced in a storage electron bombardment ion source, where particles can be trapped for a limited period of time, permitting the production of desired molecular ions out of a precursor gas mixture. The ion of choice (defined by its mass/charge ratio) can be mass selected using a source quadrupole mass filter, prior to be injected into the trap. Actual ion deceleration for confinement and cooling of the internal rovibrational modes is achieved using collisions with a buffer gas (mainly He). After undergoing the pro-

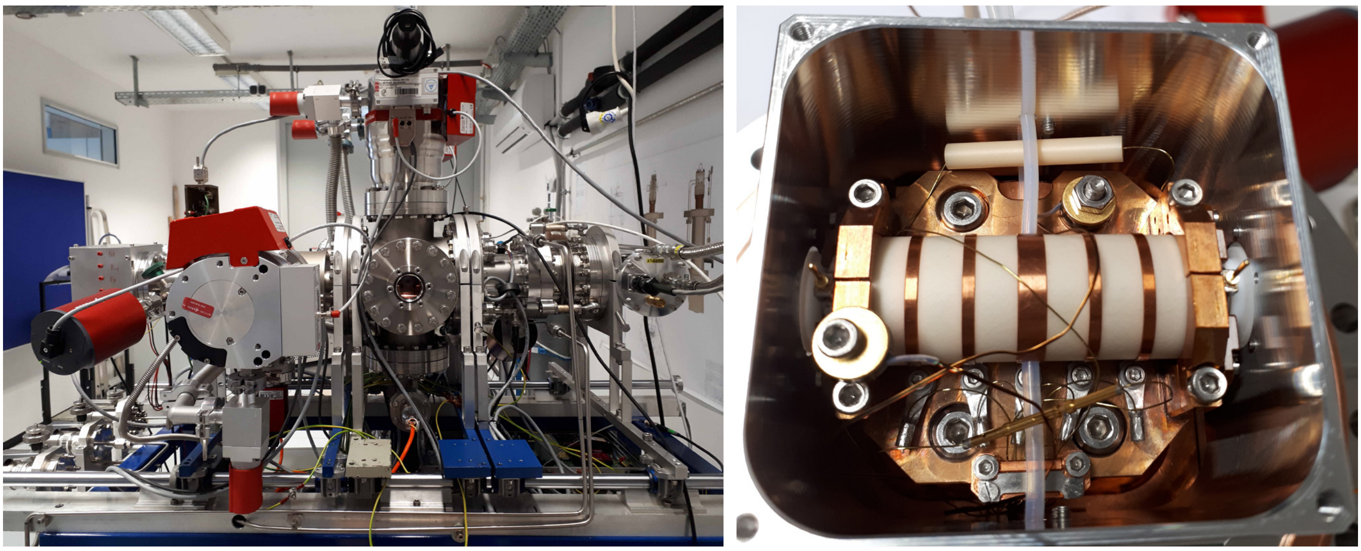

Fig. 5.2.1 Left*: The Cold CAS Ion Trap (CCIT) setup.* ***Right:*** *22 pole trap with 5 ring electrodes with the thermal shield (Aluminium).*

cess of interest in the trap, the product ions are mass selected in the detector quadrupole mass filter and counted using a Daly detector. The measurement cycle (production-storage-detection) is periodic (e.g. / usually 1 Hz). The actual measurement of interest is carried out either as a function of variable storage time (e.g. deter-mination of reaction rate, see Fig. 5.2.2 right) or the trap system is kept unchanged and external instruments tuned (e.g. spectroscopy). Where necessary or useful, the experiment can be repeated at nu-merous nominal temperatures, e.g. temperature dependent reaction rate; spectra at different popula-tions of the (rotational) states of the ion of interest. The lowest achievable nominal temperature of cca. 4 K enables attachment experiments, where rare gas atoms (He, Ne) can be attached to the bare ion of interest, in order to probe the weak ion-tag, e.g. in action spectroscopy schemes.

The main difference between the CCIT 22 pole trap and other similar 22 pole traps in use nowadays [Asv10, Jus19, Mik08], is the availability of the 5 ring electrodes surrounding the trapping volume (see Fig. 5.2.1 right). The ring electrodes, surrounding the 22 pole rods, can be used to influence the stored cold ion cloud (ion energy in meV range), since only a fraction (cca. 1%) of the electric field applied to the ring appears at the trap axis. The study of reactions like the ortho – para transition in the reac-tion of $H^+ + H_2(o) \rightarrow H^+ + H_2(p)$, where the only detectable variation is the energy release, become possible with this setup. Further application of the setup include ion-molecule reactions involving isotopologues (e.g. deuter-ation), state specific reactivity studies (e.g. defined ortho/ para H_2 reactant) and neutrals in form of a beam (access to neutrals with higher freezing points). The acquired quantitative results, mostly in form of accurate temperature dependent rate coefficients will be used in theoretical studies, i.e., complex reaction networks describing cold molecular clouds.

The construction of the Split-Ring Electrode Trap (SRET) really took in 2021, after collecting enough design information from a test bench dummy model of the trap for the reflected light detec-tion system. At the end of 2021 the vacuum system and the cryogenic system has been delivered and tested to reach the desired temperature and vacuum level with the dummy model of the final trap. The SRET instrument will use focused laser irradiation to illuminate the trapped macroscopic particle and an APD (avalanche photo-diode) to detect the collected reflected/ stray light. The variations in this collected light signal, produced by the oscillating particle inside the trap, can be analyzed in order to accurately determine the mass/charge ratio of the particle in a technique known as nanoparticle mass spectrometry (NPMS). The first version of this optical particle detection system, including a simple DAQ and Fourier transform based operator software has been tested using a paper-clip trap with ~50 µm SiO_2 grains in air (no vacuum). This experiment will allow us to characterize interstellar dust particle analogues and simple chemical processes happening on their surfaces.

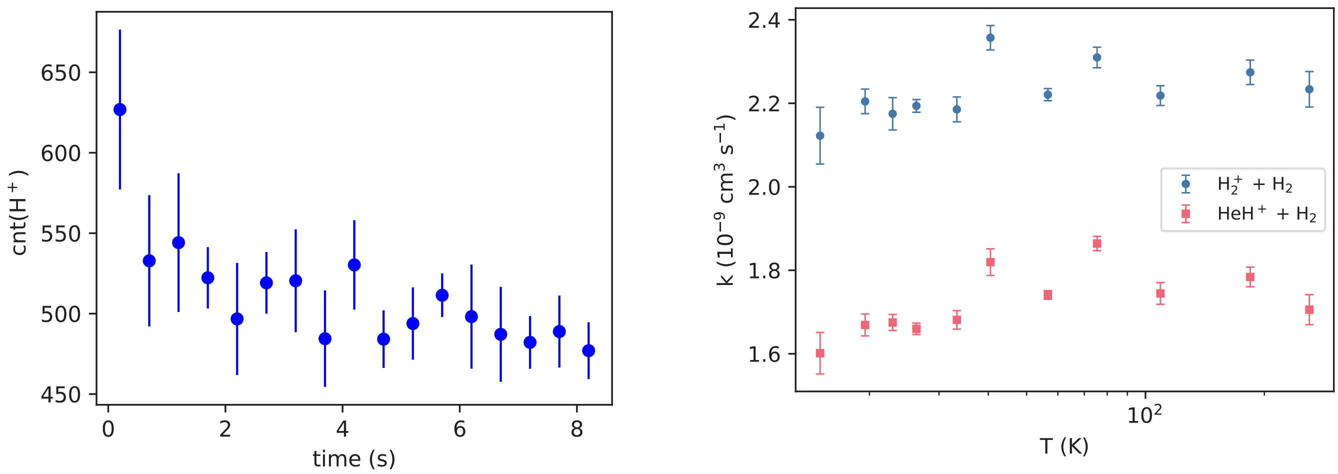

__Fig. 5.2.2 Left:__ Number of stored H⁺ ions as a function of storage time at 10 K in the CCIT trap. After initial cooling processes, the decay rate of H⁺ ions is very low, i.e., long storage times (up to tens of seconds) are possible. ***Right:*** *Measured reaction rate coefficient as a function of temperature. Reactions of H^+_2 and HeH^+ with H_2 show a flat temperature response from 15 to 300 K. Unpublished results, in prep.*

Selected References:
Asvany, O. et al. 2010, Rev. Sci. Instrum., 81, 076102
Gerlich, D. et al. 1992, Adv. Chem. Phys., vol. LXXXII, pp. 1–176
Jusko, P. et al. 2019, Faraday Discuss., 217, 172
Mikosch, J. et al. 2008, Phys. Rev. A 78, 023402

(Other CAS team members include P. Caselli, C. Endres. Former team members include Prof. D. Gerlich)

Pavol Jusko

Miguel Jiménez Redondo

5.2.2 Laboratory Characterization of Astrophysical Molecules

Molecular species in the interstellar gas carry precious information which allow astronomers to understand the physics and chemistry of the different cosmic objects. Radioastronomical identification of molecular species can be obtained, except for few cases, only when a robust laboratory spectroscopic characterisation is in hand. Since the physical and chemical conditions of the interstellar medium differ by a large extent to those on our planet, many molecular species observable in space are not stable in our day-life environment. For these reasons the gas-phase spectroscopy laboratories at CAS are equipped with a variety of different and flexible experiments allowing the study of multiple classes of molecular species, from unstable species such as ions and radicals, to larger and more complex organic molecules.

In the CAS-laboratories we have high resolution spectrometers that cover frequencies from 10 GHz to 1600 GHz. Two absorption frequency-modulated spectrometers are combined with glass tubes with the ability to apply DC-plasma discharges, and a molecular free jet apparatus (CASAC, CASJet). The broad band chirped pulse spectrometer (8 – 26 GHz, 80-120 GHz, 160-240 GHz, CP-FTS) is combined either with one of the cells or a K-band waveguide.

Radicals

Nitrogen hydride radicals are key species lying at the beginning of the reaction pathway leading to the formation of NH_3 and organic molecules of prebiotic interest (e.g. Le Gal et al. 2014) However, relatively little is known about their D-bearing isotopologues. To date, only ND has been detected in interstellar gas. To aid the identification of further deuterated nitrogen radicals, we have thoroughly re-investigated the rotational spectrum of NHD by employing two different instruments: high-resolution pure rotational spectral data of NHD have been collected in the submillimetre region with the CAS Absorption Cell, while the Far InfraRed (FIR) spectra were obtained at the AILES beamline of the SOLEIL synchrotron in Gif-sur-Yvette (Bizzocchi et al. 2020). NHD was produced in a plasma of NH_3 and D_2. A wide range of rotational energy levels have been probed thanks to the observation of high-N (up to 15) and high-Ka (up to 9) transitions. The laboratory effort on this species, and similarly the one performed on its doubly deuterated version (i.e. ND_2), allowed the discovery of both species in space. The observations, coupled with astrochemical models, put constraints on the life time of the observed protostellar core IRAS16293-2422 (Melosso et al. 2020).

Complex Molecules

The analysis of small molecular ions and radicals was recently complemented in our spectroscopy laboratories with the study of larger complex organic molecules and prebiotic compounds. Thanks to the flexibility of our spectrometers, we are indeed able to target different class of molecules by quickly adapting the experimental setup.

A large variety of complex organic molecules (COMs, carbon-containing species with more than 6 atoms) are found in different evolutionary stages of star-forming regions, and are particularly abundant in the warm, dense inner region of the envelope of young stellar objects (“hot corinos”) at temperature ranging from 100 to 300K (e.g. Jørgensen et al. 2020). COMs are thought to be precursors of prebiotic species. Their astronomical identification is not only important to constrain the physical conditions and to understand the chemical inventory of star-forming regions, but also gives constraints on their formation routes. Of particular interest are the precursors of amino acids, the building blocks of proteins. Motivated by astrochemical models, we recently studied the rotational spectrum of Propargylimine (2-propyn-1-imine, HC≡C−CH=NH; Bizzocchi et al. 2020), Allylimine (CH_2=CH-CH=NH; Alberton et al. submitted), and Aminoacrylonitrile (NH_2-CH=CH-CN, Alberton et al. in preparation), which are thought to be building blocks of prebiotic species (amino acids; Kitadai & Maruyama, 2018). Catalogs of accurate rest frequencies have been compiled to enable future astronomical searches with telescopes, like ALMA. Our laboratory work led to the detection of propargylimine in the giant molecular cloud G+0.693-0.027 located in the central molecular zone of our Galaxy (Bizzocchi et al. 2020).

Propargylimine and Allylimine were studied in our laboratories using a pyrolytic system, which is used to produce semi-unstable species (lifetime ~ 1s). A stable precursor sample is heated by an oven up to 1500 °C, and therein the target species are produced via high-temperature chemical reactions. A glass line connecting the pyrolysis oven to the absorption cell feeds directly the latter with the species to analyse, while its rotational spectrum is being probed by the electromagnetic radiation.

A static cell (2.5m-long and 10cm in diameter) has been developed last year for the characterisation of stable molecules. While in other experiments a continuous flow of the chemical sample was required to create a plasma of short-living species (i.e. ions and radical) or to be coupled to a pyrolysis system for the production of semi-unstable species, in the case of stable chemical sample the cell is built focusing on its pressure stability. The improved vacuum tightness of this cell allows measurements also minimizing the sample consumption. The static cell was involved in the measurements of Aminoacrylonitrile in combina-

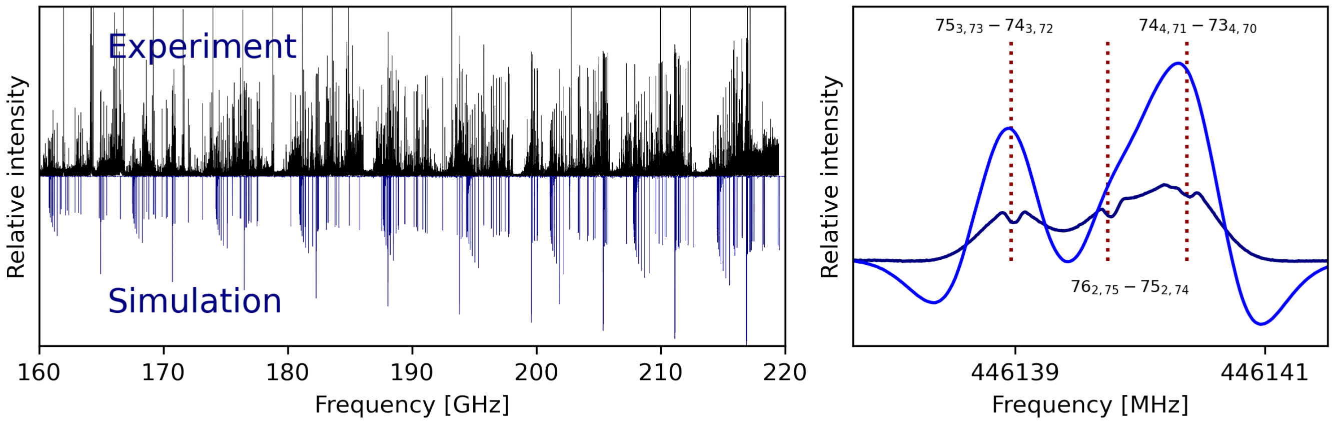

Figure 5.2.3 Left: *Spectrum of Aminoacrylonitrile recorded with the CP-FTS in the 2mm band (black). A simulation of the rotational spectrum based on the analysis is shown below in blue color.* ***Right:*** *Sub-Doppler measurement[1] (darkblue) of Aminoacrylonitrile recorded with CASAC that allows a very precise determination of transition frequencies. The spectral features overlap in the Doppler limited spectrum, which is shown in light blue for comparison.*

tion with the CP-FTS in the 80-120 GHz and 160-240 GHz bands, and the frequency modulation with bolometric detection in the 80-1100 GHz range (Fig. 5.2.3).

Sulfur-bearing substitution of known interstellar oxygen containing COMs are getting more attention lately due to the (1) higher sensitivity of modern radioastronomical receivers, which are allowing their detection in space, and (2) the still puzzling behavior of sulfur in the interstellar medium, especially in cold dark clouds (Laas & Caselli, 2019). The rotational spectrum of Methyl Isothiocyanate (CH3NCS), isovalent with CH_3NCO (detected in Sagittarius B2 and the protostellar core IRAS16293-2422B), was studied in our free-jet expansion unit (CASJet) in the frequency range 40-125 GHz. Here the molecular sample is injected into a high-vacuum expansion chamber (~10^{-6}-10^{-7} Torr / 10^{-4}-10^{-5} bar) through a 1-mm pulsed valve and undergoes to a supersonic expansion, with an adiabatic cooling of the molecular beam itself (Tonolo et al. in preparation).

COMs usually exhibit a quite complex spectrum due to large amplitude motions, e.g. the internal rotation of a methyl group, which leads not only to a splitting of each rotational level, but also to energetically low lying vibrational states. In particular in "hot core" regions, where COMs are detected at temperatures up to several hundreds of Kelvin, their lowest vibrationally excited states are significantly populated to be present in spectra of such sources (Endres et al. 2021). The spectroscopic analysis of these states is usually hampered by the high density of spectral features and strong interactions (perturbations). Using FIR spectra recorded at the Soleil synchrotron in Paris, high-level quantum chemical calculations as well as double resonance experiments in our laboratories (Fig. 5.2.4) we analyzed the rotational spectrum within such states for ethyl cyanide (Endres et al. 2021), dimethyl ether (Endres et al., in preparation) and vinylacetylene (Endres et al. 2021), that led to the identification of a number of strong features (50K) of vibrationally hot ethyl cyanide in the spectrum of the high mass star forming region G327.3−0.6.

Inelastic collisions

In the past years, the CP-FTS has been used to study inelastic collisions and to establish a new method to derive state-to-state rate coefficients experimentally (Endres et al. 2019). The studies have been extended to collisions of NH_3 with He. As NH_3-He rate coefficients have been also obtained from high level quantum chemical calculations, it is now possible to compare the experimentally obtained rates with theoretical values.

[1] The velocity distribution of the molecules observed in the measurements leads to a broadening of the spectral features caused by the Doppler effect (Doppler limited spectra). Smaller linewidths are achieved in Sub-Doppler measurements. Here, a counter-propagating beam (pump) of the same frequency as the probe beam alters the population of the molecular sample if tuned to a molecular resonance. Molecules that move along this axis are at most in resonance with ether the pump or the probe beam due to the Doppler-shift. Only molecules, whose velocity along the beam propagation is zero are in resonance with both, the pump- and probe-beam, at the same time and thus only their population is altered and probed at the same time, which is seen as a decrease in the observed absorption signal.

[2] The principle of double-resonance measurements consists of the detection of changes in signal intensities due to the excitation of a second transition that shares a common energy level with the observed transition. Here, the population of state $J_{KaKc} = 2_{21}$, v_7=1 is altered by resonant excitation (pump), which leads to stronger signal in the probed transition.

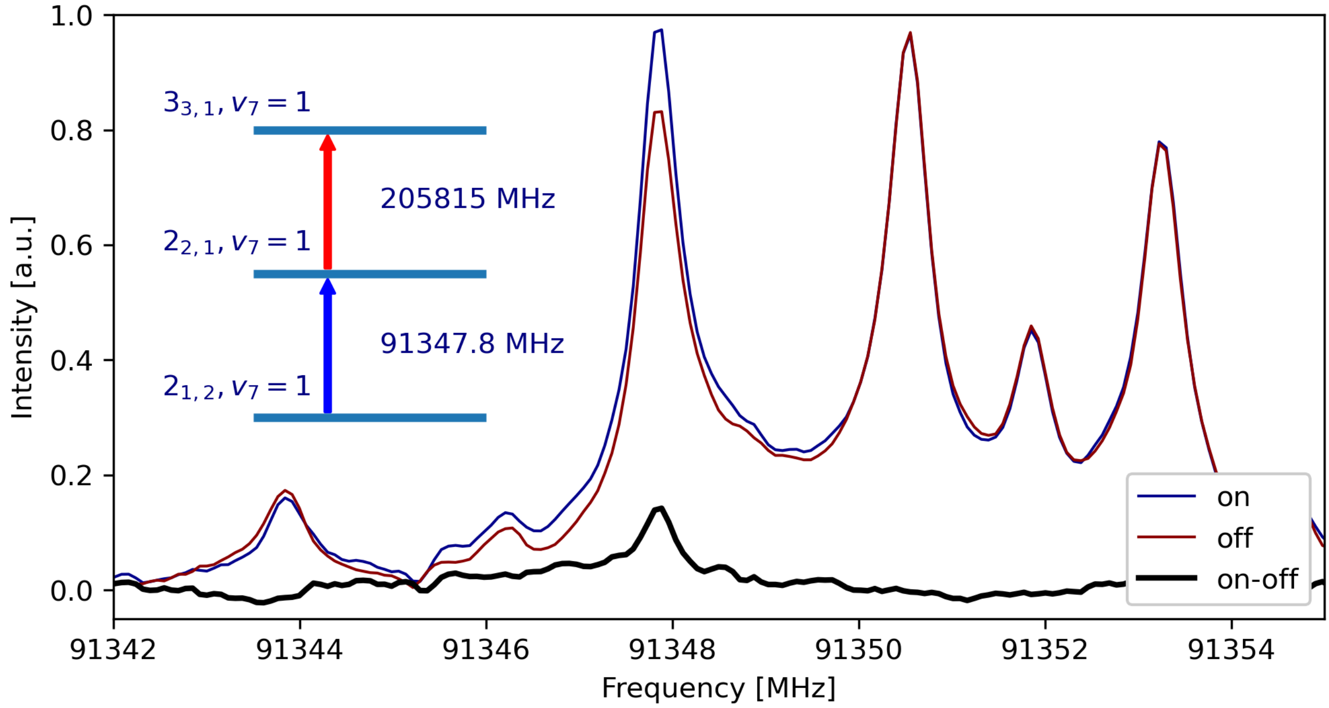

Figure 5.2.4 *Double-Resonance[2] measurement of dimethyl ether (CH_3OCH_3) recorded with the CP-FTS, which allows to determine transitions that share one rotational state. The spectrum in the vicinity of the $J_{KaKc} = 2_{21}$-2_{12}, v_7=1 (probe) is recorded twice. The sample is irradiated at the transition frequency of the $J_{KaKc} = 3_{31}$-2_{21}, v_7=1 (pump) transition in the first measurement (blue), while it is not irradiated in the second one (red). The difference spectrum is shown in black. The change in population caused by the pump radiation alters the intensity of the probe spectrum.*

Valerio Lattanzi

Christian Endres

Silvia Spezzano

(Other CAS team members include: D. Alberton, J. Ferrer Asensio, P. Caselli. Former team members include L. Bizzocchi, J. Chantzos, J. Laas, D. Prudenzano)

Selected References:

Le Gal, R. et al. 2014, A&A, 562, A83
Jørgensen, J. et al. 2020, ARAA, 58, 727
Bizzocchi, L. et al. 2020, ApJS, 247, 59
Melosso, M. et al. 2020, A&A, 641, A153
Bizzocchi, L. et al. 2020, A&A, 640, A98
Kitadai, N. & Maruyama, S. 2018, Geosci. Front., 9, 1117
Laas, J. & Caselli, P. 2019, A&A, 624, A108
Endres, C.P. et al. 2021, J. Mol. Spectrosc., 375, 111392
Endres, C.P. et al. 2019, J. Phys. Chem. Lett. 10, 17, 4836

5.2.3 Interstellar Ice Analogues

The cryogenic laboratory CASICE, originally developed and built by the CAS group, has reached the operative stage. The long-term experimental program, which started with IR spectroscopy of water and oxygen ice mixtures, has recently been extended to the analysis of more complex ice mixtures in the IR, and to the systematic measurements of the ice optical constants in the sub-mm range. The aim of these measurements is to provide reliable data needed to estimate dust opacity in dense and cold regions of pre-stellar cores and protoplanetary disks. New projects, involving Raman spectroscopy and focused on the investigation of microscopic processes in ice analogs are currently under development.

The chemical and physical processes occurring in icy mantles, which cover dust grains in many astronomical environments, are of key importance to unravel the molecular complexity observed in space. These processes are critically affected by the ice composition, and therefore it is necessary to develop a reliable methodology to identify imprints of different ices in observable properties of cosmic dust.

A combination of laboratory spectroscopic techniques provide a comprehensive reliable method to analyze a variety of chemical and physical processes in ices in a controlled environment. Over the past thirty years, laboratory experiments have been supporting and guiding the interpretation of the observational data, and they continue to serve as a unique tool helping us to understand the astrophysical processes. In order to provide a solid experimental ground to the observational data and to assist the development of chemical modeling, a complex laboratory facility specialized in the molecular spectroscopic investigation of astrophysical ice analogs has been designed and developed at CAS. During the past three years, two main research lines have been explored: the spectroscopic properties of water-based ice mixtures have been studied; and accurate measurements of the optical constants of ice analogs in the sub-mm range have been carried out.

Ice spetroscopy
The performed analysis of spectral signatures in ice mixtures led to the completion of the first PhD thesis based on the CASICE laboratory work. The early studies focused on the inclusion of homonuclear species in water-based analogs have been complemented by a more complex experimental design. The subsequent studies include the investigation of multicomponent mixtures and layered ice structures, with the feedback from chemical modelling and observational data. The conducted research improves the currently available experimental database, and aims to provide benchmarks for the upcoming JWST observations. Müller et al. 2021 and forthcoming paper Müller et al. 2022 (see Figure 5.2.5) illustrate the results of this project.

Ice optical constants and dust opacity
The interpretation of astronomical data from cold and dense regions relies on accurate measurements of dust opacity. The spectral behaviour and even the magnitude of absorption coefficient of icy mantles are practically unknown in the THz and far-infrared spectroscopic ranges. This missing information may introduce significant uncertainties in assessing the gas mass from dust continuum emission. The work by Giuliano et al. 2019 illustrates a new methodology applied for the determination of the optical constants of a reference astrophysical species (carbon monoxide). The developed approach enables direct measurements of the complex refractive index of ices in the THz range, in contrast to the standard approach which involves the use of the Kramers-Kronig relation (and may lead to uncontrolled errors in estimating the absorption coefficient). The new approach has been recently extended to the analysis of other main species comprising icy mantles, such as carbon dioxide and molecular nitrogen. Furthermore, the same methodology has been employed to derive the optical constants in a substantially broader spectral range, by combining THz measurements with data obtained in far-IR with the FTIR spectrometer available at CASICE. Two papers are currently being prepared by our new PhD student on these projects (see Figure 5.2.6).

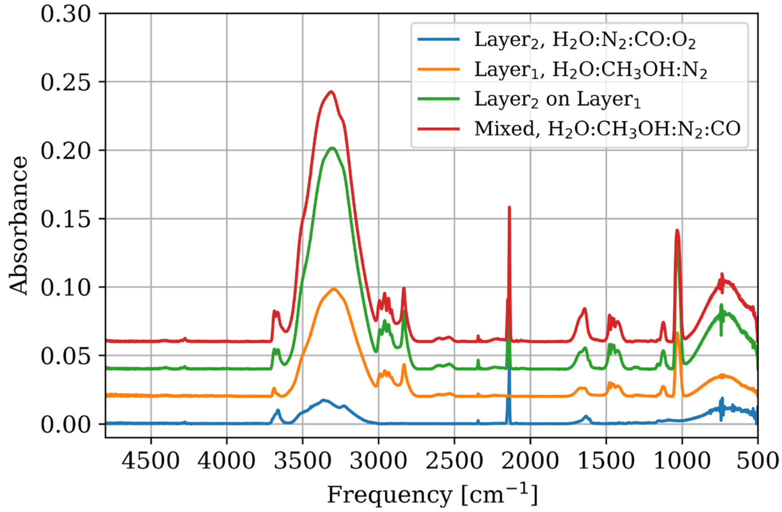

Fig. 5.2.5 *Spectra of mixed and layered ices of given composition. Relative abundances for the samples are 1:0.6:0.3:0.4 for the mixed ice, 1:0.7:0.3 (Layer 1) and 1:0.5:1.5:0.4 (Layer 2). From Müller, B. et al. 2022, submitted.*

Raman spectroscopy

A new line of research has been recently established by using confocal Raman microscopy. A customized designed cryostat is coupled to the Raman microscope installed in the laboratory, allowing detailed local analysis of samples at cryogenic temperatures. First local spectra and optical images have been recorded for water and carbon monoxide ice analogs. Matching the optical and spectroscopic information enables reconstruction of the ice properties with an unprecedented level of detail. Raman microspectroscopy is a powerful technique for the analysis of mineralogical samples of astrophysical interest, allowing us to identify the distribution of different species in the main matrix. We have started the study of meteoritic samples with the strategic goal of better understanding the interaction between ice layers and substrates of various origin. In the frame of the Origins of Life Initiative Munich network, a further application of the Raman spectroscopy has been dedicated to degradation studies of the photosensitivity of various nucleobases. One of the main aims of the project was to narrow down the vast parameter space by looking at the stability of RNA and its building blocks under various condition, simulating environments on meteorites and comets, but also settings plausible for the early Earth. We investigated the photosensitivity of various nucleobases, such as uracil, uridine, adenosine, cytidine and guanosine, performing degradation studies on high concentrated samples. The results are illustrated in Winkler et al. 2020.

Project at the ATOMKI synchrotron facility

Apart from the experimental program conducted with the CASICE instruments, we have been developing collaborations with other ice facilities across Europe – this enables access to complementary instrumentations and know-how and, thus, introduces invaluable research synergy. Recently, a fruitful collaboration has been established with the ATOMKI synchrotron facility in Debrecen, Hungary; MPE participation was funded by the Europlanet Society (through Transnational Access Programme Europlanet 2024). This project aims to investigate particular physical and chemical effects expected to occur in astrophysical ice analogs upon their bombardment by cosmic rays with the stopping power near the maximum (see section 5.4.1, paragraph *CR-induced ice chemistry and sputtering*). In particular, the first results show that the radiolysis products detected at astrophysically relevant ion fluences deviate drastically from predictions of available chemical models.

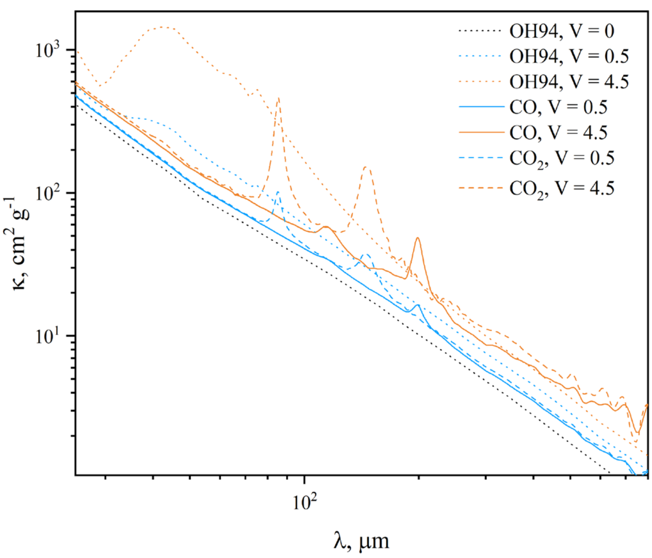

Fig. 5.2.6 *Calculated and reference opacities of astrophysical dust covered with CO and CO2 ice mantles as a function of the wavelength. Dotted lines refer to bare grains and ice mixture by Ossenkopf&Henning 1994, solid lines refer to CO data and dashed lines to CO2 data by present work. "V" indicates the volume ratio between refractory core and ice mantle. Adapted form Kruczkiewicz et al. 2022a, in prep.*

The work performed at CAS laboratory facilities will improve our understanding of the dust-ice properties, providing a better interpretation of the dust continuum emission and radiative transfer processes. The experimental data coupled with JWST observation will test our gas-grain models to provide insights into the ice analogs optical and physical properties, and their chemical processes.

Selected References:

Kruczkiewicz et al. 2022a,b, in prep.
Müller, B. et al. 2022, submitted
Müller, B. et al. 2021, A&A, 652, A126
Winkler, M. et al. 2020, ACS Earth and Space Chemistry, 4, 2320
Giuliano, B. M. et al. 2019, A&A, 629, A112

Barbara M. Giuliano

Birgitta Müller

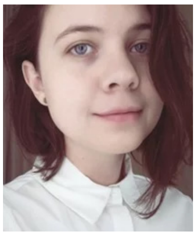

Franciele Kruczkiewicz

Max Winkler

(Other CAS members include: P. Caselli, T. Grassi, A. Ivlev)

5.3 Observations

5.3.1 Dense Cores and Filamentary Structures in Molecular Clouds

Low-mass dense cores within filaments are the birthplace of new planetary systems like our own. At CAS we use the information carried by the emission of molecules to study the chemical and physical structure of star-forming regions in order to gain insights on our astrochemical heritage and the star and planetary system formation process.

Dense cores (up to a few thousand AU long) are embedded in filamentary structures (up to a few parsec long) where low-mass stars form. The relatively high column density of dust in filaments (AV>3 mag) blocks the ambient radiation in the optical and ultraviolet wavelengths efficiently. Thanks to the shielding of the dust, molecular complexity grows. Molecules are used to derive both *the chemical and the physical structure* of star-forming regions. The chemical inventory of star-forming regions is the key information to understand their evolution, i.e. how the material is inherited from molecular clouds to forming planets. Upcoming observatories and missions like the ELT, JWST and ARIEL will characterise in detail exoplanetary atmospheres and hence enable connections from molecular clouds to the diversity of planets outside of the Solar System. Furthermore, physical properties of the core and filamentary structure like density and temperature can be inferred by observing molecular transitions. By observing different molecules towards the same object, we are able to probe different depths, and hence derive the 3D structure of a core. Moreover, molecular lines trace the kinematics of the gas, thus allowing us to peek into the dynamics of star-formation.

At CAS we use a concerted effort of observations, modelling and laboratory work to fully exploit the power of molecules in Astrophysics (see section 5.2) to derive the chemical and physical structure of star-forming regions.

Chemical structure

Isotopologue abundance ratios are pivotal for tracing the origin and evolution of the molecular material in the process of star and planetary system formation. Stable isotope ratios can, in fact, be measured in star-forming regions as well as in the Solar System. Deuteration, in particular, is crucial to understand the complexity of interstellar chemical processes, especially when they involve the interplay of gas-phase and grain-surface chemistry. At CAS, we studied the deuterium fractionation maps of HCO^+, N_2H^+, H_2CO and CH_3OH towards the prototypical pre-stellar core L1544 (Redaelli et al. 2019, Chacon-Tanarro et al. 2019). The D/H maps of N_2H^+ and HCO^+ presented in Redaelli et al. (2019) show a compact morphology around the dust peak, as their D-bearing isotopologues peak closer to the centre of the core than the corresponding normal isotopologue. As N_2H^+ is a late-type molecule, it suffers less depletion in the dense central parts of the core and reaches high levels of deuteration (~26%). HCO^+, on the other hand, traces the outer layers of the core and its deuteration fraction only reaches a value of 3.5%. Both N_2H^+ and HCO^+ and their deuterated isotopologues suffer from depletion towards the centre of the core, due to freeze-out of the parent species (N_2 and CO, respectively) on the dust grains. The depletion is more prominent for HCO+, but with this work, we could

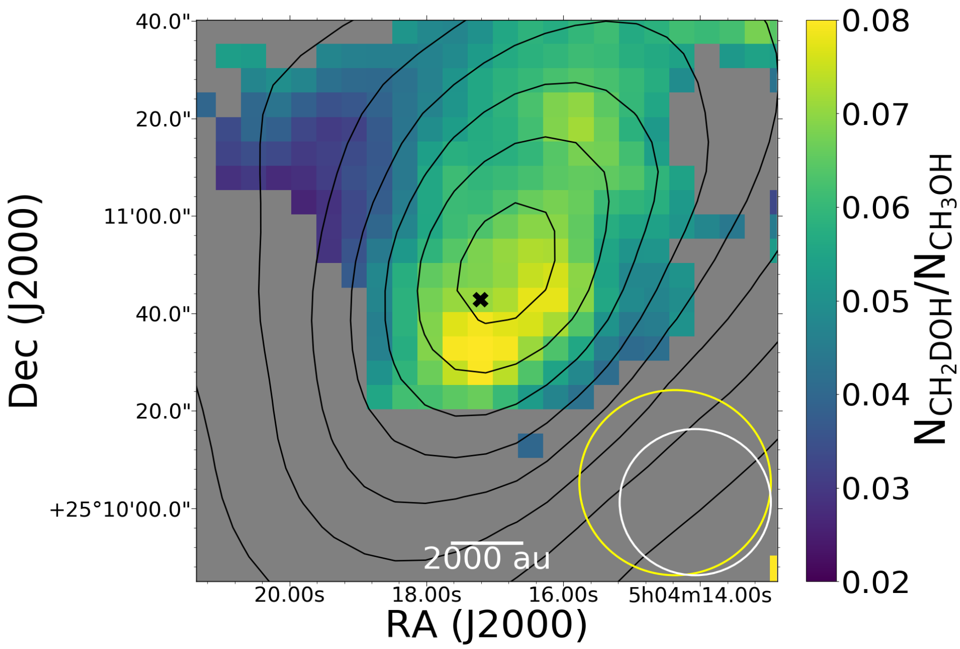

Fig. 5.3.1 *Deuterium fraction map of methanol (Chacon-Tanarro et al. 2019). The black contours represent increasing 10% steps of the peak of the Herschel N(H_2) map, presented by Spezzano et al. (2016). The beams are shown in the bottom right corner of the figure, in yellow for Herschel/SPIRE and in white for the 30m telescope. The black cross marks the dust continuum peak, and only values above the 3σ detection level are considered.*

confirm the depletion of N_2D^+ observationally, often predicted by chemical models. Unlike N_2H^+ and HCO^+, the deuteration maps of methanol and formaldehyde show a peak in deuteration that does not correspond to the dust peak, but rather is in agreement with the direction of steepest decrease of the column density of the main isotopologue (Chacon-Tanarro et al. 2019). The deuteration map of methanol, shown in Fig. 5.3.1, peaks towards the South of the dust peak and shows a more asymmetric distribution with respect to N_2H^+ and HCO^+. The deuteration maps of H_2CO instead peak towards the North-West of the dust peak. Despite being chemically related, H_2CO and CH_3OH show different emission morphologies which can be explained by the fact that H_2CO also has a gas-phase production mechanism, involving hydrocarbons, while methanol is solely formed on the surface of dust grains (Watanabe et al. 2002).

The spatial distribution of molecules towards dense cores is also a powerful tool to characterise the evolutionary stage of the observed core. In Lattanzi et al. (2020) we investigate the influence of external conditions on the chemical composition of pre-stellar cores. To this end, we compare single-pointing observations of the pre-stellar core L183 with results obtained towards L1544. Our analysis reveals clear chemical differences between both cores. While L1544 is richer in carbon-bearing species, in particular carbon chains, oxygen-containing species are generally more abundant in L183. The results are well-reproduced by our chemical model. The observed chemical differentiation between the two PSCs is caused by the different environmental conditions: the core of L183 is deeply buried in the surrounding cloud, whereas L1544 lies close to the edge of the Taurus Molecular Cloud. The obscuration of L183 from the interstellar radiation field (ISRF) allows the carbon atoms to be locked in carbon monoxide, which ultimately leads to a large abundance of O-bearing species. In contrast, L1544, being more affected by the ISRF, can keep a fraction of carbon in atomic form, which is needed for the production of carbon chains. A similar result was found in Spezzano et al. (2020) when comparing the emission maps of methanol, CH_3OH, and cyclopropenylidene, c-C_3H_2, obtained with the IRAM 30m telescope towards six starless cores embedded in different environments, and in different evolutionary stages. We infer from our maps that the chemical segregation between CH_3OH and c-C_3H_2 is driven by uneven illumination from the interstellar radiation field (ISRF). The side of the core that is more illuminated has more C atoms in the gas-phase and the formation of carbon-chain molecules like c-C_3H_2 is enhanced. Instead, on the side that is less exposed to the ISRF the C atoms are mostly locked in carbon monoxide, CO, the precursor of methanol. We conclude that large-scale effects have a direct impact on the chemical segregation that we can observe at core scale.

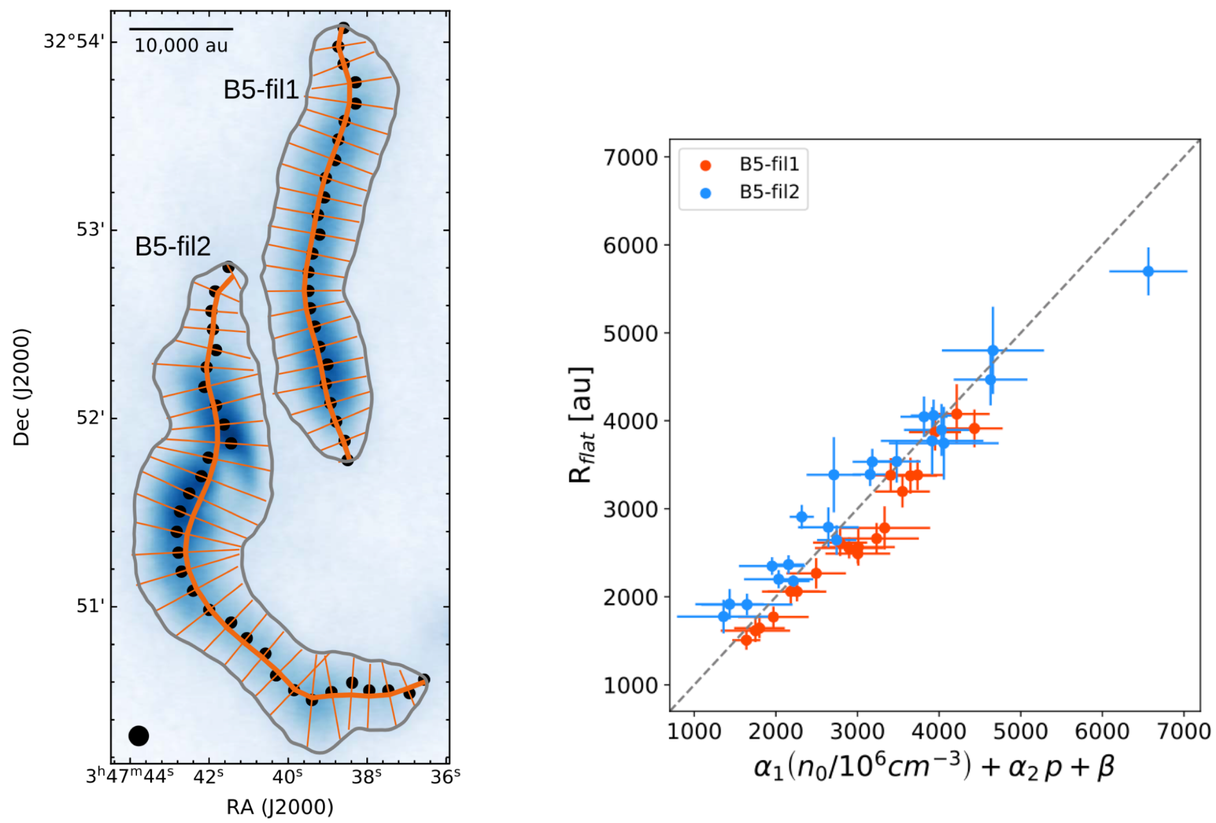

Fig. 5.3.2 Left panel: *Ammonia integrated intensity map of the masked filaments. The spines of the filaments are marked by the thick orange lines.* ***Right panel:*** *Correlation between the flattening radius Rflat, central density n0, and exponent p of the Plummer profile along the filament spines (Schmiedeke et al. 2021). .*

In Nagy et al. (2019) we showed that a substantial enrichment of sulfur-bearing molecules towards the young starless core L1521E with respect to the more evolved pre-stellar core L1544, suggesting that significant Sulfur depletion is taking place during the dynamical evolution of starless cores. Hily-Blant et al. (2021) used the NS/N_2H^+ abundance ratio as a constraint to the abundance of gas-phase atomic sulfur. They confirmed the result from Nagy et al. (2019) and found that toward L1521E, the youngest core in their sample, the abundance of atomic sulfur is comparable to the cosmic abundance of sulfur, thus demonstrating that sulfur depletes during the evolution from starless to prestellar core, as also predicted by Laas & Caselli 2019.

Physical structure

Cosmic rays are the primary ionising agent in the dense interstellar medium, thus driving the chemical complexity by forming molecular ions. Furthermore they play an essential role in the interstellar medium's chemistry and dynamics. For example, they determine the ionisation fraction, which regulates the degree of coupling between the gas and the interstellar magnetic fields and the heating of the gas. In Redaelli et al. (2021), we used observations of the molecular ions N_2H^+, N_2D^+, $HC^{18}O^+$ and DCO^+ towards the pre-stellar core L1544, coupled with state-of-the-art gas-grain chemical model, to constrain the cosmic-ray ionisation rate. The results of Redaelli et al. (2021) suggest that among the different values of cosmic-ray ionisation rate discussed in the literature (ex. Ivlev et al. 2015 and Padovani et al. 2009 and 2018), the lowest values (few 10^{-17} s^{-1}) are the ones that reproduce the observations better.

Dense cores within molecular clouds are the places where stars are formed and the final place where turbulence is dissipated. Several (large) programs have focused on the dense gas kinematics to constrain the angular momentum on dense cores, however, little has been done to understand the effect of magnetic fields on ions (affected by magnetic fields) compared to neutrals. It is expected (based on several theoretical arguments) that the non-thermal velocity dispersion (a.k.a. turbulence) should be narrower both for molecular ions (compared to neutrals) when the magnetic field inside the core is static and for molecules with higher critical density. However, a few previous observations of starless cores and IRDCs have shown suggestive evidence for broader linewidths in ions (e.g. Sokolov et al. 2019), but could not explain the cause. In Pineda et al. (2021), we compared 8 arcsec angular resolution maps of N_2H^+ (1-0), NH_3 (1,1), and NH_3(2,2) in the dense core Barnard 5 (B5) to assess this question. We find that the non-thermal velocity dispersion of the ion is subsonic and systematically higher than that of the neutral by ~20%, contrary to theoretical expectation. We explored a new and surprising possibility, that the magnetic field inside dense cores is not static, but oscillating (see the Chapter "The role of magnetic fields on the early stages of star formation", page 142).

In Schmiedeke et al. (2021), we characterise the filamentary structures found within the subsonic region of B5. We find that both filaments are shorter, steeper, narrower, and more supercritical than the large-scale "Herschel" filaments. To stabilise the B5 filaments against radial collapse, we estimate a magnetic field strength of ~500 μG is required. We analyse the filament properties as a function of position along the filament's spine. We find a correlation between the central density, the exponent, and the flattening radius of the filaments and determine an empirical relation between these three parameters (see Figure 5.3.2), showing the first clear evolution of a collapsing filament, revealing the global trends. If confirmed, this relationship could be used to calculate any of the parameters by measuring the other two.

Selected References:

Chacon-Tanarro A. et al. 2019, A&A, 622, A141
Hily-Blant et al., 2021, eprint arXiv:2112.01076
Laas J. and Caselli P., A&A, 624, A108
Lattanzi V. et al. 2020, A&A, 633, A118
Nagy Z. et al. 2019, A&A, 630, A136
Padovani M. et al. 2009, A&A, 501, 619
Padovani M. et al. 2018, A&A, 614, A111
Pineda E. J. et al. 2021, ApJ, 912, 7
Redaelli E. et al. 2019, A&A, 629, A15
Redaelli E. et al. 2021, A&A, 656, A109
Schmiedeke A. et al. 2021, ApJ, 909, 60
Spezzano S. et al. 2016, A&A, 592, L11
Spezzano S. et al. 2020, A&A, 643, A60


Silvia Spezzano


Anika Schmiedeke

(Other team members: A. Chacon-Tanarro, S. Choudhury, V. Lattanzi, Z. Nagy, J. Pineda, A. Punanova, E. Redaelli, V. Sokolov)

5.3.2 The Role of Magnetic Fields on the Early Stages of Star Formation

Magnetic fields are ubiquitous in the interstellar medium, but their properties are challenging to constrain observationally, since they are not directly observable. One of the research fields of the CAS group is to use different techniques to investigate the impact of magnetic fields in the prestellar and protostellar evolution. The field requires a strong collaboration between modellers and observers. In particular, we are interested in how B-fields are coupled to the interstellar medium, how this affects the gas dynamics and, ultimately, the formation of stars and planets. Furthermore, magnetic fields have strong influences on other key components of the interstellar medium, such as cosmic rays which —being charged particles— propagate along the field lines.

Magnetic fields in a young protostellar core

At large scales, magnetic (B-) fields are often found to be perpendicular to the main axes of filamentary molecular clouds, which hints to the importance of B-fields on the kinematics of the interstellar medium (ISM), by allowing the gas to flow mainly along the field lines. However when gravity takes over in smaller dense cores, neutral gas de-couples from the B-fields and starts to flow also perpendicular to the field lines, a process known as ambipolar diffusion. A characteristic evidence of this process is the hourglass shape exhibited by the field lines, which pinch inwards.

Polarisation observations of the dust thermal emission are commonly used to study interstellar B-fields. Anisotropic radiation causes dust grains to be aligned with their minor axis parallel to the magnetic field lines. Since grains emit preferentially along their major axis, the resulting emission is polarised perpendicularly to the local magnetic field. We used the SOFIA telescope to observe the polarised emission and to infer the magnetic field morphology in the core IRAS15398, the youngest protostar in the Lupus I molecular cloud (Redaelli et al. 2019b, see Fig. 5.3.3). The magnetic field is highly uniform and its mean direction is parallel to the large-scale magnetic field and the bipolar outflows powered by the source, as revealed by previous works. Furthermore, we detected a partial hourglass shape, the first detection made with SOFIA in the low-mass regime. We used the modified Chandrasekhar-Fermi method to infer the B-field strength, obtaining B=78μG, by assuming equipartition between kinetic and magnetic energies. The derived mass-to-flux ratio is λ=0.95, corresponding to a transcritical regime.

Overall, our data suggest that IRAS15398 evolved in a highly magnetised environment, and that the ordered magnetic field was preserved from the cloud scales to core scales. We are currently working on complementary molecular line data of $C^{18}O$ (2-1) and DCO^+ (3-2) observed with the APEX single dish telescope, which we will use to investigate the relation between the field morphology and the gas kinematics (Tabatabaei et al., in prep).

The impact of magnetic fields on the kinematics of ions and neutrals

A key question in the chemistry of the ISM is to understand how exactly magnetic fields couple with the interstellar matter. Magnetic fields exert their influence directly onto ionised particles, but neutral species are also coupled to the field lines by collisions with ions, but at high densities this coupling is expected to be imperfect. The theory hence predicts that neutral species —moving more freely— should exhibit larger velocity dispersions than ions. However, spatially-resolved evidence of this has been scarce. In Pineda et al. (2021), we performed a comparison of the kinematics properties of an ionised and a neutral species with well-resolved and high signal-to-noise observations in the isolated core Barnard 5. We analysed the N_2H^+ (1-0) transition, which was mapped using the Green Bank Telescope (GBT) at a resolution of 8" (~2400 AU at the source distance), and the NH_3 (1,1) line, observed with both the Very Large Array (VLA) and the GBT telescope. Both lines present a crowded hyperfine structure, which we fitted spectrally using dedicated python

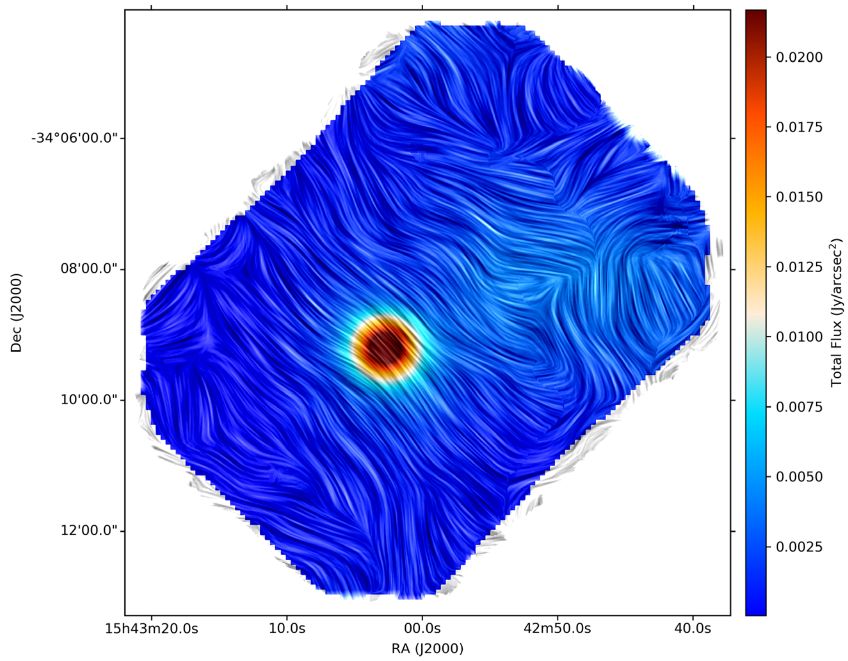

Fig. 5.3.3 *The colorscale shows the dust thermal emission at 1.4THz observed with SOFIA towards IRAS15398, with overlaid the derived field lines obtained with the line integral convolution technique. Around the central core, they bend forming the characteristic hourglass shape.*

packages, obtaining the centroid velocity and velocity dispersion maps. The two molecules exhibit consistent centroid velocity within 0.05km/s (the spectral resolution of the observations). However, the ionised N_2H^+ shows higher velocity dispersion than the neutral NH_3. In particular, the non-thermal velocity dispersion of N_2H^+ is systematically higher by 20% than that of ammonia, as shown in Fig. 5.3.4 , and the derived one-dimensional sonic mach numbers are 0.59 for N_2H^+ and 0.48 for NH_3. These results are in contrast both with magneto-hydrodynamic models, and with predictions extrapolated from empirical line-width—size relations. A possible physical explanation of this behaviour relies on the propagation of magnetohydrodynamic waves inside the coherent region. These waves affect the ions more than the neutral, hence increasing the velocity dispersion of the former with respect to the latter.

In an effort to study the initial conditions leading to core contraction, we have searched for observational hints of ambipolar diffusion in prestellar cores. To this aim, we used the IRAM 30m telescope to observe deuterated molecular species, which are known tracers of cold ($T \leq 15$ K) and dense gas ($n \geq 10^5$ cm^{-3}), toward the prestellar cores FeSt 1-457 and L1544. The velocity structure retrieved from the neutral (NH_2D) and ion (N_2D^+) maps are very similar for L1544. However, the velocity dispersion of the NH_2D line is systematically larger than the N_2D^+ for the FeSt 1-457 core, with the broader lines distributed predominantly perpendicular to the magnetic field direction reported in previous works. Our results strongly indicate that we are witnessing the onset of collapse in the FeSt 1-457 core (Alves et al. in preparation). We speculate that these two objects represent a transition in the magnetic strength, from strong enough to hamper ions motions —but not neutrals (FeSt 1-457)— to weak, after being largely dissipated by ambipolar diffusion. L1544, which is more evolved than FeSt 1-457, would hence represent this last scenario, where ions are finally free to contract and recouple to neutrals, as suggested by the similar velocity structure observed for the two species.

Cosmic rays and magnetic fields

Cosmic rays (CRs), energetic charged particles, represent the only source of ionisation at the high densities found in molecular clouds, where UV photons do not penetrate, with large impact on the physics of the ISM. At CAS we are highly interested in how CRs regulate the ISM ionisation fraction. In particular, we want to understand their effect on the chemistry (ion+neutral reactions are the most frequent in the gas phase, due to their lack of activation energy barrier), and on the dynamics of cores, as CRs indirectly determine the timescale for ambipolar diffusion. Cosmic rays are also linked to the magnetic field, as they tend to propagate along the field lines.

An important parameter to be constrained is how CRs are attenuated at high densities. As they hit and ionise hydrogen molecules, in fact, CRs lose energy. This attenuation — which translates in a decrease of the CR

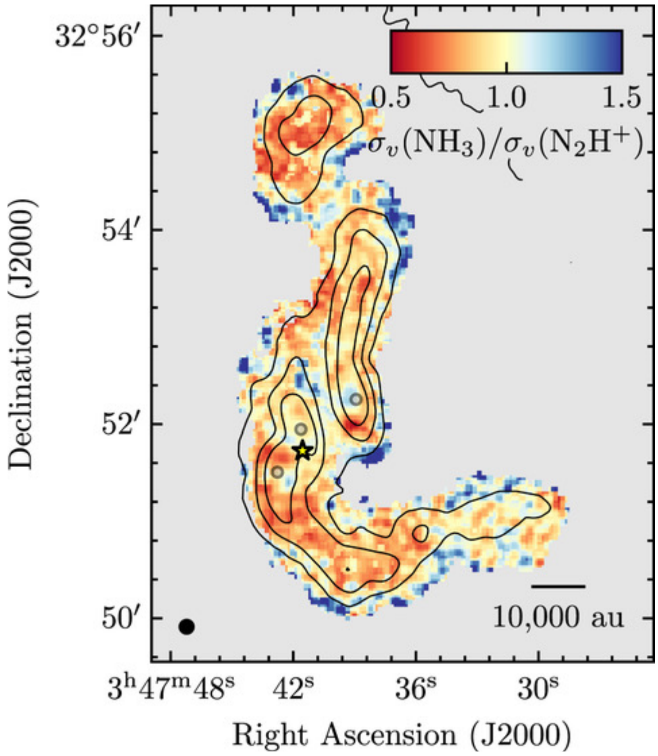

Fig. 5.3.4 Ratio of the velocity dispersion between NH3 (1,1) and N2H+ (1-0). The contours show the NH3 (1,1) integrated intensity map. The star and gray circles mark the positions of the Class I object and the condensations identified by Pineda et al. (2015), respectively. The beam and scale bars are shown in the bottom left and right corners.

ionisation rate ζ— has been theoretically investigated by several papers. However, observational evidence of this phenomenon is scarce. We performed the first dedicated study to the CRs attenuation in the prestellar core L1544 (Redaelli et al. 2021). We have coupled our gas-grain chemical code to predict molecular abundances with the physical model of the source obtained from the collapse of a Bonnor-Ebert sphere. We input different radial profiles of ζ. in the chemical code, testing different models: the standard constant value $\zeta=1.3\times10^{-17}$ s^{-1} the "high" ($\langle\zeta\rangle=10^{-16}$) s^{-1}) and "low" ($\langle\zeta\rangle=3\times10^{-17}$ s^{-1}) attenuation models developed by Padovani et al. (2018). Both of these have a shallow dependency on the column density, following $\zeta \propto N^{-0.2}$; however, a steeper profile, with $\zeta \propto N^{-1}$, is suggested by observations made in the diffuse medium. We have tested also this latter attenuation profile in our analysis.

We have produced synthetic spectral line profiles of N_2H^+ (1-0), (3-2), N_2D^+ (1-0), (2-1), (3-2), DCO^+ (1-0), (2-1), (3-2), and $HC^{18}O^+$ (1-0), and we have compared them with high-sensitivity data observed with the IRAM 30m telescope published by Redaelli et al. (2019a). Our results show that the models with high ζ (> 10^{-16} s^{-1}) or with a steep dependence on the column density are excluded by the observations. Furthermore, the model with the standard $\zeta=1.3\times10^{-17}$s^{-1} produces a worse agreement with respect to the "low" attenuation model based on Voyager observations. The single-dish data, however, are not sensitive to the attenuation of the CR profile, which changes only by a factor of two in the range of column densities spanned by the core model. Interferometric observations at higher spatial resolution, combined with observations of transitions with lower critical density, which trace the low-density envelope, are needed to observe the decrease of ζ with density. In the future, we plan extend this study to three other prestellar cores. The sources have been selected to sample different environmental properties, in order to allow us to investigate the role of the environment surrounding the cores on their ionisation properties (Redaelli et al., in prep.).

Future perspectives

Recent progress on the modeling of dust polarization in circumstellar disks has revealed that, in the Mie regime – when dust grain sizes are comparable to the wavelength of the observations – the polarization changes sign (i. e., it flips by 90°). Thus, when dust grains are radiatively aligned with the magnetic field, the polarization direction is then parallel to field lines. In this scenario, disk polarization observed with ALMA traces the morphology of the magnetic field, as a population of mm-sized grains is a key condition for future planet formation. Unpublished ALMA polarization data at 3 mm from the circumbinary disk surrounding the [BHB2007] 11 protostar shows that the polarization follows the accreting dust spirals seen in Alves et al (2019). Recent molecular line data (CH_3OH) shows a clear velocity gradient along the spirals and parallel to the polarization lines. If we assume the MIE regime, we are thus seeing magnetic field lines being dragged by the flow of gas along the spirals (Alves et al. in prep. This means that the magnetic field at scales of a few au is weak, hence shaped by the accretion flow, but still tightly coupled with the gas.

Selected references:

Alves, F. O. et al. 2019, Science, 366, 90
Redaelli, E. et al. 2019a, A&A, 629, A15
Redaelli, E. et al. 2019b, A&A, 631, A154
Redaelli, E. et al. 2021, A&A, 656, A109
Padovani, M. Et al. 2018, A&A, 614, A111
Pineda, J. E. et al. 2021, ApJ, 912, 7

Elena Redaelli

Felipe de Oliveira Alves

(Other CAS team members include A. Ivlev, J. E. Pineda, A. Schmiedeke, D. Segura-Cox, O. Sipilä, F. S. Tabatabaei, B. Zhao)

5.3.3 From Streamers to Disks

We have observed the flow of material from dense core scales down to disk scales. We identified the first robust evidence for streams of material from large distances down to disk forming scales. These features are non-axisymmetric and can dominate the infall rate, with values comparable to the protostellar accretion rates. Further, we have pushed the limits of high angular resolution observations of young embedded objects with ALMA, which led to the identification of disk substructures at very early stages. Both these results challenge the standard paradigm of star and planet formation, and open new avenues for future research.

Mass delivery to disk scales via streamers
The classical picture of star formation focuses on the material in an isolated parental dense core that undergoes gravitational collapse. In addition, all the material used to form stars and planets must pass through the dense core. In this scenario, star and disk formation can be studied in numerical simulations of isolated/closed boxes, allowing the implementation of a range of physical processes (e.g., magnetic fields, non-ideal MHD effects, dust grain-gas interaction). Recently, NOEMA observations of a Class 0 source in Perseus (Per-emb-2) revealed the presence of a large scale streamer (Pineda et al. 2020). These observations detected the streamer in molecular line emission, but not in the dust continuum emission (see left panel in Fig. 5.3.5). The derived velocity map in the streamer is smooth and it shows a streamer that begins at 10,000 au from the central YSO (beyond the classical dense core) and it is close to free-fall as it approaches disk scales. Given this strong evidence for a streamer delivering material from outside the core down to disk scales, disk formation simulations involving larger scales are needed to take into account the new observations.

Moreover, not all molecular lines trace the Per-emb-2 streamer: only those related to "chemically fresh" material (e.g., HC_3N, CCS, CS) are present, while typical dense core tracers (e.g., NH_3, N_2H^+, N_2D^+) are absent from the streamer. The chemically fresh fingerprints of the streamer indicate that if streamers are an important mass accretion pathway for the YSO, then they may alter the chemical budget at smaller scales. Thanks to the new NOEMA capabilities we detect 2 transitions of HC_3N, a good constraint of the streamer's density and total mass, enabling an estimate of the average infall rate onto the disk forming scales of 10^{-6} M_{Sun}/yr. This infall rate is comparable to the current accretion rate of 7×10^{-7} M_{Sun}/yr, which suggests that the streamer could significantly modify the protostellar accretion timescales by funnelling extra material to the central region.

Similarly, high resolution ALMA observations of the more evolved late Class I system [BHB2007] 1 presented by Alves et al. (2020) show a nearly edge-on gapped disk in the dust continuum emission. The complementary molecular line observations revealed two streamers identified in the CO (2-1) transition from ~2,000 au down to the disk edge (see right panel in Fig. 5.3.5). These streamers also present kinematics consistent with infall, and they do connect to the parental cloud-

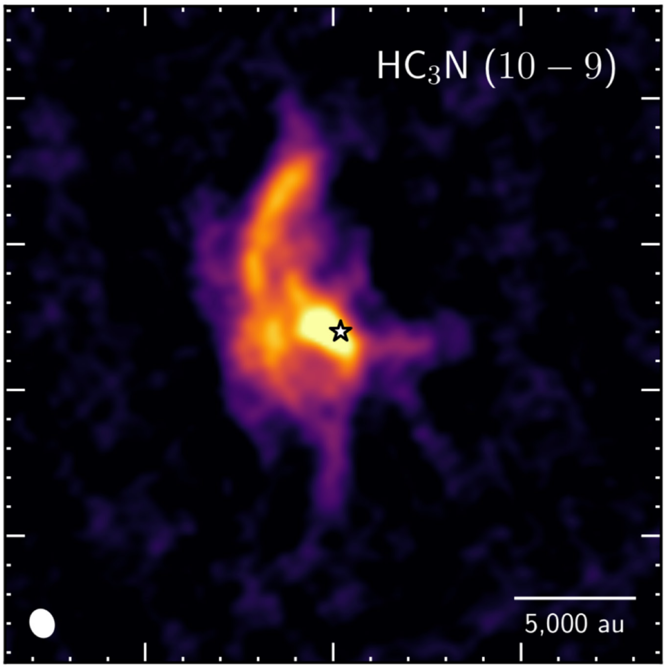

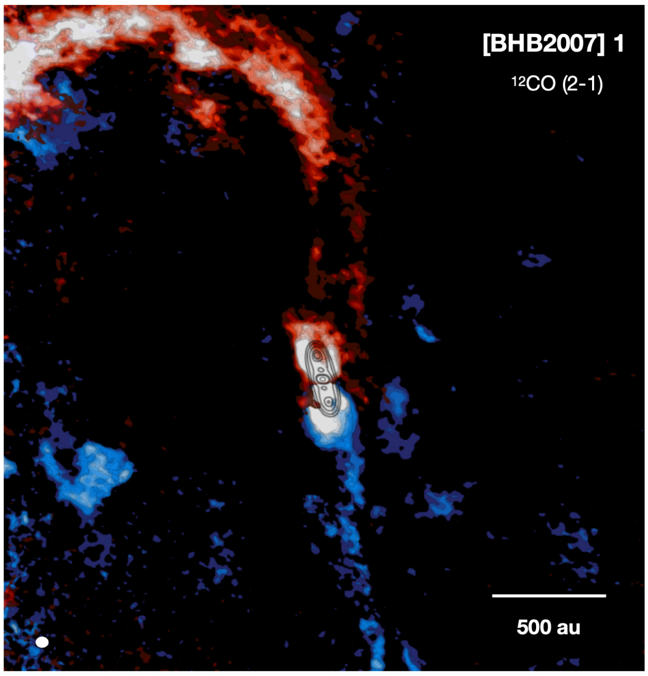

Fig. 5.3.5 Delivery of mass to disk-scales via Streamers. ***Left****: NOEMA observations revealed a large-scale streamer, confirmed by the gas dynamics, which connect scales >10,000 au down to disk scales. This reveals a strongly asymmetric mass delivery toward the young Class 0. Figure from Pineda et al. (2020).* ***Right:*** *ALMA observations of the almost edge-on system highlights the presence of two accretion streams feeding the system asymmetrically. Figure from Alves et al. (2020).*

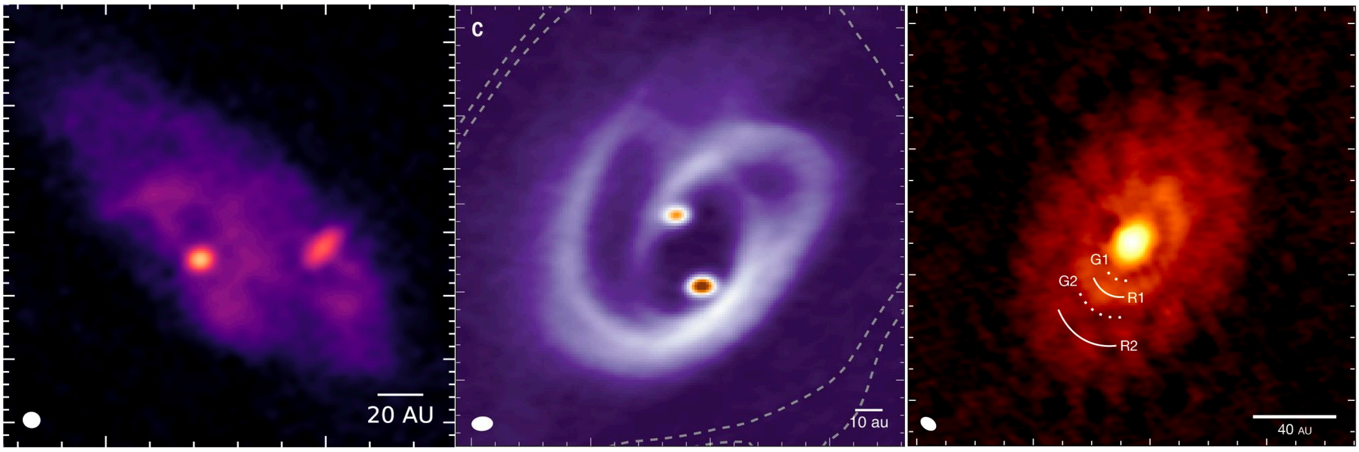

Fig. 5.3.6 *Substructures at disk scales seen in dust continuum with ALMA around protostars in different evolutionary stages.* ***Left:*** *Substructures seen around the highly-embedded Class 0 proto-binary IRAS 16293, revealing compact circumstellar disks within a sub-structured and clumpy circumbinary disk. Figure from Maureira et al. (2020).* ***Middle:*** *The complex morphology of the Class 0/I [BHB2007] 11 circumbinary disk shows that the accretion to the pair of young stars occurs via narrow accretion streams. Figure from Alves et al. (2019).* ***Right:*** *The youngest rings and gaps revealed in the disk of the Class I protostar IRS 63. Figure from Segura-Cox et al. (2020).*

seen at lower angular resolutions. A follow-up analysis of VLA and VLT/NACO observations confirmed the presence of a substellar object within the disk. This presents further evidence that the presence of a streamer does not hinder the formation of companions in disks; streamers can be present in a variety of evolutionary phases, and they should be taken into account in the star and planet formation process.

Disk substructures at different evolutionary stages

A variety of disk substructures have been found in dozens of Class II protostars with ALMA; however, studies of substructures in younger embedded disks (Class 0 and I) have only started to be probed for a handful of sources. We investigated the presence of substructures in the prototypical Class 0 object IRAS16293 in Maureira et al. (2020). These were the highest angular resolution observations of the system, and they provided the first confirmation of its binary nature. Moreover, these observations revealed the small circumstellar disks and clumpy substructures in the circumbinary disk (see left panel in Fig. 5.3.6). This highlights that disks even in the earliest stages of evolution are not smooth, which may impact early planet formation or binary accretion processes.

We also examined the circumbinary material around the slightly more evolved Class 0/I binary system [BHB2007] 11 in Alves et al. (2019). These ALMA continuum observations showed that the circumbinary disk feeds the material to the protostars via spiral streams reaching the circumstellar disks (see middle panel in Fig. 5.3.6). Velocities of small-scale CO line emission trace the flow of material from the spiral streams to the protostars, and demonstrate the prevalence of non-axisymmetric accretion structures at few au scales. These observations of extremely young protostars show the complexity of the disk structure and accretion process, which can directly influence the planet formation process.

Finally we observed the disk emission around the Class I protostar IRS 63 (Segura-Cox et al. 2020). These ALMA high-resolution observations revealed the youngest, so far, rings and gaps found in a disk (see right panel in Fig. 5.3.6). In the older Class II systems, rings and gaps in disks commonly found with ALMA are often attributed to the interactions between sizable planet embryos and the disk. The rings of IRS 63 are either the earliest evidence for a planet already in the act of formation, or at minimum, the rings provide stable zones for agglomeration of dust needed to start the planet formation process. In either case, these results present important evidence for the onset planet formation beginning at times earlier than ever seen before.

Selected References:

Pineda, J. E. et al. 2020, Nature Astronomy, Volume 4, pp. 1158-1163
Segura-Cox, D. et al. 2020, Nature, Volume 586, pp. 228–231
Alves, F. O. et al. 2019, Science, Volume 366, Issue 6461, pp. 90-93
Alves, F. O. et al. 2020, The Astrophysical Journal, Volume 904, Issue 1, id.6
Maureira, M. J. et al. 2020, The Astrophysical Journal, Volume 897, Issue 1, id.59

Jaime E. Pineda

Dominique Segura-Cox

(Other CAS team members include P. Caselli, F. Alves, M.J. Maureira, M.T. Valdivia-Mena, B. Zhao, A. Schmiedeke)

5.4 Theory

5.4.1 Cosmic Rays in Molecular Gas

Galactic cosmic rays (CRs) are a ubiquitous source of ionization and heating of the interstellar gas. In dense astrophysical environments, such as molecular clouds and pre-stellar cores (where UV and x-ray photons are extinguished), the ionization and heating are completely dominated by CRs. One of the principal aims of the CAS-Theory group is to understand the physics of low-energy CRs in molecular gas, by combining advanced methods of the kinetic theory and plasma physics and applying available observational constraints. These efforts will enable self-consistent modeling of key physical and chemical processes governed by CRs. Below we present several recent highlights of our research.

Theory of CR penetration into dense gas

Diffusive vs. free-streaming propagation of CRs. The penetration of Galactic CRs into molecular clouds and their further transport in dense gas is a complex physical phenomenon. Depending on a number of conditions, CRs can either move freely along the local magnetic field lines, or experience significant scattering on small-scale field fluctuations and propagate diffusively. Also, CRs lose energy due to ionizing collisions with gas molecules. In combination with the realized transport regime, this shapes the local energy spectrum of CRs and thus sets the local ionization rate ζ – the chief parameter that controls a variety of physical and chemical processes. Given that different transport regimes result in quite different dependencies of ζ on gas column density N, the CR transport could be constrained from available and future observations. We have derived analytical expressions for ζ vs. N, generally applicable to describe the diffusive or free-streaming regimes of CR propagation (Silsbee et al. 2019). Observational data suggest a relatively steeply decreasing ζ(N) in molecular cloud envelopes, which is matched better with the model of diffusive propagation. While the currently available data are not precise enough for drawing solid conclusions, our theoretical work provides the essential basis for the analysis of upcoming data – which will eventually allow us to identify the dominant regime of CR transport in molecular clouds.

Secondary CR ionization. CRs interacting with the gas generate electron-ion pairs, with electrons having sufficient energy to produce further ionization. These processes of primary and secondary ionization are characterized by the respective ionization rates, ζ_p and ζ_{sec}. While ζ_p can be straightforwardly derived for a given CR spectrum, computing ζ_{sec} is a much more difficult problem. Recently, we have rigorously calculated the energy spectrum of electrons that are produced by interstellar CRs penetrating dense molecular gas (Ivlev et al. 2021). Fig 5 4.1 illustrates our findings (see more details in the abstract by Ivlev), showing the derived dependence of ζ_{sec}/ζ_p on N. We see that this ratio steadily increases with gas column density. This behavior is quite different from the assumption of a constant ζ_{sec}/ζ_p, traditionally accepted in the literature. Knowing the exact spectrum of secondary electrons makes it possible to accurately evaluate characteristics of various important processes driven by CRs in molecular gas, such as the local rates of gas heating and H_2 dissociation, the local magnitude of the UV field (due to H_2 fluorescence), generation of x-ray emission as well as of IR emission (due to H_2 rovibrational transitions), etc.

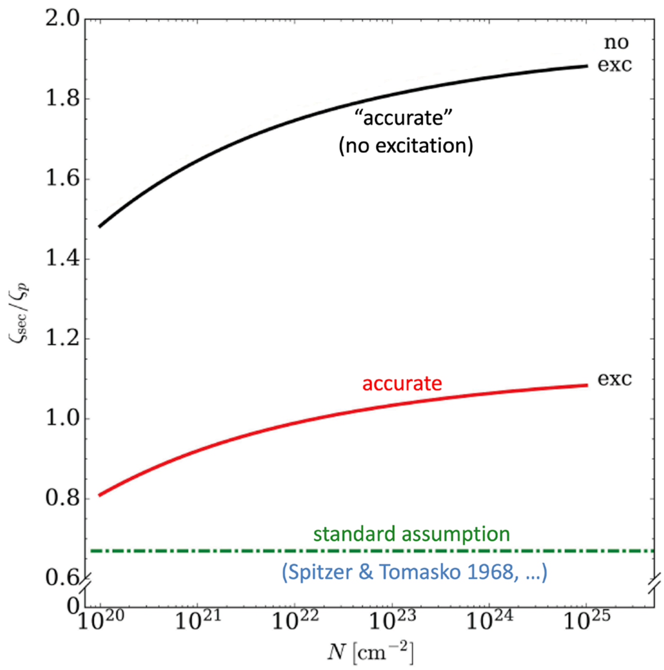

Fig.5.4.1 *Ratio of the secondary to primary ionization rates of H_2 as a function of the gas column density. The red curve ("exc") shows the exact case where excitation collisions with H_2 are included. For methodological reasons, we also plot the model case of no excitation ("no exc", illustrating the importance of excitation energy losses compared to ionization losses). The horizontal dashed–dotted line indicates the "standard" value of ζ_{sec}/ζ_p often adopted in the literature.*

Implications for physics and chemistry in clouds and disks

Icy mantles on dust grains. Dust grains in cold pre-stellar cores can grow icy mantles, where abundant gas-phase species can freeze out. Existing gas-grain chemical models predict formation of thick icy mantles of a few hundred monolayers around 0.1 μm dust particles, containing mainly water and CO. Collision of CRs with grains represent the main physical mechanism that controls the structure and composition of icy mantles at different evolutionary stages. We have computed the desorption rate of icy mantles as a function of the size and composition of both the grain and the mantle (Silsbee et al. 2021). Combining existing models of CR-induced desorption with our models of CR transport allowed us to accurately calculate the desorption rates in dark regions of molecular clouds. We showed that different desorption mechanisms dominate for grains of different sizes and in different regions of the cloud, leaving some grains free of volatile material, as illustrated in Fig. 5.4.2.

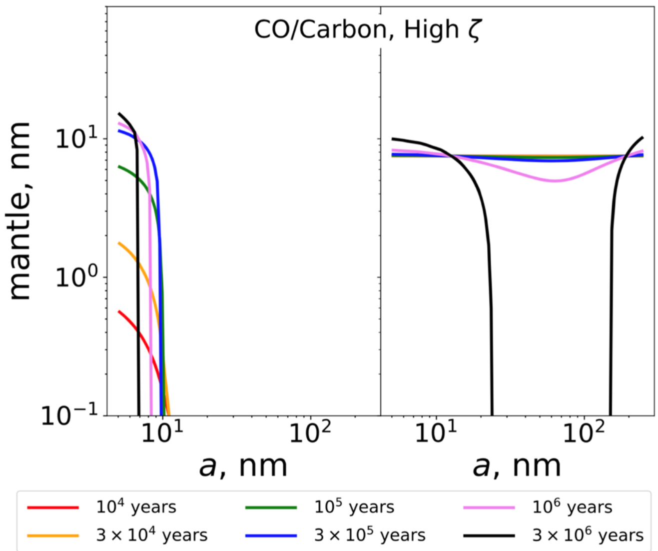

***Fig. 5.4.2** Thickness of icy mantles as a function of grain size, assuming an MRN size distribution and a free-streaming penetration of CRs into a molecular cloud core. All mantle material is in the gas phase at time t = 0, different colour curves correspond to different evolutionary times. The left and right panels correspond to an outer (n~10^4 cm^{-3}) and inner (n~10^6 cm^{-3}) core region, respectively. The composition of the mantle and the grain (CO ice on amorphous carbon material) is labelled on the panels.*

CR processing of ice. A large body of experimental work has shown that the interaction between CRs and ices similar to those coating interstellar grains can result in the efficient production and desorption of various chemical species observed in cold cores. Yet, understanding of these phenomena critically depends on the knowledge of microphysical processes occurring in ices upon the impact of individual CRs. We have shown that CR tracks in amorphous solid water can be approximated as a cylindrical volume with an average radius that is a function of the initial CR energy (Shingledecker et al. 2020). Interactions between energetic ions and ice targets were simulated using a Monte Carlo code, which allowed us to track secondary electrons down to sub-excitation energies in the material, as depicted in Fig. 5.4.3. We found the peak track-core radii to be as large as ~10 nm, substantially larger than the value often assumed in astrochemical models.

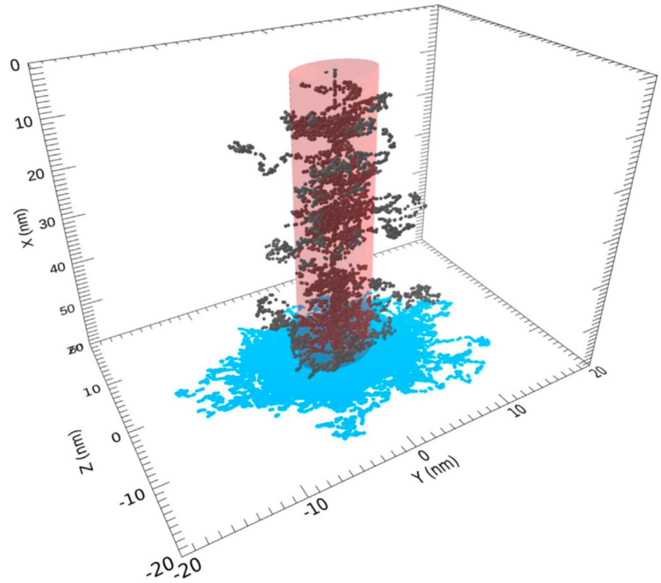

***Fig. 5.4.3** Portion of the track for a 0.1 MeV proton moving vertically through amorphous water ice, with the cylindrical track-core region depicted in pink and the projection of individual electron tracks onto the yz plane shown in blue.*

Outlook

Our group is currently working on several topics related to the physics of low-energy CRs. Below we illustrate two important directions that demonstrate long-term perspectives of our research, and also highlight collaborations with experimental groups. One direction is focused on understanding fundamental microphysics occurring in astrophysical ices bombarded by CRs. The other is the analysis of various CR-induced processes in the ISM, that can be imprinted in the emission detectable in different spectral ranges (from radio to x-ray) with available and next-generation telescopes.

CR-induced ice chemistry and sputtering. This work, whose aim is to study generic processes driven by CRs in pure astrophysical ice analogs, is conducted in close collaboration with experimentalists (see section 5.2.3, paragraph **"Project at the ATOMKI synchrotron facility"**). We utilize the fact that the energy of secondary electrons generated in ice in primary ionization events has a significant dependence on the energy of incident ions, if the latter is chosen near the maximum of ion stopping power (the rate of energy deposition in ice). Thus, by selecting pairs of ion beam energies on both sides of the stopping-power peak, we are able to probe the effect of electron-impact excitation and ionization of ice molecules – the processes that are sensitive to the electron energy, and are believed to play a crucial role in the ice radiolysis and sputtering. The first results of these dedicated experiments indicate that both the radiolysis products detected at astrophysically relevant ion fluences and the measured sputtering yield reveal a strong dependence on the energy of secondary electrons (Ivlev et al. in prep.; Giuliano et al. in prep.).

Observational signatures. To confront the theoretical models with observations, we are working on including them in the 2D radiation thermo-chemical model ProDiMo (Protoplanetary Disk Model). With ProDiMo we are able to model protoplanetary disks and embedded sources (ClassI/0), to make predictions for current (e.g. ALMA) and upcoming (e.g. ngVLA, JWST) telescopes. Our first simulations show how individual ionization sources (CRs, x-rays, stellar energetic particles) impact the spatial distribution of spectral line emission of molecules such as HCO+ and N2H+. It is crucial to understand the contributions of the various ionization sources to the total ionization rate, as this consequently allows us to provide constraints on the individual ionization rates. With such models, we can then test the various transport models for energetic particles in a global scenario, where other ionization sources that may drive ion chemistry (e.g. X-rays, UV) are also included. Furthermore, this allows us to properly interpret existing observations and to produce synthetic observables to, e.g., identify the best molecular tracers for studying ionization in planet-forming disks and embedded objects (Rab et al. in prep.).

Alexei Ivlev

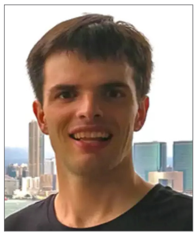

Kedron Silsbee

Christian Rab

(Other CAS team members: P. Caselli, B.M. Giuliano, T. Grassi, Ch. Shingledecker)

Selected References:

Giuliano, B.M. et al. in prep.
Ivlev, A.V. et al. 2019, ApJ 884,176
Ivlev, A.V. et al. 2021, ApJ 909, 107
Ivlev, A.V. et al. in prep.
Rab et al. in prep.
Shingledecker, C.N. et al. 2020, ApJ, 904, 189
Silsbee, K. et al. 2019, ApJ 879, 14
Silsbee, K. et al. 2021, MNRAS 507, 6205

5.4.2 Magneto-Hydrodynamic Simulations of Protoplanetary Disks

In this report, we show the profound impact of the magnetic field on protoplanetary disks and planet formation. Using numerical simulations, our group explores the effect of magnetic fields on disk formation, evolution, substructure, and grain growth within the disks. The relative strengths of non-ideal MHD effects determine whether a disk can form at all, as well as the orientation of the disk. Ambipolar diffusion, one important non-ideal MHD effect, removes small grains from the disk, which in turn changes the ambipolar diffusivity and promotes disk formation. The growth of larger grains also depends on the magnetic field: the magneto-rotational instability generates turbulence in the disk, which can result in much faster grain growth compared to the hydrodynamic Kolmogorov turbulence. Finally, the interplay between the magnetic field and the grain growth creates a wealth of substructures in the disks, carving out gaps and rings, where planet formation may occur.

The interplay between non-ideal MHD effects in protoplanetary disk formation

The formation of rotationally supported disks (RSDs) was previously shown to be difficult due to the so-called magnetic braking "catastrophe". By carefully investigating the ionization chemical network, we uncovered a unified picture of protostellar collapse in which non-ideal MHD effects work together in the diffusion of the magnetic field, allowing the formation of RSDs for typical prestellar core conditions. Based on our previous results of the depletion of very small grains (VSGs≤100 Å; Zhao et al. 2016, Silsbee et al. 2020) in protostellar envelope, we further investigated the intricate interplay between the non-ideal MHD effects, especially for ambipolar diffusion (AD) and Hall effect (Zhao et al. 2020, 2021), in the protostellar envelopes and disks. We discovered that despite the dispersive nature of the Hall effect which may counteract the diffusion of magnetic fields by AD and Ohmic dissipation, the net effect of non-ideal MHD in the protostellar envelope is to move the magnetic field radially outward against collapse. (see Fig. 5.4.4). As a result, disk formation should be relatively common for typical prestellar core conditions, with the observed range of cosmic-ray ionization rate (few 10^{-18} /s to few 10^{-16} /s; Caselli et al. 1998; Padovani et al. 2009). We also find that the magnetic field polarity does not affect disk formation, but can cause the disk to rotate in either retrograde or prograde fashion with respect to its surrounding envelope, if microphysics favors a strong Hall effect.

Depletion of small dust grains by ambipolar diffusion

We explored a novel mechanism for the removal of small dust grains in molecular clouds and prestellar cores. In poorly ionized regions of the interstellar medium, there is typically motion between ionized and neutral species, termed ambipolar diffusion. In prestellar cores, grains smaller than a few tens of nanometers across are typically tied to the magnetic field lines, while larger grains are dragged inwards across the field lines by the neutral gas. This results in a relative velocity, typically several tens of meters per second, between large and small grains, causing the small grains to paste themselves onto the larger ones. We showed in Silsbee et al. (2020) that in the absence of any grain fragmentation, proper accounting for ambipolar diffusion in calculating grain motions results in the near-complete removal of grains smaller than ~20 nm in a prestellar core (see Fig. 5.4.5). This work justifies the consideration of models such as in Zhao et al. (2020, 2021), in which the smallest grains are assumed to be entirely absent from the size distribution.

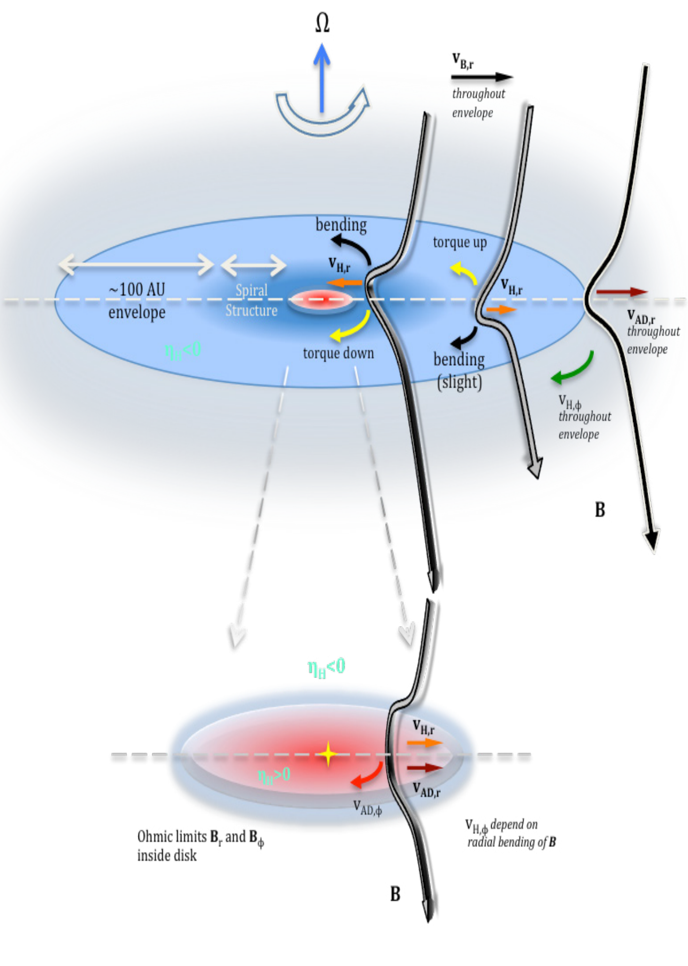

Fig. 5.4.4 *Adapted from Zhao et a. (2020).*

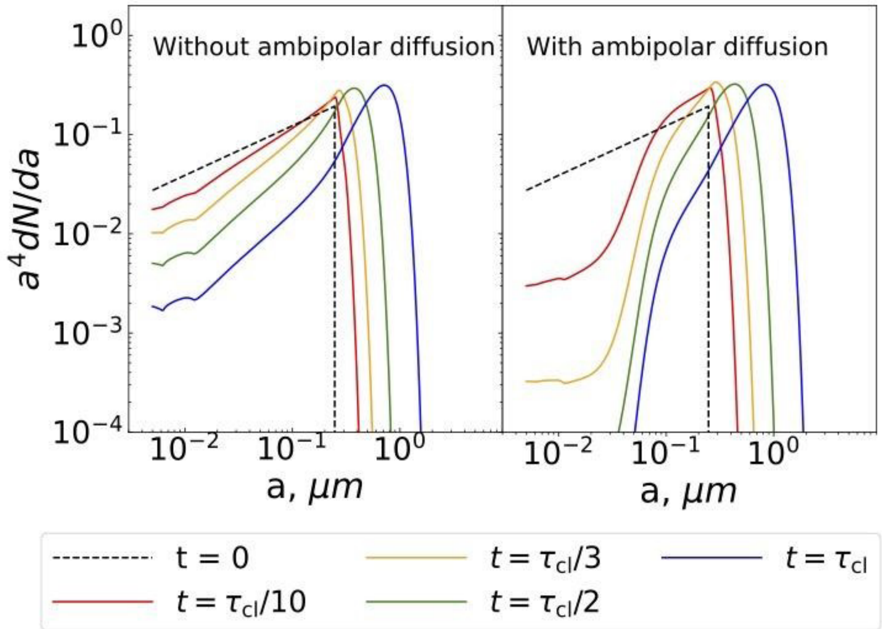

Fig. 5.4.5 *Evolution of the dust size distribution with and without ambipolar diffusion. In both cases, grain velocities arising from gas turbulence and Brownian motion were considered. Different color curves correspond to different amounts of time over which the size distribution has evolved, in units of the estimated cloud lifetime τcl. It is apparent that with ambipolar diffusion, the smallest grains are nearly completely removed in a small fraction of the cloud lifetime. Adapted from Silsbee et al. (2020).*

Effects of non-ideal MHD on ring formation

Radial substructures have now been observed in a wide range of proto-planetary disks (PPDs), from young to old systems, however, the mechanism of formation of these structures is still an area of vigorous debate. Recent magneto-hydrodynamic (MHD) simulations have shown that rings and gaps can form naturally in PPDs when parameterized non-ideal MHD effects are included (e.g. Suriano et al 2018, Riols & Lesur 2019). In Nolan et al 2022 we remove the parameterization of these terms by including simple chemistry and grain modeling to calculate the non-ideal effects in a more self-consistent way. Including ambipolar diffusion, we find that large grain populations (> 1 μm), and those including a population of very small polyaromatic hydrocarbons (PAHs) facilitate the growth of periodic, stable rings, while intermediate-sized grains suppress ring formation. Including Ohmic diffusion removes the positive influence of PAHs, with only large grain populations still producing periodic ring and gap structures. We aim next to include Hall diffusion and more accurate chemistry modeling, to determine whether non-ideal effects can reproduce the ring structures seen in PPDs.

Magneto-rotational instability and grain growth

Grain growth in protoplanetary disks is the first step towards planet formation. One of the most important pieces in the grain growth model is calculating the collisional velocity between two grains in turbulent gas. The collisional velocities in previous works are obtained based on the assumption that the turbulence is hydrodynamic with the Kolmogorov power spectrum. However, realistic protoplanetary disks are magnetized, and turbulent motions can be induced by the magneto-rotational instabilities (MRI). In Gong et al. (2020), we use magneto-hydrodynamic (MHD) simulations of MRI to investigate turbulence properties in protoplanetary disks. We observe a persistent kinetic energy spectrum of 4/3, shallower than the Kolmogorov spectrum of 5/3. In our subsequent work of Gong et al. (2021), we study the impact of turbulence properties on grain collisional velocities, and find that for the modeled cases of the Iroshnikov-Kraichnan turbulence and the turbulence induced by the magneto-rotational instabilities, collisional velocities of small grains are much larger than those for the standard Kolmogorov turbulence. This leads to faster grain coagulation in the outer regions of protoplanetary disks, resulting in rapid increase of dust opacity in mm-wavelength and possibly promoting planet formation in very young disks (Fig. 5.4.6).

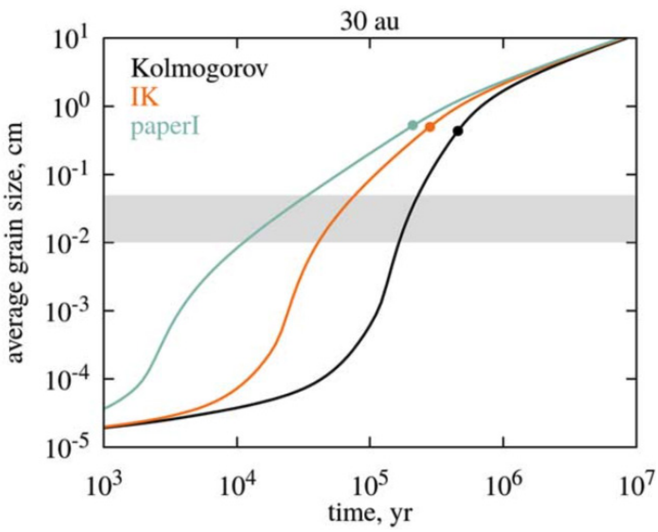

Fig. 5.4.6 *Evolution of the average grain size in the disk midplane at 30 AU, for Kolmogorov (black), Iroshnikov-Kraichnan (orange) and MRI (green) turbulence. The gray shaded region marks the size range that contributes the most to the dust emission at millimeter wavelengths. The filled circles indicate radial drift barriers for each turbulence model. Compared to the standard Kolmogorov turbulence assumption, MRI turbulence results in faster coagulation of small grains, possibly promoting planet formation. Adapted from Gong et al. (2021).*

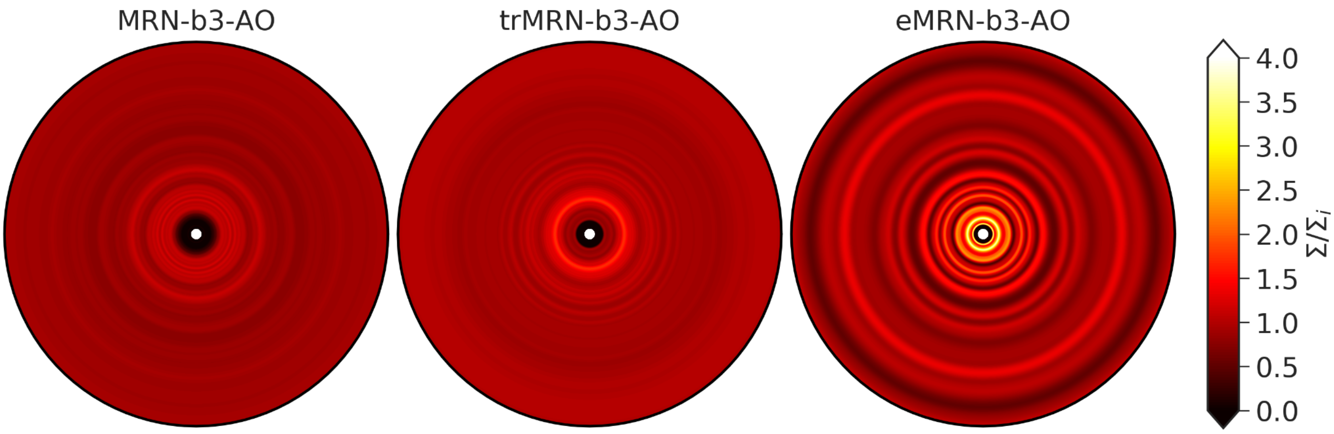

Fig. 5.4.7 *Face-on surface density profiles normalized to their initial radial distribution (out to a radius of 35 au) at t/t0=2500, for grain distributions of increasing size, from 0.005-1 um (MRN) to 1-100um (eMRN). Adapted from Nolan et al. (2022).*

Munan Gong

Bo Zhao

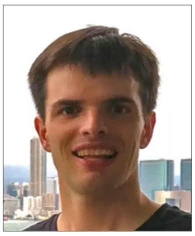

Kedron Silsbee

Chris Nolan

(Other CAS team members include: A. Ivlev, P. Caselli)

Selected References:

Gong, M., Ivlev, A. V., Akimkin, V., Caselli, P., 2021, ApJ, 917, 82
Gong, M., Ivlev, A. V., Zhao, B., Caselli, P. 2020, ApJ, 891, 172
Nolan, C. A., Zhao, B., Caselli, P. 2022, in preparation
Silsbee, K., Ivlev A. V., Sipilä, O,. Caselli, P., & Zhao, B. 2020 A&A, 641, 39
Zhao, B. et al., 2020, MNRAS, 492, 3375
Zhao, B. et al., 2021, MNRAS, 505, 5142

5.4.3 Astrochemical Modeling

Cosmic rays impact the chemical evolution in star-forming regions not only through gas heating, but also due to their ability to deposit energy into dust grains which leads to the sublimation of the ice covering the grains. Time-dependent effects due to changes in the ice composition affect the efficiency of this process, which has so far been explored only through simulations that ignore the time-dependence of the cooling. An impinging cosmic ray may also generate excited electrons as it passes through the ice, and these electrons further excite neighboring molecules, leading to a local enhancement in reactivity. In this Section we describe recent modeling efforts to constrain the interplay between cosmic rays and chemical evolution in the interstellar medium, as well as the fate of sulfur in molecular clouds.

The astrochemical modeling efforts at CAS aim to understand the chemical composition of interstellar matter, both in the gas phase and in the ices on the surfaces of interstellar dust grains. To this end, many distinct modeling studies have been undertaken at CAS. In the present Report, we concentrate on models that quantify the effect of cosmic rays on the structure and chemical composition of interstellar ices, as well as the elusive element sulfur.

Cosmic-ray induced desorption

A cosmic ray deposits energy into a dust grain upon striking and passing through it. For grains up to a few tenths of a micron in radius, the energy deposition leads to the transient heating of the entire grain to a higher temperature. The grain cools subsequently back to its equilibrium temperature by radiating away the excess heat, or via the (partial) desorption of the ice mantle on it. The latter mechanism is called cosmic-ray induced desorption (CRD). The efficiency of CRD depends on how often a grain is struck by a cosmic ray and to how high a temperature it is raised upon the cosmic ray strike, as well as on the molecular content of the ice. A numerical description of CRD has been provided by Hasegawa & Herbst (1993), who assumed a single grain radius of 0.1 μm, that the incoming cosmic rays consist of iron nuclei only (with a specific energy per nucleon), and that the ice on the grains is made up of a molecule with CO-like properties. Under these assumptions they derived a transient maximum grain temperature of 70 K as well as an efficiency parameter which characterizes the desorption rate, defined as the ratio of the grain cooling time (via desorption) to the average time interval between successive cosmic ray strikes. This description of CRD is adopted in nearly all astrochemical models that consider this process, regardless of the assumed grain size or the actual ice content.

Realistically, it is expected that the size of the grain and the grain material properties, as well as the composition of the impacting cosmic rays, all affect the maximum transient grain temperature, which will have a direct impact on desorption — a higher temperature leads to enhanced desorption. On the other hand, the chemical composition of the ice determines the cooling timescale. If the grain is covered by strongly-bound molecules such as water, the cooling time will be decidedly longer than if the grain is covered by weakly-bound molecules. At CAS, we have in the recent years undertaken new projects to understand better the CRD process by relaxing the strong assumptions made in previous works, and to explore the implications on the results of chemical simulations.

In Sipilä et al. (2020), we quantified the effect of the grain size on the efficiency of CRD by deriving the transient maximum temperatures for a range of grain sizes (see also Zhao et al. 2018) — assuming still the constant cooling efficiency from Hasegawa & Herbst. We also explored the effect of the grain size on the equilibrium temperature of the grains. It was found that grain-size dependent grain heating has consequences for gas-phase and grain-surface chemistry. For the latter, our model shows that the ice composition depends strongly on the grain size, and not in a straightforward manner. Some molecules (e.g. CH_3OH, c-C_3H_2) are most abundant on the smallest grains, while others present highest abundances on larger grains (e.g., HCN, HNC) — though not necessarily on the largest grains in the distribution. One of the main conclusions of this work is that the ice composition going into the protostellar stage could be very different as compared to the case of monodisperse grains if the smallest grains are removed from the distribution through grain-grain collisions before or during gravitational collapse.

In Sipilä et al. (2021), we revised the Hasegawa & Herbst description of CRD by accounting for the time-dependent ice composition to determine the grain cooling time (defined as a competition between desorption and radiative dissipation). We also modified the heating scheme to account for the attenuation of cosmic rays. We applied the revised CRD scheme to physical conditions typical to star-forming regions. Fig. 5.4.8 shows the calculated grain cooling time at two different volume densities, at constant 10 K temperature. Evidently, the cooling time as calculated by our new dynamic CRD model deviates significantly from the Hasegawa & Herbst constant value of 10^{-5} s at advanced simulation times. This has in some cases a large impact for the chemical composition in the gas phase – ice abundances are however affected only rather marginally.

Although the models described above have already improved greatly our understanding of the interaction between cosmic rays and chemical evolution in the interstellar medium, a lot remains to be done. We are currently working on expanding the dynamic CRD scheme to relax the assumption of constant transient maximum temperature reached by a grain upon a cosmic ray impact — cosmic rays rarely pass through the center of the grain, and for larger impact factors less energy is deposited. Another avenue for further research is to investigate the effect of grain size variations, in combination with the newly developed dynamic CRD scheme.

Bulk reactivity

Icy mantles are typically modeled considering a separation between the top few monolayers (the surface) and the rest of the ice under the surface (the bulk). For example, only surface species can be affected by photoprocesses and return to the gas phase via desorption. Species in the bulk are thought to be less mobile than those in the surface layers, affecting the chemistry and possibly maintaining a large fraction of radicals. These assumptions are however very rough and there is a crucial need to measure diffusion processes in the laboratory (one of the plans we have for the near future with the use of our Raman Microscope, see sect. 5.2.3). Shingledecker et al. (2019) simulated experimental work on proton-irradiation of O_2 and H_2O ices using astrochemical models accounting for radiation chemistry. This work clearly showed that to reproduce the experimental results, radicals and other reactive species produced via radiolysis in the bulk react quickly and non-diffusively with neighbours in the ice. This implies that the standard approaches to bulk chemistry based on thermal diffusion or quantum tunnelling through diffusion barriers reproduce less accurately the experimental data (especially at low temperature) and that bulk diffusion should not be considered in future modelling.

The fate of sulfur in molecular clouds

It is still an open question what happens to sulfur in the transition from diffuse to molecular clouds and dense cores (e.g., Ruffle et al. 1999 and references therein). Although diffuse clouds show elemental sulfur abundances close to the cosmic abundance, chemical models of molecular clouds need to consider two to three orders of magnitude of sulfur depletion to reproduce observations of CS and other S-bearing species. *Where does the sulfur go?* The missing sulfur cannot all be adsorbed onto dust grains, as it will then be hydrogenated and transformed in H_2S ice, which is not observed. We decided to explore this problem by running gas-grain chemical models of molecular clouds with the inclusion of radiation chemistry, by merging the chemical code of Vasyunin et al. (2017) with the code of Laas & Caselli (2019), where sulfur chemistry has been updated. Then, we included radiation chemistry to simulate the impact of low-energy cosmic rays on icy mantles. The results of this work are described in Shingledecker et al. (2020), where we show that a significant fraction of the H_2S is reprocessed into sulfur allotropes, in particular the most stable S_8. As shown in Fig. 5.4.9, our chemical model, starting with cosmic abundance of sulfur in the gas phase, predicts that without bulk diffusion a large fraction of S atoms is trapped in unobservable allotropes, in particular S_8, which is refractory and hard to remove from the ice. We propose this as a possible solution to the “missing sulfur” problem.

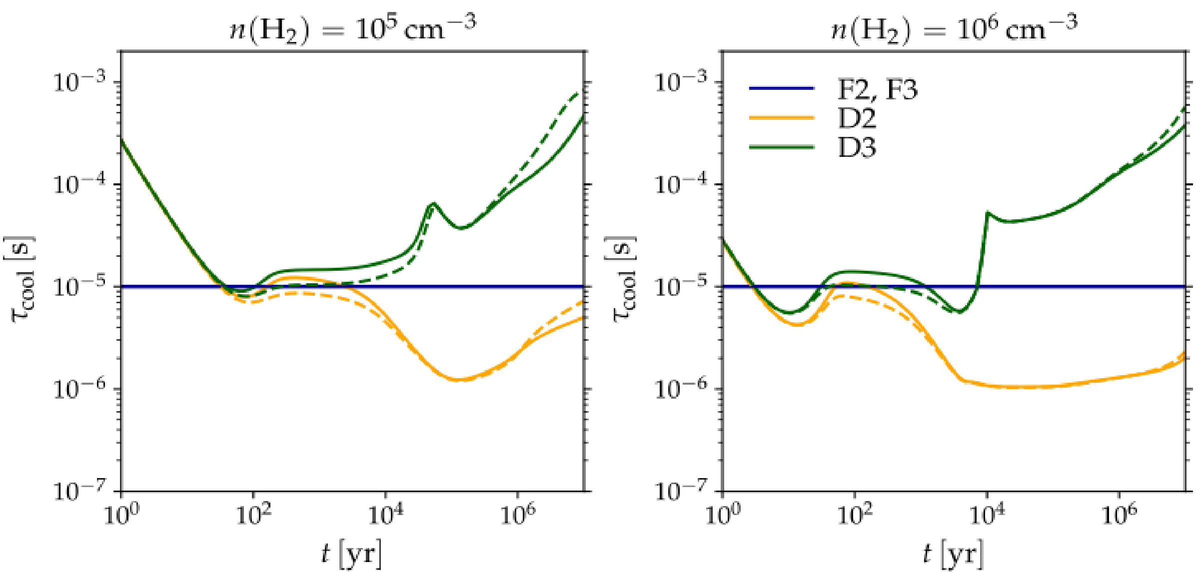

Fig. 5.4.8 *Grain cooling time at two different H_2 volume densities (10^5 cm^{-3}, left; 10^6 cm^{-3}, right) as a function of simulation time. The curves labeled “F” correspond to the Hasegawa & Herbst formalism with a constant grain cooling time, while the curves labeled “D” represent the new dynamic cooling scheme. The suffix in each model denomination shows whether the model is a two-phase (gas-phase chemistry + single reactive ice bulk) or a three-phase (gas-phase chemistry + ice separated into a single reactive surface layer on top of a chemically inert bulk) model. (Adapted from Sipilä et al. 2021.)*

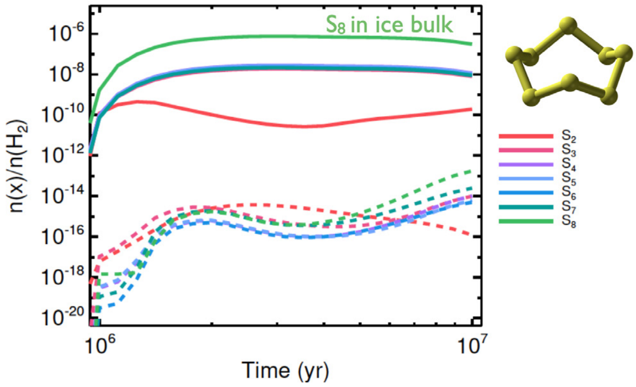

Fig. 5.4.9 *Abundances of sulfur allotropes (S_n, n ∈ [2,8]) in molecular clouds, within the bulk in models with bulk diffusion (dashed lines) and models without bulk diffusion (solid line). This shows that a significant fraction of sulfur can become trapped in the unobservable and refractory S_8 (depicted in the top right of the Figure), thus providing a plausible solution to the "missing sulfur" problem. (From Shingledecker et al. 2020).*

Selected References:

Hasegawa, T. I., & Herbst, E. 1993, MNRAS, 261, 83
Laas, J. C., & Caselli, P. 2019, A&A, 624, A108
Ruffle, D. P., Hartquist, T. W., Caselli, P., Williams, D. A. 1999, MNRAS, 306, 691
Shingledecker, C. N., Vasyunin, A., Herbst, E., Caselli, P. 2019, ApJ, 876, 140
Shingledecker, C. N., Lamberts, T., Laas, J. C., et al. 2020, ApJ, 888, 52
Sipilä, O., Zhao, B., & Caselli, P. 2020, A&A, 640, A94
Sipilä, O., Silsbee, K., & Caselli, P. 2021, ApJ, 922, 126
Vasyunin, A., Caselli, P., Dulieu, F., et al. 2017, ApJ, 842, 33
Zhao, B., Caselli, P., & Li, Z.-Y. 2018, MNRAS, 478, 2723

Olli Sipilä Christopher Shingledecker

(Other CAS team members include: B. Zhao, K. Silsbee, P. Caselli)

6 The Institute

6.1 Technical Services

The realisation of our scientific ideas would be impossible without the support of MPE's central technical services division. This mainly consisting of three different groupings of specialists in electrical engineering, mechanical engineering, and information technology. These specialists work closely together, and the scientific departments and project groups.

Electronic Engineering

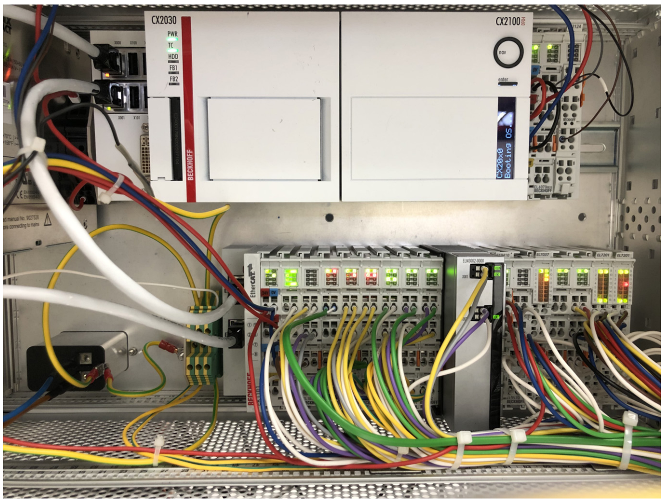

Fig. 6.1.1 *MICADO cryogenic mechanism test controller.*

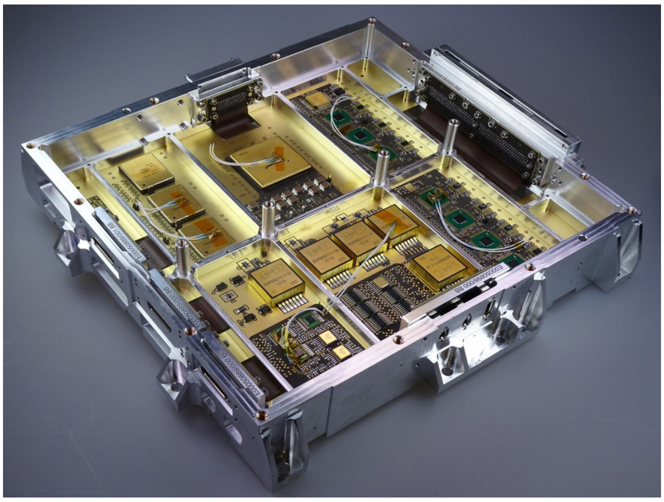

Fig. 6.1.2 *ATHENA-WFI Frame Processing Module: preliminary engineering model.*

The electronics engineering department consists of three groups: electronics development, electronics manufacturing, and building and utilities management. Approximately 30 staff members work in the entire department. In addition, a fluctuating number of students is working every year in the group by doing internships, bachelor and master theses.

Electronics engineering at MPE provides all professional skills required for the design, development, manufacturing and testing of scientific instruments. The group's experience covers a broad range, such as PCB (Printed Circuit Board) schematic and layout, electric cabinet construction and wiring, cryo-vacuum technology, PLC (Programmable Logic Controller) programming, processor- or FPGA-based (Field Programmable Gate Array) embedded systems and test setup automation, electronics system engineering, functional or environmental performance verification and circuit simulation.

The electronic equipment is provided for various applications, e.g. instrument control systems in electronics cabinets, highly integrated circuits for space-based electronics or test setups for laboratory experiments. In the years 2019 to 2022, the following MPE projects have benefited from the technical support of electronics engineers, technicians and other skilled workers in the electronics department: eROSITA, GRAVITY, ARGOS, ERIS, EUCLID, MICADO and ATHENA-WFI. Furthermore, new laboratory facilities and equipment were set up for the science group "Center for Astrochemical Studies".

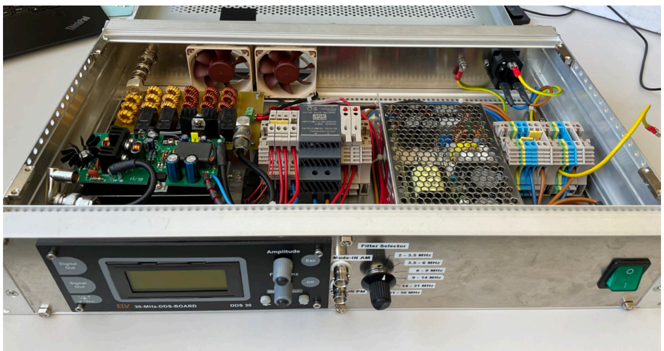

Fig. 6.1.3 *CAS cryogenic ion trap RF generator.*

Mechanical Enineering

Fig. 6.1.4 *Computer-aided design and manufacturing on high precision 5-axis CNC machine (CAD/CAM) at MPE*

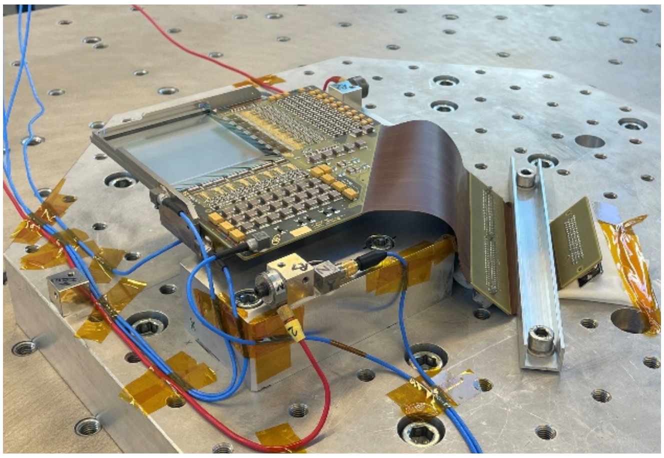

Fig. 6.1.5 *The Wide Field Imager (WFI) large detector quadrant on the shaker for vibration qualification tests.*

Fig. 6.1.6 *The ERIS Instrument on the Cassegrain focus of VLT UT4.*

The department has 43 staff plus eight apprentices and several student trainees. It is subdivided into three groups: the mechanical design office, the precision mechanical workshop including the training workshop and the integration and test facilities.

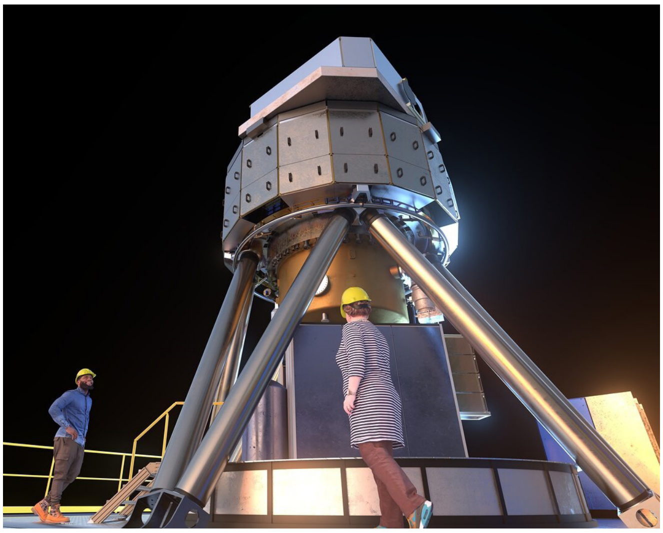

Fig. 6.1.7 *CAD view of MICADO imaging camera for the ELT*

The departments's qualified specialists deal with a wide range of tasks, reaching from optical- and mechanical design, structural- and thermal analyses to system engineering and product assurance. The complexity in the developments results from the highly demanding requirements, such as extreme cleanliness, stress due to vibration loads during a rocket launch, the required functioning of instruments in vacuum and at very low temperatures. For the mechanical design development and analysis, high-end CAD/CAE/CAM and PLM (Product Lifetime Management) tools are used. In the mechanical workshops, the sophisticated instruments

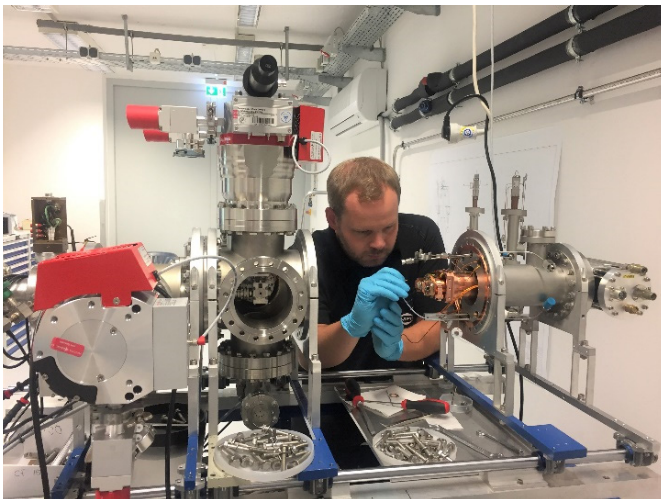

Fig. 6.1.8 *The open Cold CAS Ion Trap (CASTRAP)*

are manufactured on conventional as well as on large high precision 5-axis CNC machines. For environmental tests and for space qualification services, a shaker and several thermal vacuum chambers are available in the department.

The Mechanical Engineering department develops, manufactures, integrates and tests complex space and ground-based instruments for experimental astronomy. These instruments are based on cutting-edge technologies and innovative concepts and are built in close cooperation with the scientists and project groups, and partly also together with space industry.

In the years 2019 to 2022 the mechanical engineering department supported the following main MPE projects: the X-ray telescope eROSITA launched on July 13, 2019, the Einstein Probe mission with the Follow-up X ray Telescope (FXT), the Wide Field Imager (WFI) for ESA's ATHENA satellite mission and the EUCLID satellite payload NISP. For astrochemical studies, the CAS Cold Ion Trap unit (CASTRAP) for cryogenic ion-molecule interaction studies and the Split-Ring Electrode Trap (CASSRET) for nanoparticle mass spectrometry were developed. For ground-based astronomy, the focus was on: ERIS, the Enhanced Resolution Imager and Spectrograph successfully installed at the Cassegrain focus of the VLT-UT4 in 2021, GRAVITY+, GRAVITY's VLTI upgrade for milliarcsecond resolution interferometric imaging, and MICADO, the first light imaging camera for ESO's Extremely Large Telescope (ELT).

Information Technology

Data management and processing is generally a collaborative task of the MPE IT group and the individual research groups. The IT people cover the central tasks and, in addition, support with their IT-knowledge and manpower the science groups in their specific work.

Computing and data processing activities are coordinated and handled by a committee with representatives from all science groups of the Institute. This IT committee plays an important role in steering the Institute's IT strategy, and ensuring that the needs of the scientific groups are being fully accounted for. The main tasks of this committee are to advise on MPE's longer-term IT strategy, to advice and asses central IT projects, to coordinate and to evaluate new hardware as well as software, and the hard- and software procurement. In addition, the committee is co-ordinating the collaboration with the Max Planck Computing and Data Facility (MPCDF).

The members of the central IT support group maintain the central installations, i.e. network, server workstations, printers, and the official WWW pages, with up-to-date information about the Institute. They are also part-time involved in the data processing of and software development for our main science projects like eROSITA, GRAVITY+, ERIS, MICADO and EUCLID..
This guarantees the horizontal flow of information and experience.

6.2 General Services

The Institute's administration supports the scientific management for two Max Planck Institutes (MPI for Astrophysics and MPI for Extraterrestrial Physics) and the Computing Center / Max Planck Computing and Data Facility (MPCDF). Organizationally, the administration is divided into four areas:
Human Resources, Finance, Procurement/Purchasing, and General Services (including housekeeping, motor pool, and gate/reception services).

Fig. 6.2.1 *Personnel at MPE's administration*

Looking back, there have again been a number of new challenges over the past three years, such as the introduction of electronic invoicing, the switch to the travel expense reporting module from SAP (formerly Wintrip), and the implementation of the virtual workplace (vAP) in the wake of advancing digitization.
The latter change (vAP) in particular proved to be a blessing during the last two years of the pandemic, as working from home was made much easier here.
Together with our on-site IT, this went almost silently. However, digitization is far from complete and opportunities for optimization are always opening up.

The large number of research projects to be supervised in the area of third-party funding has not decreased, and the administrative work is not made any easier by further changes
in the area of public procurement law and labor law/occupational health and safety (pandemic).

The Astrobibliothek is the joint library for MPE and MPA. At present it holds a unique collection of about 54000 books and journals, about 7300 reports and observatory publications, as well as print subscriptions for about 140 journals and manages online subscriptions for about 500 periodicals. In addition it maintains an archive of MPA and MPE publications, two slide collections (one for MPA and one for the MPE), a collection of approximately 800 nonprint media, and store copies of the Palomar Observatory Sky Survey (on photographic prints) and of the ESO/SERC Sky Survey (on film). The library catalogue includes books, conference proceedings, periodicals, and theses, in print and online as well.

Fig. 6.2.2 *The joint MPE/MPA Library*

6.3 Vocational Training and Education

Fig. 6.3.1 Mechanical Apprentices at work.

Fig. 6.3.2 Mechanical Apprentices at work.

Education is a socio-political task to which the MPI for Extraterrestrial Physics is committed as a publicly funded research institute. In addition to the next generation of scientists, the professional training of young people is also promoted at our institute.

In each of the past three years (2019, 2020, 2021), eight apprentices - 2 per apprenticeship year - have been trained in the Institute's training workshop as industrial mechanics in the field of fine equipment construction (training period 3 1/2 years). Occasionally, students also complete a work placement in the workshop to prepare for their professional career.

In the first two years of the apprenticeship, the apprentices mainly receive basic training in a wide range of occupational fields. The focus is on working on various projects to teach the basic qualifications. Independent and team-oriented work as well as the observance of occupational safety regulations are particularly promoted. From the middle of the second year of training, the apprentices already support the precision mechanics workshop with simple turning, milling and assembly work. In the third year of training, the apprentices work in the precision mechanics workshop for three and a half months, where they are taught further technical qualifications. In the process, they already make significant productive contributions to the Institute.

Through strict adherence to hygiene rules, sufficient distance and permanent mask-wearing, the training operation was able to continue as normal for the most part during the Corona pandemic. Only internships were temporarily suspended.

Fig. 6.3.3 Mechanical Workshop.

The International Max-Planck Research School (IMPRS) on Astrophysics at the Ludwig-Maximilians University of Munich

IMPRS is a graduate school offering a broad PhD program in astrophysics, astrochemistry and cosmology.

Open for students worldwide, the school provides a world-class teaching and research program with sufficient attraction to compete successfully with other well-known graduate schools. IMPRS comprises all Munich astrophysics institutes, i.e. MPE, MPA and the University Observatory of the Ludwig-Maximilians-University of Munich (USM). ESO participates as an associated partner.

The school was founded in 2001 and was successfully evaluated several times. In 2021, IMPRS celebrated its 20th anniversary, which gave time to take stock about the program: Not only the statistical figures but also the reports of directors, lecturers, doctoral students and alumni of the program's values showed that the IMPRS of Astrophysics is a scientific success story.

There are less than a handful of such places worldwide that can compete in breadth and level of research with our participating institutes. The large number of active scientists who are involved in IMPRS teaching and student supervision guarantees that state-of-the-art knowledge is presented to the students.

Right now, it is funded by the Max-Planck-Society (MPG) until September 2025. The MPG funding, however, supports only a small minority of our students. The majority is funded through the IMPRS member institutions themselves, either via their own budgets or via external third-party funds.

The training program of our IMPRS is highly structured, aiming for a PhD at the end of three to four years. It is designed to attract young scientists with outstanding qualifications and is advertised worldwide.

354 students out of 41 different countries applied for the IMPRS program 2022. In total, the school has received more than 4250 applications from 103 different countries since 2001. Based on their excellence as proven by their university record, by letters of recommendation and by a successful interview during a three-day recruitment workshop in Garching, on average 25 applicants are offered a position every year. The acceptance rate is about 75%.

Coursework, research opportunities, evaluation and mentoring are all managed uniformly across the program, which aims for a broad understanding of the essential elements of astrophysics, astrochemistry and

Fig. 6.3.4 *Participants of the IMPRS introductory workshop 2015.*

Fig. 6.3.5 *First seminar for IMPRS class of 2021.*

cosmology. The joint education of all students in a well-defined set of courses also creates a well-developed esprit de corps throughout the whole student body and forges links that can support them throughout their careers. We are in contact with the majority of previous IMPRS participants via our alumni program. It includes e.g. an alumni network platform as well as regular Career Seminars, where former students give insights in a working life after the PhD!

Since 2001, nearly 350 students finished successfully. Of them about 66% held a post-doc position, about 26% took a job in industry and about 8% started an academic career.

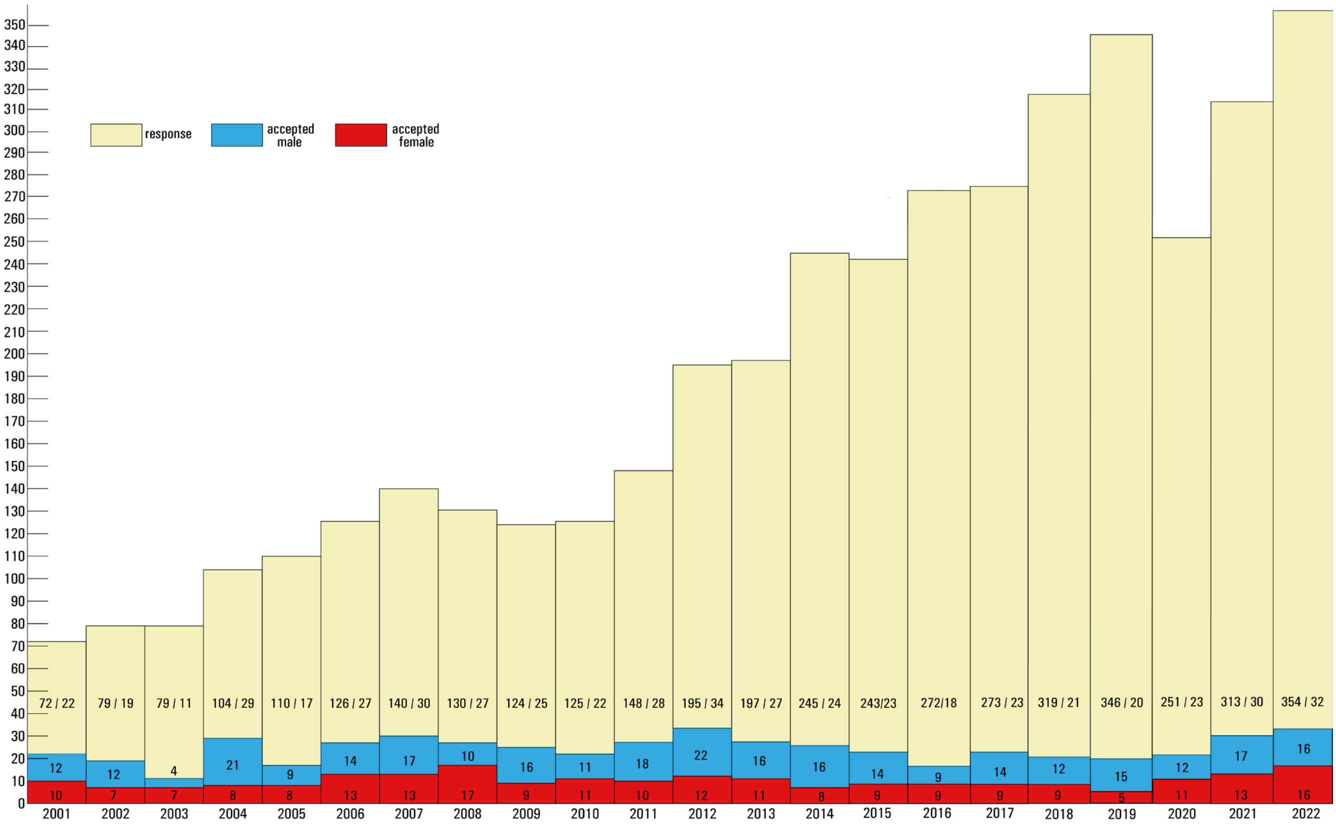

__Fig. 6.3.6__ Applicant statistics for IMPRS since 2001.

6.4 Public Outreach

A modern technological society needs basic research for a successful future. As fundamental research is mainly funded by tax revenue, it is essential to report our work to and seek the support of the general public. Therefore our Institute actively communicates its activities and results to a broad audience, and makes the argument for science as an integrated and basic part of a vital and developing society, even if the benefits to an individual's daily live are not immediate and obvious.

The MPE public outreach team consists primarily of media production head of the press office and another communication specialist, who mainly takes care of Social Media and scientific administration tasks. This team, supported by a team assistant and by many MPE members, organized several, quite different activities in and outside MPE during the past three years.

A special day in every respect was the 6th of October 2020, when it was announced that MPE-Director Reinhard Genzel was to receive the **Nobel Prize for Physics 2020**. On the same day, a press conference was organised and MPE and Genzel received about 50 press inquiries. Up to today, there have been more than 180 inquiries, which had been answered by Genzel or colleagues from his group.

In general, the Nobel Prize for Reinhard Genzel have resulted in an enormous media coverage. The day after the announcement, more than 8000 news had been registered all over the world, along with 18000 mentions on Social Media. In the following week, there have been another 6000 news and 8000 social media mentions. Since then, Genzel gave about 70 public talks and many more interviews.

Every two years, the Institute actively par ticipates in the **Open House** event on the Garching campus. However, the last Open House has happened in 2017. In 2019, there was no Open House because the Technical University of Munich didn't participate, and in 2020 and 2021 the COVID pandemic made it impossible for the MPE to open its doors for visitors.

Every year since 2008, the Institute participates in the nationwide **Girls' Day**. Sponsored by the European Union, the Federal Ministry of Education and Research (BMBF) and the Federal Ministry for Families, Senior Citizen, Women and Young People (BMFSFJ), the yearly Girls' Day initiative has been established in Germany in 2001. Although on average girls do reach a higher level of education at school than their male peers, they still tend to choose traditional female fields of occupa-

Fig. 6.3.7 *Prof. Dr. Reinhard Genzel presents the Nobel Medal to the Bavarian Minister for Science and Arts, Bernd Sibler. On the left: Director of OPINAS group, Prof. Dr. Ralf Bender.*

Fig. 6.3.8 *Due to COVID restrictions, the Girls' Day 2021 was held virtually.*

tion. By providing girls, aged between 14 and 16 years, with contact to professionals and an insight to modern working places in the area of technology, IT and natural sciences, it is often possible to catch their interest and encourage them to pursue a career in these fields.

In 2019, 40 girls participated in the Girls' Day at MPE, another 5 visited the MPE Workshop. The Girls' Day 2020 had to be cancelled due to COVID restrictions. However, to enable young women a glance into MPE, the Girls' Day 2021 was organized virtually. 50 girls listened to several online presentations by female MPE scientists, along with a live stream from the MPE Workshop.

In addition to such special events and the preparation of singular documents like brochures and flyers, the MPE public outreach team regularly fulfills a number of tasks. MPE offers guided tours for groups through the Institute on request. The tours are available in German and English, as well as some other languages. After a general introduction, scientists of the various groups of the Institute will guide the visitors through their departments. This service is requested quite frequently (about 25 to 30 groups per year) and it can be really challenging to meet the requirements of the different visitors as the groups can be as diverse as e.g. high school and university students, senior citizens, interested hobby astronomers or even colleagues from other scientific institutions.
Since the last report, 24 guided tours have been organised at the MPE, mostly for scientific interested school classes, and mainly in 2019 and early 2020.

On the 14th of July 2021, the Bavarian Minister for Science and Arts, Bernd Sibler visited MPE, along with some assistants from his ministerial office. The group was first welcomed by Nobel Prize Laureate and MPE Director Reinhard Genzel, who gave a presentation with general information about MPE, followed by some lab visits.

On the 22nd of September 2021, the MPE welcomed 16 winners of "Jugend Forscht" (Youth Researchers). The junior scientists listened to a talk by Nobel Prize Laureate Reinhard Genzel, visited a lab and joined a discussion with doctorate candidates.

On a regular basis, MPE scientists give public talks/ lectures for a scientifically interested audience. MPE scientists are invited to e.g. planetariums, schools, or special events to provide their expertise. About 40 such talks or lectures are delivered every year – due to COVID most of them online.

Finally, MPE offers the possibility for doing internships at the Institute, both for high school and university students. Every year about 10 to 15 high school students (1 to 2 weeks) and 5 to 10 university students (4 to 8 weeks) gain an inside-look at a scientific institute by participating under the supervision of a scientist in a small research project. Since March 2020, those numbers declined drastically as – due to COVID – no personal supervision at MPE could be established.

MPE's website (http://www.mpe.mpg.de) exists both in German and English and is regularly updated with research news as well as events such as technical achievements or awards. Each year, about 20 to 30 new science results of MPE scientists are presented with an eye to the popular press. High-impact science results are issued as press releases, often in cooperation with other scientific institutes. MPE regularly receives journalist inquiries, which range from simple questions to large visits by TV film crews.

Since June 2021, the MPE has been operating its own Twitter account (@MPE_Garching). As of 31 December 2021, the account had 760 followers and posted 322 tweets and re-tweets. The account on LinkedIn (MPE-Garching) was also managed more intensively lately, and by the end of the year 2021, the MPE had accumulated 1518 followers there.

6.5 Social Events

Getting to know one's colleagues not only through formal workplace interaction, but also from joint social activities, can help to form a positive atmosphere in the Institute. These activities help to link people from sometimes quite separate areas, but can also serve to integrate new MPE-members. Our social activities range from small group-internal celebrations (e.g. the success of a certain scientific project, a PhD defence, special birthdays etc.) to MPE-wide celebrations like the Christmas party and the three well-established annual trips: the skiing excursion, the summer trip, and the visit to the Munich Oktoberfest in autumn.

On the 21st of February 2019, a ski trip for MPE employees was organized to Elmau/Hartkaiserbahn in Tirol/Austria with joint dinner at Ellmauer Hof.

For the summer trip on the 4th of July 2019, we went to Herrsching am Ammersee: After initial difficulties with the booked bus company during the journey, the participating employees met in Herrsching at the Realschule. From there, they went on a joint walk to a "fishy surprise". At the fish sandwich king (Matos fish shop in Herrsching), a fish sandwich and a glass of prosecco or orange juice awaited each participant for a good start to the company excursion. Afterwards, the day was free. The participants met again for dinner at the Gasthof zur Post in Herrsching before the return journey.

Each year, a large MPE crowd spends a pleasant afternoon - and most also the evening – together at the famous Munich Oktoberfest. They may enjoy the fun rides as well as the entertainment in the outdoor festival area but also Bavarian sociability inside the “Wiesn Tents”. Many colleagues dress up for this occasion in traditional Bavarian costumes. The unique atmosphere of eating, drinking and celebrating together is very favourable for deepening existing connections between MPE staff members, students and guests, as well as making new ones. On 25th of September 2019, a contingent of 100 was reserved for MPE in the Hofbräutent, which was quickly exploited by MPE staff.
On the 19th of December 2019, a Christmas Party was organized at MPE. A great amount of MPE staff enjoyed warm food from the buffet and talking to colleagues.

Since then, due to the Corona pandemic, no more trips, excursions or parties could have been done.